

# Corrosion and microbiological resistance of modified epoxy coating for pipe protection

---

**Samardžija, Marina**

**Doctoral thesis / Doktorski rad**

**2024**

*Degree Grantor / Ustanova koja je dodijelila akademski / stručni stupanj:* **University of Zagreb, Faculty of Chemical Engineering and Technology / Sveučilište u Zagrebu, Fakultet kemijskog inženjerstva i tehnologije**

*Permanent link / Trajna poveznica:* <https://urn.nsk.hr/urn:nbn:hr:149:651451>

*Rights / Prava:* [In copyright](#)/[Zaštićeno autorskim pravom.](#)

*Download date / Datum preuzimanja:* **2025-03-13**



*Repository / Repozitorij:*

[Repository of Faculty of Chemical Engineering and Technology University of Zagreb](#)





University of Zagreb

FACULTY CHEMICAL ENGINEERING AND TECHNOLOGY

Marina Samardžija

**CORROSION AND MICROBIOLOGICAL  
RESISTANCE OF MODIFIED EPOXY COATING FOR  
PIPE PROTECTION**

DOCTORAL THESIS

Zagreb, 2024.

SVEUČILIŠTE U ZAGREBU  
FAKULTET KEMIJSKOG INŽENJERSTVA I TEHNOLOGIJE

Kandidatkinja Marina Samardžija

predala je dana: 6. rujna 2024. doktorski rad izrađen pod mentorstvom izv. prof. dr. sc. Ivana Stojanovića, Sveučilište u Zagrebu Fakultet strojarstva i brodogradnje i prof. dr. sc. Helene Otmačić Ćurković, Sveučilište u Zagrebu Fakultet kemijskog inženjerstva i tehnologije.

Povjerenstvo za ocjenu doktorskog rada u sastavu:

1. prof. dr. sc. Sanja Martinez, Sveučilište u Zagrebu Fakultet kemijskog inženjerstva i tehnologije
2. prof. dr. sc. Marija Vuković Domanovac, Sveučilište u Zagrebu Fakultet kemijskog inženjerstva i tehnologije
3. prof. dr. sc. Vesna Alar, Sveučilište u Zagrebu Fakultet strojarstva i brodogradnje

pozitivno je ocijenilo doktorski rad doktorandice Marine Samardžija, a Fakultetsko vijeće Sveučilišta u Zagrebu Fakulteta kemijskog inženjerstva i tehnologije na sjednici održanoj dana 28. listopada 2024. prihvatilo je ocjenu i odobrilo obranu doktorskog rada pred istim povjerenstvom.

Obrana doktorskog rada održana je dana 28. studenog 2024.

D e k a n

prof. dr. sc. Ante Jukić



University of Zagreb

FACULTY CHEMICAL ENGINEERING AND TECHNOLOGY

Marina Samardžija

**CORROSION AND MICROBIOLOGICAL  
RESISTANCE OF MODIFIED EPOXY COATING FOR  
PIPE PROTECTION**

DOCTORAL THESIS

Zagreb, 2024.



Sveučilište u Zagrebu

FAKULTET KEMIJSKOG INŽENJERSTVA I TEHNOLOGIJE

Marina Samardžija

**KOROZIJSKA I MIKROBIOLOŠKA OTPORNOST  
MODIFICIRANE EPOKSIDNE PREVLAKE ZA  
ZAŠTITU CIJEVI**

DOKTORSKI RAD

Zagreb, 2024.



University of Zagreb

FACULTY OF CHEMICAL ENGINEERING AND TECHNOLOGY

Marina Samardžija

**CORROSION AND MICROBIOLOGICAL  
RESISTANCE OF MODIFIED EPOXY COATING FOR  
PIPE PROTECTION**

DOCTORAL THESIS

Supervisors:

Assoc. Prof. Ivan Stojanović, PhD  
Prof. Helena Otmačić Ćurković, PhD

Zagreb, 2024.



Sveučilište u Zagrebu

FAKULTET KEMIJSKOG INŽENJERSTVA I TEHNOLOGIJE

Marina Samardžija

**KOROZIJSKA I MIKROBIOLOŠKA OTPORNOST  
MODIFICIRANE EPOKSIDNE PREVLAKE ZA  
ZAŠTITU CIJEVI**

DOKTORSKI RAD

Mentori:

Izv. prof. dr. sc. Ivan Stojanović  
Prof. dr. sc. Helena Otmačić Ćurković

Zagreb, 2024.

## Bibliografski podaci

UDK: 621.793:66.094.39(043.3)=111  
Znanstveno područje: Tehničke znanosti  
Znanstveno polje: Kemijsko inženjerstvo  
Znanstvena grana: Kemijsko inženjerstvo u razvoju materijala  
Institucije: Sveučilište u Zagrebu, Fakultet strojarstva i brodogradnje,  
Zavod za materijale

### Voditelji rada:

izv. prof. dr. sc. Ivan Stojanović, Sveučilište u Zagrebu Fakultet strojarstva i brodogradnje  
prof. dr. sc. Helena Otmačić Čurković, Sveučilište u Zagrebu Fakultet kemijskog inženjerstva i tehnologije

Broj stranica: 154

Broj slika: 23

Broj tablica: 10

Broj literaturnih referenci: 155

Datum obrane: 28.11.2024.

### Sastav povjerenstva za obranu:

1. prof. dr. sc. Sanja Martinez, Sveučilište u Zagrebu Fakultet kemijskog inženjerstva i tehnologije
2. prof. dr. sc. Marija Vuković Domanovac, Sveučilište u Zagrebu Fakultet kemijskog inženjerstva i tehnologije
3. prof. dr. sc. Vesna Alar, Sveučilište u Zagrebu Fakultet strojarstva i brodogradnje

### Rad je pohranjen u:

Nacionalnoj i sveučilišnoj knjižnici u Zagrebu, Hrvatske bratske zajednice bb;  
Knjižnici Fakulteta kemijskog inženjerstva i tehnologije Sveučilišta u Zagrebu, Marulićev trg 20.

Tema rada prihvaćena je na 8. sjednici Fakultetskog vijeća Fakulteta kemijskog inženjerstva i tehnologije u Zagrebu, održanoj dana 10. srpnja 2023. te odobrena na sjednici Senata Sveučilišta u Zagrebu 19. prosinac 2023.

The topic of the doctoral thesis was accepted at the 8th session of the Faculty Council of the Faculty of Chemical Engineering and Technology in Zagreb, held on July 10, 2023, and approved at the session of the Senate of the University of Zagreb held on December 10, 2023.



## **Supervisor information**

### **Assoc. Prof. Ivan Stojanović, PhD**

Ivan Stojanović [REDACTED] where he finished elementary and technical high school. In 2003 he graduated from Zagreb University's Faculty of Mechanical Engineering and Naval Architecture with a degree in Naval Engineering. After graduating, he worked for Uljanik, a shipbuilding company based in Pula. Since 2004 he has been working at the Chair of Materials Protection at the Zagreb Faculty of Mechanical Engineering and Naval Architecture. In January 2011, he earned a PhD in Mechanical Engineering Technologies with a thesis entitled "Influence of Technological Parameters on Corrosion Protection Properties of Waterborne Coatings". He was promoted to the research and teaching position of assistant professor in May 2015 and to the scientific grade of senior research associate in April 2018. In September 2020, he was promoted to the scientific grade of Associate Professor. He currently works at the Department of Welded Structures, Chair of Materials Protection, and teaches a variety of courses including Mechanisms of Corrosion Protection, Fundamentals of Technology, Robotized Welding and Surfacing, Heat Treatment and Surface Protection, Corrosion Protection in Shipbuilding and Protection by Organic Coatings. He is author and co-author of 88 scientific and professional papers in the field of corrosion and materials protection, of which 17 scientific papers in CC and SCI expanded journals. He is co-author of the university textbook Corrosion and Coatings issued by the Faculty of Mechanical Engineering and Naval Architecture in Zagreb in 2014. He is head of the international scientific research project between the Republic of Croatia and the People's Republic of China titled Self-healing Coating for Corrosion Protection Based on Microcapsules/Nano-particles for the period 2018 – 2020. He is editor-in-chief of five proceedings books of international scientific conferences, as well as programme and organizing committee member of conferences. He is editorial board member of three scientific journals and reviewer for many international and national journals, as well as for international conference proceedings. He reviewed two books. He is a certified FROSIO Inspector for Surface Treatment and Croatian Accreditation Agency expert in the inspection area corrosion and fire protection. He is Secretary of the Croatian Society for Materials Protection and its representative in the European Federation of Corrosion (EFC) and International Corrosion Council (ICC). He has been President of the Public Relations Committee of the Zagreb Faculty of Mechanical Engineering and Naval Architecture since 2014.

## **Prof. Helena Otmačić Ćurković, PhD**

Prof. Helena Otmačić Ćurković, Ph.D. graduated in 2000 at the Faculty of Chemical Engineering and Technology of the University of Zagreb. In the same year, she was employed as a research assistant at the Department of Electrochemistry of the Faculty of Chemical Engineering and Technology of the University of Zagreb and got enrolled in the postgraduate course in Chemical Engineering. She received her master's degree in 2004, with the topic of her master's thesis "Copper corrosion inhibitors in a neutral medium".

From October to December 2004, she conducted her research at the Electrochemical Laboratory (Laboratoire Interfaces et Systemes Electrochimiques) of the Pierre et Marie Curie University in Paris, France. She defended her doctoral thesis entitled "Inhibiting Action of Imidazole Derivatives on Metal Corrosion" at the Faculty of Chemical Engineering and Technology of the University of Zagreb in 2007. She was elected to the position of assistant professor in the field of technical sciences, chemical engineering in 2010, to the position of associate professor in 2017, and in 2022 to the position of full professor at the Faculty of Chemical Engineering and Technology of the University of Zagreb.

Prof. Helena Otmačić Ćurković, Ph.D. mentored 27 final and 27 graduate theses. She was also the mentor of three and commentor of four doctoral theses. She teaches several courses in the field of corrosion and metal protection at undergraduate, graduate and postgraduate studies.

Her scientific research work is related to the research of corrosion processes on metals and metal protection by using corrosion inhibitors and organic coatings. She led two research projects financed by the Croatian Science Foundation and was a collaborator on two more projects. She also led three international bilateral projects. Her scientific-research work resulted in the publication of 52 original scientific papers, two of which were published as book chapters, forty-eight original scientific papers in journals cited in tertiary databases and two papers published in journals cited in secondary databases. In addition to the above, prof. Ph.D. Helena Otmačić Ćurković had a large number of presentations at international and domestic scientific meetings. She received several awards for her work: in 2001, the Croatian Energy Institute's "Hrvoje Požar" award, for the best graduate thesis in the field of energy, in 2004, the "Society of University Teachers and Other Scientists in Zagreb" award to young scientists and artists, in 2005 Award to young chemical engineer of the Croatian Society of Chemical Engineers and Technologists, and in 2010 the Award to the young scientist "Vera Johanides" awarded by the Croatian Academy of Technical Sciences.

## **Zahvala**

---

*Zahvaljujem mentorima izv. prof. dr. sc. Ivanu Stojanoviću i prof. dr. sc. Heleni Otmačić Ćurković na stručnom vodstvu, savjetima i podršci tijekom izrade rada.*

*Zahvaljujem članovima Povjerenstva prof. dr. sc. Mariji Vuković Domanovac, prof. dr. sc. Sanji Martinez i prof. dr. sc. Vesni Alar na korisnim prijedlozima i raspravama.*

*Veliko hvala svim kolegama Katedre za zaštitu materijala, Fakulteta strojarstva i brodogradnje, na prijateljstvu, podršci i ugodnoj radnoj atmosferi. Posebno hvala prof. dr. sc. Vesni Alar na korisnim savjetima, spremnosti za objašnjavanje i prenošenju znanja koji su mi omogućili pisanje ovog rada. Hvala i dr. sc. Marinu Kurteli na vrlo ugodnim diskusijama, izmjenama ideja, razmišljanja, prijedlozima i kritikama. Tehničarki Dubravki Ulaga na uvijek vedrom i nasmijanom licu i brzim ugovorenim pripremama uzoraka.*

*Zahvaljujem se djelatnicama Zavoda za kemiju Rudarsko-geološko-naftnog fakulteta na velikodušnoj podršci, prof. dr. sc. Frankici Kapor na riječima podrške i ohrabrenja, prof. dr. sc. Gordani Bilić na lijepim razgovorima i savjetima, dragoj cimi dr. sc. Gabrijeli Ljubek na spremnosti za pomoć u svakom trenutku, te tehničaru Tomislavu Škarici na stvaranju ugodne radne okoline.*

*Posebno se zahvaljujem prof. dr. sc. Mariji Vuković Domanovac na trudu i razvijanju ideje za ispitivanje antibakterijskih svojstava prevlake.*

*Veliko hvala dr. sc. Vedrani Špadi i dr. sc. Suzani Jakovljević, na brojnim interpretacijama SEM i EDS analize.*

*Dugujem zahvalnost i dr. sc. Michaeli Hrušková Hasan, na detaljnom objašnjenju i analizi uzoraka na atomskoj apsorpcijskoj spektrometriji.*

*Hvala dragoj kolegici dr. sc. Lauri Bačani na motivaciji, zajedničkim druženjima i svim ispijenim kavama kroz sve ove godine.*

*Za kraj, najveće hvala obitelji na bezuvjetnoj ljubavi, koja mi je uvijek bila velika potpora u trenucima uspjeha i izazova, kroz svaki uspon i pad.*

*Ovaj doktorski rad izrađen je u sklopu provedbe projekta KK. 01.1.1.07.0045 pod nazivom „Razvoj sustava antikoroziivne zaštite za višenamjensku uporabu cijevi“ koji financira Europski fond za regionalni razvoj čija je voditeljica prof. Vesna Alar.*

*This doctoral thesis was prepared as part of the realization of the project KK. 01.1.1.07.0045 entitled „Development of anti-corrosion protection system for multipurpose pipe use”, which is financed by the European Fund for Regional Development under the of prof. Vesna Alar, PhD.*

## *Abstract*

---

One of the leading issues in industry and municipal infrastructure is the occurrence of corrosion damage, which poses a serious challenge due to its ability to cause significant financial losses and operational disruptions. This process not only reduces the lifespan of metal structures but also increases the costs of maintenance, repairs, and replacements, thereby directly impacting on the economic sustainability of projects. In response to this challenge, various surface protection methods have been developed that are based on isolating the metal surface from the aggressive environment through protective layers, which can be in the form of coatings, linings, or surface treatments.

This work focuses on corrosion protection of underground pipes, which are particularly exposed to aggressive conditions such as seawater and wastewater, microbiological environments, high humidity, and cyclic temperature changes. For this purpose, a multi-layer coating system made from chemically inert high-molecular polymeric materials containing epoxy groups is commonly used. Over the time, damage occurs to the epoxy coating, leading to the formation of micropores, microcracks, and swelling, making it necessary to further modify such organic coatings to extend the lifespan of the protection they provide.

To expand existing knowledge, this doctoral thesis investigates an active nanocomposite coating for the corrosion protection of drainage pipes. The examined system includes an epoxy matrix and fillers in the form of metal nanoparticles, whose role is to improve the coating's corrosion and microbiological resistance.

The experimental work is based on a series of input variables, which include the testing of different types and concentrations of metal nanoparticles, methods of their incorporation into the epoxy coating, and the interaction between the nanoparticles and the epoxy paint or pure epoxy resin. The effectiveness of the developed coatings was tested on a grey cast iron substrate. The addition of nanoparticles improved some of the key properties of the epoxy coating. The structural and morphological characteristics of the nanoparticles, unmodified epoxy coating, and nanocomposite coatings were determined using scanning electron microscopy (SEM) and energy-dispersive X-ray spectroscopy (EDS). Based on the tested physical properties, it was found that the addition of nanoparticles improves one of the most critical parameters for coating durability, namely, the adhesion of the coating to the metal surface. Special attention was given to enhancing the anticorrosion and antibacterial properties of the modified coatings. For this purpose, three types of metal nanoparticles were used: aluminum, silver, and nickel. By using

the electrochemical impedance spectroscopy, it was found that the nanocomposite coating containing 1% silver nanoparticles exhibits the best anticorrosive properties, followed by the nanocomposite coatings with nickel and aluminum. Additionally, the antibacterial properties of the epoxy coating and nanocomposite coatings were determined, revealing that the nanocomposite coatings with aluminum and silver yielded the best results, while the nanocomposite coating with nickel had minimal antibacterial activity. The nanocomposite with 1% aluminum nanoparticles showed significant migration, while the nanocomposites with silver and nickel nanoparticles exhibited the lowest migration values from the epoxy coating into wastewater. The amount of migrated aluminum nanoparticles initially increased gradually but reached a constant concentration of aluminum (1 mg/L) after 10 days of exposure to wastewater. The surface of the nanocomposite coating with 1% aluminum nanoparticles was analyzed by using the scanning electrochemical microscopy, and it was found that only these nanoparticles were capable of forming a passive oxide film on their surface, thus preventing the degradation of the coating. Therefore, samples modified with aluminum nanoparticles were tested in accelerated corrosion tests, including salt spray tests, high humidity conditions, and in a climate chamber.

Based on the conducted research, a nanocomposite coating containing aluminum nanoparticles was developed. These nanoparticles can migrate and oxidize in the event of corrosion or bacterial attack, thereby improving the corrosion and microbiological stability of the epoxy coating, with potential commercialization that could ultimately contribute to a longer lifespan of buried pipes.

**Keywords:** antibacterial action, anticorrosive action, corrosion, epoxy coating, migration, nanoparticles

## *Prošireni sažetak*

---

Jedan od vodećih problema u industriji i komunalnoj infrastrukturi je pojava korozijskog oštećenja koje predstavlja ozbiljan izazov jer uzrokuje velike financijske gubitke i prekide u radu. Ovaj proces ne samo da smanjuje vijek trajanja metalnih konstrukcija, već i povećava troškove održavanja, popravaka i zamjene, čime direktno utječe na ekonomsku održivost projekata. Kao odgovor na ovaj izazov, razvile su se različite metode površinske zaštite koje se baziraju na odvajanju površine metala od agresivne okoline pomoću zaštitnih slojeva, koji mogu biti u obliku prevlaka, obloga ili tretmana površine.

U fokusu ovog rada je korozijska zaštita podzemnih cijevi koje su posebno izložene agresivnim uvjetima, poput morske i otpadne vode, mikrobiološke atmosfere, visoke vlage, te cikličkih promjena temperature. U tu svrhu uobičajeno se koristi višeslojni sustav prevlaka napravljen od kemijskih inertnih visokomolekulskih polimernih materijala koji sadrže epoksidne skupine. Tijekom vremena eksploatacije dolazi do oštećenja epoksidne prevlake i nastanka mikropora, mikropukotina i bubrenja, zbog čega je potrebno dodatno modificirati takvu organsku prevlaku kako bi se produljio vijek zaštite koju pruža.

U cilju proširenja dosadašnjih saznanja, u ovom doktorskom radu istraživana je aktivna nanokompozitna prevlaka za zaštitu odvodnih cijevi od korozije. Ispitivani sustav uključuje epoksidnu matricu i punila u obliku metalnih nanočestica čija je uloga poboljšanje korozijske i mikrobiološke otpornosti prevlake

Eksperimentalni rad počiva na nizu ulaznih varijabli koje podrazumijevaju ispitivanje različitih vrsta i koncentracija metalnih nanočestica, te metode njihove ugradnje unutar epoksidne prevlake, kao i međudjelovanje između nanočestica i epoksidne boje ili čiste epoksidne smole. Učinkovitost zaštite razvijenih prevlaka ispitana je na podlozi od sivog lijeva. Dodavanje nanočestica poboljšalo je neka od ključnih svojstava epoksidne prevlake. Strukturne i morfološke karakteristike nanočestica, nemodificirane epoksidne prevlake i nanokompozitnih prevlaka određene su primjenom pretražne elektronske mikroskopije (SEM) i disperzivne rendgenske spektroskopije (EDS). Na temelju ispitanih fizikalnih svojstava, utvrđeno je da s dodatkom nanočestica poboljšava se jedan od najvažnijih parametara za trajnost prevlake, tj. povećava se prionjivost prevlake uz metalnu površinu. Posebna pozornost posvećena je poboljšanju antikorozivskih i antibakterijskih svojstava modificiranih prevlaka. U tu svrhu korištene su tri vrste metalnih nanočestica: aluminij, srebro i nikal. Pomoću elektrokemijske impedancijske spektroskopije, utvrđeno je da nanokompozitna prevlaka koja sadrži 1%

nanočestica srebra pokazuje najbolja antikorozivna svojstva, nakon čega slijedne nanokompozitne prevlake s niklom i aluminijem. Osim toga, određena su i antibakterijska svojstva epoksidne prevlake i nanokompozitnih prevlaka, te je ustanovljeno da nanokompozitna prevlaka s aluminijem i srebrom daju najbolje rezultate, dok nanokompozitna prevlaka s niklom ima vrlo malo antibakterijsko djelovanje. Nanokompozit s 1% aluminijevih nanočestica pokazao je značajnu migraciju, dok su nanokompoziti s nanočesticama srebra i nikla pokazali najmanju vrijednost migracije iz epoksidnog premaza u otpadnu vodu. Količina migriranih nanočestica aluminijska u početku je postupno rasla, ali nakon 10 dana izloženosti u otpadnoj vodi poprimila je konstantnu vrijednost koncentracije aluminijska (1 mg/L). Pomoću pretražne elektrokemijske mikroskopije analizirana je površina nanokompozitne prevlake s 1% aluminijevih nanočestica, te je ustanovljeno da su jedino ove nanočestice bile sposobne stvoriti pasivni oksidni film na svojoj površini i na taj način spriječiti degradaciju prevlake. Stoga su uzorci modificirani aluminijevim nanočesticama ispitani u ubrzanim korozivnim testovima, uključujući ispitivanja u slanoj magli, uvjetima visoke vlažnosti i u klima komori.

Na temelju provedenih istraživanja razvijena je nanokompozitna prevlaka koja sadrži nanočestice aluminijska, koje mogu migrirati i oksidirati u slučaju korozivnog i bakterijskog napada i tako poboljšati korozivnu i mikrobiološku stabilnost epoksidne prevlake, a čija bi potencijalna komercijalizacija u konačnici mogla pridonijeti dužem životnom vijeku ukopanih cijevi.

**Ključne riječi:** antibakterijsko djelovanje, antikorozijsko djelovanje, korozija, epoksidna prevlaka, migracija, nanočestice



## Nomenclature

### Abbreviations

AC	alternating current
Ag NP	silver nanoparticles
Al NP	aluminium nanoparticle
<i>B. subtilis</i>	<i>Bacillus subtilis</i>
CPE	coating protection efficiency
DC	direct current
DIN EN	Deutsches Institut für Normung, European Norm
DSC	Differential Scanning Calorimetry
EDX/EDS	Energy-dispersive X-ray spectroscopy
EIS	Electrochemical impedance spectroscopy
FB mode	feed back mode
ISO	International Standardization Organization
ic-ac	intermittent contact – alternating current
MIC	Microbiologically influenced corrosion
Ni NP	nickel nanoparticles
NP	nanoparticles
<i>P. aeruginosa</i>	<i>Pseudomonas aeruginosa</i>
ROS	reactive oxygen species
SECM	Scanning Electrochemical Microscopy
SEM	Scanning electron microscope
SG/TC	substrate generation/tip collection

TGA	Thermogravimetric analysis
TG/SC	tip generator/sample collector
UME	UltraMicroElectrode

### Variables

$C_{\text{coat}}$	capacitance of the coating
CFU	colony forming unit, CFU/mL
CPE	Constant Phase Element, $Ss^n$
EOC	Open circuit potential, V
$R_{\text{coat}}$	coating resistance, $\Omega$
$R_e$	electrolyte resistance, $\Omega$
$R_{\text{ct}}$	charge transfer resistance, $\Omega$
$n$	constant describing non-ideal capacitive behaviour (0–1)
$T_g$	glass transition temperature, $^{\circ}\text{C}$
$\Delta m$	mass loss, %
wt. %	weight percentage

### Subscripts

coat	coating
dl	double layer
ct	charge transfer
g	glass transition

## List of tables

Table 1. Investment in the renovation and development of water supply system in Croatia and the city of Zagreb in the period from 2019 to 2023 [25–29].....	6
Table 2. Classification of nanomaterials [68, 69]. .....	18
Table 3. Review of publications from 2016 to 2024 on “antibacterial and anticorrosion nanocomposite epoxy coating” in Web of Science database. ....	20
Table 4. Modifications of epoxy coatings (EP) with nanoparticles. ....	21
Table 5. Methods for preparation of epoxy nanocomposite coatings. ....	23
Table 6. Data resulted for measured $R_{\text{coat}}$ values and calculated $C_{\text{coat}}$ values for the samples immediately after of immersion in a tap water. ....	56
Table 7. Results of thermal decomposition parameters of epoxy paint nanocomposite with 0.5%, 0.75% and 1% of Al NPs. ....	59
Table 8. Measured $R_{\text{coat}}$ values and calculated $C_{\text{coat}}$ and $\Phi_t$ values for the samples made of epoxy resin in a tap water. ....	61
Table 9. Measured $R_{\text{coat}}$ values and calculated $C_{\text{coat}}$ and $\Phi_t$ values for the samples made of epoxy paint in a tap water. ....	62
Table 10. Summary of individual contributions for presented articles (Article 1, Article 2, Article 3, and Article 4) with united scientific contribution for doctoral thesis as a whole. ...	62

## List of figures

Figure 1. Data from newspapers on burst pipes in Zagreb in the period from 2019 to 2023 [31]. .....	7
Figure 2. Amounts of discharged municipal wastewater expressed in m <sup>3</sup> /year in the Republic of Croatia and the City of Zagreb for the period from 2019 to 2022 [33–36]. .....	7
Figure 3. Closer view of pipe wall in cross section; arrows point to corrosive attack at inner and outer surfaces. Reprinted from ref. [21]. .....	9
Figure 4. Graphitic corrosion of grey cast iron in pipeline. ....	10
Figure 5. Extracellular electron transfer MIC occurs when outermembrane cytochromes scavenge electrons from a surface via (a) direct contact, (b) conductive pili or (c) delivery through soluble electron shuttles. Metabolite MIC occurs when corrosive bacterial metabolic products or their derivatives degrade a surface (d). Reprinted from ref. [54]. .....	13
Figure 6. Steel substrate immersed in (a) sterile medium and (b) in bacterium, <i>P. aeruginosa</i> inoculated medium for 28 days after exposing to environment. Reprinted from ref. [58]. ....	15
Figure 7. Organic coating components. ....	16
Figure 8. The number of publications during 2015 to 2024 on “nanoparticles in epoxy coating and corrosion” in Web of Science search database [74]. .....	20
Figure 9. (a) The damage mechanism in steel coated by epoxy and epoxy filled with micro/nano Al <sub>2</sub> O <sub>3</sub> particles after being subjected to tensile loading. The barrier properties of steel coated by epoxy and epoxy filled with micro/nano Al <sub>2</sub> O <sub>3</sub> particles when immersed in (b) 3.5 wt% NaCl and (c) citric acid solution [96]. .....	25
Figure 10. Schematic illustration of the corrosion inhibition mechanism of zinc fibres in the epoxy coating [98]. .....	26
Figure 11. Schematic of the modified SiO <sub>2</sub> dispersion influence on the barrier properties of coating (a) pure coating (b) small amount of SiO <sub>2</sub> (c) appropriate amount of SiO <sub>2</sub> and (d) excess SiO <sub>2</sub> [100]. .....	28
Figure 12. (a) The antibacterial mechanisms of nanoparticles. (b) Antibacterial activities of Al <sub>2</sub> O <sub>3</sub> nanoparticles against <i>E. coli</i> , <i>S. aureus</i> , and <i>S. mutans</i> . Antimicrobial activities of TiO <sub>2</sub> -APTES nanohybrid coatings against <i>S. aureus</i> [104, 106, 107]. .....	29
Figure 13. SECM device with marked display of all components (type Biologic M470). .....	30
Figure 14. Schemes of (a) positive feedback, (b) negative feedback, (c, d) generation-collection (G/C) modes of SECM [111]. .....	31
Figure 15. ac- SECM measurement above a non-conducting surface. ....	32

Figure 16. SECM topographic images of a scratched (a) neat epoxy coating and epoxy coating with ZrO <sub>2</sub> , TiO <sub>2</sub> , Mg, and CeO <sub>2</sub> nanoparticles coated carbon steel, after 8 hours in 3.5% NaCl. SECM and SEM image of (b) a neat epoxy coating and coating with Si nanoparticles after 8h in 0.1 M NaCl solution. SECM image of the organic coating with a defect (c) the image with a size of 500×500 μm corresponding to an immersion time of 1 and 48 h [115 –119].	33
Figure 17. 3D laser microscopy micrograph of the scratched test area (a) and the self-healed scratch (b) on the epoxy resin coating. AC-SECM image of (c, d) self-healing coating surface immersed in a solution of 0.6 M NaCl. DC potential: 0 V. Amplitude of the AC potential signal: 10 mV, and different range of frequency [121].	35
Figure 18. The Nyquist and Bode plots for nanocomposite with (a,b) 0.5%, 1%, 1.5% Ag NPs, and (c,d) 1%, 2%, 3% Ni NPs after 24 h in 3.5 wt. % NaCl solution.	38
Figure 19. Pourbaix diagram for: (a) silver, (b) nickel, (c, d) aluminium in Cl – H <sub>2</sub> O system at 25 °C [128,129,130].	42
Figure 20. (a) Nyquist and (b) Bode plots for 1% Al NP nanocomposite exposed to 3.5% NaCl solution for 1, 5, 10 and 20 days.	51
Figure 21. (a) Combined color map of the segment on the oxidized Al NP surface captured using the SEM/EDS method at 6 000x magnification. Partial color maps showing the distribution of individual chemical elements on the oxidized Al NP surface, captured using the SEM/EDS method at 6,000x magnification: b) aluminum (Al) and c) oxygen (O).	52
Figure 22. SEM image of the surface of (a) Al NPs and (b) oxidized Al NPs powder at a magnification of 10 000x.	53
Figure 23. Results of EDS analysis with partial staining of the distribution of aluminium particles on the cross-sectional surface for a sample of 1% Al NP epoxy nanocomposite prepared by (a) mechanical mixing and (b) ultrasonic homogenizer.	55

## *Contents*

---

1. INTRODUCTION.....	1
2. LITERATURE REVIEW.....	4
2.1. Corrosion and its impact on pipelines.....	4
2.2. Grey cast iron.....	4
2.3. Pipeline corrosion.....	5
2.3.1 Frequency and consequences of pipeline failure in the Zagreb.....	5
2.3.2. Degradation process for wastewater pipeline.....	8
2.3.3. Chemical factors.....	10
2.3.4. Physical factors.....	11
2.3.5. Biological factors.....	12
2.4. Pipe surface protection.....	15
2.4.1. Protective coatings.....	16
2.5. Application of nanotechnology in organic coatings.....	17
2.5.1. Modification of the epoxy coating with nanoparticles.....	19
2.5.2. Preparation of epoxy nanocomposite coating.....	23
2.5.3. Effect of nanoparticles on the barrier properties of epoxy coating.....	24
2.5.4. Corrosion inhibition by metal nanoparticles in epoxy coating.....	26
2.5.5. Labyrinth effect of nanoparticles in epoxy coating.....	27
2.5.6. Antibacterial effect of nanoparticles in epoxy coating.....	28
2.6. New approaches in characterization of nanoparticles in epoxy coating.....	29
2.6.1. Introduction to SECM.....	29
2.6.2. dc – SECM analysis of epoxy coating.....	32
2.6.3. ac- SECM analysis of epoxy coating.....	34
3. DISCUSSION.....	36
4. CONCLUSIONS.....	65
5. BIBLIOGRAPHY.....	69
6. ORIGINAL SCIENTIFIC PAPERS.....	84
Article 1.....	84
Article 2.....	100
Article 3.....	118
Article 4.....	136

6. BIOGRAPHY OF THE AUTHOR ..... 152

# 1. INTRODUCTION

Grey cast iron is the most common material used for drainage pipes for the distribution of wastewater because of the low cost, ease of fabrication, adequate corrosion resistance and availability. This material also has many other applications such as for pumps, valve bodies, engines, decorations, and it is very important in many industries such as automotive and petrochemical industries.

Pipeline corrosion is a complex process because different chemical, physical and biological factors can affect pipeline damage. Cast irons are resistant to uniform corrosion due to their microstructure, building components (graphite and phosphate eutectic), and due to the resistant and compact surface formed by cooling after casting [1]. However, plumbing systems are exposed to aggressive atmospheric or soil environments for decades or even centuries, making them susceptible to corrosion. It is commonly held that in this form of corrosion attack, the ferric ion content of the surface layers is leached out during the corrosion process, leaving behind a porous residue consisting of a graphite matrix. This form of corrosion is called graphitic or selective corrosion. Graphitic corrosion on the inner side of pipelines occurs due to aggressive components present in the media flowing through the pipe. This is one of the leading problems of the city of Zagreb. According to information from the media, about 10,000 breakdowns in the water supply network occur in the city of Zagreb every year, which means that problems occur in 20 to 30 places every day. The renovation of the water supply and drainage pipes of a metropolis, of 641 km<sup>2</sup>, would amount to around 265 million euros. In addition to different physical causes, corrosion is one of the main factors leading to pipe failure. More recently, research has shown that the corrosion process can be stimulated with bacteria found in wastewater. Corrosion of a material when the presence of microorganisms plays a role is known as the microbiologically influenced corrosion (MIC). Examples of corrosion-related microorganisms are *Sulphate reducing bacteria*, *Pseudomonas aeruginosa*, *Escherichia coli*, *Salmonella*, *Bacillus subtilis* and similar. Over the past decades, MIC has attracted wide interest to investigate and control the problem [2]. The influence of microorganisms on cast iron has not yet been fully explained [3] and, therefore, there are several theories describing the interaction between bacteria and metal. The mechanisms of action of bacteria and carbon steel were described in detail by the authors Blackwood [4] and Lv and co-authors [5]. In their work, they explained the cathodic depolarization theory and the extracellular electron transfer, as well as microbiologically stimulated corrosion caused by microbial products.



In order to extend the life of distribution pipes, a surface protection made of a multi-layer coating system is used. The epoxy coating proved to be a good solution due to its good protective barrier properties, high adhesion, easy application and low cost [6]. During the exploitation process, the epoxy coating is gradually damaged and the formation of micropores, microcracks, and swelling occurs, and therefore it is necessary to additionally modify such organic coating to extend the life of the protection it provides [7]. Likewise, epoxy coatings are not resistant to bacterial attacks because they do not possess antibacterial properties.

Development of a new generation of coatings that will have both anti-corrosion and antibacterial properties is enhanced by using nanotechnology. Nanotechnology today has branched out in a large number of different areas of sciences because of its significant benefits in terms of improving the performance in many fields [8]. It also provides new tools to combat corrosion attacks caused by aggressive components or bacterial action, showing a great potential in surface transformation. Advanced materials using nanotechnology may extend service life, reduce failure rates, limit the potential for environmental damage and enhanced corrosion protection [9].

Due to all the reasons mentioned, the objectives of the proposed work are as follows:

- to develop an active nanocomposite system with anticorrosion and antibacterial properties for the protection of drainage pipes.
- to investigate the influence of different types of nanoparticles (Al, Ni, and Ag) on the growth of bacteria and behaviour of the prepared nanocomposite system under corrosion conditions and conditions of microbiologically induced corrosion.
- to select a nanocomposite system that meets corrosion and bacterial resistance requirements and to evaluate the influence of the concentration and method of nanocomposite preparation on its protective properties in accelerated corrosion conditions.

Research hypothesis of this work is:

By adding nanoparticles to the epoxy coating, it is possible to increase the resistance to electrochemical corrosion and improve the antibacterial properties of the coating.

The research hypothesis is confirmed by four scientific papers focusing on different aspects of development and characterization of an active nanocomposite system with anticorrosion and antibacterial properties for the protection of drainage pipes:

**Paper 1:** M. Samardžija, I. Stojanović, M. Vuković Domanovac, V. Alar, V. Epoxy Coating Modification with Metal Nanoparticles to Improve the Anticorrosion, Migration, and Antibacterial Properties, *Coatings*, 13 (2023), 1201.

**Paper 2:** M. Samardžija, V. Alar, V. Špada, I. Stojanović, Corrosion Behaviour of an Epoxy Resin Reinforced with Aluminium Nanoparticles, *Coatings*, 12 (2022), 1500.

**Paper 3:** M. Samardžija, M. Kurtela, M. Vuković Domanovac, V. Alar, Anticorrosion and Antibacterial Properties of Al NP–Epoxy Nanocomposite Coating on Grey Cast Iron, *Coatings*, 13 (2023), 898.

**Paper 4:** M. Samardžija, I. Stojanović, M. Kurtela, V. Alar, Influence of aluminum nanoparticles in epoxy resin and epoxy coating for anticorrosion and antibacterial protection in pipeline industry, *J. Appl. Polym.*, 141 (2023), 1–14.

## **2. LITERATURE REVIEW**

### **2.1. Corrosion and its impact on pipelines**

Corrosion is a process that results in an irreversible damage of the surface of materials (metal, ceramic, and polymer) due to chemical, physical, and biological factors [10,11]. All materials can corrode, but research on metal corrosion is of great economic importance because it shortens the life of metal products, leading to significant financial losses and posing risks to both people and the environment [12]. For this reason, extensive research is conducted with the aim to better understand corrosion processes and to find new or improve existing methods of corrosion protection, that will extend the lifetime of metal structures.

Iron-based metals are the most widely used as construction materials for pipelines. Pipes are connected and placed in the concrete in buildings or in the ground to transport various products, either a few meters or cross-country to the location of use [13]. In water distribution systems, metal constructions are typically made of cast iron. The commercial development of cast iron pipes and their application to water transmission and distribution resulted in a significant improvement in public health [14].

### **2.2. Grey cast iron**

Grey cast iron is a broad term used for a number of cast irons whose microstructure is characterized by the presence of flake graphite in the ferrous matrix [15]. Most cast irons have chemical composition of 2.5 to 4.0% carbon, 1.0 to 3.0% silicon, and the remainder is iron [16]. The composition of grey iron must be selected in such a way as to satisfy three basic structural requirements[17]:

1. the required graphite shape and distribution,
2. the carbide-free (chill-free) structure,
3. the required matrix.

Grey cast iron has been widely used in pipes serving as water mains due to unique characteristics that include a combination of good mechanical and thermal properties, good friction and wear characteristics, relatively low melting temperature, excellent castability, and economical production processes [18–20]. Cast irons are resistant to uniform corrosion due to

their microstructure, component compounds (graphite and phosphate eutectic), and due to the resistant compact surface formed by cooling after casting [1]. Even after many years of operation, much of the cast iron infrastructure still remains in a satisfactory condition for continued use, however there is an increasing risk of failure of these pipes due to corrosion loss of material [21].

### **2.3. Pipeline corrosion**

A pipeline can be defined as a continuous, long, tubular structure used to transport significant amounts of liquid or liquefied materials and gases over long distances [22]. Pipeline defects can be classified as [22]:

1. built-in defects (construction of the pipeline),
2. long-term defects (bad realization of joints, corrosion, erosion) and
3. one-time events (terrorist activity, earthquakes, landslides).

Fluids inside the pipeline can lead to a reduction in its structural integrity and eventual failure [23]. Generally, fluid transfer pipelines can be categorized into different groups including [12]:

1. oil and gas (crude oil, natural gas, and products obtained from oil refinement),
2. clean water and wastewater (aqueduct and sewage), industrial material (ammonia, hydrogen, carbon dioxide, etc.),
3. pipeline transport fluids on small scale (beer, biofuel, etc.).

#### **2.3.1 Frequency and consequences of pipeline failure in the Zagreb**

One of the leading problems of the city of Zagreb (area 641 km<sup>2</sup>) is the deterioration and damage to water transport pipes. Zagreb's water supply network is 3,230 kilometres long and supplies water to more than 750,000 inhabitants. The water supply area covers the cities of Zagreb, Samobor, Sveta Nedjelja and the municipality of Stupnik, and it is being repaired and renovated every day. [24]. Two key reasons for the frequent pipe bursts are long-lasting pipes and insufficient investment in underground infrastructure. Table 1 shows all investments in drainage pipes in the last 5 years at the level of the whole of Croatia and in the city of Zagreb. These investments in underground infrastructure include:

1. construction of transport pipelines,
2. rehabilitation of pipelines and networks with cracks in the water supply system,
3. reconstruction of the water supply network.

Table 1. Investment in the renovation and development of water supply system in Croatia and the city of Zagreb in the period from 2019 to 2023 [25–29].

<b>Year</b>	<b>2019.</b>	<b>2020.</b>	<b>2021.</b>	<b>2022.</b>	<b>2023.</b>
Investment in the water supply system in Croatia, EUR	24.644.236	35.610.325	37.044.793	37.415.356	50.824.502
Investment in the water supply zones of the city of Zagreb, EUR	729.975	982.148	530.891	2.421.660	-
%	2.96	2.75	1.43	6.47	-

In addition to financial expenses caused by burst pipes, the consequences may include floods, large loss of water, damage to property, an increase in the price of water for citizens, and similar.

The frequency of bursting of water pipes in the city of Zagreb in a period of 5 years is shown in Figure 1. The graph indicates that the most significant damage to the water supply occurred in 2022, with 30 cases of burst pipes that caused floods. This statement is also confirmed by Table 1, which shows that in 2020, 6.47% of funds were allocated to Zagreb, from the total budget for the whole of Croatia, for investment in the renovation of a section of the water supply network. Likewise, Figure 1 shows the distribution of pipe bursts by month, and no significant difference was observed between seasons. The reason for this is that in the past five years, there were no extremely low temperatures that could freeze the water in the pipes, which can cause the pipe wall to expand and burst. In general, as a result of hot and cold temperatures, pipes endure dimensional changes due to the expansion and contraction of the material. These dimensional changes create increased axial loads in the pipe which can result in cracking [30].

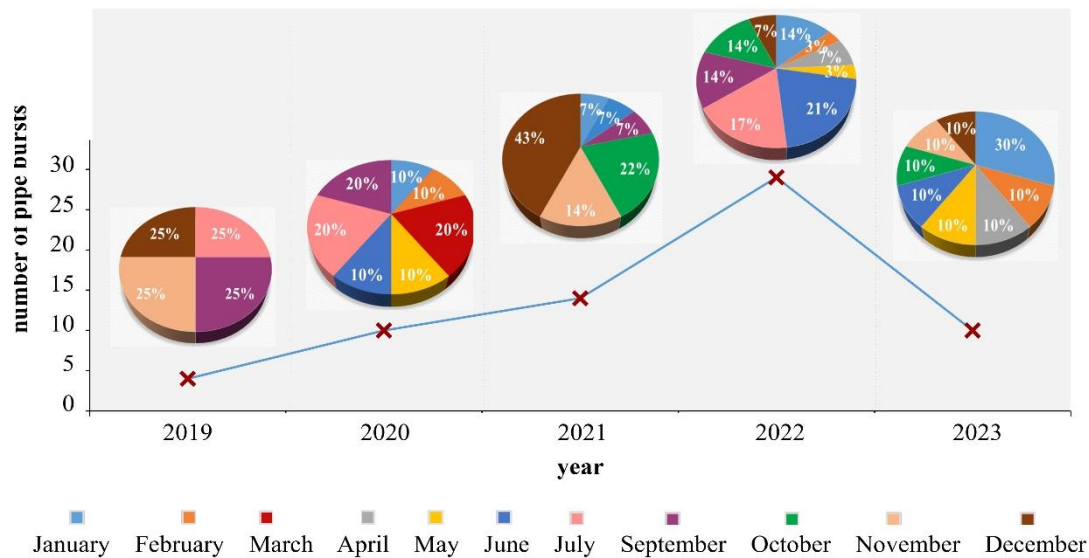


Figure 1. Data from newspapers on burst pipes in Zagreb in the period from 2019 to 2023 [31].

One of the major global problems linked to industrial development and population growth is the increasing amount of environmental pollution and wastewater produced from domestic activities, industry, and stormwater outflows [32]. In Republic of Croatia, approximately 350 million m<sup>3</sup> wastewater are produced every year, while in City of Zagreb is about 173 million m<sup>3</sup> wastewater (Figure 2). This problem has raised great concern due to its potentially dangerous effects. Drainage systems are heavily loaded, leading to exposure to harsh environmental conditions that accelerate degradation of pipelines.

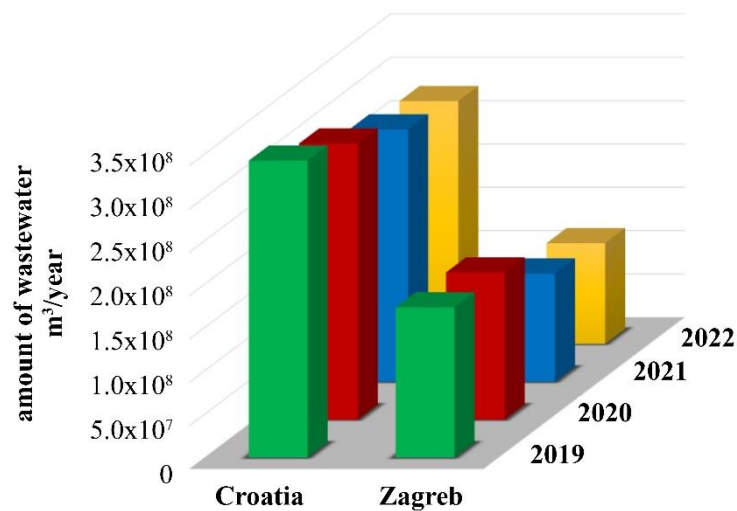


Figure 2. Amounts of discharged municipal wastewater expressed in m<sup>3</sup>/year in the Republic of Croatia and the City of Zagreb for the period from 2019 to 2022 [33–36].

Corrosion is one of the leading causes of failures in onshore transmission pipelines (wastewater) in Zagreb (Croatia). Corrosion that occurs as a result of the age of the pipeline system, which is more than 50 years old. Pipeline cracking can also be the result of a number of influencing parameters, such as: method and quality of installation, internal and external load, damage to the pipeline during construction works, environmental conditions in which the pipe is located, and similar. Damage to pipelines can lead to leakage of transported material and reduction (or even ceasing) of the transport of life-sustaining supplies, with potentially disastrous humanitarian, social, economic, and ecological consequences. Generally, the consequences of a pipeline break include:

1. direct costs (cost of repair, cost of water loss, cost of damage to surrounding infrastructure and property, liabilities),
2. indirect costs (cost of supply interruption, cost of potentially increased deterioration rate of surrounding infrastructure and property, cost of decreased fire-fighting capacity),
3. social costs (cost of water quality degradation due to contaminant intrusion, cost of decrease in public trust and quality of water supply, cost of disruption of traffic and business, cost of disruption of water supply to special facilities).

Therefore, the assessment and monitoring of pipeline conditions are essential for early emergency response and for the mitigation of environmental hazards [22].

### **2.3.2. Degradation process for wastewater pipeline**

In terms of corrosive environments leading to infrastructure degradation, industrial and domestic wastewater has garnered substantial attention due to high toxicity [12]. The corrosive damage to pipelines often results in large scale pollution of the hydrosphere and lithosphere [37]. The precise nature of material degradation depends on various factors, including the chemistry of the water (e.g., pH, ionic composition including chloride, sulphate, phosphate, carbonate, calcium, etc.), temperature, flow rate, and the construction materials. Additionally, piping materials may react with species in water to form protective films and scales, which can reduce the rate of their degradation [38].

Study developed by Jur and co-authors [21] showed a piece of pipe with corrosive attack at both the inner and outer surfaces (Figure 3). The corroded part of the pipe remained in its

original or almost original dimension, which is characteristic of graphite corrosion and indicates that the pipe is made of cast iron.



Figure 3. Closer view of pipe wall in cross section; arrows point to corrosive attack at inner and outer surfaces. Reprinted from ref. [21].

Misiunas [39], analyzed the process of pipe deterioration. He described the life of the pipes in five steps:

1. installation of new intact pipe,
2. after the pipe has been in operation for some time, the corrosion processes start on the interior or exterior (or both) surface of the pipe,
3. formation of crack before leak,
4. the leak or burst will be initiated depending on the size of the crack,
5. the complete failure of the pipe can be caused by a crack, corrosion pit, already existing leak/burst or a third-party interference.

Most grey cast iron pipes fail because of a combination of factors that may include external loading, internal pressure, manufacturing flaws and corrosion damage. However, while the external forces and the final failure modes are understood, the mechanisms that link the application of the force to the actual failure have not been as thoroughly investigated [20]. In



the review paper of Ossai and co-authors [40] are analyzed corrosion mechanisms in oil and gas transmission pipelines, that can be caused by chemical, physical and biological factors.

### 2.3.3. Chemical factors

Generally, cast irons perform well in water environments due to the formation of a protective layer on the inside wall of the pipe, typically composed of carbonate.

However, water containing carbon dioxide in solution, acid effluents, chlorides, etc., is significantly more corrosive [41]. Graphite corrosion, a form of galvanic corrosion, occurs through electrochemical processes [21, 42]. It is commonly accepted that in this type of corrosion, the ferritic iron component in the alloy dissolves, leaving behind a porous residue consisting of graphite flakes interspersed with iron oxides and other insoluble products such as siliceous compounds and phosphide eutectic stringers [42]. Corrosion of drainage pipes made of cast iron was studied by Melchers [18]. Graphitic corrosion is shown in Figure 4.

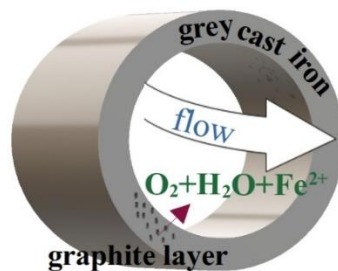


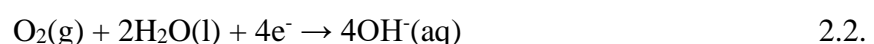
Figure 4. Graphitic corrosion of grey cast iron in pipeline.

When the ferrous iron component of the cast iron pipe wall is exposed to an electrolytic environment, two processes take place simultaneously [42, 18]:

1. the dissolution of iron at the anode:



2. the reduction of water in a neutral medium (pH=7) on residual graphite serving as a cathode:



Although no dimensional changes take place, graphitic corrosion can cause significant problems as the cast iron loses its strength and metallic properties. During graphitic corrosion, the porous graphite network, which makes up 4%–5% of the total mass of the alloy, is

impregnated with insoluble corrosion products. As a result, the cast iron retains its appearance and shape but it is structurally weaker [1].

#### **2.3.4. Physical factors**

Ossai et al. [40] and Agala et al. [44] studied pipe degradation caused by physical factors. The study by Ossai et al. divides the physical factors of corrosion into structural properties, and product properties. Agala explains these factors by using the examples of pipes made of cast iron. Comprehensive list of parameters affecting wastewater pipe performance is presented by the author Angkasuwansiri et al [31]. According to their research, the physical effects on cast iron pipes are:

##### 1. Structural properties:

a) material properties – depend on the method of preparation of cast iron and there are two influencing parameters: impact of porosity and impact of inclusions. A porous structure may be created during manufacturing, but this phenomenon is less acute in grey iron pipes, in which air can more readily escape through the inner wall of the pipe. Inclusions are unintended additions that find their way into materials. These materials then cause stress concentrations, decrease the cross-sectional area of the pipe, and result in crack formations.

b) design factors – poor installation can result in inadequate bedding and/or possible damage to the pipe itself. If too long a pipe is installed, it can lead to increased stresses as a result of differential ground movement transverse to the pipe axis. A pipeline that is not properly supported can suffer beam stresses.

##### 2. Product properties:

a) temperature gradient – causes stresses and cracks can form which can result in leaks.

b) pressure – results in hoop or tensile stress acting on pipes. When tensile stress passes a given threshold, it results in longitudinal cracks appearing on the pipe wall, while axial stress can lead to circumferential cracking.

c) flow rate – excessive velocities lead to mechanical surface wear and greater levels of corrosion as results of higher oxygen levels.

Of all the parameters mentioned, fluid velocity plays a significant role in pipe corrosion [44]. Along the wall of the pipe, there is a small laminar layer of media which allows incubation of bacteria. On the other hand, high fluid flow velocities increase the shear stress on the pipeline wall, inhibiting cell attachment and even causing the release of already adhered cells [45]. This is a biological factor in corrosion and is described in the following chapter.

### **2.3.5. Biological factors**

Microbiologically influenced corrosion (MIC), also known as microbial induced corrosion, microbial corrosion, bacterial corrosion, bio-corrosion, was defined by Videla (1996) as “an electrochemical process in which the microorganisms are present to initiate, facilitate, and accelerate the corrosion reactions” [46, 47]. Such microorganisms can be from any of three main branches of evolutionary descent, i.e. bacteria, archaea (methanogens) and eukaryotes (fungi) [48]. While all three groups can contribute to MIC, bacteria receive the most attention regarding their influence on corrosion processes.

Municipal wastewater flowing through pipes contains of multiple pathogens and non-pathogenic bacteria, organic/inorganic chemicals, suspended and dissolved compounds, which can cause corrosion, damage, reduction in the water transport capacity, and an increase in the habitat of pathogenic and opportunistic bacteria [49, 50, 5]. The microbiological community in wastewater typically consists of various types of bacteria, including: *Enterobacter cloacae*, *Enterococcus faecalis*, *Escherichia coli*, *Klebsiella pneumoniae*, *Proteus vulgaris*, *Pseudomonas aeruginosa*, *Salmonella*, *Shigella genera*, and *Escherichia coli* [31, 51]. Some of these bacteria have the ability to colonize metal surfaces in aqueous environments, initiating electrochemical reactions that lead to microbiologically induced corrosion. For instance, *Pseudomonas aeruginosa* can produce a mature biofilm in 5-7 days [52]. On a metal surface, bacteria use iron for survival and growth, leading to the metal surface underneath the biofilm becoming an anodic area due to the corrosion process induced by the bacteria using iron as an energy source. At the same time, the surface outside the biofilm, which is not directly exposed to the bacteria, acts as a cathodic area with the oxygen reduction reaction occurring in that region. This process creates an electrochemical couple that accelerates metal corrosion, further damaging its structure and integrity.

The influence of microorganisms on cast iron has not yet been fully explained and, therefore, there are several theories on interaction between bacteria and metal [3]. The mechanisms of

action of bacteria and carbon steel were described in detail by the authors Blackwood [4] and Lv et al [5]. In their work, they explained the cathodic depolarization theory and the extracellular electron transfer, as well as microbiologically stimulated corrosion caused by microbial products.

The cathodic depolarization theory is the first theory which assumes that accelerated corrosion is due to the consumption of cathodic hydrogen by sulphate-reducing bacteria and its enzyme hydrogenase [4]. However, this theory is not applicable to bacteria that do not utilize hydrogen, leading to the emergence of the theory of extracellular electron transfer. According to the literature, such bacteria are in direct contact with the metal substrate and consume electrons released by metal oxidation causing a much higher rate of corrosion. A review of consequences and accelerated corrosion by such bacteria that can be found in the literature is presented by Blackwood [4]. Maji [53] classified MIC into two basic types: (i) electrical MIC (EMIC), which triggers direct corrosion by the consumption of electrons from metals, (ii) chemical/metabolite MIC (CMIC), where the metal is indirectly affected when microbes produce corrosive metabolites. EMIC takes more attention due to extracellular electron transfer (EET). Extracellular electron transfer can occur when cytochromes scavenge electrons from a surface either via direct contact (Figure 5a), conductive pili (Figure 5b) or delivery through soluble electron shuttles (Figure 5c). Figure 5d shows metabolite MIC where surfaces are affected directly by corrosive metabolites.

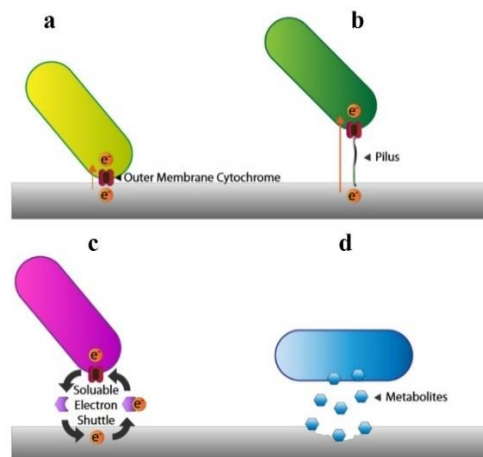


Figure 5. Extracellular electron transfer MIC occurs when outermembrane cytochromes scavenge electrons from a surface via (a) direct contact, (b) conductive pili or (c) delivery through soluble electron shuttles. Metabolite MIC occurs when corrosive bacterial metabolic products or their derivatives degrade a surface (d). Reprinted from ref. [54].

In EET bacteria use the cytochrome c protein to transport an electron from the inner membrane. Direct transmission is also possible via conductive nanowires (pili) [55].

However, there are some issues regarding the direct electron theory. From an electrochemical perspective, charge transfer in a single step at the electrode-electrolyte interface would not occur at distances greater than 2 nm, which is much less than the thickness of the cell wall which ranges from 7.5 to 10 nm. Another mechanism of direct electron transfer, via conductive pili, also raises some issues. Pili are thought to behave like microbial nanowires, using the concept of extracellular electron transfer. However, this brings up the problem of the pili's length, which is on the order of 1  $\mu\text{m}$ . For electron transfer along the entire length of the pili, some form of electronic hopping would be necessary. Even if this were possible, the question remains of how to generate the electric field required to drive this hopping process. [4].

Microbial electrochemical activity can occur via mediated electron transfer where soluble electron shuttle molecules (with examples being flavins, melanin, phenazines, and quinines) transfer electrons from the metallic substrates to the microbial cell [54]. However, the redox mediator does not have to be one of the species present in the original culture medium; it can also be a product of metabolic reactions. Additionally, if the redox mediator is continuously regenerated in a metabolic reaction, it does not need to be present in high concentrations, which makes its detection more challenging [4].

Over the time, microorganisms will begin to grow, colonize the metal surface and begin to produce extracellular polymeric substances (EPS) [56]. Strongly adhesive EPS, are mainly high molecular weight secretions of microorganisms and consist of various organic substances such as polysaccharides, proteins, nucleic acids and lipids) [56, 57]. However, some studies showed that EPS can influence on metal corrosion. In the study by Hamzah et al. [58], results of the XRD analysis of the biofilm made by *Pseudomonas aeruginosa* bacteria on a steel substrate were presented. They showed the presence of iron(III) oxyhydroxide ( $\text{FeO}(\text{OH})$ ), iron oxide ( $\text{FeO}$  and  $\text{Fe}_3\text{O}_4$ ) and magnetite ( $\text{FeO}\cdot\text{Fe}_2\text{O}_3$ ). The appearance of the metal surface in the sterile medium and in the medium with the presence of bacteria for 28 days is shown in Figure 6.

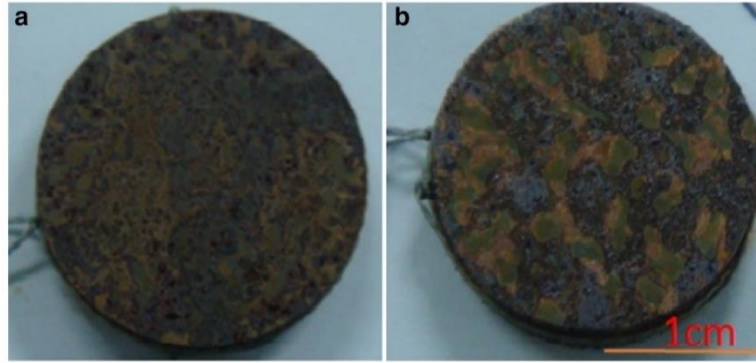


Figure 6. Steel substrate immersed in (a) sterile medium and (b) in bacterium, *P. aeruginosa* inoculated medium for 28 days after exposing to environment. Reprinted from ref. [58].

EPS are acidic and possess functional groups (hydroxyl, carboxylic, sulphate, phosphate, pyruvate, and succinate) that complex metal ions (iron ions, copper ions, etc.) and, thus, accelerate the dissolution of the anode [56, 59, 60]. The weak electrostatic interactions between EPS and metal ions have been shown to accelerate metal corrosion [61]. However, there are also studies showing that the attachment of EPS can have an inhibitory effect on the corrosion of a metal, mainly because EPS adsorb on the surface of a material and can form a protective film [60].

Microbiologically stimulated corrosion of cast iron will be accelerated due to the rough surface on which microorganisms can easily adhere and begin to develop a biofilm. For all the above reasons, the surface of cast iron needs to be protected from the influence of microbes.

#### **2.4. Pipe surface protection**

Corrosion protection methods are based on reducing or cancelling the corrosion driving force or increasing the resistance that resists the action of that driving force. There are three ways of corrosion protection:

1. by changing the construction material,
2. by changing external factors (temperature, medium, stresses, and similar),
3. separating the structural material from the media.

The third method showed the best results and widely applied [62].

### 2.4.1. Protective coatings

Coating is a general name for one or more interconnected layers on a substrate that create a dry film. In corrosion protection metallic, organic and inorganic (ceramic) coatings are used, although organic coatings are the most common. The components of an organic coating are shown in Figure 7.

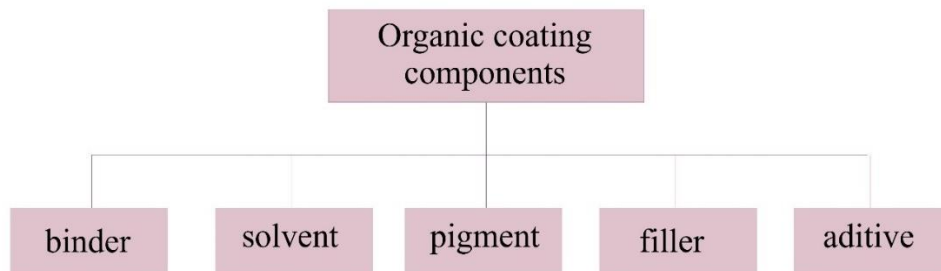


Figure 7. Organic coating components.

All organic coatings contain a binder (epoxy, alkyd, and vinyl resin, polyurethanes, cellulose derivatives and similar), which forms the membrane of the coating, and a solvent that dissolves the binder and regulates the viscosity. In addition, coating agents can contain insoluble powders (pigments and fillers) that give colours and shades and make the coating opaque, as well as various additives [62].

The most effective way to achieve good corrosion protection is to apply a multi-layered coating system. In case of waste water pipelines, epoxy coatings are used as they have good protective barrier properties, high adhesion to the metal substrate, are easy to apply, and are not expensive [6]. During the exploitation, the properties of the epoxy coating deteriorate and this leads to coating blistering and the creation of micropores and microcracks [7]. Therefore, it is necessary to improve these organic coatings to extend their durability.

Recently, with the development of nanotechnology, the term “nanocomposite” has appeared for composites with the filler with at least one dimension on the nanometre scale [63, 64]. Nanoparticles have been widely used as resin fillers to block micropores and improve the corrosion resistance and the mechanical properties of the resins due to their greater surface-to-volume proportion with respect to conventional macroscopic materials [65].

## **2.5. Application of nanotechnology in organic coatings**

Since the term “nanotechnology” was presented by Nobel laureate Richard P. Feynman during his well famous 1959 lecture “There’s Plenty of Room at the Bottom” (Feynman, 1960), there were made various revolutionary developments [66]. In this lecture, Feynman made the hypothesis “Why can’t we write the entire 24 volumes of the Encyclopedia Britannica on the head of a pin?” and described a vision of using machines to construct smaller machines and down to the molecular level [67]. Nowadays, this idea has turned nanotechnology into main scientific driver for the development of new innovations that will be translated into products on the market. It is the ability to convert the nanoscience theory to useful applications by observing, measuring, manipulating, assembling, controlling and manufacturing matter at the nanometer scale [67]. The term “nano” origins from the Greek word “nanos” that means “dwarf” or something extremely small [8]. In general, nanotechnology uses the properties of nanostructures on atoms and molecules to create new materials and structures for the needs of various scientific fields. By incorporating at least one of the new dimensions is in the nanoscale, i.e. smaller of 100 nm into the existing material, a nanostructured material is obtained that will have additional properties that it did not have before. Based on their dimensionalities, nanomaterials are placed into four different classes which are shown in Table 2.



Table 2. Classification of nanomaterials [68, 69].

nanomaterials	<b>Zero-dimensional nanomaterials</b>	<b>One-dimensional nanomaterials</b>	<b>Two-dimensional nanomaterials</b>	<b>Three-dimensional nanomaterials</b>
	(0-D)	(1-D)	(2-D)	(3-D)
	all dimensions in the nanoscale range (x, y, z)	2 dimensions in the nanoscale range (x, y)	1 dimension in the nanoscale range (x)	0 dimensions in the nanoscale range
properties	prone to physical or chemical crosslinking with polymer resins  the surface activity is high due to the lack of coordination atoms on their surfaces, so nanoparticles tend to aggregate	the ability to cross each other to form a dense layer that prevents the invasion of media  good electrical properties and better mechanical properties	interatomic interactions within the layer are much larger than those between the layers,  form a "labyrinth effect" in materials, prolonging the penetration path of the media, improving the protective effectiveness of the surface	composed of a multiple arrangement of nano size crystals in different orientations
examples	quantum dots, fullerenes, and nanoparticles	nanotubes, nanofibers, nanorods, nanowires, and nanohorns	nanosheets, nanofilms, and nanolayers	bulk powders, dispersions of nanoparticles, arrays of nanowires and nanotubes

The fundamental components of nanotechnology are nanoparticles (NP). Nanoparticles are defined as particulate dispersions or solid particles with a size in the range of 10-1000 nm [65]. There are two main factors causing nanomaterials to behave significantly differently than the

same materials of larger dimensions: surface effects and quantum effects [68]. Nanoparticles have attracted much interest because of their unique physical and chemical properties, which originate from the high area to volume ratio and elevated quantity of surface atoms [70]. The surface to volume ratio of nanoparticle is 35-45% times higher as compared to large particles [71]. In fact, as the diameter decreases, the available surface area of the particle dramatically increases, and, consequently, there is an increase in surface reactivity which is size dependent [70, 71]. This feature makes nanoparticles superior to macroparticles and exceptional candidates for use as resin fillers to block micropores and improve the corrosion resistance and the mechanical properties of coatings. Nanoparticles tend to occupy small hole defects formed from local shrinkage during curing of the epoxy resin and act as a bridge interconnecting more molecules. For instance, inorganic filler particles at nanometer scale can be dispersed within the epoxy resin matrix to form an epoxy nanocomposite. The incorporation of nanoparticles into resins offers durability to coatings, since the fine particles dispersed in coatings can fill cavities and cause crack bridging, crack deflection and crack bowing [72]. For all the above reasons, researchers began to modify coatings with nanoparticles.

### **2.5.1. Modification of the epoxy coating with nanoparticles**

Nanocomposite coatings, which involve adding inorganic nanofillers to a polymer matrix, represent a new class of corrosion protection methods that exhibit superior corrosion resistance and mechanical performance compared to conventional composite coatings [73]. Various studies have reported that the mechanical, thermal, anticorrosion, antibacterial, and physicochemical properties of epoxy coating can be improved through addition of nanoparticles and thus developing nanocomposites. Pourhashem et al. [73], presented a diagram illustrating publications on "anti-corrosion nanocomposite polymer coatings" in the period from 2002 to 2019, revealing growing trend in the research of nanocomposites for protecting metal structures from corrosion. Additionally, the number of publications on nanoparticles in epoxy coatings for use as anti-corrosion protection for the period from 2015 to 2024 is shown in Figure 8.

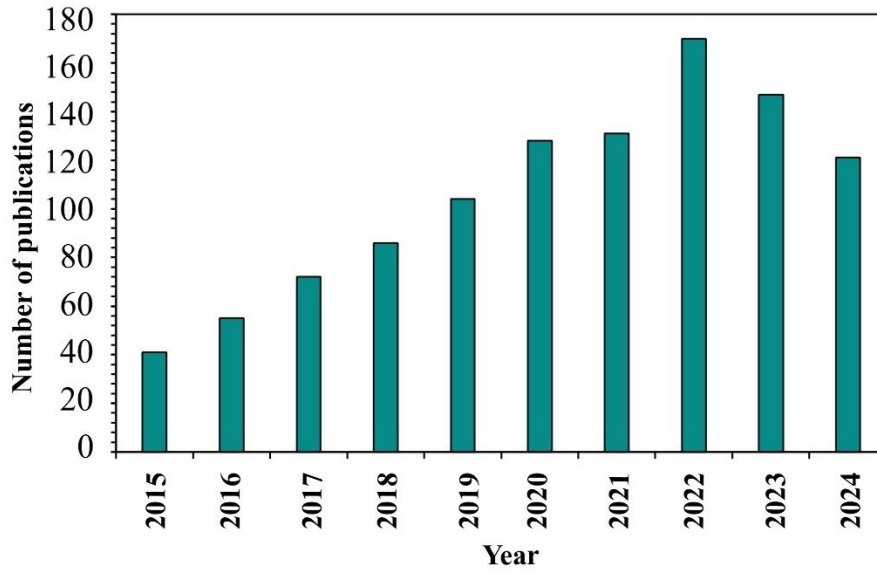


Figure 8. The number of publications during 2015 to 2024 on “nanoparticles in epoxy coating and corrosion” in Web of Science search database [74].

Figure 8 shows the growth trend of the number of publications on nanoparticles in epoxy coatings and corrosion, with a gradual increase in the number of published papers until 2022, after which a slight decline is recorded. To further narrow down this search and focus on works that specifically explore epoxy coatings with nanoparticles providing both anticorrosive and antibacterial properties, we can refer to the data presented in Table 3.

Table 3. Review of publications from 2016 to 2024 on “antibacterial and anticorrosion nanocomposite epoxy coating” in Web of Science database.

Year	2016	2018	2019	2020	2021	2022	2023	2024
Number of publications	1	1	3	4	6	2	7	3

The idea of developing a nanocomposite epoxy coating with anticorrosive and antibacterial properties began in 2016 with the work of the author El Saeed [75]. In this study, Cu<sub>2</sub>O nanoparticles were incorporated into epoxy resin at ratios ranging from 0.1 to 1.0 wt. %. The research demonstrates that the inclusion of small amounts of Cu<sub>2</sub>O nanoparticles significantly enhances various properties of the coatings, including improved epoxy coating resistance to surface damage such as scratches and abrasions, as well as increased microbial resistance,

compared to the virgin resins. Table 4 provides additional literature examples of the incorporation of nanoparticles with both anticorrosive and antibacterial properties into epoxy coatings.

Table 4. Modifications of epoxy coatings (EP) with nanoparticles.

Nanocomposite	Properties	Ref.
EP/Fe <sub>2</sub> O <sub>3</sub>	Iron oxide nanoparticles enhance the adhesion and mechanical characteristics (bending, abrasion, and hardness) of epoxy nanocomposite films on the steel surfaces and decrease corrosion rate was most pronounced for the specimens containing high percent of nanoparticles.	[75]
EP/Si	Coating is durable and mechanically stable and provides good resistance to wear and corrosion.	[76]
EP/SiO <sub>2</sub>	Increase of SiO <sub>2</sub> content from 1% to 3% and further to 5% greatly increases corrosion resistance of epoxy coatings. With the increase in the exposure time, coatings are deteriorated because of water uptake, but still possess higher anticorrosive properties.	[77]
EP/Cu	Epoxy/Cu NPs composites with 3 wt. % and 4 wt. % copper nanoparticles provide high reactivity against <i>E. coli</i> bacteria.	[78]
EP/TiO <sub>2</sub> EP/FAS-TiO <sub>2</sub>	Epoxy coatings with the addition of TiO <sub>2</sub> and FAS-TiO <sub>2</sub> nanoparticles reduced <i>E. coli</i> adhesion due to the antibacterial effect of the anatase TiO <sub>2</sub> .	[79]
EP/TiO <sub>2</sub> -CuO	Enhanced corrosion resistance and antibacterial properties of epoxy coatings after addition of CuO/TiO <sub>2</sub> nanocomposite, assessed by observing the growth of Gram-negative bacterium and <i>E. coli</i> .	[80]
EP/Zn	Epoxy coatings containing appropriate proportions of Zn NPs exhibit remarkable barrier properties in corrosion protection without deteriorating the physical and mechanical properties of the coating. Reduced pitting corrosion tendency by reducing blistering	[81]

	in aqueous solution containing chloride ( $\text{Cl}^-$ ) ions such as HCl or NaCl.	
EP/ZnO	Nanocomposite exhibited good antibacterial activity against both <i>E. coli</i> and <i>S. aureus</i> .	[82]
EP/AgO	AgO nanoparticles as nanofillers significantly improved the anticorrosion and mechanical properties of epoxy coatings, and deliver antibacterial activity, showing promising solution for protection of steel substrates in the marine environment.	[83]
EP/F-Ag	Released silver ions from the nanoparticles react with the membrane of the microorganism, which results in a reduced level of ATP, oxidative stress, and significant damage to cellular structures and finally cellular death.	[84]

According to Table 4, metal and metal oxide NPs are very promising candidates for antibacterial agents. Nanomaterials derived from silver, silver oxide, zinc, zinc oxide, copper, copper oxide, titanium and titanium oxide showed good corrosion and antibacterial properties within the epoxy coating. Several parameters can influence the anticorrosion and bactericidal property of the nanoparticles, including size, shape, morphology, stability and surface functionalization [85]. Some study indicated that particle size and size distribution are the most important characteristics of nanoparticle systems, but it is generally believed that the shapes and types of nano-particles play a great role in determining the nanocomposite coatings properties [65, 86]. Smaller particles tend to dissolve more quickly and flow more easily, leading to higher suspension viscosities compared to larger particles. Likewise, more spherical particles tend to flow more easily than high-aspect-ratio particles, which are NPs with a length many times that of their width [87]. However, it is essential to ensure the successful formation of a 'nanoorganic coating' to retain these desired properties. Agglomeration of nanoparticles within the organic coating can lead to the loss of expected properties [88].

### 2.5.2. Preparation of epoxy nanocomposite coating

Aggregation, a common yet complex phenomenon for small particles is problematic in the production and application. In the manufacturing process of nanocomposites, one of the most significant challenges is achieving uniform dispersion of nanoparticles within the matrix material. This is crucial because only well-separated nanoparticles can impart unique properties to the composite, such as simultaneous improvements in toughness and stiffness, even at very low filler contents [89]. Agglomeration of particles is a basic process that results in a reduction of surface free energy by increasing their size and decreasing their surface area [90]. Two mechanisms commonly contribute to the agglomeration of nanoparticles:

1. Brownian agglomeration is mechanism that leads to particles collision and stick together because of their random motion.
2. Gravitational agglomeration is dependent on the size of the particles and their terminal velocity. The slowly settling particles are caught by the more rapidly settling particles, leading to the formation of clusters [87].

In literature, different methods are used to obtain nanocomposite coatings. For example, Shen and co-authors [83] applied gentle mechanical stirring, while Xavier dispersed nickel(II) oxide nanoparticles in a polymer matrix by stirring at 3000 rpm [91]. Alam and co-authors used an ultrasonic homogenizer to avoid agglomeration of nanoparticles [77]. Table 5 summarizes various techniques for the dispersion of nanoparticle in epoxy coating.

Table 5. Methods for preparation of epoxy nanocomposite coatings.

Nanocomposite	NPs	Incorporation of NP in EP	Ref.
EP/Fe <sub>2</sub> O <sub>3</sub>	0.1, 1.0, 10.0 wt. %	ultrasonication (amplitude 25%, 25 min)	[75]
EP/Si	1.0 g Si NP mixed in 5 g of toluene	planetary centrifugal mixer (2 min at 1000 rpm, 1 min at 2200 rpm)	[76]
EP/SiO <sub>2</sub>	1.0, 3.0, 5.0 %	stirred (5000 rpm for 45 min) and then left for 10 min to get stabilization	[77]
EP/Cu	1.0, 2.0, 3.0, 4.0 wt. %	magnetic stirrer (30 min)	[78]

EP/TiO <sub>2</sub>	3 wt. %	spin-coated	[79]
EP/FAS-TiO <sub>2</sub>			
EP/ CuO-TiO <sub>2</sub>	5.0, 10.0, 20.0 %	NPs, acetone and hardener sonicate (10 min) and EP added with laboratory mixer	[80]
EP/Zn	0.5, 1.0, 1.5 wt. %	ultrasonication (10 min), bubbles removing in a vacuum oven (at -0.75 bar for 10 min)	[81]
EP/ZnO	0.01, 0.05, and 0.1 M in acetone solvent	mixing (30 min), stabilized for 10 min	[82]
EP/AgO	0.5, 1.0, 1.5, 2.0 wt. %	mixing (5 – 10 min)	[83]
EP/F-Ag	1.0, 3.0, 5.0 wt. %	mixing (15 min, 60 °C)	[84]

Table 5 highlights several techniques employed to achieve uniform dispersion of particles in nanocomposites. Among these methods, mechanical stirring and ultrasonic homogenization are the most commonly used. Ultrasonic irradiation, in particular, is well-known for its efficiency in dispersing particles due to the cavitation effect [92]. However, for high viscosity epoxy resins, additional considerations are necessary. When applying ultrasonic irradiation, it is essential to reduce the resin's viscosity by heating to ensure low damping and allow the sonotrode to vibrate at its resonance frequency. Conversely, during sonication, the epoxy resin heats up and must be externally cooled to prevent degradation [93].

### 2.5.3. Effect of nanoparticles on the barrier properties of epoxy coating

It is well known that cross-linking density and ionic resistance are among the main parameters affecting the barrier properties of organic coatings when exposed to corrosive electrolyte. A decrease in cross-linking density can lead to an increase in electrolyte permeation into the coating matrix. [94]. According to Haddadi et al., the inclusion of nanoparticles in the epoxy coating resulted in an increase in coating film resistance, which could be attributed to the barrier effect of the nanoparticles. Generally, properties of epoxy coating depend on the concentration

of nanoparticles. For instance, the optimum amount of nano Al powder in the epoxy coating is about 1 wt. %. Adding nano Al particles into the epoxy resins, the intrinsic pores can be jammed and the barrier performance of the coating can be increased [95]. Saber et al. [96] studied the effect of nano and micro  $\text{Al}_2\text{O}_3$  particles on the barrier properties of epoxy coating. Figure 9a shows the damage mechanism in steel coated by epoxy and epoxy filled with  $\text{Al}_2\text{O}_3$  micro and nano particles after being subjected to tensile loading. The pure epoxy coating (2E) exhibited the worst results, whereas the addition of micro (M1N1 sample with 1% wt. %  $\text{Al}_2\text{O}_3$  and M2N1 sample with 2% wt. %  $\text{Al}_2\text{O}_3$ ) and nano (EN1) particles improved the adhesion properties of the coating. Figures 9b and c demonstrate that the lowest water absorption was detected for the M1N1 composite coating, followed by the M2N1 composite coating.

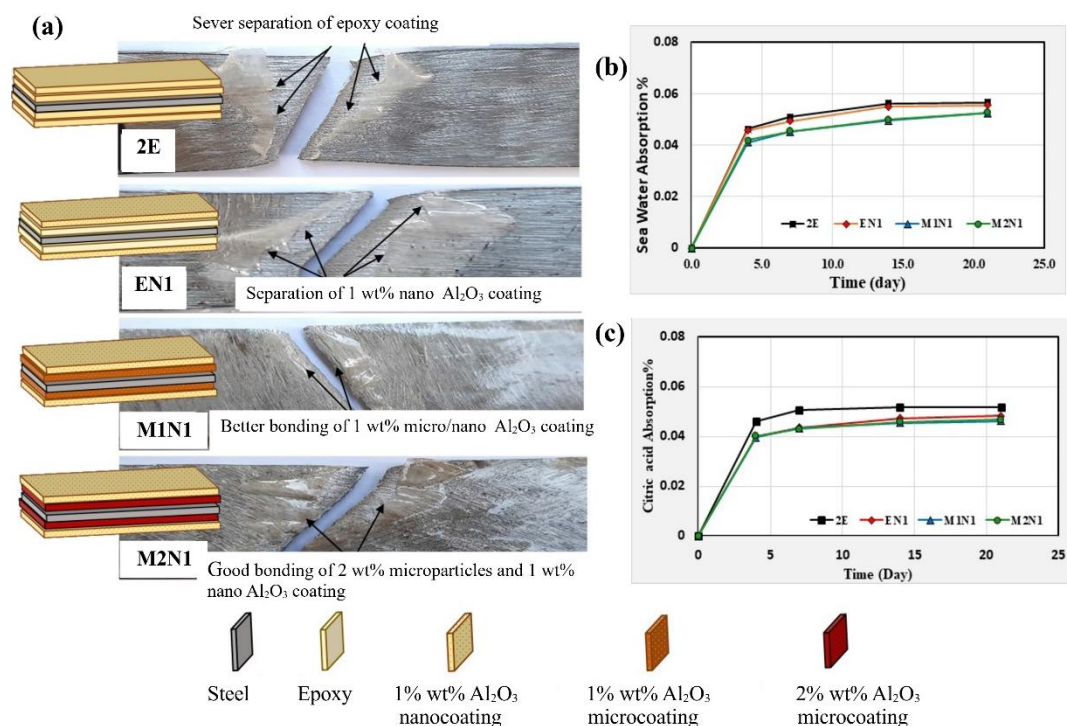


Figure 9. (a) The damage mechanism in steel coated by epoxy and epoxy filled with micro/nano  $\text{Al}_2\text{O}_3$  particles after being subjected to tensile loading. The barrier properties of steel coated by epoxy and epoxy filled with micro/nano  $\text{Al}_2\text{O}_3$  particles when immersed in (b) 3.5 wt% NaCl and (c) citric acid solution [96].

The nanosized inclusions reduce the rate of water absorption due to the barrier properties of these nanoparticles, by decreasing the voids and the zigzag diffusion path for deleterious species. Nanoparticles effectively block the corrosive medium, reduce the tendency of



blistering or delamination of the layer, and improve the anticorrosive properties of the composite coating.

In this case of the addition of a higher concentration of nanoparticles, for examples  $\text{Fe}_2\text{O}_3$  and  $\text{SiO}_2$  nanoparticles, the properties of the epoxy coating deteriorated due to agglomeration of the nanoparticles [95].

#### **2.5.4. Corrosion inhibition by metal nanoparticles in epoxy coating**

In a literature review, the author Esuyankpa [97] described the mechanisms of the anticorrosive effect of nanoparticles. The author emphasizes the key properties of nanoparticles that contribute to their effectiveness as corrosion inhibitors. Nanoparticles, with dimensions from 1 to 100 nanometres, have unique characteristics that are extremely suitable for use in corrosion protection. One of the most important properties relevant for this application is their large specific surface area. It is this large specific surface area that allows nanoparticles to establish multiple points of interaction with corrosive agents, which enables them to create a comprehensive protective barrier.

Qi et al [98] demonstrated that active zinc particles serve as an anode and sacrificially corrode to protect the steel substrate, which becomes the cathode. This cathodic protection is effective as long as there are enough active zinc particles.

As shown in Figure 10, at the early stage, when zinc fibres and steel are in contact with in corrosive species at damaged areas of the coating, the surrounding nanoparticle are activated forming a galvanic cell with the exposed steel.

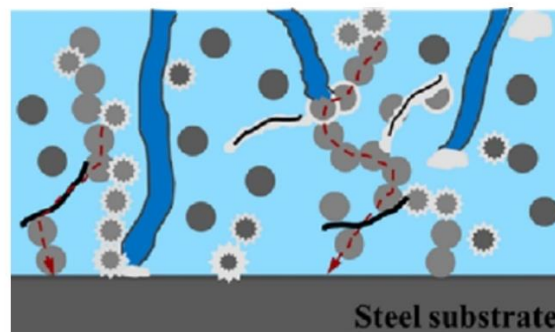


Figure 10. Schematic illustration of the corrosion inhibition mechanism of zinc fibres in the epoxy coating [98].

Additionally, Zn ions form complexes with the product of the cathodic reaction ( $\text{OH}^-$ ) and create a protective layer that inhibits the flow of cathodic current. This process results in the clogging of pores or cracks within the epoxy coating [98].

According to author Liang [99], aluminium nanoparticles have the ability to cut electrolyte penetration through the epoxy coating through the passivation mechanism. In a neutral medium, these nanoparticles will undergo an anodic dissolution reaction, forming passive films on their surface, including  $\text{Al}(\text{OH})_3$ ,  $\text{AlOOH}$  and  $\text{Al}_2\text{O}_3$ . In addition, aluminium expands moderately in volume after oxidation, which makes it possible to fill voids in the coating without creating significant internal stress. In this system, aluminium nanoparticles act as a sacrificial anode that protects the metal surface from corrosion, while simultaneously reducing the transfer of the corrosive medium into the coating.

#### **2.5.5. Labyrinth effect of nanoparticles in epoxy coating**

The labyrinth effect occurs in an epoxy coating containing dispersed lamellae that form complex barriers, elongating the diffusion path of the corrosive medium and resulting in a slower corrosion rate. This effect is most commonly observed in epoxy coatings containing dispersed lamellae, such as graphene or MXene, but it can also occur with certain nanoparticles [98]. For example, a single water-borne epoxy coating is porous (Figure 11a). Figure 11b shows that a small amount of  $\text{SiO}_2$  is not capable of effectively filling the pores in epoxy resin while Figure 11c illustrates that when the coating is uniformly dispersed with an appropriate amount of  $\text{SiO}_2$ , pores can be effectively plugged, and penetration path of corrosive media is significantly increased [100].

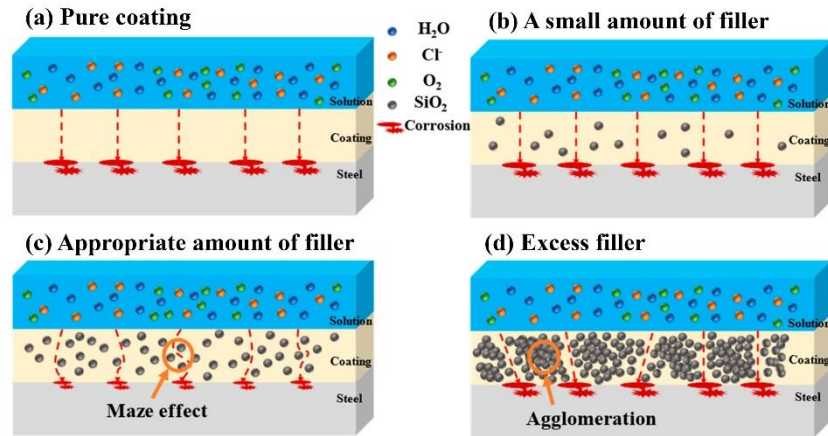


Figure 11. Schematic of the modified SiO<sub>2</sub> dispersion influence on the barrier properties of coating (a) pure coating (b) small amount of SiO<sub>2</sub> (c) appropriate amount of SiO<sub>2</sub> and (d) excess SiO<sub>2</sub> [100].

### 2.5.6. Antibacterial effect of nanoparticles in epoxy coating

In the quest for a novel and efficient system providing simultaneous corrosion and antibacterial protection, promising initial results are emerging from composite systems incorporating metal powder nanoparticles [83]. Metal nanoparticles and metal oxides exhibit exceptional resistance to microorganisms and heat, making them viable antimicrobial agents [101]. Nanoparticles of metals or metal oxides such as Ag, AgO, Cu, TiO<sub>2</sub>, Fe<sub>2</sub>O<sub>3</sub> have a great ability to suppress the growth of bacteria [84, 83, 102, 103].

Although the mechanisms behind the antibacterial activity of metallic nanostructures are not yet fully understood, various antibacterial actions have been proposed in Figure 12a. Nanoparticles have the ability to release ions continuously, which is important for killing the microbes. Positively charged ions can adhere to the negatively charged cell wall due to electrostatic attraction and affinity to sulphur proteins [104]. Furthermore, nanoparticles, owing to their minute size, can penetrate into bacterial cells, which typically range from 0.5 to 3 microns in size [105]. After the uptake of free ions into the cells, the respiratory enzymes can be deactivated, generating reactive oxygen species that cause the interruption of adenosine triphosphate production, disruption of the cell membrane and modification of deoxyribonucleic acid. Additionally, nanoparticles can eliminate bacteria by accumulating in pits formed on the cell wall after anchoring to the cell surface [104].

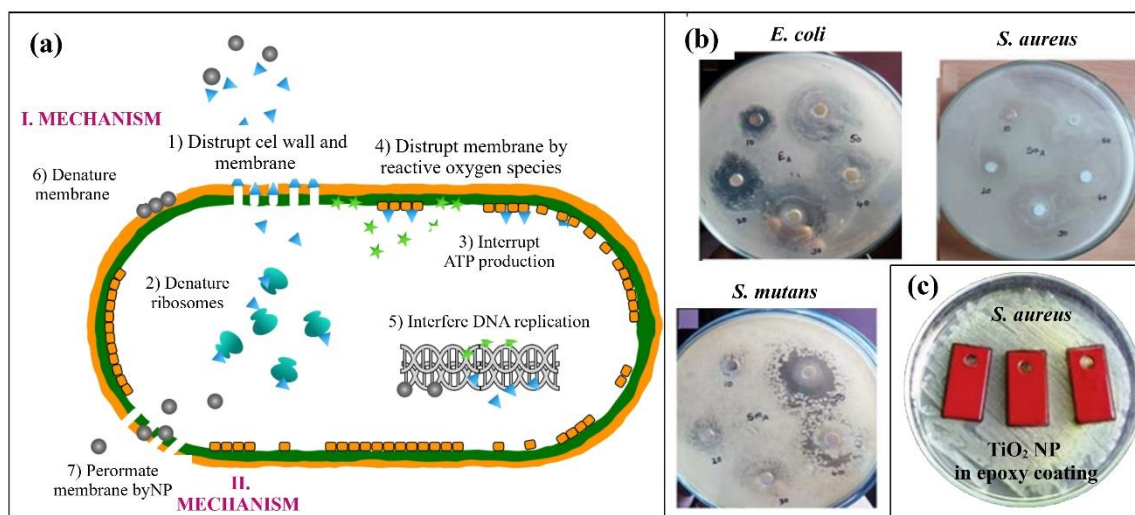


Figure 12. (a) The antibacterial mechanisms of nanoparticles. (b) Antibacterial activities of  $\text{Al}_2\text{O}_3$  nanoparticles against *E. coli*, *S. aureus*, and *S. mutans*. Antimicrobial activities of  $\text{TiO}_2$ -APTES nanohybrid coatings against *S. aureus* [104, 106, 107].

Figure 12b presents an example of testing the antibacterial activity of  $\text{Al}_2\text{O}_3$  nanoparticles for various bacteria in a well diffusion technique [105]. Furthermore, Saravanan et al. [107] investigated the effect of  $\text{TiO}_2$  nanoparticles with 3-aminopropyltriethoxysilane (APTES) which was used as a coupling agent to surface treats. The authors of this study successfully developed an antibacterial epoxy coating, with the best result achieved using 3%  $\text{TiO}_2$ -APTES nanoparticles, as clearly shown in Figure 12c.

## 2.6. New approaches in characterization of nanoparticles in epoxy coating

### 2.6.1. Introduction to SECM

Scanning Electrochemical Microscopy (SECM) was first mentioned in the middle of '80s by Bard and Engstrom. SECM is defined as a technique where the current flowing through a very small electrode tip (typically an ultramicroelectrode with a tip diameter of 10 pm or less) near a conductive, semiconductive, or insulating substrate immersed in a solution is used to characterize processes and structural features at the substrate as the tip is moved near the surface [108]. Since its introduction, SECM has found a wide range of applications, from degradation reaction, catalysis, and chemical corrosion to the study of microorganisms. Consequently, the scientific output utilizing SECM has steadily increased over the years, with reports of applications in various research areas [109].

Figure 13 shows typical SECM setup with an electrochemical cell containing the substrate, tip (UME), reference, and auxiliary electrodes.

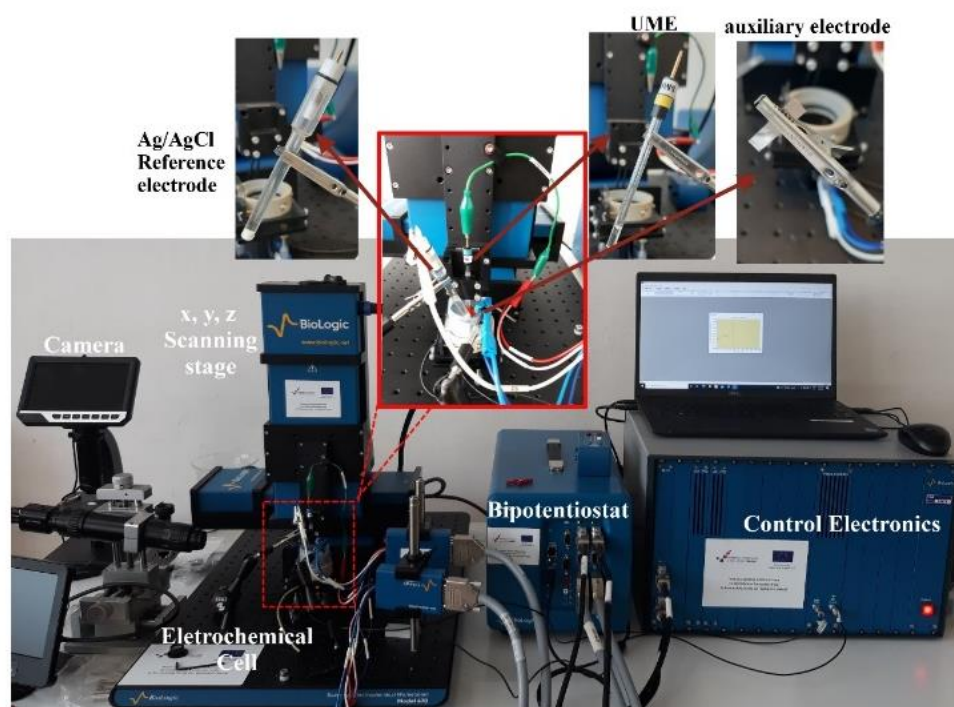


Figure 13. SECM device with marked display of all components (type Biologic M470).

In SECM, the imaging process relies on the interaction of the substrate with a species electro-generated at the tip. During measurement, SECM can utilize either a direct current (dc) or alternating current (ac) signal. Both dc- and ac- SECM can be performed in constant-height or constant-distance mode supported by the intermittent contact (ic-) SECM technique. In SECM, electrochemical data may be collected in three main modes namely voltammetry (amperometric), potentiometric, and ac- modes [110].

The foundation of amperometric operation is the change in the measured current at the surface of a biased microelectrode occurring when it is moved near the surface of a substrate immersed in an electrolyte solution containing a redox mediator [111]. There are two distinctive modes of SECM data collection, namely positive (Figure 10a) or negative (Figure 10b) feedback and generation/collection modes which can be tip generation/substrate collection (TG/SC) (Figure 10c), and substrate generation/tip collection (SG/TC) (Figure 10 d).

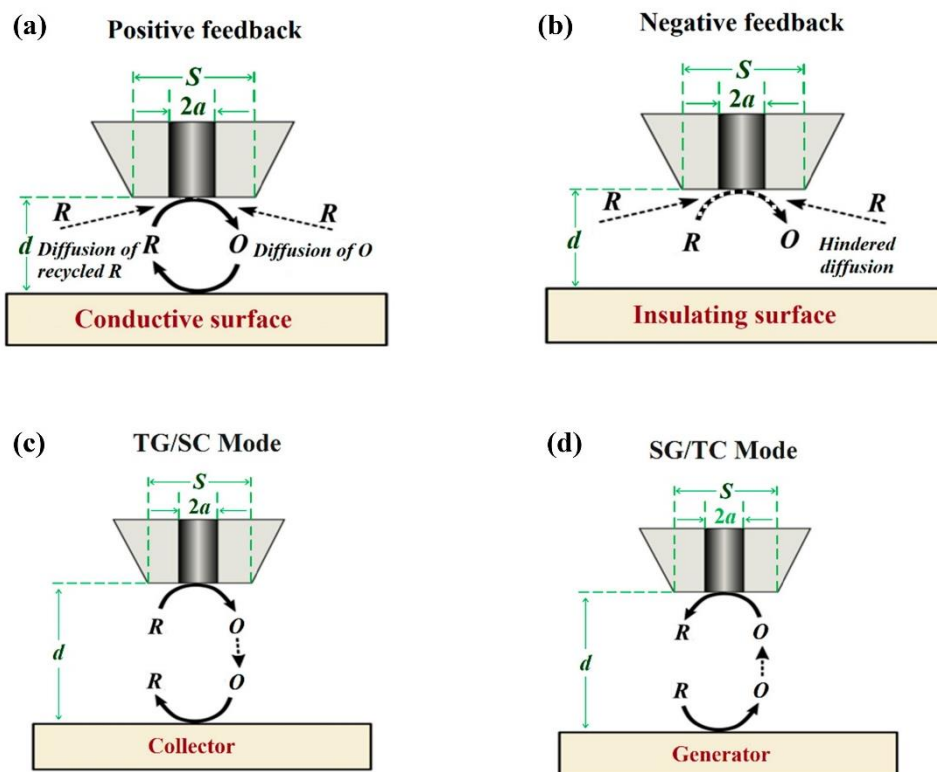


Figure 14. Schemes of (a) positive feedback, (b) negative feedback, (c, d) generation-collection (G/C) modes of SECM [111].

When SECM uses dc- methods, the choice of redox mediator is very important because the wrong choice can lead to an enhanced or inhibited corrosion effect, therefore ac- methods are most often used.

Recently, ac- SECM was introduced as a mediator – independent mode for imaging local variations in surface conductivity [111]. Ac- SECM imaging comprises of recording impedance (imaginary and real) and phase shift via counter electrode (CE) as a response to the ac- signal applied at the UME at a set frequency and excitation amplitude. As the tip approaches the insulator, the electrolyte layer between the UME and the surface decreases, the impedance increases, and the current decreases (Figure 15) [112].

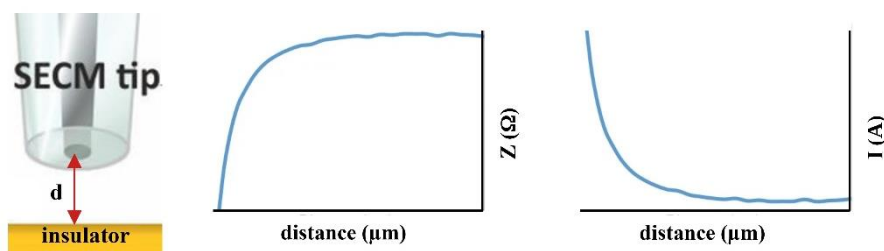


Figure 15. ac- SECM measurement above a non-conducting surface.

Surface activities and surface topography mapping in electrochemical measurement (dc- or ac) can also be combined with intermittent contact (ic-SECM). Catarelli et al. [113] elucidate the principle of ic-technique. The probe's vibration spectrum is recorded, and a frequency slightly lower than the resonant frequency is selected. Then, the tip amplitude, which should not damage the sample, and the set point for surface mapping are determined. The approach to the surface is executed until the tip oscillation amplitude reaches the predefined set point by probe interaction (damping of vibration) with the surface. Throughout the mapping, a constant tip amplitude is maintained, and the topography is determined through mechanical interaction, while the electrochemical measurement (dc or ac) is run independently.

### 2.6.2. dc – SECM analysis of epoxy coating

Traditional and simple techniques have been used in the evaluation of coatings for many years. However, with the advancement of modern methods for protecting metal substrates, the necessity for sophisticated approaches has arisen. For instance, the mechanisms of small pigments of 20-30 nm (nanotechnology) or coatings that respond intelligently to external stimuli (smart coatings) cannot be adequately explained by traditional techniques [114]. In corrosion science, SECM has emerged as a valuable tool for characterizing both organic and inorganic coatings applied on metals. This technique has found diverse applications, including microscopic chemical imaging, the measurement of physicochemical constants and coefficients, and as a micromachining tool. Figure 16 illustrates three exemplary applications of SECM that highlight the method's versatility in corrosion research.

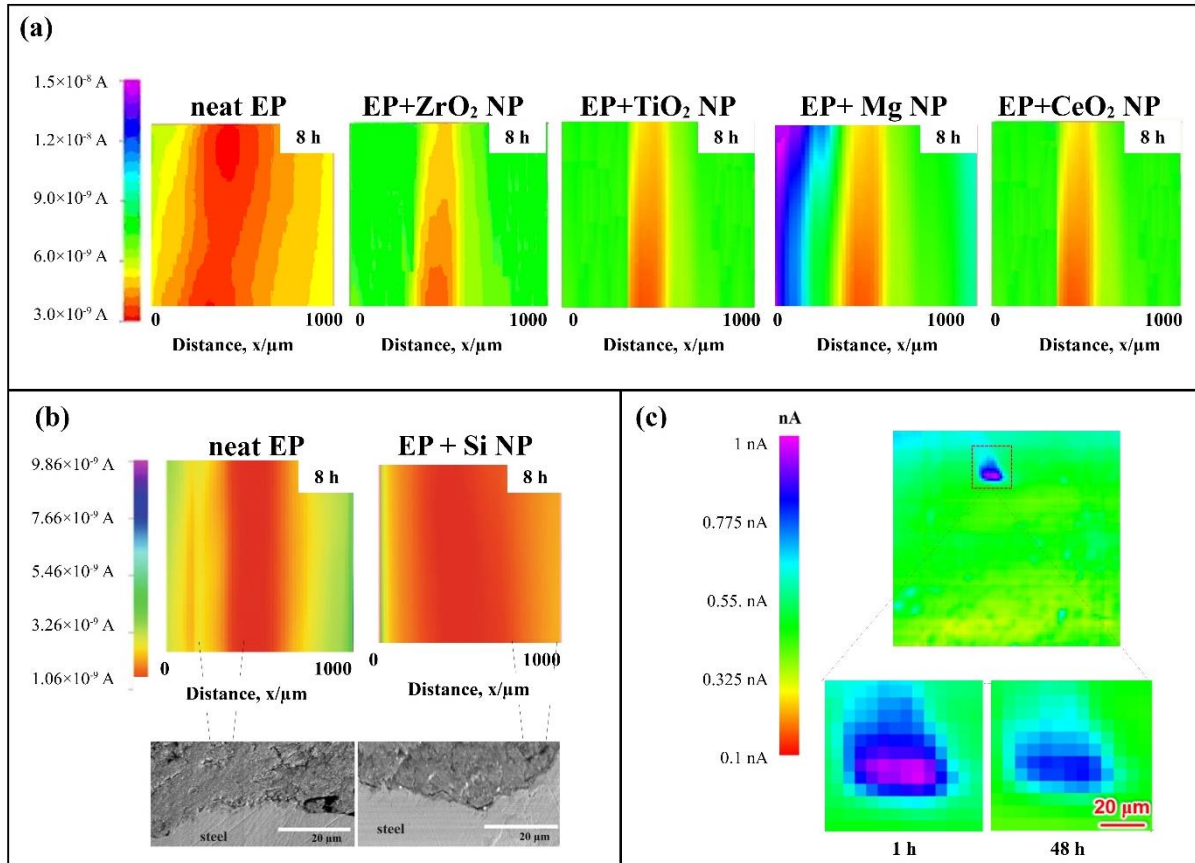


Figure 16. SECM topographic images of a scratched (a) neat epoxy coating and epoxy coating with ZrO<sub>2</sub>, TiO<sub>2</sub>, Mg, and CeO<sub>2</sub> nanoparticles coated carbon steel, after 8 hours in 3.5% NaCl. SECM and SEM image of (b) a neat epoxy coating and coating with Si nanoparticles after 8h in 0.1 M NaCl solution. SECM image of the organic coating with a defect (c) the image with a size of 500 × 500 μm corresponding to an immersion time of 1 and 48 h [115–119].

Extensive research was done by the Xavier (Figure 16a) who focused on the impact of corrosion reduction from nanoparticles (TiO<sub>2</sub>, ZrO<sub>2</sub>, Mg, Ce) within an epoxy coating in salt water [115–118]. In this study, a platinum microelectrode traversed the damaged area of the epoxy coating, providing information about the dissolved oxygen as a cathode current. As the reduction in oxygen is predominant in the cathodic process of corrosion, changes in the concentration of dissolved oxygen due to corrosion reactions were the primary focus. Results indicated that all nanoparticles led to decrease in current on the damaged epoxy coating compared to the sample without nanoparticles. This suggests that the presence of nanoparticles in the epoxy coating reduces the dissolution of iron from the metal surface by forming complexes on the surface.



The formation of these complexes provides additional barrier protection to the surface, in addition to the film resistance.

Similar research was done by Madhankumar et al [119]. In their study (Figure 16b), the behavior of Si NPs on a scratched sample inside an epoxy coating was observed. SEM and EDS analysis revealed that Si NP migrated from the film to the scratched area during the exposure time. It is hypothesized that Si was dissolved in the solution as ions ( $\text{Si}^{n+}$ ) and then transferred from the film to the scratched area. Thus, this result implies a sacrificial effect of Si from the film against steel corrosion.

Furthermore, Xia et al. [120] investigated defects in coatings by using cyclic voltammetry in the presence of ferrocenylmethanol as the redox mediator (Figure 16c). SECM results indicate that the defect initially increased and then decreased, attributed to the accelerated corrosion of carbon steel in the initial stage and subsequently the formation of corrosion product.

### **2.6.3. ac- SECM analysis of epoxy coating**

Wang et al [121] employed a combination of high and low perturbing frequency of ac- signal in SECM measurements on coating sample with scratches and healed coatings. They concluded that the ac- SECM image of the sample surface were significantly influenced by the probing frequency as well as the selection of the image for the exact part of the impedance response. Figure 17a and b shows the coating surface characterized by 3D laser microscopy. In Figure 17c and d, the ac- SECM graphs with a high perturbing frequency (60 000 Hz) could clearly distinguish the scratch topography while ignoring the spatial resolution of surrounding areas. Conversely, the ac- SECM graph with a low perturbing frequency (200 Hz) could distinguish the scratch topography with little spatial resolution, resulting in probing around the scratch area as well. The ac- SECM graph with 3464 showed results very similar to those obtained at high frequency (60,000 Hz). These results demonstrated that ac- SECM offered a wider set of local electrochemical topographies, illustrating the self-healing procedure at different ac-frequencies.

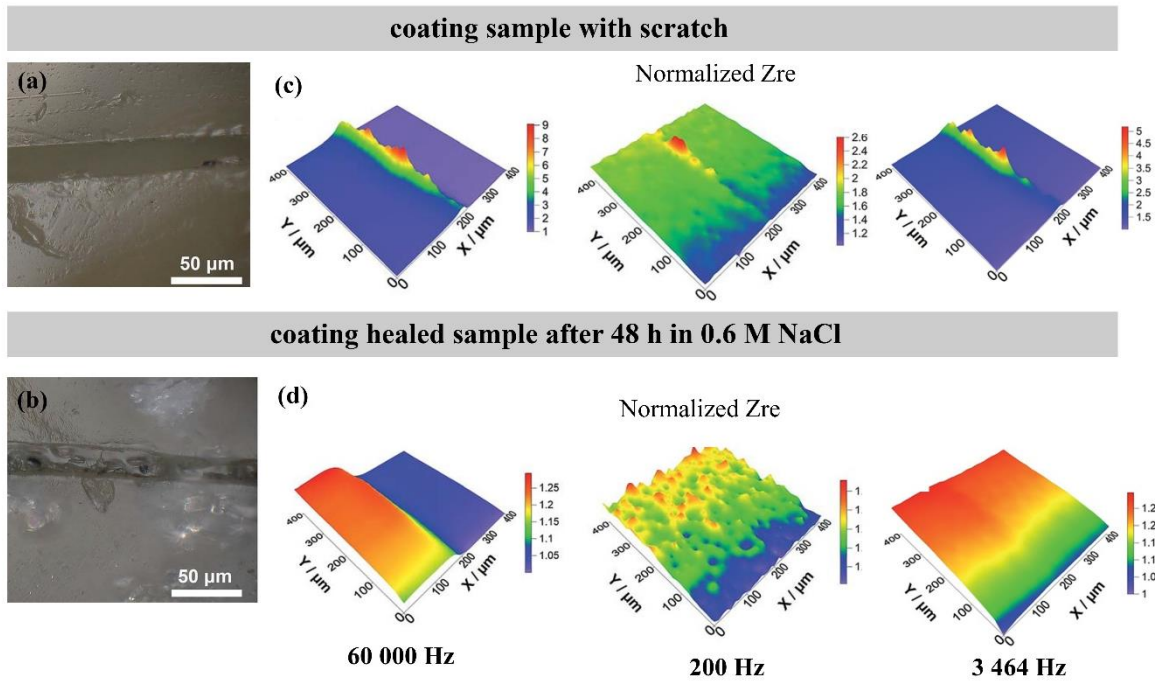


Figure 17. 3D laser microscopy micrograph of the scratched test area (a) and the self-healed scratch (b) on the epoxy resin coating. AC-SECM image of (c, d) self-healing coating surface immersed in a solution of 0.6 M NaCl. DC potential: 0 V. Amplitude of the AC potential signal: 10 mV, and different range of frequency [121].

### 3. DISCUSSION

**Article 1** presents research and development of a new and effective epoxy coating system that combines anticorrosive and antibacterial properties, specifically designed for protecting cast iron in pipelines. This industry segment requires a high level of protection due to constant exposure to conditions that can cause rapid material degradation, such as corrosion and bacterial infections. For effective protection of cast iron from corrosion and bacterial attacks in pipelines, it is crucial to develop and improve coatings that not only offer exceptional corrosion protection but also possess reliable mechanical properties that extend the lifespan of the pipeline. Classic epoxy resins, although widely used, often do not meet all modern requirements without additional enhancements. To increase the resistance of epoxy coatings to corrosion and bacterial attacks, special additives, including nanoparticles that act as effective corrosion inhibitors, are incorporated into the epoxy resin. Due to their small size and high specific surface area, nanoparticles can create a dense and uniform protective layer on the metal surface. This layer acts as a barrier, preventing the penetration of moisture, oxygen, and corrosive chemicals, thereby significantly reducing the risk of damage to the underlying substrate [122]. By incorporating various nanoparticles such as  $\text{Fe}_2\text{O}_3$ ,  $\text{ZnO}$ ,  $\text{SiO}_2$ ,  $\text{CeO}_2$ ,  $\text{TiO}_2$ , graphene, and MXene, nanocomposite coatings based on epoxy have been developed that demonstrate exceptional performance. These coatings offer excellent adhesion to metal substrates, provide a strong barrier against aggressive substances, and possess high resistance to salt, water, and oxygen ingress [123]. The application of these advanced nanocomposite coatings can significantly enhance the longevity and safety of infrastructure, especially in industries facing harsh operating conditions. Further research and optimization of these materials could lead to even more effective solutions for protecting cast iron and other materials in similar applications.

Article 1 investigated the effects of aluminium (Al), nickel (Ni), and silver (Ag) nanoparticles (NPs) integrated within an epoxy coating, aiming to develop an advanced nanocomposite coating. This new coating is intended to provide significant improvements in anticorrosive and antibacterial properties. To achieve the desired goals, experiments were conducted to analyse the performance of different metallic nanoparticles mixed with epoxy resin. The applicability of Al, Ni and Ag nanoparticles was examined through various aspects, including their impact on the coating's corrosion resistance and its ability to inhibit bacterial growth. The development of this advanced nanocomposite coating could significantly enhance the durability and

functionality of protective coatings compared to conventional coatings, which is crucial for applications in the interior of drainage pipes where corrosion and bacterial depositions are serious issues.

All studied metal nanoparticles (Al, Ni and Ag) and epoxy coating (Bisphenol A) were commercially available. A detailed description of the experimental procedure for the preparation of the epoxy nanocomposite coating, and the SEM, EDS, and XRF characterization of metal nanoparticles (Figure 1, and Table 1) can be found in the Materials and Methods section of Article 1. The prepared nanocomposite coatings with 1% of studied nanoparticles were also tested in aggressive corrosion conditions in a 3.5 wt. % NaCl solution after 24 h and 10 days.

Pure epoxy coating contains, besides the resin alone, different components such as fillers, additives, and pigments. Similarly, the studied commercial epoxy coating contained 0.85% of aluminium microparticles which were used as a pigment in the epoxy coating. The SEM and EDS analyses of pure epoxy coating, as well as the epoxy nanocomposites containing 1% Al NP, 1% Ni NP, and 1% Ag NP, are depicted in Figure 2 in Article 1. They have revealed that the surface morphology of coating did not change with the addition of nanoparticles.

In this research corrosion protection by pure epoxy coatings in a 3.5 wt.% NaCl solution was examined by electrochemical impedance spectroscopy measurements (EIS) as a non-destructive method that enables following the corrosion behaviour in time. The recorded impedance spectra for all samples, both after 24 hours of testing and after 10 days, were analysed using the equivalent electrical circuit shown in Figure 3 in Article 1. This model allows for a detailed understanding of the various elements present in the system. The equivalent electrical circuit illustrates three key types of resistance affecting the behavior of alternating current in the system. The first resistance encountered by the alternating current is the electrolyte resistance,  $R_e$ , followed by the coating resistance,  $R_{coat}$ , and the charge transfer resistance,  $R_{ct}$ . Electrical circuit contains also capacitive elements, however real electrochemical systems usually do not exhibit ideal capacitive behaviour, for this reason constant phase element (CPE) was used for description of coating dielectric behaviour,  $CPE_{coat}$  and capacitance of electrochemical double layer  $CPE_{dl}$ .

All samples presented in Article 1 are made of 1% nanoparticles. Concentrations of 1% were chosen based on to the electrochemical measurement shown in Figure 18.

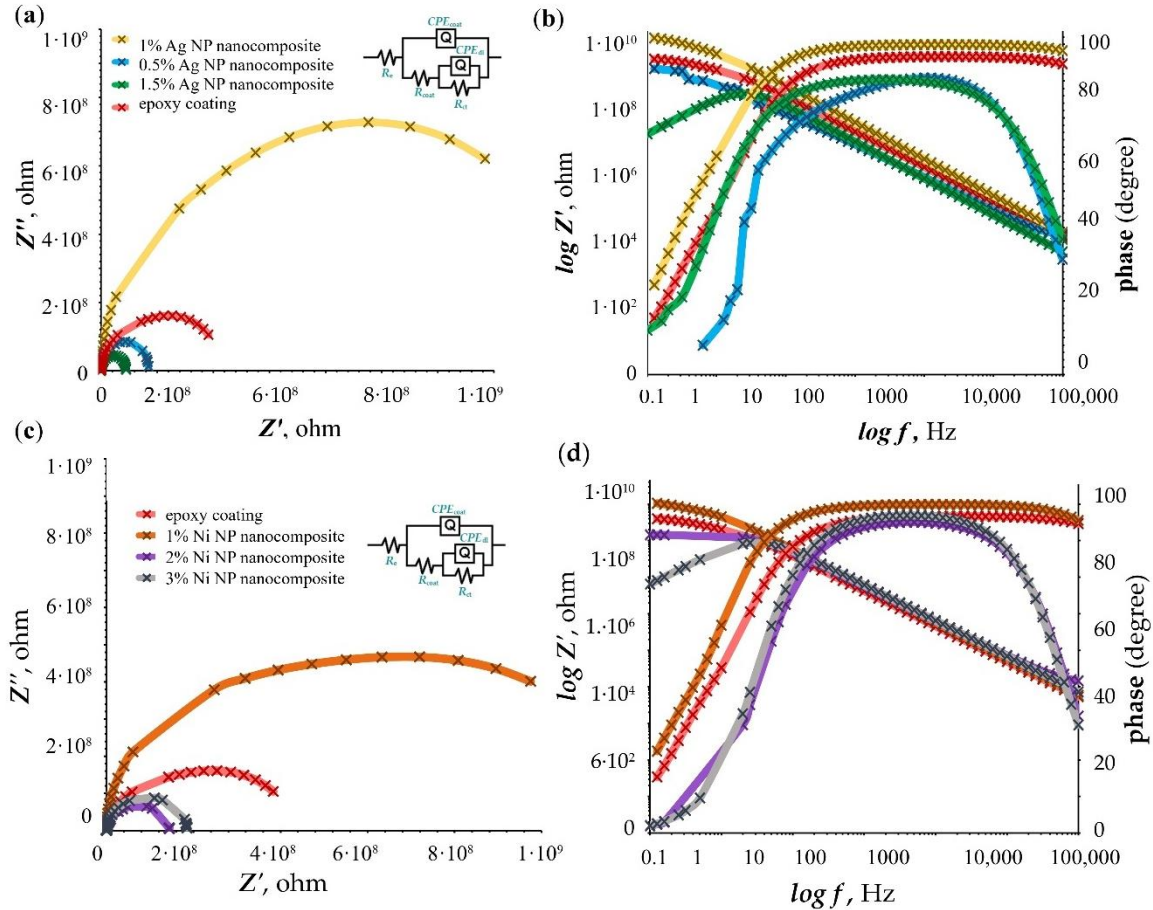


Figure 18. The Nyquist and Bode plots for nanocomposite with (a,b) 0.5%, 1%, 1.5% Ag NPs, and (c,d) 1%, 2%, 3% Ni NPs after 24 h in 3.5 wt. % NaCl solution.

To determine the optimal concentration of nanoparticles within an epoxy coating, various mass fractions of nanoparticles were tested in a 3.5% NaCl solution after 24 hours of exposure. According to the literature, the optimal concentration of Ag NPs within the epoxy coating is 1% [124]. Therefore, concentrations of 0.5%, 1%, and 1.5% Ag NPs were chosen for the study. As shown in Figure 18a, the addition of 1% Ag NPs exhibits the best anticorrosive properties, which is consistent with previous research and literature. This result confirms that a concentration of 1% is ideal for achieving optimal corrosion protection, while lower or higher concentrations may result in less effective protection. It can be seen that at low frequencies (10 mHz) on the Bode plot, the sample with 1% Ag NPs shows the highest impedance (Figure 18b). At high frequencies, the Bode diagram for the sample without nanoparticles, as well as the sample with 1% Ag NP, shows a high phase angle value of approximately 90°, which extends to a frequency of 10 Hz. This high phase angle value at high frequencies reflects the behavior of the coating. A high phase angle value indicates that the coating has no significant damage and is in good condition immediately after application. It has low high electrical resistance due

to the good dielectric properties [125]. However, after below the frequency of 10 Hz, the phase angle value begins to decrease, which may indicate the presence of micropores within the coating. On the other hand, samples with 0.5% and 1.5% Ag NP show lower phase angle values at both high and low frequencies, which may be a sign of possible coating damage. For the lower concentrations of silver nanoparticles within the epoxy coating EIS suggest that these concentrations have very little potential to improve the properties of the coating, and therefore minimally affect its performance and durability [84]. To determine the optimal concentration of Ni NPs within an epoxy coating, different concentrations were tested: 1%, 2%, and 3%. The literature shows the incorporation of nickel oxide within the epoxy matrix. According to [91], the optimal concentration of nickel(II) oxide within the epoxy coating that provides the best anticorrosive properties is 2%. However, based on the results shown in Figure 18c, the optimal concentration of Ni NPs in epoxy coating is 1%. A possible reason for this deviation from the literature could be in the different method of preparing the nanocomposite coating. Differences in preparation can significantly affect the distribution of nanoparticles within the matrix, which may lead to variations in coating performance. To better understand the reasons for these differences, other factors such as the size and shape of the nanoparticles, as well as their interaction with the epoxy resin, should be considered, as all these parameters can impact the final properties of the coating [66]. In the Bode plot (Figure 18d), it can be observed that the behavior of Ni NP is similar to that of Ag NP. The optimal concentration of 1% Ni NPs, in combination with the epoxy coating, shows a wide constant value of the phase angle in the frequency range, from 100 kHz to 10 Hz. On the other hand, coatings with 2% and 3% Ni NP concentrations show reduced phase angle values across the whole frequency spectrum, as well as the lower impedance modulus values. This could be the consequence of excessive nanoparticle concentration, which may agglomerate and form microdefects in the coating, leading to a decrease in anticorrosive efficiency [88].

The tested concentrations of Al NPs within the epoxy coating were 0.5%, 0.75%, 1%, 3%, and 6%. Each of these concentrations was analyzed to evaluate its effectiveness under corrosive conditions. A detailed analysis of the behavior of these concentrations in a corrosive medium is presented and explained in Articles 2, 3, and 4.

On the Nyquist diagrams (Figure 4a in Article 1), an increase in the diameter of the capacitive semicircles and the impedance modulus is evident in all cases where 1% of different metallic nanoparticles was added to epoxy coating which confirms improved anticorrosive properties of modified epoxy coatings. The nanocomposite with 1% Ag NPs exhibits exceptional corrosion

resistance after 24 hours of exposure in a 3.5% NaCl solution. The resistance of this coating, read from the Nyquist and Bode diagram, is 889 M $\Omega$ , which represents a significant enhancement compared to the initial unmodified epoxy coating, whose resistance is 255 M $\Omega$ . These results suggest that Ag NP increased the resistance of the nanocomposite by approximately 71% compared to the unmodified coating. This improved resistance can be attributed to silver's high capacity to inhibit corrosion processes and protect the substrate from the harmful effects of chlorides. Ni NPs within the epoxy coating also show a significant improvement in corrosion resistance compared to the initial epoxy coating after 24 hours of exposure in a corrosive medium. Although the increase in resistance caused by Ni NP is somewhat lower compared to that provided by Ag NP, it still amounts to a significant 67%. This improved resistance can be attributed to nickel's ability to act as a protective barrier against the penetration of corrosive agents. Furthermore, the incorporation of Al NPs within the epoxy coating also results in increased coating resistance. In this case, the resistance increases by about 55% compared to the initial unmodified epoxy coating. This change indicates that, although Al NP does not provide the same level of protection as Ag NP or Ni NP, they still significantly contribute to improving the anticorrosive resistance of the system. The increase in coating resistance with the addition of nanoparticles can also be tracked on the Bode impedance modulus diagram (Figure 4b in Article 1).

On the Bode diagram, the sample with Ag NP shows the highest impedance values at low frequencies (0.1 Hz), followed by samples with Ni NP, Al NP, and finally the epoxy coating without nanoparticles. This indicates that the nanoparticles provide a good barrier function, preventing the passage of electrolytes and corrosive agents through the coating to the substrate. All tested samples show, at high frequencies, value of the phase angle close to 90°, which indicates a predominantly capacitive behaviour of the coating.

With an increase in immersion time in the 3.5% NaCl solution, a decrease in the resistance of all tested coatings was observed after 10 hours. Although there was a decrease in resistance, the coatings still provide satisfactory anticorrosive properties (Figure 4c in Article 1). However, it was noted that the unmodified epoxy coating shows the greatest decline in anticorrosive protection, which is reflected in a significant reduction in the measured coating resistance values,  $R_{coat}$ , which is 5.87 M $\Omega$ . This drop indicates that the epoxy coating is particularly susceptible to corrosive effects during prolonged exposure. In contrast, coatings enriched with nanoparticles show improved effectiveness in corrosion protection, as shown in Table 3 in Article 1. Specifically, the sample with Ag NP retains the best anticorrosive properties, with a

coating resistance of 25.7 M $\Omega$ , showing a high level of protection even after prolonged exposure to the corrosive medium. On the other hand, after 10 days of immersion in the corrosive medium, nickel nanoparticles (Ni NP) showed the lowest resistance values, indicating reduced effectiveness in anticorrosive protection. Conversely, Al NP provided significantly better protection, maintaining higher resistance compared to nickel nanoparticles, suggesting better corrosion resistance under these conditions. These trends are also clearly visible impedance modulus plots in Bode diagram (Figure 4d in Article 1). It is important to notice that the epoxy coating without nanoparticles shows the greatest drop in impedance modulus values at low frequencies, in time. The Bode diagram also reveals that the end of the phase angle plateau around  $-90^\circ$  starts at higher frequencies for spectra measured after 10 day than for spectra measured after 24 h. This trend further confirms that the samples, after prolonged exposure to the corrosive medium, began to lose their protective properties, but compared to the unmodified epoxy coating, the samples with nanoparticles still exhibit satisfactory anticorrosive properties.

Table 3 in Article 1 indicates that the addition of nanoparticles increased the value of the coating protection efficiency, demonstrating an improvement over time. According to literature, metal particles can be converted to a more chemically stable oxides, hydroxide, chloride, or sulphide components when reacting with the surroundings and which then results in a better barrier and corrosion properties [95, 126, 127].

Since the experimental part of the work used a neutral 3.5% NaCl aqueous solution, the corrosive behavior of nanoparticles within the epoxy coating can be described in more detail using Pourbaix diagrams. These diagrams show the dependence of electrochemical potential on pH and are used to predict the stability of various metals and their compounds in aqueous solutions. Pourbaix diagrams for silver, nickel, and aluminum in chloride aqueous solutions are shown in Figure 19.



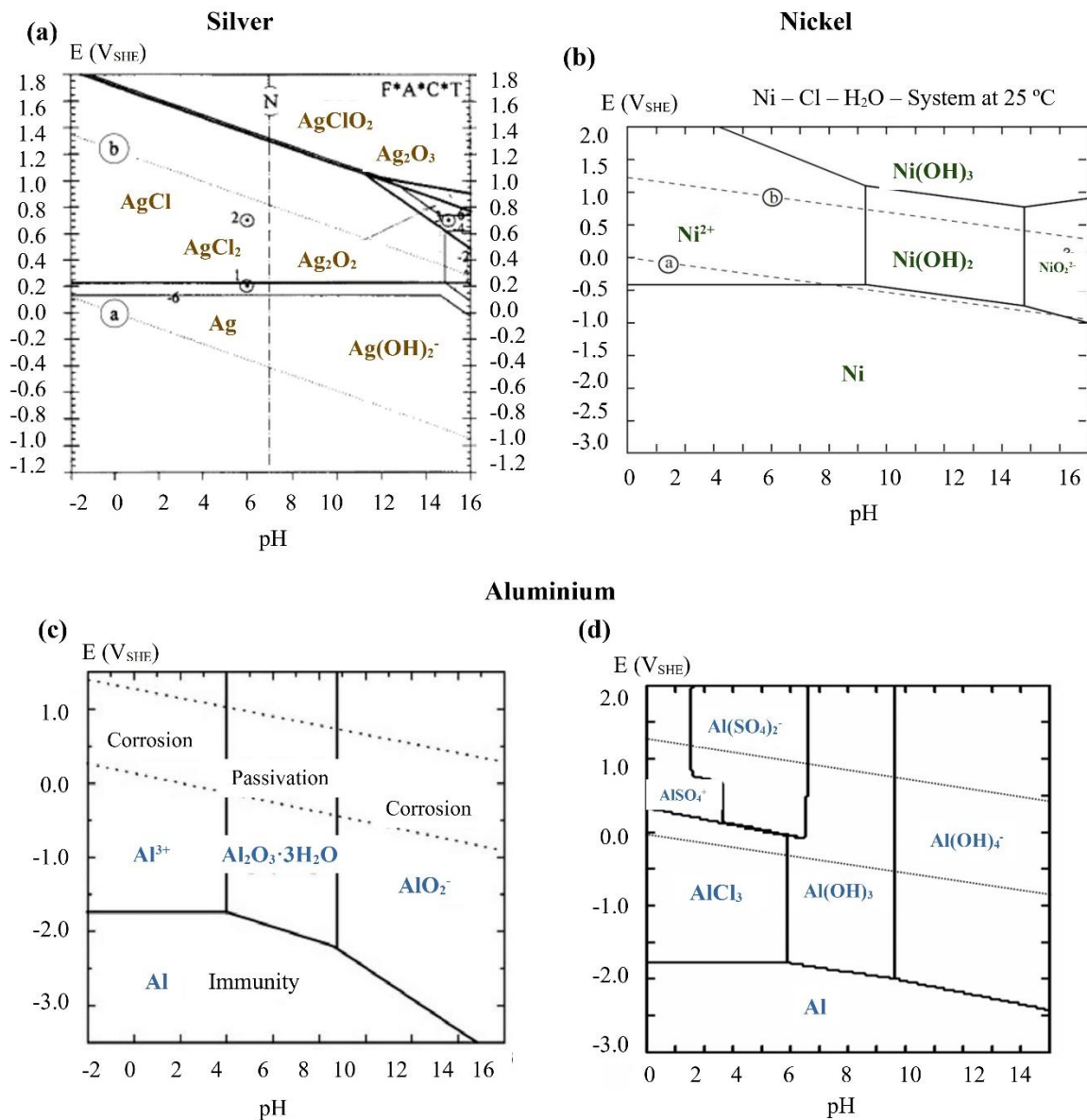


Figure 19. Pourbaix diagram for: (a) silver, (b) nickel, (c, d) aluminium in Cl – H<sub>2</sub>O system at 25 °C [128,129,130].

Pourbaix diagrams allow us to understand the stability (immunity), corrosion (activity), and the conditions under which the listed metals can form insoluble compounds (e.g., oxides or hydroxides) that can further contribute to protecting the metal from corrosion (passivity). The Pourbaix diagrams provide insight into the expected corrosive behavior of Ag NP, Ni NP, and Al NP when they get in contact with neutral medium like a 3.5% NaCl solution that is penetrating into the epoxy coating when samples are exposed to corrosive medium.

Since silver is a noble metal, its affinity for oxygen is low. According to the Pourbaix diagram, in a neutral solution and at an electrochemical potential of 0.799 V, a layer of AgCl will form on the silver surface. The formation of this insoluble AgCl creates a chemical barrier within the epoxy coating, slowing down further penetration of corrosive substances to the substrate and in this significantly improving the corrosion resistance of the coating.

On the other hand, Ni NP does not exhibit passive behavior in such conditions. According to the Pourbaix diagram, passive oxide films should appear at a pH of 10, which is not the case in a neutral solution. Therefore, the increase in volume of Ni NP, which would cause plugging of the pores in coating, is not expected. In an article by Pavapootanont et al. [131], it was reported that a passive layer containing NiO<sub>2</sub>, Ni<sub>2</sub>O<sub>3</sub>, Ni<sub>3</sub>O<sub>4</sub> and Ni(OH)<sub>2</sub> could be formed on nickel surfaces in basic aqueous solution. Consequently, nickel nanoparticles showed decreased electrochemical resistance, as they were unable to form a surface film, unlike aluminium and silver nanoparticles.

When aluminum comes into contact with a corrosive medium, it reacts with oxygen in a neutral solution and begins to form oxide layers on its surface. These oxide layers act as a protective cover, preventing further oxidation of aluminum and improving its corrosion resistance. The formation of insoluble Al(OH)<sub>3</sub>, AlO(OH), Al<sub>2</sub>O<sub>3</sub> and AgCl leads to the creation of a chemical barrier within the epoxy coating, which results in a prolonged path of the corrosive medium into the coating, and ultimately delays the onset of corrosion of grey cast iron [132, 133].

Based on these observations, we can conclude that metallic nanoparticles significantly enhance the corrosion resistance of the epoxy coating, but the effectiveness of protection depends on the type of nanoparticles and the conditions they are in. Silver and aluminum provide significant protection through the formation of insoluble compounds, while nickel offers protection through various mechanisms of protective layer formation under specific conditions.

The antimicrobial properties of nanoparticles are influenced by several important parameters, including particle size, shape, surface area, surface chemistry, morphology, solubility or dissolution rate, purity, agglomeration state, net charge, and physicochemical properties [134, 90]. These parameters collectively contribute to the diverse mechanisms through which nanoparticles exert their antimicrobial effects. The results of antibacterial test against *P. aeruginosa* and *B. subtilis* of pure metal nanoparticles (Al, Ni, and Ag) are shown in Figure 6 in Article 1. The diameter of the inhibitory zone indicates that spherical Al NP had a larger zone of inhibition compared to irregular shaped Ag NP. However, research on the

morphological design of nanomaterials to mimic bacterial shapes and the impact of nanoparticle shape on antimicrobial efficiency remains limited [135]. Spherical nanoparticles have demonstrated superior antimicrobial effects due to their ability to release more ions, facilitated by their larger surface area [134]. Cheon et al. [136] show the ability to control the antibacterial activity of Ag NPs by manipulating their shape. In their study, spherical Ag NPs exhibited the highest antibacterial activity against *E. coli* and *P. aeruginosa*, while triangular plate shape of Ag NPs showed lowest inhibition zone against *E. coli* and almost no antibacterial activity against *P. aeruginosa*. The different shapes of Al and Ag nanoparticle may contribute to the superior antibacterial properties of Al nanoparticles. Additionally, Chaudhary et al. [137] showed that Ni NPs, with a crystalline size of approximately 30 nm, exhibit strong toxicity against bacterial pathogens. It is hypothesized that due to their small size, Ni NPs penetrate the bacterial cell membrane and bind to functional groups of proteins, leading to their denaturation [138].

Previous studies have shown that the antimicrobial nature of nanoparticles is dependent on their size and shape, with smaller nanoparticles displaying better antimicrobial activity [139]. It was assumed that due to their large size range and the potential for agglomeration in aqueous media, Ni NPs may not efficiently penetrate the membrane of bacterial cells, resulting in weak antibacterial properties (as depicted in Figure 6b and d of Article 1).

The potential release of nanoparticles from a polymer nanocomposite exposed to the environment is closely tied to the degradation of the polymer matrix. This release of nanoparticles is particularly relevant in antimicrobial food packaging, where preventing foodborne diseases is crucial [140, 141]. Inspired by this concept, the migration of nanoparticles from an epoxy coating was studied. Assessing the migration of nanoparticles from epoxy coating is highly important, as it introduces a new property for drainage pipe protection. Therefore, the mass concentration of Al, Ag, and Ni nanoparticles migrating from the epoxy coating to simulated wastewater were determined as depicted in Figure 7 of Article 1.

The nanoparticles containing 1% aluminium (Al NP) exhibited significant migration, with the wastewater reaching a constant concentration of aluminium (1 mg/L) after 10 days of exposure. As discussed previously, only aluminium nanoparticles were capable of forming an oxide film on their surface. The resulting oxide film covered the surface of the epoxy coating, decreasing the dissolution and migration of other nanoparticles located deeper within the coating. Subsequent experiments were conducted to evaluate the antibacterial activity of the epoxy coating and 1% Al, 1% Ag, and 1% Ni epoxy nanocomposites against *P. aeruginosa* and *B.*

*subtilis* over a 24-hour period, following the ISO 22196 standard [142]. It was found that the antimicrobial activity was decreasing in the order of 1% of Al NP epoxy nanocomposite > 1% of Ag NP epoxy nanocomposite > 1% Ni NP epoxy nanocomposite > pure epoxy coating (Table 4 and Figure 8 in Article 1). Additionally, Table 4 in Article 1 indicates that samples exposed to the Gram-positive bacterium *B. subtilis* exhibited lower antibacterial activity, likely due to the presence of a thick outer cell wall that can hinder nanoparticle penetration into the peptidoglycan layer.

In continuation of the research presented in Article 1, **Article 2** was developed, which addresses a different approach in the preparation of nanocomposite material. While in the literature nanocomposite materials are mostly prepared by using mechanical mixing and ultrasonic probes, this study explores different concentrations (0.5, 0.75, 1, 3, 6 wt. %) of Al NPs within an epoxy coating in addition to the standard mechanical preparation of samples. In the previous work (Article 1), the behaviour of nanocomposite materials prepared with Ag, Ni, and Al nanoparticles was compared. For further analysis and consideration, the aluminium nanocomposite epoxy coating was selected. This coating demonstrated a satisfactory increase in anticorrosion properties, while also achieving the best antibacterial properties among the tested samples. Although Ag NP showed outstanding results, they were not selected for further study as they have already been extensively researched and documented in the existing literature. Aluminium nanoparticles, on the other hand, provided an opportunity for additional research due to their potential in enhancing the functionality of epoxy coatings, particularly in the context of corrosion resistance and antimicrobial efficiency.

To further investigate the behaviour of Al NP within the epoxy coating, extensive testing was conducted using various analytical methods. First, SEM and EDS analyses were applied, providing detailed insights into the morphology and composition of Al NP, as well as their distribution within the epoxy material. These analyses provided key information on how the nanoparticles integrate into the coating matrix, which is crucial for understanding their impact on the overall properties of the material. In addition to analysing morphology and composition, physical tests of the epoxy coatings were conducted, including measurements of hardness, adhesion, thickness, and colour change. These tests were performed under specific low-temperature conditions, simulating the icing/deicing process within a climate chamber. These conditions were designed to mimic the characteristics of a moderate winter continental climate, common in enclosed, unheated spaces. Testing under these conditions allowed for the

assessment of the coatings' resistance to extreme temperature changes, which is essential for the application of materials in real, demanding environments. The results obtained through these methods contributed to a better understanding of how Al NP within the epoxy matrix enhance the mechanical and aesthetic properties of the coatings, opening new possibilities for their application in various industrial sectors.

The dispersion of nanoparticles and the homogeneity of the layer were observed with the EDS analysis (as depicted in Figure 6 and 7 of Article 2). The sample containing 1% Al NPs exhibited the best distribution, while large agglomerates were observed in the samples containing 3% and 6% Al NPs in the epoxy nanocomposite. The results of physical properties such as discoloration, hardness, and coating adhesion to the metal substrate are presented in Tables 3 to 5 of Article 2. Consistent with findings reported by Bello et al. [143], the addition of Al NPs to epoxy resulted in improved mechanical properties, whereas the same concentration of microparticles led to their deterioration.

A review of the relevant literature leads to the conclusion that the finer size of Al NP compared to aluminium microparticles enables better interaction with the epoxy matrix. The smaller particle size ensures a larger specific surface area, resulting in better dispersion within the epoxy coating and potentially improved material properties. In this study, increase in the concentration of Al NP in the epoxy coating did not significantly affect the material's hardness, suggesting that the addition of nanoparticles does not substantially alter the coating's mechanical resistance. However, despite this, significant improvements were observed in the aesthetic and functional properties of the coating, particularly in colour and adhesion, compared to the pure epoxy coating. These improvements can be attributed to better integration of the nanoparticles with the epoxy matrix, leading to a more homogeneous structure and better adhesion of the coating to the substrate. Additionally, testing conducted in a climate chamber, which simulated the icing/deicing process, did not result in a reduction of the physical properties of the nanocomposite coating. These results indicate the resistance of epoxy coatings enriched with Al NP to extreme temperature changes, which is crucial for their application in conditions characterized by a moderate winter continental climate. The stability of physical properties under such conditions further confirms the potential of these materials for wide industrial use, especially in demanding environments.

EIS measurements were conducted to investigate the effect of increasing the concentration of Al NP in the epoxy matrix on the corrosion resistance of the coating. The testing included evaluating the behavior of the coatings in a 3.5 wt. % NaCl solution and in a climate chamber.

The results were recorded at two key time points: immediately after the coating was dried and after 10 days of immersion in the corrosive medium and exposure to the conditions of the climate chamber. This dual assessment allowed for the analysis of both the initial corrosion resistance and the long-term effects of exposure to corrosive conditions. The results were interpreted by using the EEC model, which is detailed and described in Figure 8 of Article 2.

Electrochemical measurements showed that increasing the concentration of Al NP within the epoxy coating from 0.5 to 1 wt. % leads to a significant improvement in the material's corrosion resistance (as depicted in Figure 9a Article 2). However, at concentrations higher than 1 wt. % Al NP, a decrease in anticorrosive properties was observed immediately after the coating was immersed in a corrosive medium. In samples with concentrations of 3 and 6 wt. % Al NP, the formation of agglomerates occurred, resulting in reduced coating efficiency in corrosion protection. The agglomeration of nanoparticles disrupts the uniformity of the coating and creates microscopic voids or weak points within the structure, through which corrosive agents can more easily penetrate [144].

This phenomenon is illustrated in Figure 7 of Article 2, where the agglomeration of Al NP in the epoxy coating is visualized. The optimal concentration of Al NPs in the epoxy matrix, which in this study is approximately 1 wt. %, allows for achieving maximum corrosion resistance. In this case, the corrosion resistance reached a value of 18.8 GΩ. After 10 days of immersing the samples in a 3.5% NaCl solution, a decrease in the corrosion resistance of all tested samples was recorded, as shown in Figure 9c of Article 2. During this period, a particularly noticeable reduction in resistance was observed in the sample with 1% Al NP. In contrast, the sample with 0.75% Al NP exhibited the best performance in maintaining corrosion resistance. The decline in resistance in the sample with 1% Al NP can be attributed to the uneven distribution of nanoparticles within the epoxy coating, which led to the formation of a small number of agglomerates. These agglomerations are visualized in Figure 7h of Article 2 and may significantly impact the integrity of the coating.

Figures 9b and 9d in Article 2 show Bode plots for all samples, both immediately after application and after 10 days of immersion in a 3.5 wt. % NaCl solution. Comparing these two plots reveals a significant decrease in the real impedance of all coatings after 10 days of exposure to the corrosive medium. Additionally, after 10 days, a drastic reduction in the phase angle is observed in EIS spectra of all samples. This decrease in the phase angle indicates that the protective properties of all coatings have significantly deteriorated during exposure. The

phenomenon of the phase angle decrease is often associated with the occurrence of defects and degradation within the coating, resulting in reduced effectiveness in corrosion protection.

Additionally, according to Figure 10 in Article 2, an increase in the  $CPE_{coat}$  value was observed after 240 hours of immersing the samples in the corrosive medium. This increase in the  $CPE_{coat}$  value suggests that the coating has absorbed water that the corrosive medium has penetrated into the pores of the coating. The increased  $CPE_{coat}$  value could be a result of corrosion products forming on the surface of the grey cast iron. These corrosion products may block the pores in the coating which enhances the coating's resistance ( $R_{coat}$ ). As a result, a significant increase in the protective efficiency of the nanocomposite systems was recorded, as detailed in Table 6 of Article 2.

Additionally, Figure 11 in Article 2 provides a schematic representation of the possible incorporation of Al NPs into the added hardener and directly into the epoxy coating via hydroxyl groups.

Throughout the curing process, several reactions between the nanoparticle surface and the reaction mixture are possible, depending on the particle size, chemical component, surface functional, which all can influence the dispersion structure in the cured nanocomposite [145, 146]:

1. Nanoparticles can bind to the epoxy matrix through physical interactions such as:
  - (a) Van der Waals forces: these are weak attractive forces that enable the adsorption of nanoparticles on the surface of the epoxy resin.
  - (b) Mechanical anchoring: nanoparticles can be "trapped" within micropores or rough surfaces of the epoxy resin, contributing to mechanical bonding.
2. If nanoparticles are functionalized (coated with chemical groups), they bind to the epoxy resin via chemical bonds such as:
  - (a) Covalent bonds: functionalization of nanoparticles allows the formation of covalent bonds between nanoparticles and epoxy monomers, creating a strong and stable bond.
  - (b) Hydrogen bonds: nanoparticles with functional groups (such as -OH, -COOH) can form hydrogen bonds with the epoxy matrix.

Figure 12a in Article 2 illustrates the consequences of agglomerates within the nanocomposite, as numerous studies have indicated their detrimental effects, including the production of defects

and stress concentrations that worsen sample properties [147]. The behaviour of the nanocomposite containing up to 1% Al NPs is depicted in Figure 12b in Article 2, highlighting the appearance of oxide layers on nanoparticles during epoxy coating degradation as a result of successful nanoparticle incorporation.

Epoxy coatings have a porous structure due to the presence of micropores, which allows corrosive media to pass through and can lead to corrosion of the underlying structural material. This study investigated the effect of different concentrations of aluminium nanoparticles within epoxy coatings on their anticorrosive properties. Mechanical mixing of small amounts of nanoparticles (0.5%) into the epoxy resin is insufficient to fill the voids and pores in the resin. Such a concentration of nanoparticles is not enough to significantly improve the barrier properties of the coating. However, when the concentration of nanoparticles is increased to 0.75% or 1%, a significant improvement in the anticorrosive properties of the coating is observed. On the other hand, using larger amounts of nanoparticles, such as 3% or 6%, can lead to the formation of agglomerates within the resin. Due to inadequate mixing, after 10 days of exposure to a corrosive medium, a deterioration in coating properties was noticed in all samples.

The study of the impact of ultrasonic preparation of nanocomposite materials and their effects on the performance of epoxy coatings is the focus of **Article 3**. One of the major challenges in manufacturing nanocomposites lies in achieving uniform dispersion of nanoparticles within the matrix material. Only well-separated nanoparticles can impart unique properties to the composite, such as simultaneous enhancement in toughness and stiffness even at very low filler contents [93]. Ultrasonic treatment offers numerous advantages over mechanical stirring, including high frequency mixing, good directionality and transmissibility, high energy concentration, strong reflectivity, and easy availability. Despite its widespread use in synthesizing various nanomaterials and their composites, the mechanism by which ultrasound influences on the size and dispersibility of particles remains poorly understood. When researching literature on ultrasonic dispersion of nanoparticles in epoxy resin, one can find a significant variation in information regarding the optimal processing time. Ultrasonication, a process where ultrasonic waves are used to disperse nanoparticles within the resin, can cause the epoxy resin to heat up. This heating may lead to the resin reaching temperatures that exceed its degradation threshold. Therefore, it is crucial to apply external cooling during sonication to ensure that the resin temperature remains below this critical limit, thus preventing its degradation [93].



This part of the work primarily focuses on studying and providing a clear explanation of the differences in test results between nanocomposite coatings prepared using mechanical stirring and ultrasonic homogenization. Figure 1 in Article 3 illustrates the ultrasonic preparation of the Al epoxy nanocomposite in different ratio (0.50, 0.75. and 1.0 % Al NPs). Additionally, the article investigates the physical properties of the coatings in humid and climatic chambers, including during icing/deicing processes. Moreover, the article provides a detailed analysis of the anticorrosion mechanism of Al nanoparticles in epoxy coating.

According to Table 2 in Article 3, it is evident that there was no change in the thickness and hardness of the coating on the samples despite the addition of Al NPs and exposure of the coating to corrosive conditions. However, the adhesion of the coating to the metal substrate showed a small increase with the addition of Al NPs. Samples that were exposed to the humid and climatic chambers also showed a small increase in adhesion.

Figure 4 of Article 3 presents the EIS results for epoxy paint and nanocomposite samples with different concentrations of Al NPs (0.50%, 0.75%, and 1%), which were prepared using ultrasonic homogenization. The results are shown in Nyquist and Bode diagrams. According to Figure 4a in Article 3, it is evident that the highest resistance is provided by the nanocomposite with 1% Al NPs, while lower concentrations of nanoparticles did not provide adequate protection when exposed to 3.5% NaCl solution. Therefore, when an appropriate amount of nanoparticles (1%) is present, that are evenly distributed, there is a significant improvement in the coating's resistance. Evenly distributed nanoparticles enhance adhesion and compatibility with the epoxy matrix. They also reduce the pathways for corrosive electrolytes to pass through the coating, resulting in a decrease in the coating's capacitance. As a result, the coating acts as a more efficient barrier and exhibits increased corrosion resistance. Small quantities of nanoparticles (0.5% and 0.75%) are not sufficient to adequately fill the voids and pores in the epoxy resin. Such amounts of nanoparticles are not enough to significantly improve the barrier properties of the coating [100]. Figure 4b shows the Bode phase angle plot that reveals that all samples, immediately after immersion in a 3.5% NaCl solution, exhibit high dielectric properties. This is evident as the phase angle is approximately  $80^\circ$ , and this value is maintained across a broad frequency range, from high frequencies of 100 kHz down to low frequencies of 10 Hz. Figure 4c in Article 3 illustrates the time dependence of the coating resistance of all tested samples over 100 days of exposure to a 3.5% NaCl solution. The diagram clearly shows that all samples maintain almost constant resistance values during the first 50 days. After this period, there is a slight decrease in resistance for samples with unmodified coatings, which may

indicate the beginning of degradation of the coating protective properties. In contrast, nanocomposite coatings exhibit a gradual increase in resistance after 50 days, suggesting an improvement in their protective properties over time. Notably, the most significant increase in resistance is observed for the sample containing 1% Al NP, indicating superior corrosion resistance of this sample compared to the others.

By comparing the diagrams in Figures 4a and 4c in Article 3, it can be observed that after 10 days, there is a significant drop in resistance for all samples. However, following this initial decline, Figure 4c shows a continuation of stable real resistance values over the subsequent period, particularly for the nanocomposite coatings. Among them, the sample with 1% Al NP exhibited the best protective properties, although it also experienced a drop in resistance during the first 20 days. This initial drop, reflecting the temporary impact of the aggressive medium, is detailed in the following diagram, where the specific behaviour of this sample during the early exposure period can be tracked (Figure 20).

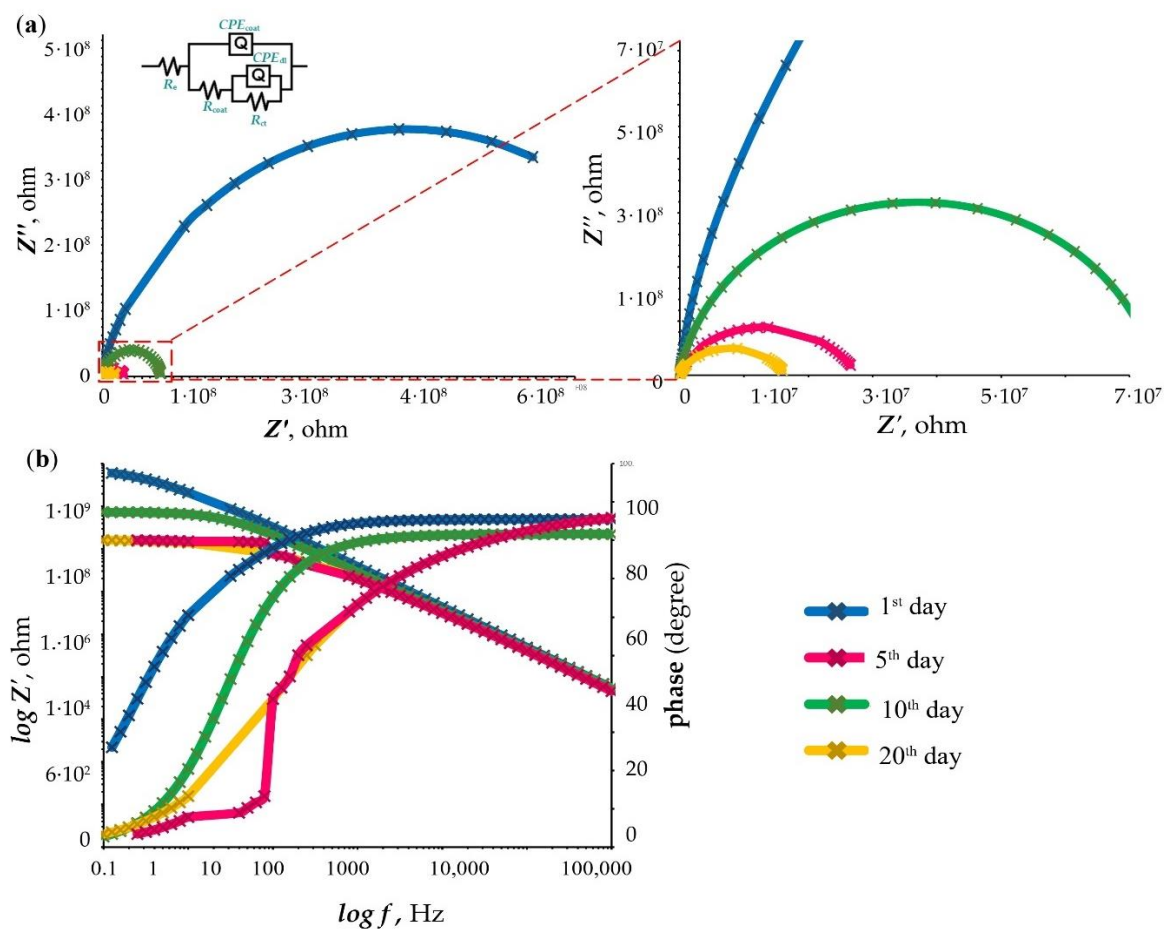


Figure 20. (a) Nyquist and (b) Bode plots for 1% Al NP nanocomposite exposed to 3.5% NaCl solution for 1, 5, 10 and 20 days.

According to the Nyquist plot shown in Figure 20a, it can be observed that the coating's resistance begins to improve after approximately 20 days of exposure to a 3.5% NaCl solution. In the initial stages of exposure, the plot shows a decrease in impedance, indicating early degradation of the coating. However, after 20 days, there is a shift in the shape of the Nyquist plot, suggesting an improvement in the electrochemical properties of the coating. This favourable trend may be attributed to the formation of a protective layer on Al NPs that enhances the coating's resistance to further corrosion.

Furthermore, as stated in Table 3 of Article 3, the value of  $CPE_{\text{coat}}$  for nanocomposites decreases with the addition of nanoparticles. This reduction in the  $CPE_{\text{coat}}$  value indicates improved corrosion resistance. A lower capacitance of the coating typically implies a reduced capacity for corrosive interaction with the environment [146].

Al NPs that are not embedded in the epoxy coating but are exposed to a humid atmosphere (distilled water), will oxidize within 10 days. The chemical composition of the examined point/area on the surface of the oxidized aluminium powder is shown in Figure 5 of Article 3. The results of the EDS analysis show the presence of aluminium (Al) and oxygen (O) on the same surface area. For better clarity, an enlarged view is provided in Figure 21.

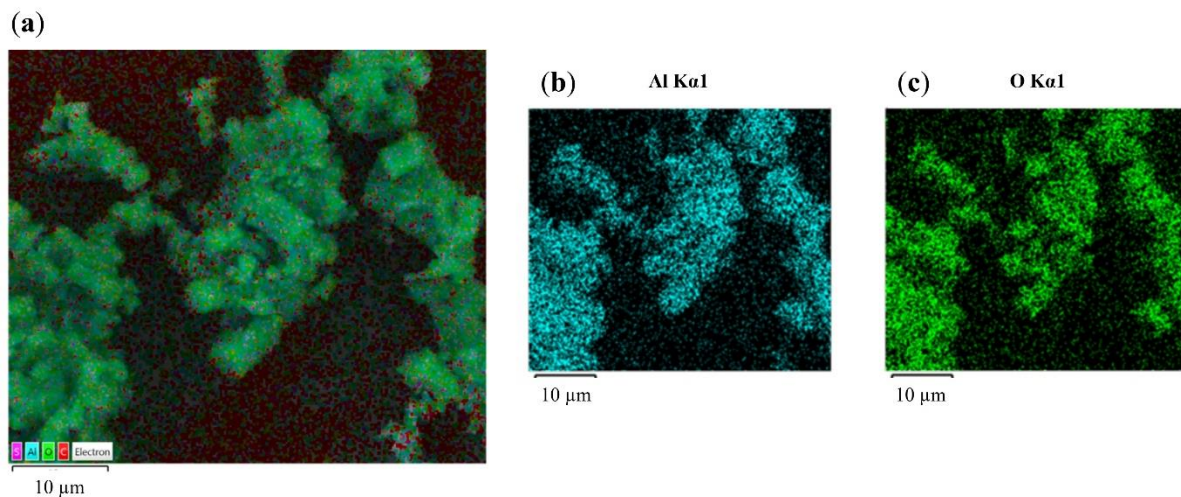


Figure 21. (a) Combined color map of the segment on the oxidized Al NP surface captured using the SEM/EDS method at 6 000x magnification. Partial color maps showing the distribution of individual chemical elements on the oxidized Al NP surface, captured using the SEM/EDS method at 6,000x magnification: b) aluminum (Al) and c) oxygen (O).

The mechanism of Al NP oxidation is proposed in Figure 6 of Article 3. According to literature, during the oxidation process, the outer layer consists of a mixture of  $\text{Al}_2\text{O}_3$  and a hydrated layer, primarily in the form of amorphous  $\text{Al}(\text{OH})_3$ , while the inner part mainly comprises  $\text{Al}_2\text{O}_3$  and a small amount of aluminium oxyhydroxide in the form of  $\text{AlO}(\text{OH})$  when the nanoparticles are in contact with the aqueous medium [148].

The degradation process of the nanocomposite coating is depicted in Figure 7 of Article 3. The aluminium nanoparticles, when in contact with the aqueous medium, form aluminium oxide and smaller amounts of aluminium hydroxide and oxyhydroxide, which increases the volume of the nanoparticles. In the SEM images shown in Figure 7 of Article 3, it is evident that the non-oxidized nanoparticles have a size of up to 100 nm, while the volume of the oxidized Al NPs increases to approximately 15  $\mu\text{m}$ . If SEM images of Al NPs and oxidized Al NPs are normalized to the same magnification as shown in Figure 2 of Article 3, the following image comparison is obtained.

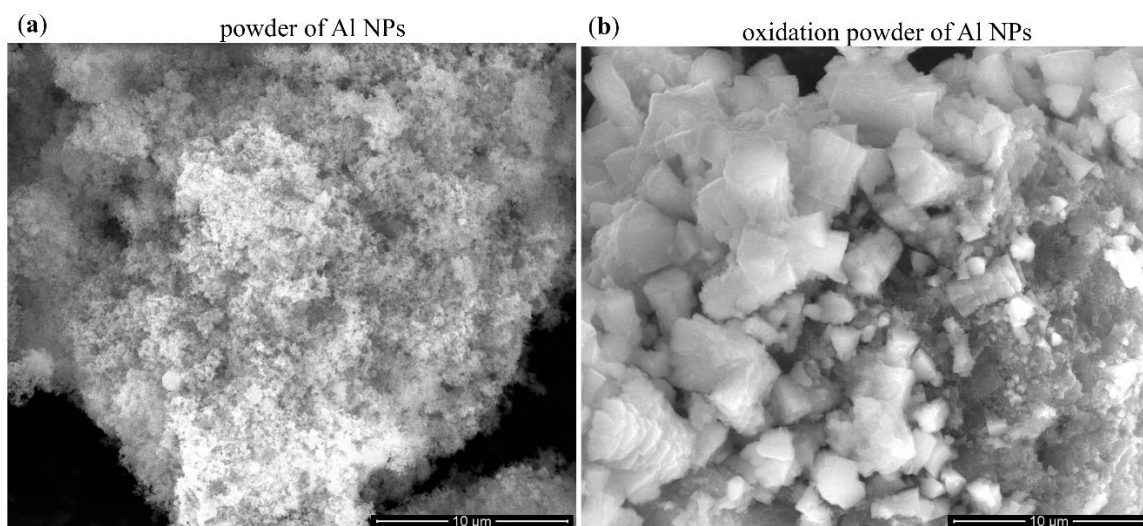


Figure 22. SEM image of the surface of (a) Al NPs and (b) oxidized Al NPs powder at a magnification of 10 000x.

The SEM images in Figures 22a and 22b show a significant difference in the microstructure of pure Al NPs versus those exposed to aqueous media. The surface of Al NPs is a fluffy powder. At a magnification of 10 000x, it was not possible to accurately determine the size of the nanoparticles due to their small size. On the other hand, oxidized Al NPs display notable differences. Their images show the presence of particles several micrometers in size, with a smooth surface but irregular shapes. These particles suggest a well-developed surface structure, likely resulting from oxidation, which has influenced their shape and texture.

The mechanism shown in Figure 7 of Article 3 suggests that well-dispersed nanoparticles have a significant impact on improving the corrosion resistance. According to this mechanism, the nanoparticles create a “labyrinth effect”, which extends the path of corrosive media through the coating. This extended pathway slows down the contact of corrosive agents with the underlying material, ultimately delaying the onset of corrosion. The “labyrinth effect” arises due to the complex distribution of nanoparticles, which impedes the direct access of corrosive agents, thereby enhancing the durability and protection of the material against corrosion [131].

Figure 8 in Article 3 shows a SEM image of a cross-sectional view of a sample containing 1% Al NPs prepared using ultrasound and mechanical mixing. This analysis is related to the investigations conducted in Article 2.

Where it was found through EIS measurements that the anticorrosive properties of the coating improved over a short period. The improvement of the coating in a short time period of 10 days is the result of the specific method of preparation of the nanocomposite, which was confirmed by cross-sectional analysis. Figure 8 from Article 3 shows the SEM analysis of the cross-section of the samples, where the samples were made using an ultrasonic homogenizer (Figure 8a, Article 3) and a mechanical mixer (Figure 8b, Article 3). By using ultrasonic mixing, better anticorrosive properties were achieved over a longer period. Figure 8a in Article 3 shows a cross-section of the nanocomposite without air bubbles. Figure 8b in Article 3 shows that a sample made using a mechanical stirrer contains air bubbles within its structure. Comparing the EDS analysis of the surface of these samples, we can see that the nanocomposite system obtained through mechanical mixing contains agglomerates in its structure (Figure 23a), while the sample obtained with an ultrasonic homogenizer shows a uniform distribution of particles without agglomerates (Figure 23b).

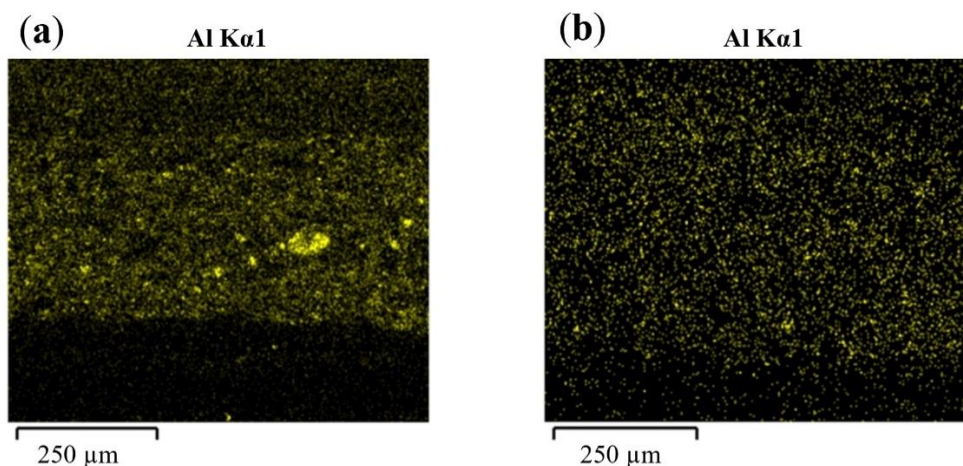


Figure 23. Results of EDS analysis with partial staining of the distribution of aluminium particles on the cross-sectional surface for a sample of 1% Al NP epoxy nanocomposite prepared by (a) mechanical mixing and (b) ultrasonic homogenizer.

Additionally, the advantages and disadvantages of using mechanical and ultrasonic mixing in the preparation of nanocomposite coating are summarized in Table 4 of Article 3. Better corrosion resistance and stability of the sample were obtained by ultrasonic preparation of nanocomposites due to better dispersion of nanoparticles and the absence of air bubbles.

Figure 9 in Article 3 shows the SEM and EDS analysis of the surface of an epoxy nanocomposite sample with 1% Al NP, prepared using an ultrasonic homogenizer. In this figure, the overlap of EDS maps of aluminum and oxygen elements is clearly visible. Such overlap suggests that the aluminum microparticles, added to the coating as a pigment, have an oxide layer on their surface. This is consistent with the assumption that the aluminum microparticles present in the epoxy matrix undergo oxidation during the preparation process.

Figure 10 in the same article shows Al NPs dispersed in pure epoxy resin, without the presence of additional aluminum microparticles. The EDS analysis of this sample did not detect the presence of oxygen atoms, indicating that during the mixing of Al NPs into the epoxy matrix, no oxidation of the aluminum nanoparticles occurred. This result suggests that the aluminum nanoparticles in this case remained stable without forming an oxide layer.

To complement the EIS measurements on a macro scale, impedance measurements were conducted on a micro scale at high frequency (100 kHz), where the capacitive behavior of the coating was observed. The Intermittent Contact-Scanning Electrochemical Microscopy (ic-ac-SECM) test was conducted on pure epoxy resin, pure epoxy coating, and epoxy resin/coating

nanocomposite with 1% of Al NP to observe real impedance distribution over a certain area (Figure 12 in Article 3). Small variations in the measured impedance distribution values indicate a homogeneous structure, while larger deviations are interpreted as consequences of the action of added coating components, such as additives in the epoxy paint. The sample containing 1% Al NPs in the epoxy paint showed the highest resistance (ranging from 143 kΩ to 1.12 MΩ). These values, depicted in Figure 12 in Article 3, for coating resistance were utilized to calculate the nanocomposite protection efficiency, the results of which are presented in Table 5 of Article 3. Nanoparticles in pure epoxy resin increased the protection efficiency by 25.75%, and in the epoxy coating by 40.89%.

Capacitance is an important parameter to measure the amount of water and corrosive ions penetration into the coating [149]. At the micro level, the capacitance of the coating ( $C_{coat}$ ) was calculated according to the following expression [150]:

$$\omega = \frac{1}{R_{coat} \cdot C_{coat}} \quad (1)$$

At high frequencies (100 kHz), the capacitive resistance ( $R_{coat}$ ) shows lower values (Figure 4b in Article 3) due to measurements at these frequencies provide insight into the coating's ability to absorb the electrolyte. In Table 6, the calculated values for  $C_{coat}$  for all samples are presented, based on the data taken from Figure 12 in Article 3, using Equation 1.

Table 6. Data resulted for measured  $R_{coat}$  values and calculated  $C_{coat}$  values for the samples immediately after of immersion in a tap water.

<b>sample</b>	<b>epoxy resin</b>	<b>epoxy paint</b>	<b>1% Al NP epoxy resin nanocomposite</b>	<b>1% Al NP epoxy paint nanocomposite</b>
<b><math>R_{coat}</math>, kΩ</b>	447	662	602	1120
<b><math>C_{coat}</math>, F</b>	$3.56 \cdot 10^{-9}$	$2.41 \cdot 10^{-10}$	$2.64 \cdot 10^{-10}$	$1.42 \cdot 10^{-10}$

According to Table 6, the addition of Al NPs leads to an increase in the coating resistance ( $R_{coat}$ ), which decreases the electrolyte absorption capacity ( $C_{coat}$ ). In addition to providing information about the coating's capacitance, this method offers a more detailed surface insight into the distribution of impedance values across the surface. This is a significant advantage over the classical EIS method, which only provides an aggregate impedance value and does not

allow for detailed mapping of variations across the coating's surface. This advancement enables more precise analysis and optimization of protective coatings under various conditions.

The antibacterial properties of pure Al NPs against *P. aeruginosa* and *B. subtilis* were tested using the diffusion method. The test results are shown in Figure 13 in Article 3. The inhibition zone diameter indicated that Al NPs had a great antimicrobial effect. Pure Al NPs produced zones of inhibition of 25 mm against *P. aeruginosa* and 23 mm against *B. subtilis*.

After successfully incorporating aluminium nanoparticles into the epoxy coating via ultrasonication, a detailed examination was conducted to investigate whether other added components in the epoxy coating affect the nanoparticles. For this reason, the analyses were also performed on pure epoxy resin as presented in **Article 4**.

In addition to SEM, EDS, and mechanical resistance assessments of nanocomposites, differential scanning calorimeter (DSC) and thermogravimetric analyses (TGA) were also performed. Figure 1 in Article 4 shows the SEM and EDS images of pure epoxy resin and 1% Al NP epoxy resin nanocomposite. The EDS analyses, as depicted in Figure 1g of Article 4, confirmed the homogeneous distribution of Al NPs in the epoxy resin, with particles uniformly dispersed at the nano level. Notably, mixing with the ultrasonic probe prevented agglomeration of the Al NPs.

The pure epoxy coating, before modification, contained a small number of aluminium microparticles (Figure 2c and d in Article 4). The ultrasonic homogenizer, in addition to ensuring the good distribution of nanoparticles, was also effective in breaking up the aluminium agglomerates added as pigments (Figure 2h in Article 4).

According to Table 1 in Article 4, it is evident that the addition of 1% Al NPs did not change physical properties such as thickness and hardness of the epoxy resin and epoxy coating. Adhesion of the coating to the metal substrate showed a small increase with the addition of Al NPs to the epoxy. A significant change is visible in the colour of the coating. All samples exhibited stability of mechanical properties in the salt chamber.

DSC analysis for all samples is presented in Table 2 in Article 4. It is evident that with an increase in the proportion of Al NPs, there is a shift of glass-transition temperature ( $T_g$ ) to lower temperatures, indicating that the nanoparticles are not completely absorbed by the epoxy resin/paint and still have intact free nanoparticle surfaces.



Figure 3 in Article 4 illustrates the thermal stability behaviour of pure epoxy resin, 1% Al NP epoxy resin nanocomposite, epoxy paint, and 1% Al NP epoxy paint nanocomposite, while the TGA parameters are listed in Table 3 in Article 4. In Figure 3 of Article 4, in addition to the TGA curve, its derivative (DTG) is shown on the secondary axis of the coordinate system with unit of %/°C. TGA curves for nanocomposites of epoxy resin and 1% Al NP epoxy resin show degradation in two phases (Figure 3a,b in Article 4). In both cases, the first stage of degradation starts around 100 °C, with the weight loss for the epoxy resin being 13.29% and for the 1% Al NP epoxy resin nanocomposites being 11.05%. The DTG curve in this phase gradually increased from a lower value. For the pure epoxy resin, the DTG curve reached a value of 179.25°C, whereas for the 1% Al NP epoxy resin, a slight increase was recorded at 182.73°C. The second phase of weight loss, for both samples, started above 300 °C during which the weight loss for both samples was approximately 80%. The DTG curve continued to rise in this phase. For the epoxy resin, two peaks appear, while the 1% Al NP epoxy nanocomposite reaches its maximum peak. From the DTG curves, it can be observed that the rate of mass change with temperature at the maximum peaks for both samples is similar, approximately 25%/°C.

From the obtained results according to Figure 3c,d in Article 3, it can be concluded that the epoxy paint and 1% Al NP epoxy nanocomposite decompose in three stages. The first phase of weight loss started above 100 °C and continued until approximately 400 °C. This may correspond to the removal of solvent residues or other volatile substances trapped during curing due to the complex cross-linked structure of epoxy and reactant residues, as well as the degradation of low molecular weight polymer fractions [30]. In this phase, the DTG curve rises sharply. For the epoxy resin, at a temperature of 334.03 °C, the mass change rate is about 2.5%/°C. In contrast, for the 1% Al NP sample, a slightly higher mass change rate of 3.5%/°C was recorded at 347.15°C. The second and third stages of weight loss started above 400 °C and continued up to 510 °C during which the weight loss for blank epoxy coating and 1.0% Al NP epoxy nanocomposite was approximately 27.08, 32.51% and 13.43, 10.87%. The use of an ultrasonic homogenizer did not affect the solvent loss during the preparation of the nanocomposite. In this phase, the DTG curve for the epoxy resin shows results similar to those in the first phase, with a consistent rate of mass change. For the 1% Al NP sample, the DTG curve displays a lower peak at 446.59 °C, with a mass change rate of about 1.9%/°C. At 600°C, a significant amount of solid residue appears, which may be related to the presence of additives.

Table 3 in Article 4 shows all results of TGA analysis for samples of epoxy resin, nanocomposite. The onset decomposition temperature ( $T_5$ ), defined as the temperature at which a 5% mass loss occurs, decreases with the addition of Al NPs to the epoxy resin, while remaining constant for samples made with epoxy paint. The reduction in  $T_5$  indicates a decrease in thermal stability. The sample with 1% Al NPs within the epoxy resin shows the widest decomposition temperature range, from 169.5 to 423.5 °C. In the first stage of decomposition, which involves the evaporation of water, or some solvent used, all samples exhibit similar mass losses ( $\Delta m_1$ ): 13.3% for the epoxy resin, 11.1% for the samples with added Al NPs, 0.49% for the epoxy paint, and 0.43% for the samples made with added Al NPs. The second and third stages of decomposition are related to the remaining components in the samples. The temperatures at the maximum decomposition rate ( $T_{max}^2$ ,  $T_{max}^3$ ) show slight differences with the addition of Al NPs. The mass loss in the second stage of decomposition ( $\Delta m_2$ ) is very similar for all samples, while in the third stage ( $\Delta m_3$ ), the sample with epoxy resin shows a decrease with the addition of Al NPs, whereas the sample with epoxy paint exhibits a slight increase. At 600 °C, the samples with epoxy resin show a smaller amount of solid residue compared to the sample made with epoxy paint.

Table 7 shows the thermal degradation of the epoxy coating with different proportions of Al NPs, at concentrations of 0.5%, 0.75% and 1% within the epoxy paint.

Table 7. Results of thermal decomposition parameters of epoxy paint nanocomposite with 0.5%, 0.75% and 1% of Al NPs.

<b>samples</b>	<b>0.5 % Al NP epoxy paint nanocomposite</b>	<b>0.75 % Al NP epoxy paint nanocomposite</b>	<b>1 % Al NP epoxy paint nanocomposite</b>
$T_{5\%}, ^\circ\text{C}$	289.4	286.5	277.4
$T_{fin}, ^\circ\text{C}$	469.6	470.4	468.2
$T_{max}^1, ^\circ\text{C}$	105.9	101.9	103.0
$\Delta m_1, \%$	0.43	0.41	0.43
$T_{max}^2, ^\circ\text{C}$	352.1	347.2	347.2
$\Delta m_2, \%$	24.8	29.8	32.5
$T_{max}^3, ^\circ\text{C}$	448.1	449.1	446.6
$\Delta m_3, \%$	12.7	11.1	10.9
<b>Residue, 600 °C</b>	57.8	58.2	55.5

According to the values in Table 7, the nanocomposite systems with 0.5% and 0.75% Al NPs show similar thermal decomposition as the sample with 1% Al NPs, with three distinct stages of decomposition. With the addition of Al NPs, there is a decrease in the temperature at which 5% mass loss occurs ( $T_{5\%}$ ). The sample with 1% Al content has the widest decomposition temperature interval from 277.4 to 468.2 °C. Mass loss in the second stage of decomposition  $\Delta m_2$  increases with the increase in the proportion of Al, while in the third stage of decomposition  $\Delta m_3$  decreases. At 600 °C, a large proportion of solid residue appears as observed for previous samples.

The study of the electrochemical properties of the coating can be found in Figure 5 in the Electrochemical impedance spectroscopy section of Article 4. Epoxy coating (Figure 5c in Article 4) shows better corrosion resistance than pure epoxy resin (Figure 5a in Article 4), indicating that the incorporation of Al NPs into epoxy coating will enhance its properties.

From the Bode diagram shown in Figure 5b in Article 4, it is clearly visible that at high frequencies, both the epoxy resin and the epoxy resin nanocomposite with 1% Al NPs exhibit a low phase angle value. This phase angle begins to increase as the frequency decreases. At a frequency of around 100 Hz, the phase angle for both samples decreases, but in the nanocomposite with 1% Al NP, the phase angle starts to increase again toward lower frequencies, down to 0.01 Hz. This increase in phase angle in the nanocomposite can be interpreted as an indicator of better protective properties compared to pure epoxy resin. Specifically, the Al NPs present in the epoxy nanocomposite provide additional resistance, which may explain the rise in phase angle at lower frequencies. It is believed that the nanoparticles within the coating matrix contribute to greater protective capacity, resulting in enhanced barrier properties and, consequently, better corrosion resistance. In contrast to epoxy resin, samples made of epoxy paint show a high value of the phase angle, approximately 90°, at higher frequencies. This value remains stable and constant up to a frequency of 100 Hz for epoxy paint, while in the case of 1% Al NP epoxy coating nanocomposite (Figure 5d in Article 4) the constancy of the phase angle extends up to 1 Hz. Such high phase angle value over wide frequency range is typical for highly protective coatings.

According to Table 4 in Article 4, the same amount of Al NP in the epoxy coating provided better corrosion protection by approximately 51.41% compared to epoxy resin. The reason for this deviation could be attributed to the presence of additives and aluminium microparticles, as

well as the superior initial corrosion resistance of pure epoxy coating. Therefore, in addition to the EIS measurement, scanning electrochemical microscopy analysis of the samples was conducted, providing a surface a representation of the coating in different shades corresponding to the electrochemical activity during 30 days of exposure in a 3.5 wt. % NaCl solution. The surface distribution of real impedance resistances on epoxy resin and 1% Al NP epoxy resin nanocomposite after 1, 15, and 30 days of exposure in a 3.5 wt. % NaCl solution is depicted in Figures 6 and 7 in Article 4. The measurements were conducted in tap water, at a frequency of 100 kHz, and on a surface area of 0.5 mm<sup>2</sup>, with the aim of monitoring changes in the capacitance of coatings. According to Figure 6 in Article 4, the impedance value distribution across the surface is observed for samples made from epoxy resin. Pure epoxy resin, as well as the sample with the addition of 1% Al NP, exhibit a homogeneous structure, as the change in impedance values across the surface is minimal. After 30 days of exposure to a 3.5% NaCl solution, the epoxy resin shows a slight decrease in resistance, from 366 kΩ to 301 kΩ. In contrast, the nanocomposite with 1% Al NP records an increase in resistance, from 506 kΩ to 654 kΩ. According to equation (1), the capacitance values of the epoxy resin and the nanocomposite with 1% Al NP epoxy resin during 30 days of exposure in a 3.5% NaCl solution are shown in Table 8.

Following equation (1), it is possible, using the relation given by the authors Monetta [151] and Deflorian [152], to calculate the percentage of the amount of water that can be absorbed during exposure to a corrosive medium. This amount of water can be estimated based on the capacity of the coating, and is calculated using the following commands:

$$\Phi_t = 100 \cdot \frac{\log \left( \frac{C_{coat,t}}{C_{coat,0}} \right)}{\log 80} \quad (2)$$

where  $\Phi_t$  is the amount of water at the time  $t$ ,  $C_{coat,t}$  is the capacitance after the time  $t$  and  $C_{coat,0}$  is the initial capacitance. Table 8 also shows the calculated values of the percentage of water for the samples prepared in epoxy resin.

Table 8. Measured  $R_{coat}$  values and calculated  $C_{coat}$  and  $\Phi_t$  values for the samples made of epoxy resin in a tap water.

days	parameters	epoxy resin	1% Al NP epoxy resin nanocomposite
1	$R_{coat}$ , kΩ	366	506
	$C_{coat}$ , F	$4.35 \cdot 10^{-10}$	$3.14 \cdot 10^{-10}$

15	$R_{\text{coat}}$ , $\text{k}\Omega$	341	597
	$C_{\text{coat}}$ , F	$4.66 \cdot 10^{-10}$	$2.66 \cdot 10^{-10}$
	$\Phi_t$ %	1.57	-
30	$R_{\text{coat}}$ , $\text{k}\Omega$	301	654
	$C_{\text{coat}}$ , F	$5.29 \cdot 10^{-10}$	$2.43 \cdot 10^{-10}$
	$\Phi_t$ %	4.46	-

Table 8 shows that the addition of Al NPs leads to an increase in the resistance of the coating, which reduces the electrolyte absorption capacity. In the epoxy resin, the volume of absorbed electrolyte increased, from 1.57% to 4.46% over a period of 30 days, indicating a significant increase in moisture absorption in the coating. On the other hand, the 1% Al NP epoxy resin nanocomposite sample shows a completely different behavior profile. This sample maintains a constant capacitance value over the same time period of 30 days, suggesting that no electrolyte absorption has occurred.

According to equations (1) and (2), Table 9 shows the values of capacitance and volume fraction of water for samples of epoxy paint and nanocomposite with 1% Al NP epoxy paint during 30 days of exposure in 3.5% NaCl solution.

Table 9. Measured  $R_{\text{coat}}$  values and calculated  $C_{\text{coat}}$  and  $\Phi_t$  values for the samples made of epoxy paint in a tap water.

days	parameters	epoxy paint	1% Al NP epoxy paint nanocomposite
1	$R_{\text{coat}}$ , $\text{k}\Omega$	670	990
	$C_{\text{coat}}$ , F	$2.38 \cdot 10^{-9}$	$1.61 \cdot 10^{-9}$
15	$R_{\text{coat}}$ , $\text{k}\Omega$	522	897
	$C_{\text{coat}}$ , F	$3.05 \cdot 10^{-9}$	$1.77 \cdot 10^{-9}$
	$\Phi_t$ %	5.66	2.16
30	$R_{\text{coat}}$ , $\text{k}\Omega$	451	793
	$C_{\text{coat}}$ , F	$3.53 \cdot 10^{-9}$	$2.00 \cdot 10^{-9}$
	$\Phi_t$ %	9.00	4.95

Table 9 shows that the resistance of the epoxy paint gradually decreases during 30 days of exposure to a corrosive environment, which is reflected in the increase in capacitance. Increased

capacitance indicates a deeper penetration of the electrolyte into the coating, which reduces the protective properties of the coating. This is additionally confirmed by the calculated percentage of the amount of absorbed electrolyte, which after 30 days is 9%. On the other hand, the nanocomposite with 1% Al NPs in epoxy paint shows significantly better corrosion resistance. During the same period of 30 days, the nanocomposite maintains an almost stable resistance value, which indicates a minimal change in capacitance and thus better protection against electrolyte penetration. The percentage of absorbed electrolyte in this sample is only 4.95%, which is significantly lower compared to pure epoxy coating. These results confirm that the addition of 1% Al NP significantly improves the resistance of the coating to electrolyte penetration and makes it more effective in preventing corrosive processes.

The Equation (1) in Article 4 calculate coating protection efficiency values for all samples. Table 5 in Article 4 confirms that the efficiency of samples of 1% Al NP epoxy resin nanocomposite increases with greater exposure to the medium, possibly indicating the beginning of oxide film formation. The distribution of real impedances on the surface of epoxy coating and 1% Al NP epoxy nanocomposite is illustrated in Figure 7 in Article 4. The addition of Al NPs to the epoxy paint increases the value of the relay impedance on the surface, thereby improves the anti-corrosion properties of the coating. According to Table 6 in Article 4, the addition of Al NPs results in a smaller increase in coating efficiency compared to samples made of epoxy resin. The pure epoxy coating exhibits higher corrosion stability than the epoxy resin coating, making electrolyte penetration more difficult and hindering the incorporation of Al NPs into the epoxy coating.

The release of Al NPs from epoxy resin, epoxy paint, and nanocomposite in simulated wastewater was measured at intervals of up to 30 days, as illustrate in Figure 8a in Article 4. The release rate of Al NPs is faster in epoxy resin than in epoxy coating. Both samples, after a certain time (10 days of exposure), show a constant mass concentration of aluminium in the wastewater. The constant value of the mass concentration of aluminium in the wastewater could be attributed to the oxidation of Al NPs on the surface of the epoxy coating, and the possibility of the release of a new Al NPs due to the formation of aluminium oxide.

The antibacterial activity of the epoxy resin, epoxy coating, 1% Al epoxy resin nanocomposite, and 1% epoxy coating nanocomposite against *P. aeruginosa* and *B. subtilis* is presented in Figure 8c and 8d in Article 4. Both nanocomposites made with epoxy resin and epoxy coating exhibited similar antibacterial effect (Table 7 in Article 4).

The metal NPs slowly release metal ions capable to punctuating holes in the bacterial cell membrane and disrupting cellular processes from inside the cell [153, 154]. The toxicity of  $Al^{3+}$  ions can lead to excessive generation of reactive oxygen species, increased peroxidation and/or breakdown of membrane lipids, and elevated levels of free radicals. These effects can result in irreparable damage to nucleic acids, proteins, membranes, and organelles, ultimately leading to the activation of cell death [155].

To summarise the discussion, Table 6 shows the main contributions of all four articles represented as well as their relevance to the doctoral thesis as a whole.

Table 10. Summary of individual contributions for presented articles (Article 1, Article 2, Article 3, and Article 4) with united scientific contribution for doctoral thesis as a whole.

<b>Main individual scientific contributions</b>			
<b>Article 1</b>	<b>Article 2</b>	<b>Article 3</b>	<b>Article 4</b>
<p>- investigate potential of Al, Ni, and Ag NP for development of epoxy nanocomposite coating with dual functionalities: anticorrosion and antibacterial protection,</p> <p>- propose an anticorrosion mechanism of action for the NPs within the epoxy coating based on existing literature and experimental findings,</p> <p>- performed detailed antibacterial characterization of all nanoparticles and nanocomposites to understand their efficacy against bacterial strains.</p>	<p>- investigate the influence of mechanical stirring on the preparation of aluminium epoxy nanocomposites,</p> <p>- study the effect of different concentration of Al NPs in epoxy coating on the properties of the nanocomposites,</p> <p>- perform detailed physical characterization of the nanocomposites in a climatic chamber to assess their stability under varying environmental conditions.</p>	<p>- investigate the influence of ultrasonic homogenization on the preparation of aluminium epoxy nanocomposites,</p> <p>- study the effect of different concentration of Al NPs in epoxy coating on the properties of the nanocomposites ,</p> <p>- perform detailed physical characterization of the nanocomposites in both humidity and climatic chamber conditions,</p> <p>- the advantages and disadvantages of using</p>	<p>- investigate the influence of Al NP in epoxy resin and epoxy coating on their properties,</p> <p>- perform detailed physical characterization of the nanocomposite in a salt chamber to assess its behavior under corrosive conditions,</p> <p>- conduct microanalysis of the transformation/degradation of the nanocomposite system surface in a corrosive medium to confirm the formation of a passive film on the coating surface,</p>



<p>- successfully develop Al and Ag epoxy nanocomposites and evaluate their performance in terms of anticorrosion and antibacterial properties.</p>		<p>mechanical and ultrasonic mixing in the preparation of nanocomposite coatings were evaluated, - microanalysis of the surface of the nanocomposite system was investigated in order to understand its behavior and changes in the corrosive medium.</p>	<p>- propose an antibacterial mechanism of action for nanoparticles within the epoxy coating based on existing literature and experimental findings.</p>
---	--	---	--

**United scientific contribution**

The epoxy nanocomposite coating described in Article 1, enhanced with Al, Ni, and Ag nanoparticles, demonstrates superior efficiency and profitability, particularly evident in the case of Al nanoparticles compared to Ni nanoparticles. Moreover, nanocomposite coatings with varying concentrations of Al nanoparticles, prepared through both mechanical stirring (Article 2) and ultrasonic homogenization (Article 3), exhibit enhanced anticorrosion properties relative to pure epoxy resin and unmodified epoxy coatings (as discussed in Article 4). The mechanism of action of Al nanoparticles within the epoxy coating (discussed in Article 3) and epoxy resin (detailed in Article 4) is scrutinized at a micro level by observing the surface transformation of the nanocomposite system over time under corrosive conditions. This microanalysis provides insights into how the incorporation of nanoparticles influences the coating's behavior and performance. Furthermore, the epoxy nanocomposite modified with Al nanoparticles in Article 1 demonstrates potential antibacterial properties against *P. aeruginosa* and *B. subtilis*, with the mechanism

elucidated in Article 4. It becomes apparent that the modification of the coating with nanoparticles depends significantly on the size, shape, and concentration of the incorporated nanoparticles, as evidenced by comparing the properties of the nanocomposite coating with unmodified counterparts. In summary, this doctoral thesis shows that adequately prepared nanocomposite Al/epoxide coatings provide enhanced corrosion and antibacterial protection to cast iron substrates and present a promising solution for protection of wastewater pipelines.

## 4. CONCLUSIONS

Nanocomposite coating as a simple and affordable method for metal protection have good prospects for wider application. The interaction and mode of action between nanoparticles and epoxy coating is explained in detail in this doctoral thesis. Three different metal nanoparticles were used to increase the anticorrosion and antibacterial properties of coating. Since the main problem is to incorporate nanoparticles inside the epoxy coating without agglomeration, two mixing methods were tested. The nanocomposite system, which showed both anticorrosive and antibacterial properties, was analyzed in detail under accelerated corrosion conditions, in pure epoxy resin, where the mechanism of action of the nanoparticles themselves was observed. Therefore, based on the conducted analyses, the following conclusions were reached:

- Electrochemical tests confirm that the addition of nanoparticles to the epoxy coating significantly increases the impedance values. Results from EIS demonstrate that Al and Ag nanoparticles embedded in nanocomposites markedly enhance anticorrosive properties and inhibit bacterial growth, while Ni NPs exhibit lower efficiency. Embedded Al and Ag nanoparticles within the epoxy coating interact with the electrolyte, creating a chemical barrier against further penetration of corrosive species and forming a passive layer on their surface. Extended exposure to a corrosive medium leads to a decrease in electrochemical resistance for Ni nanoparticles due to the absence of passive film formation, particularly in neutral media.
- Nanoparticles containing 1% Al NPs showed significant migration, but after 10 days of exposure, the wastewater reaches a constant value of aluminium concentration of 1 mg/L. Further analysis of the antibacterial activity of epoxy coatings and 1% Al, 1% Ag and 1% Ni epoxy nanocomposite against *P. aeruginosa* and *B. subtilis* reveals that the antimicrobial activity follows the order: 1% Al NP epoxy nanocomposite > 1% Ag NP epoxy nanocomposite > 1% Ni NP epoxy nanocomposite > pure epoxy coating.
- Nanocomposite samples containing up to 1% concentration of Al nanoparticles (Al NPs) were successfully dispersed within the epoxy resin and coating, exhibiting uniform distribution without agglomerates or air bubbles. This dispersion was confirmed through SEM, EDS, and SECM analyses. However, higher concentrations of nanoparticles (3% and 6%) led to agglomeration.
- The remarkable properties of Al nanoparticles, including high reactivity, the ability to form a homogeneous structure, bacterial resistance, cost-effectiveness, and limited

exploration in the literature, prompted significant interest. Consequently, Al NPs were selected for further analyses and investigations.

- Mechanical property testing of the Al NP epoxy nanocomposite, prepared via both mechanical stirring and ultrasonic homogenization methods, revealed several key findings:
  1. the addition of Al NPs induced a change in the color of the nanocomposite from red to grey,
  2. the hardness of the nanocomposite remained consistent compared to the epoxy coating, indicating that the incorporation of Al NPs did not significantly alter the material's hardness,
  3. notably, the adhesion of the nanocomposite to the cast iron substrate exhibited a remarkable increase compared to the epoxy coating alone, suggesting enhanced bonding properties attributed to the presence of Al NPs.
- Based on the conducted electrochemical impedance spectroscopy (EIS) analyses, the following observations were made regarding the resistance of the samples to aggressive media:
  1. For samples prepared by mechanical stirring and immediately immersed in the aggressive media, the sample containing 1.0% Al nanoparticles (Al NPs) initially exhibited the best resistance. However, after 240 hours in the aggressive medium, the sample containing 0.75% Al NPs demonstrated the highest resistance. Conversely, samples prepared by ultrasonic mixing consistently exhibited higher impedance values compared to those prepared by mechanical mixing.
  2. Among the samples prepared by ultrasonic mixing, the highest resistance was observed in the sample containing 1% Al NPs, which was tested by immersion in a 3.5% NaCl solution for 100 days.
- Based on the results obtained from mechanical mixing and ultrasonic mixing methods, the following observations were made regarding the anticorrosive properties and stability of the nanocomposite samples:
  1. mechanical mixing resulted in an improvement in the anticorrosive properties of the coating within a short period (10 days). However, SEM cross-section analysis revealed the presence of air bubbles within the samples, indicating potential issues with dispersion and stability. In contrast, ultrasonic mixing led to better anticorrosive properties and enhanced stability of the samples over a longer period. This

improvement can be attributed to the more effective dispersion of nanoparticles and the absence of air bubbles in the nanocomposite matrix.

2. the release of air bubbles during sample preparation was attributed to the heating of the coating, which reduced the viscosity of the liquid. As the viscosity decreased with increasing temperature, air bubbles were released more easily, potentially leading to even dispersion and increase stability of the samples.

- The embedding of nanoparticles, specifically Al NPs, within both epoxy resin and epoxy coating yields consistent mechanical, corrosion, antibacterial, and migration properties. This consistency suggests that the presence of additives within the epoxy coating, such as pigments, additives, and fillers, does not adversely affect the efficacy of the nanoparticles. In other words, the desired properties conferred by Al NPs remain unaffected and stable despite the presence of other components within the epoxy matrix. This observation underscores the robustness and versatility of Al nanoparticles as additives for enhancing the performance of epoxy-based coatings, regardless of the presence of additional ingredients.
- The SECM analysis of a 1% Al NP epoxy nanocomposite sample reveals a progressive distribution of higher impedance resistance across the surface over time. This phenomenon can be attributed to the reactivity of aluminium nanoparticles when in contact with the electrolyte. Upon contact, aluminum nanoparticles react with water molecules, as well as  $H^+$  and  $OH^-$  ions present in the electrolyte solution, initiating the formation of an oxide film on their surface. The oxide film formed is characterized by its compact nature, and the volume of oxide produced is substantial compared to that of the metal nanoparticles themselves. Consequently, as degradation progresses, the oxide film originating from the nanoparticles disperses across the surface of the epoxy coating. This dispersion of the oxide film contributes to the observed increase in impedance resistance, indicating the formation of a protective layer that enhances the coating's corrosion resistance over time.
- The nanoparticles embedded within the epoxy coating have the potential to undergo slow and continuous release from the surface. This release process may involve cell penetration, as well as adsorption or diffusion of nanoparticles on the cell surface, which often serves as the initial step in the stages leading to microbial cell inhibition. In particular, the toxicity of aluminum ions ( $Al^{3+}$ ) can induce the excessive formation of reactive oxygen species (ROS), which play a significant role in causing DNA damage in bacterial cells. The presence of ROS can disrupt cellular processes and lead to

irreparable damage to nucleic acids, proteins, membranes, and organelles within the bacterial cell. As a result, the antibacterial properties of the epoxy coating, attributed to the release of nanoparticles and subsequent generation of ROS, contribute to the inhibition of microbial growth.

## 5. BIBLIOGRAPHY

- [1] M. Sykora, K. Kreislova, P. Pokorny, Corrosion of historic grey cast irons: indicative rates, significance, and protection, *Int. J. Comp. Meth. And Exp. Meas.* 8 (2020) 162-174.
- [2] B. Wei, J. Xu, C. Sun, Y. F. Chen, Internal microbiologically influenced corrosion of natural gas pipelines: A critical review, *J. Nat. Gas Sci. Eng.* 102 (2022) 104581.
- [3] G. Zhang, B. Li, J. Liu, M. Luan, L. Yue, X. T. Jiang, K. Yu, Y. Guan, The bacterial community significantly promotes cast iron corrosion in reclaimed wastewater distribution system, *Microbiome* 6 (2018) 1-18.
- [4] D. J. Blackwood, An Electrochemist Perspective of Microbiologically Influenced Corrosion, *Corros. Mater. Degrad.* 1 (2018) 59-76.
- [5] M. Lv, M. Du, A review: microbiologically influenced corrosion and the effect of cathodic polarization on typical bacteria, *Rev. Environ. Sci. Biotechnol.* 17 (2018) 431-446.
- [6] P. Khodaei, M. Shabani-Nooshabadi, M. Behpour, Epoxy-Based nanocomposite coating reinforced by a zeolite complex: Its anticorrosion properties on mild steel in 3.5 wt% NaCl media, *Prog. Org. Coatings* 136 (2019) 105254.
- [7] M. Wang, J. Wang, W. Hu, Preparation and corrosion behavior of Cu-8-HQ@HNTs/epoxy coating, *Prog. Org. Coat.* 139 (2020) 105434.
- [8] S. Kargozar, M. Mozafari, Nanotechnology and Nanomedicine: Start small, think big, *Mater. Today Proc.* 5 (2018) 15492-15500.
- [9] J. F. Wansah, A. E. Udounwa, A. D. Ahmed, A. A. Essiett, E. U. Jackson, Application of Nanotechnology in The Corrosion Protection of Steel Oil Pipes, *Heal. Environ.* (2014) 103-111.
- [10] S. Harsimran, K. Santosh, K. Rakesh, Overview of corrosion and its control: a critical review, *Proc. Eng. Sci.* 3 (2021) 13-24.

- [11] M. Aliofkhaezrai, Developments in Corrosion Protections, u A. Popoola, OE olorunniwo, OO. Ige, Corrosion Resistance Through the application of anti-corrosion coatings, IntechOpen, London, 2014, p. 241.
- [12] S. Foorginezhad, M. Mohseni-Dargah, K. Firoozirad, V. Aryai, A. Razmjou, R. Abbassi, V. Garaniya, A. Behesti, M. Asadnia, Recent advances in sensing and assessment of corrosion in sewage pipelines, *Process Saf. Environ. Prot.* 147 (2021) 192-213.
- [13] M. E. Orazem, Underground pipeline corrosion Detection, analysis, and prevention, Woodhead Publishing, Cambridge, 2014.
- [14] L. Osborn, M. Najafi, Pipelines 2007: Advances and experiences with trenchless pipeline protects, u A. E. Romer, P. J. Passaro, Risk Management and Pipeline Safety Committee Presentation, American Society of Civil Engineers, Reston, 2007, 1-8.
- [15] R. Singh, Applied welding engineering processes, code, and standards: Cast iron and cast steel, Elsevier, London, 2020, p. 61-76.
- [16] D. Gross, C. Ancel, L. Gulielmi, Fatigue design and safety factor for scroll compressor wraps. Woodhead Publishing Limited, 2013, p. 12-15.
- [17] ASM Handbook, Properties and Selection: Irons, Steels, and High-Performance Alloys, u D. M. Stefanescu, Classification and Basic Metallurgy of Cast Iron. Vol. 1, ASM International, Materials Park, 1990, p. 3-11.
- [18] R. E. Melchers, Post-perforation external corrosion of cast iron pressurised water mains, *Corros. Eng. Sci. Technol.* 52 (2017) 514-546.
- [19] M. Samardžija, M. Kurtela, M. Vuković Domanovac, V. Alar, Anticorrosion, and antibacterial properties of Al NP – epoxy nanocomposite coating on grey cast iron, *Coatings* (2023) 898.
- [20] A. R. Riahi, A. T. Alpas, Wear map for grey cast iron, *Wear* 255 (2003) 401-409.
- [21] T. A. Jur, J. I. Middleton, A. A. Yurko, R. L. Windham, and J. R. Grey, Case studies in graphitic corrosion of cast iron pipe, *J. Fail. Anal. Prev.* 21 (2021) 376-386.



- [22] B. Glisic, Sensing solutions for assessing and monitoring pipeline systems. Vol. 1. Woodhead Publishing Limited, Cambridge, 2014, p. 422-460.
- [23] A. P. Teixeira, C. Guedes Soares, T. A. Netto, S. F. Estefen, Reliability of pipelines with corrosion defects, *Int. J. Press. Vessel. Pip.* 85 (2008) 228-237.
- [24] FIDON, Elaborat zaštite okoliša za ocjenu o potrebi procjene utjecaja na okoliš za zahvat: Magistralni vodoopskrbni cjevovod od vodocrpilišta kosnica do spoja na 4. Etapu radničke ceste, Grad Zagreb i Zagrebačka županija, Zagreb, 2022.
- [25] Hrvatske vode, Izvješće o izvršenju plana upravljanja vodama za 2019. godinu, Zagreb, 2020.
- [26] Hrvatske vode, Izvješće o izvršenju plana upravljanja vodama za 2020. godinu, Zagreb, 2021.
- [27] Hrvatske vode, Izvješće o izvršenju plana upravljanja vodama za 2021. godinu, Zagreb, 2022.
- [28] Hrvatske vode, Izvješće o izvršenju plana upravljanja vodama za 2022. godinu, Zagreb, 2023.
- [29] Hrvatske vode, Druge izmjene i dopune plana upravljanja vodama za 2023. godinu, Zagreb, 2023.
- [30] T. Angkasuwansiri, V. Tech, S. K. Sinha, Comprehensive list of parameters affecting wastewater pipe performance, *Technol. Interface Int. J.* 13(2013) 68-79.
- [31] M. Samardžija, F. Kapor, V. Alar, M. Kurtela, Metode analize ispitivanja epoksidnih prevlaka, 26. Međunarodno savjetovanje o zaštiti materijala i industrijskom finišu, Zagreb (2024) 108-119.
- [32] L. Perelomov, O. Sizova, M. M. Rahman, I. Perelomova, T. Minkina, S. Sokolov, Y. Atroshchenko, Metal-tolerant bacteria of wastewater treatment plant in a large city, *Sustain.* 14 (2022) 1-11.
- [33] M. Beuk, G. Graovac, Ž. Korica, Z. Vranar, A. C. Thavenet, Đ. Požgaj, Izvješće o podacima iz Registra onečišćavanja okoliša za 2019. godinu, Republika Hrvatska Ministarstvo gospodarstva i održivog razvoja, Zagreb, 2020.

- [34] M. Beuk, G. Graovac, Ž. Korica, Z. Vranar, A. C. Thavenet, Đ. Požgaj, Izvješće o podacima iz Registra onečišćavanja okoliša za 2020. godinu, Republika Hrvatska Ministarstvo gospodarstva i održivog razvoja, Zagreb, 2021.
- [35] M. Beuk, G. Graovac, Ž. Korica, Z. Vranar, A. C. Thavenet, Đ. Požgaj, Izvješće o podacima iz Registra onečišćavanja okoliša za 2021. godinu, Republika Hrvatska Ministarstvo gospodarstva i održivog razvoja, Zagreb, 2022.
- [36] M. Beuk, G. Graovac, Ž. Korica, Z. Vranar, A. C. Thavenet, Đ. Požgaj, Izvješće o podacima iz Registra onečišćavanja okoliša za 2022. godinu, Republika Hrvatska Ministarstvo gospodarstva i održivog razvoja, Zagreb, 2023.
- [37] E. V. Moskvicheva, P. A. Sidyakin, D. V. Shitov, Method of corrosion prevention in steel pressure pipelines in sewerage systems, *Procedia Eng.* 150 (2016) 2381-2386.
- [38] M. Kutz, Handbook of environmental degradation of materials u S. Brossia, Corrosion of pipes in drinking water systems, Elsevier, Amsterdam, 2018, p. 1-9.
- [39] D. Misiunas, Failure Monitoring and Asset Condition Assessment in Water Supply Systems, Doctoral Thesis, Lund Institute of Technology, 2005.
- [40] C. I. Ossai, B. Boswell, I. J. Davies, Pipeline failures in corrosive environments- A conceptual analysis of trends and effects, *Eng. Fail. Anal.* 53 (2015) 36-58.
- [41] S. Adair, E. Ajuong, R. akid, M. G., Alvarez, H. Alves, A. Anderko, V. Ashworth, C. Atkins, Shreir's Corrosion u A. Reynaud, Corrosion of cast iron. Vol. 3, Elsevier, Amsterdam, 2010, p. 1737-1788.
- [42] C. Nejneru, M. Cristina Perju, D. Doru Burduhos Nergis, A. Victor Sandu, C. Bejinariu, Galvanic corrosion behaviour of phosphate nodular cast iron in different types of residual waters and couplings, *Rev. Chim.* 70 (2019) 3597-3602.
- [43] [R. Logan, M. J. Mulheron, D. A. Jesson, Graphitic corrosion of a cast iron trunk main: Implications for asset management, *WIT Trans. Built Environ.* 139 (2016) 411-422.
- [44] A. Agala, M. Khan, A. Starr, Degradation mechanisms associated with metal pipes and the effective impact of LDMs and LLMs in water transport and distribution, *Proc. Inst. Mech. Eng. Part C J. Mech. Eng. Sci.* 237 (2023) 1855-1876.

- [45] V. S. Liduino, J. C. Payão Filho, C. Cravo-Laureau, M. T. Lutterbach, E. F. Camporese Sérvulo, Comparison of flow regimes on biocorrosion of steel pipe weldments: Fluid characterization and pitting analysis, *Int. Biodeterior. Biodegrad.* 144 (2019) 104750.
- [46] C. A. Loto, Microbiological corrosion: mechanism, control and impact-a review, *Int. J. Adv. Manuf. Technol.* 92 (2017) 9-12.
- [47] T. Muzadzi, Microbiologically Influenced Corrosion (MIC) Mechanisms and mitigation, Doctoral Thesis, Faculty of the Russ College of Engineering and Technology of Ohio University, 2013.
- [48] B. J. Little, J. S. Lee, Microbiologically influenced corrosion: An update, *Int. Mater. Rev.* 59 (2014) 384-393.
- [49] J. Wang, G. H. Liu, J. Wang, X. Xu, Y. Shao, Q. Zhang, Y. Liu, L. Qi, H. Wang, Current status, existent problems, and coping strategy of urban drainage pipeline network in China, *Environ. Sci. Pollut. Res.* 28 (2021) 43035-43049.
- [50] H. Sun, B. Shi, D. A. Lytle, Y. Bai, D. Wang, Formation and release behavior of iron corrosion products under the influence of bacterial communities in a simulated water distribution system, *Environ. Sci. Process. Impacts* 16 (2014) 576-585.
- [51] M. Cyprowski, A. Stobnicka-Kupiec, A. Ławniczek-Wałczyk, A. Bakal-Kijek, M. Gołofit-Szymczak, R. L. Górny, Anaerobic bacteria in wastewater treatment plant, *Int. Arch. Occup. Environ. Health* 91 (2018) 571-579.
- [52] N. Høiby, O. Ciofu, H. K. Johansen, Z. Song, C. Moser, P. Ø. Jensen, S. Molin, M. Givskov, T. Tolker-Nielsen, T. Bjarnsholt, The clinical impact of bacterial biofilms, *Int. J. Oral Sci.* 3 (2011) 55-65.
- [53] K. Maji, M. Lavanya, Microbiologically Influenced Corrosion in Stainless Steel by *Pseudomonas aeruginosa*: An Overview, *J. Bio-Tribo-Corros* 10 (2014) 1–18.
- [54] P. Vuong, A. McKinley, P. Kaur, Understanding biofouling and contaminant accretion on submerged marine structures, *npj Mater. Degrad.* 7 (2023) 1–11.
- [55] H. Li, D. Xu, Y. Li, H. Feng, Z. Liu, X. Li, T. Gu, K. Yang, Extracellular electron transfer is a bottleneck in the microbiologically influenced corrosion of C1018 Carbon

- steel by the biofilm of sulfate-reducing bacterium *Desulfovibrio vulgaris*, PLOS One 10 (2015) 1-12.
- [56] S. Chitra, B. Anand, R. Vaidyanathan, V. Balasubramanian, A Review on microbial mediated corrosion on mild steel by inactivating the extracellular polysaccharide secreted by aerobic/anaerobic microorganism, Chem. Sci. Rev. Lett. 3 (2014) 56-62.
- [57] J. Jin, G. Wu, Z. Zhang, Y. Guan, Effect of extracellular polymeric substances on corrosion of cast iron in the reclaimed wastewater, Bioresour. Technol. 165 (2014) 162-165.
- [58] E. Hamzah, M. F. Hussain, Z. Ibrahim, A. Abdolahi, Corrosion behavior of carbon steel in sea water medium in presence of *P. aeruginosa* bacteria, Arab. J. Sci. Eng. 39 (2014) 6863-6870.
- [59] P. M. Visakh, C. Della Pina, E. Fallatta, Polyaniline blends, composites, and nanocomposites, u S. Thambidurai, K. Pandiselvi, Polyaniline/natural polymer composites and nanocomposites. Elsevier, Amsterdam, 2017, p. 235-256.
- [60] Y. Wang, R. Zhang, J. Duan, X. Shi, Y. Zhang, F. Guan, W. Sand, B. Hou, Extracellular polymeric substances and biocorrosion/biofouling: Recent advances and future perspectives, Int. J. Mol. Sci. 23 (2022) 5566.
- [61] J. P. Busalmen, M Vázquez, S.R de Sánchez, New evidence on the catalase mechanism of microbial corrosion, Electrochim. Acta 47 (2002) 1857-1865.
- [62] I. Eshi, Z. Dugi, tehnologija tzaštite od korozije, Školska knjiga, Zagreb, 1990.
- [63] R. Bertani, A. Bartolozzi, A. Pontefisso, M. Quaresimin, M. Zappalorto, Improving the antimicrobial and mechanical properties of epoxy resins via nanomodification: An overview, Molecules 26 (2021) 1-24.
- [64] H. Yuan, F. Qi, N. Zhao, P. Wan, B. Zhang, H. Xiong, B. Liao, X. Ouyang, Graphene oxide decorated with titanium nanoparticles to reinforce the anti-corrosion performance of epoxy coating, Coatings 10 (2020) 10020129.
- [65] V. J. Mohanraj, Y. Chen, Nanoparticles – a review, Trop. J. Pharm. Res. 5 (2006) 561-573.

- [66] I. Khan, K. Saeed, I. Khan, Nanoparticles: Properties, applications, and toxicities, *Arab. J. Chem.* 12 (2019) 908-931.
- [67] S. Bayda, M. Adeel, T. Tuccinardi, M. Cordani, F. Rizzolio, The history of nanoscience and nanotechnology: From chemical-physical applications to nanomedicine, *Molecules* 25 (2020) 1-15.
- [68] N. Joudeh, D. Linke, Nanoparticle classification, physicochemical properties, characterization, and applications: a comprehensive review for biologists, *J. Nanobiotechnology* 20 (2022) 1-29.
- [69] H. Yao, L. Li, W. Li, D. Qi, W. Fu, N. Wang, Application of nanomaterials in waterborne coatings: A review, *Resour. Chem. Mater.* 1 (2022) 184-200.
- [70] M. Rai, R. Shegokar, Metal Nanoparticles in Pharma, u A. Brandelli, A. C. Ritter, F. F. Veras, *Antimicrobial Activities of Metal Nanoparticles*, Springer Link, 2017, p. 337-363.
- [71] P. G. Jamkhande, N. W. Ghule, A. H. Bamer, M. G. Kalaskar, Metal nanoparticles synthesis: An overview on methods of preparation, advantages and disadvantages, and applications, *J. Drug Deliv. Sci. Technol.* 53 (2019) 101174.
- [72] X. Shi, T. A. Nguyen, Z. Suo, Y. Liu, R. Avci, Effect of nanoparticles on the anticorrosion and mechanical properties of epoxy coating, *Surf. Coatings Technol.* 204 (2009) 237-245.
- [73] S. Pourhashem, F. Saba, J. Duan, A. Rashidi, Polymer/inorganic nanocomposite coatings with superior corrosion protection performance: A review, *J. Ind. Eng. Chem.* 88 (2020) 29-57.
- [74] URL: <https://www.webofscience.com/wos/woscc/basic-search> (access 10.9.2024.)
- [75] A. M. El Saeed, M- Adb El-Fattah, A. M. Azzam, M. M. Datdir, M. M. Badr, Synthesis of cuprous oxide epoxy nanocomposite as an environmentally antimicrobial coating, *Int. J. Biol. Macromol.* 89 (2016) 190–197.
- [76] D. Sebastian, C. Yao, L. nipa, I. Lian, G. Twu, Corrosion Behavior and Mechanical Properties of a Nanocomposite Superhydrophobic Coating, *Coatings* 11 (2021) 652.

- [77] M. A. Alam, U. A. Samad, E-S. M. Sherif, A. M. Poulouse, J. A. Mohammed, N. Alharthi, A. M. Al-Zahrani, Influence of SiO<sub>2</sub> content and exposure periods on the anticorrosion behavior of epoxy nanocomposite coatings, *Coatings* 10 (2020) 118.
- [78] H. K. Talabi, B. O. Adewuyi, O. Olaniran, P. O. Ayekusibe, Reinforcement efficiency of copper nanoparticles on epoxy matrix bactericide composite, *J. Chem. Technol. Metall.* 56 (2021) 321-326.
- [79] A. Kocijan, M. Conradi, M. Hočevár, The influence of surface wettability and topography on the bioactivity of TiO<sub>2</sub>/epoxy coatings on AISI 316L stainless steel, *Materials* 12 (2019) 1877.
- [80] A. M. Kumar, A. Khan, R. Suleiman, M. Qamar, S. Saravanan, H. Dafalla, Bifunctional CuO/TiO<sub>2</sub> nanocomposite as nanofiller for improved corrosion resistance and antibacterial protection, *Prog. Org. Coat.* 114 (2017) 9-18.
- [81] M. Apsak, A. Akdemir, F. Karabork, S. Yazman, Investigation effect of zinc nanoparticles on the mechanical and anticorrosion properties of epoxy coatings on stainless steel surface, *Gazi Univ. J. Sci.* 34 (2021) 864-877.
- [82] S. Amirsoleimani, H. R. Ghorbani, Preparation of antibacterial coating film using ZnO nanoparticles and epoxy resin, *J. Nanoanalysis* 7 (2020) 96-103.
- [83] W. Shen, T. Zhang, Y. Ge, L. Feng, H. Feng, P. Li, Multifunctional AgO/epoxy nanocomposites with enhanced mechanical, anticorrosion and bactericidal properties, *Prog. Org. Coat.* 152 (2021) 106130.
- [84] R. Manjumeena, R. Venkatesan, D. Duraibabu, J. Sudha, N. Rajendran, P. T. Kalaichelvan, Green nanosilver as reinforcing eco-friendly additive to epoxy coating for augmented anticorrosive and antimicrobial behavior, *Silicon* 8 (2016) 277-298.
- [85] P. A. Prashanth, R. S. Raveendra, R. H. Krishna, S. Ananda, N. P. Bhagya, B. M. Nagabhushana, K. Lingaraju, H. R. Naika, Synthesis, characterizations, antibacterial and photoluminescence studies of solution combustion-derived  $\alpha$ -Al<sub>2</sub>O<sub>3</sub> nanoparticles, *J. Asian Ceram. Soc.* 3 (2015) 345-351.
- [86] M. A. Deyab, Anticorrosion properties of nanocomposites coatings: A critical review, *J. Mol. Liq.* 313 (2020) 113533.

- [87] S. S. Mohapatra, S. Ranjan, N. Dasgupta, R. K. Mishra, S. Thomas, Applications of Targeted Nano Drugs and Delivery Systems: Nanoscience and Nanotechnology in Drug Delivery (Micro and Nano Technologies) u A. Singer, Z. Barakat, S. Mohapatra, S. S. Mohapatra, Nanoscale drug-delivery systems: in vitro and in vivo characterization, Elsevier, Amsterdam, 2019, p. 395-419.
- [88] A. Mathiazhagan, R. Joseph, Nanotechnology-a new prospective in organic coating – review, *Int. J. Chem. Eng. Appl.* 2 (2011) 225-237.
- [89] M. A. Megahed, A. A. Megahed, H. E. M. Sallam, U. A. Khashaba, Ultrasonic mixing of nanoparticles in epoxy resin, *Int. Conf. on Nano-Technology for Green and Sustainable Construction*, (2022) 1-10.
- [90] I. Gosens, J. A. Post, L. JJ de la Fonteyne, E. HJM Jansen, J. W. Geus, F. R. Cassee, W. H. de Jong, Impact of agglomeration state of nano- and submicron sized gold particles on pulmonary inflammation, *Part. Fibre Toxicol.* 7 (2010) 1-11.
- [91] J. R. Xavier, Electrochemical, mechanical, and adhesive properties of surface modified NiO-epoxy nanocomposite coatings on mild steel, *Mater. Sci. Eng. B Solid-State Mater. Adv. Technol.* 260 (2019) 114639.
- [92] S. Sumitomo, H. Koizumi, M. A. Uddin, Y. Kato, Comparison of dispersion behavior of agglomerated particles in liquid between ultrasonic irradiation and mechanical stirring, *Ultrason. Sonochem.* 40 (2017) 833-831.
- [93] B. Bittmann, F. Hauptert, A. K. Schlarb, Ultrasonic dispersion of inorganic nanoparticles in epoxy resin, *Ultrason. Sonochem.* 15 (2009) 622-628.
- [94] B. Ramezanzadeh, M. M. Attar, M. Farzam, A study on the anticorrosion performance of the epoxy-polyamide nanocomposites containing ZnO nanoparticles, *Prog. Org. Coat.* 72 (2011) 410-422.
- [95] L. Xue, L. Xu, Q. Li, Effect of nano Al pigment on the anticorrosive performance of waterborne epoxy coatings. *J. Mater. Sci. Technol.* 23 (2007) 563–567.
- [96] D. Saber, A. H. Alghtanib, E. M. Ahmedc, B. F. Felemban, H. T. Alib, M. Megahedd, K. A. El-Aziz, Enhancement of barrier and mechanical performance of steel coated with epoxy filled with micron and nano alumina fillers, *Mater. Res.* 25 (2022) 1-11.

- [97] M. B. Etsuyankpa, I. Hassan, S. T. Musa, J. T. Mathew, E. Y. Shaba, A. Andrew, A. I. Muhammad, K. T. Muhannad, N. A. Jibrin, M. K. Abubakar, J. Maurice, J. Hussaini, A. Mamman, Comprehensive review of recent advances in nanoparticle-based corrosion inhibition approaches, *J. Appl. Sci. Environ. Manage.* 28 (2024) 2269-2286.
- [98] C. Qi, C. E. Weinell, K. Dam-Johansen, H. Wu, Assessment of anticorrosion performance of zinc-rich epoxy coatings added with zinc fibers for corrosion protection of steel, *ACS Omega* 8 (2022) 1912-1922.
- [99] Y. Liang, F. C. Liu, M. Nie, S. Zhao, J. Lin, E. H. Han, Influence of Nano-Al Concentrates on the Corrosion Resistance of Epoxy Coatings. *J. Mater. Sci. Technol.* 29 (2013) 353–358.
- [100] B. Fan, J. Yang, L. Cao, X. Wang, J. li, y. Yang, Q. Wang, P. Zhang, F. Vogel, W. Li, Z. Lin, Revealing the impact of micro-sio2 filler content on the anti-corrosion performance of water-borne epoxy resin, *Polymers* 15 (2023) 3273.
- [101] K. S. Khashan, G. M. Sulaiman, A. H. Hamad, F. A. Abdulameer, A. Hadi, Generation of NiO nanoparticles via pulsed laser ablation in deionised water and their antibacterial activity, *Appl. Phys. A Mater. Sci. Process.* 123 (2017) 1-10.
- [102] A. K. Chatterjee, R. Chakraborty, T. Basu, Mechanism of antibacterial activity of copper nanoparticles, *Nanotechnology* 25 (2014) 135101.
- [103] R. Rawashdeh, Y. Haik, Antibacterial mechanisms of metallic nanoparticles: a review, *Dyn. Biochem. Process Biotechnol. Mol. Biol.* 3 (2009) 12-20.
- [104] I. X. Yin, J. Zhang, I. S. Zhao, M. L. Mei, Q. Li, C. H. Chu, The antibacterial mechanism of silver nanoparticles and its application in dentistry, *Int. J. Nanomedicine* 15 (2020) 2555-2562.
- [105] E. Ukpong, J. Udechukwu, Analysis of coliform bacteria in WSPs at ALSCON using macconkey broth and locally made solution, *Glob. J. Eng. Res.* 13 (2015) 21-34.
- [106] D. Manyasree, P. Kiranmayi P., R. V. S. S. N. Ravi Kumar, Synthesis, characterization and antibacterial activity of aluminium oxide nanoparticles, *Int. J. Pharm. Pharm. Sci.* 10 (2018) 1-4.



- [107] P. Saravanan, K. Jayamoorthy, S. Ananda Kumar, Design and characterization of non-toxic nano-hybrid coatings for corrosion and fouling resistance, *J. Sci. Adv. Mater. Devices* 1 (2016) 367-378.
- [108] A. J. Bard, F. R. F. Fan, J. Kwak, O. Lev, Scanning electrochemical microscopy. Introduction and principles, *Anal. Chem.* 61 (1989) 132-138.
- [109] J. J. Santana, J. Izquierdo, R. M. Souto, Uses of scanning electrochemical microscopy (SECM) for the characterization with spatial and chemical resolution of thin surface layers and coating systems applied on metals: A review, *Coatings* 12 (2022) 637.
- [110] S. S. Jamali, Developing scanning electrochemical microscopy method for studying bio-corrosion of magnesium alloys and protective surface treatments, Doctor of Philosophy thesis, Intelligent Polymer Research Institute, University of Wollongong, 2016.
- [111] M. Etienne, A. Schulte, W. Schuhmann, High resolution constant-distance mode alternating current scanning electrochemical microscopy (AC-SECM), *Electrochem. commun.* 6 (2004) 288-293.
- [112] K. Eckhard, W. Schuhmann, Alternating current techniques in scanning electrochemical microscopy (AC-SECM), *Analyst* 133 (2008) 1486-1497.
- [113] S. R. Catarelli, D. Lonsdale, L. Cheng, J. Syzdek, M. Doeff, Intermittent contact alternating current scanning electrochemical microscopy: A method for mapping conductivities in solid Li ion conducting electrolyte samples, *Front. Energy Res.* 4 (2016) 1-8.
- [114] S. Farrokhpay, Application of spectroscopy and microscopy techniques in surface coatings evaluation: A review, *Appl. Spectrosc. Rev.* 47 (2012) 233-243.
- [115] J. R. Xavier, R. Nallaiyan, Application of EIS and SECM studies for investigation of anticorrosion properties of epoxy coatings containing ZrO<sub>2</sub> nanoparticles on mild steel in 3.5% NaCl solution, *J. Fail. Anal. Prev.* 16 (2016) 1082-1091

- [116] J. R. Xavier, T. Nishimura, Evaluation of the corrosion protection performance of epoxy coatings containing Mg nanoparticle on carbon steel in 0.1 M NaCl solution by SECM and EIS techniques, *J. Coatings Technol. Res.* 14 (2017) 395-406.
- [117] J. R. Xavier, Investigation on the effect of nano-ceria on the epoxy coatings for corrosion protection of mild steel in natural seawater,” *Anti-Corros. Methods Mater.* 65 (2018) 38-45.
- [118] X. J. Raj, T. Nishimura, Electrochemical investigation into the effect of nano-titania on the protective properties of epoxy coatings on mild steel in natural seawater, *Int. J. Petrochemical Sci. Eng.* 2 (2017) 29-37.
- [119] A. Madhankumar, N. Rajendran, T. Nishimura, Influence of Si nanoparticles on the electrochemical behavior of organic coatings on carbon steel in chloride environment, *J Coat Technol Res* 9 (2012) 609-620.
- [120] D. H. Xia, J. Wang, Z. Wu, Z. Qin, L. Xu, W. Hu, Y. Behnamian, J. L. Luo, Sensing corrosion within an artificial defect in organic coating using SECM,” *Sens. Actuators B: Chem.* 280 (2018) 235-242.
- [121] W. Wang, L. Xu, H. Sun, X. Li, S. Zhao, W. Zhang, Spatial resolution comparison of AC-SECM with SECM and their characterization of self-healing performance of hexamethylene diisocyanate trimer microcapsule coatings, *J. Mater. Chem. A* 3 (2015) 5599-5607.
- [122] M. A. Deybab, M. M. Alghamdi, A. A. El-Zahhar, O. A. A. El-Shamy, Advantages of CoS<sub>2</sub> nano-particles on the corrosion resistance and adhesiveness of epoxy coatings, *Sci Rep* 14 (2024) 14684.
- [123] T. V. Nguyen, V. D. Truc, T. A. Nguyen, D. L. Tran, Synergistic effect of oxide nanoparticles and inorganic inhibitor on anti-corrosion performance of epoxy coating, *ACMM* 71 (2024) 225–240.
- [124] L. Xue, L. Xu, Q. Li, Effect of nano Al pigment on the anticorrosive performance of waterborne epoxy coatings. *J. Mater. Sci. Technol.* 23 (2007) 563–567.
- [125] F. Deflorian, L. Fedrizzi, S. Rossi, P.L. Bonora, Organic coating capacitance measurement by EIS: ideal and actual trends, *Electrochim. Acta* 44 (1999) 424–4249.

- [126] P. Jain, B. Patidar, J. Bhawsar, Potential of nanoparticles as a corrosion inhibitor: A review, *J. Bio- Tribo-Corrosion* 6 (2020) 1-12.
- [127] V. J. Keast, Atmospheric corrosion of silver and silver nanoparticles, *Corros. Mater. Degrad.* 3 (2022) 221-234.
- [128] A. J. Betts, D. P. Dowling, M. L. McConnell, C. Pope, The influence of platinum on the performance of silver–platinum anti-bacterial coatings, *Mater. Des.* 26 (2005) 217–222.
- [129] E. S. Skilbred, Corrosion of Nickel-Aluminium Bronze - How does the different alloying elements effect the corrosion properties?, M. Sc. Thesis, NTNU, 2016.
- [130] M. Fousova, V. Valesova, D. Vojtech, Corrosion of 3D-Printed AlSi9Cu3Fe Alloy, *Manuf. Technol.* 19 (2019) 29–36.
- [131] G. Pavapootanont, P. Wongpanya, E. Vianit, G. Lothongkum, Corrosion behavior of Ni steels in aerated 3.5-wt. % NaCl solution at 25°C by potentiodynamic method, *Eng. J.* 22 (2018) 1-12.
- [132] B. Feichtenschlager, S. Pabosch, J. Svehla, H. Peterlik, M. Sajjad, T. Koch, G. Kickelbick, Epoxy resin nanocomposites: the influence of interface modification on the dispersion structure—a small-angle-x-ray-scattering study, *Surfaces* 3 (2020) 664-682.
- [133] S. Bordbar, M. Rezaeizadeh, A. Kavian, Improving thermal conductivity and corrosion resistance of polyurea coating on internal tubes of gas heater by nano silver, *Prog. Org. Coat.* 146 (2020) 105722.
- [134] M. Ozdal, S. Gurkok, Recent advances in nanoparticles as antibacterial agent,” *ADMET & DMPK* 10 (2022) 115-129.
- [135] F. A. Z. Sayed, N. G. Eissa, Y. Shen, D. A. Hunstad, K. L. Wooley, M. Elsbahy, Morphologic design of nanostructures for enhanced antimicrobial activity, *J. Nanobiotechnology* 20 (2022) 1-18.
- [136] J. Y. Cheon, S. J. Kim, Y. H. Rhee, O. H. Kwon, W. H. Park, Shape-dependent antimicrobial activities of silver nanoparticles, *Int. J. Nanomedicine* 14 (2019) 2773-2780.

- [137] R. G. Chaudhary, J. A. Tanna, N. V. Gandhare, A. R. Rai, H. D. Juneja, Synthesis of nickel nanoparticles: Microscopic investigation, an efficient catalyst and effective antibacterial activity, *Adv. Mater. Lett.* 6 (2015) 990-998.
- [138] A. Hussain, M. N. Ahmad, F. Jalal, M. Yameen, S. Falak, S. Noreen, S. Naz, A. Nazir, S. Iftikhar, G. A. Soomro, M. Iqbal, Investigating the antibacterial activity of POMA nanocomposites, *Polish J. Environ. Stud* 28 (2019) 4191-4198.
- [139] B. Khalandi, N. Asadi, M. Milani, S. Davaran, A. J. N. Abadi, E. Abasi, A. Akbarzadeh, A review on potential role of silver nanoparticles and possible mechanisms of their actions on bacteria, *Drug Res. (Stuttg)* 67 (2017) 70-76.
- [140] T. Nguyen, B. Pellegrin, C. Bernard, X. Gu, J. M. Gorham, P. Stutzman, D. Stanley, A. Shapiro, E. Byrd, R. Hettenhouser, J. Chin, Fate of nanoparticles during life cycle of polymer nanocomposites, *J. Phys. Conf. Ser.* 304 (2011) 012060
- [141] M. Carbone, D. T. Donia, G. Sabbatella, R. Antiochia, Silver nanoparticles in polymeric matrices for fresh food packaging, *J. King Saud Univ. - Sci.* 28 (2016) 273-279.
- [142] ISO 22196:2007. Plastics — Measurement of antibacterial activity on plastics surfaces, International Organization for Standardization: Geneva, Switzerland, 2007.
- [143] S. A. Bello, J. O. Agunsoye, J. A. Adebisi, S. B. Hassan, Effect of aluminium particles on mechanical and morphological properties of epoxy nanocomposites, *Acta Period. Technol.* 48 (2017) 25-38.
- [144] P. Buaphuen, P. Tongpon, W. Vittayakorn, Effect of Surface Modification on Corrosion Resistance, Mechanical and Electrical Properties of Epoxy Resin-Based Nanocomposites, *Integr Ferroelectr* 238 (2023) 25–38.
- [145] H. Gong, Y. Song, G. Liang Li, G. Xie, J. Luo, A highly tough and ultralow friction resin nanocomposite with crosslinkable polymer-encapsulated nanoparticles, *Compos. Part B* 197 (2020) 108157.
- [146] B. Feichtenschlager, S. Pabisch, J. Svehla, H. Peterlik, M. Sajjad, T. Koch, G. Kickelbick, Epoxy Resin Nanocomposites: The Influence of Interface Modification on the Dispersion Structure—A Small-Angle-X-ray-Scattering Study, *Surfaces* 3 (2020) 664–682.

- [147] Y. Zare, Study of nanoparticles aggregation/agglomeration in polymer particulate nanocomposites by mechanical properties, *Compos. Part A Appl. Sci. Manuf.* 84 (2016) 158-164.
- [148] A. Trentin, A. Pakseresht, A. Duran, Y. Castro, D. Galusek, Electrochemical characterization of polymeric coatings for corrosion protection: A review of advances and perspectives, *Polymers* 14 (2022) 2306.
- [149] S. Niroumandrad, M. Rostami, B. Ramezanzadeh, Effects of combined surface treatments of aluminium nanoparticle on its corrosion resistance before and after inclusion into an epoxy coating. *Prog. Org. Coat.* 101 (2016) 486–501.
- [150] A. C. Lazanas, M. I. Prodromidis, Electrochemical Impedance Spectroscopy—A Tutorial. *ACS Meas. Sci. Au.* 3 (2023) 162–193.
- [151] T. Monetta, F. Belluci, L. Nicodemo, L. Nicolais, Protective properties of epoxy-based organic coatings on mild steel, *Prog. Org. Coat.* 21 (1993) 353–369.
- [152] F. Deflorian, L. Fedrizzi, S. Rossi, P. L. Bonora, Organic coating capacitance measurement by EIS: ideal and actual trends, *Electrochim. Acta* 44 (1999) 4243–4249.
- [153] N. Doskocz, K. Affek, M. Załęska-Radziwiłł, Effects of aluminium oxide nanoparticles on bacterial growth, *E3S Web Conf.* 17 (2017) 1-17.
- [154] S. V. Gudkov, D. E. Burmistrov, V. V. Smirnova, A. A. Semenova, A. B. Lisitsyn, “A mini review of antibacterial properties of Al<sub>2</sub>O<sub>3</sub> nanoparticles, *Nanomaterials* 12 (2022) 1-18.
- [155] L. Ponsone, A. Fabra, S. Castro, Interactive effects of acidity and aluminium on the growth, lipopolysaccharide and glutathione contents in two nodulating peanut rhizobia, *Symbiosis* 36 (2004) 193-204

## 6. ORIGINAL SCIENTIFIC PAPERS

### Article 1

M. Samardžija, I. Stojanović, M. Vuković Domanovac, V. Alar, V. Epoxy Coating Modification with Metal Nanoparticles to Improve the Anticorrosion, Migration, and Antibacterial Properties, *Coatings*, 13 (2023), 1201.

#### Author Contributions:

Marina Samardžija	conceptualization, methodology, software, validation, formal analysis, investigation, data curation, writing—original draft preparation, writing—review and editing, visualization
Ivan Stojanović	resources, supervision, project administration
Marija Vuković Domanovac	conceptualization, methodology, validation, investigation, supervision
Vesna Alar	conceptualization, resources, supervision, project administration, funding acquisition

This paper is published in an open access journal (<https://doi.org/10.3390/coatings13071201>).

## Article

# Epoxy Coating Modification with Metal Nanoparticles to Improve the Anticorrosion, Migration, and Antibacterial Properties

Marina Samardžija <sup>1,\*</sup>, Ivan Stojanović <sup>2</sup>, Marija Vuković Domanovac <sup>3</sup>  and Vesna Alar <sup>2</sup>

<sup>1</sup> Department of Chemistry, Faculty of Mining-Geology-Petroleum Engineering, University of Zagreb, 10110 Zagreb, Croatia

<sup>2</sup> Department of Welded Structures, Faculty of Mechanical Engineering and Naval Architecture, University of Zagreb, 10000 Zagreb, Croatia; ivan.stojanovic@fsb.unizg.hr (I.S.); vesna.alar@fsb.unizg.hr (V.A.)

<sup>3</sup> Department of Industrial Ecology, Faculty of Chemical Engineering and Technology, University of Zagreb, 10000 Zagreb, Croatia; mvukovic@fkit.unizg.hr

\* Correspondence: marina.samardzija@rgn.unizg.hr; Tel.: +385-1-5535-912

**Abstract:** Nanoparticles are capable of making more durable and stronger materials with better chemical resistance. They are used for a wide range of applications. Likewise, the potential of metal nanoparticles as antimicrobial agents has been widely studied. In this work, we investigate various nanoparticles (Al, Ni, Ag) incorporated into epoxy coating. The anticorrosion and antibacterial properties of the unmodified and modified coatings were evaluated. According to the SEM and EDS analyses, the coating did not contain agglomerates, which confirms the quality of the dispersion of inorganic nanoparticles in the coating. After 24 h and 10 days immersions in a 3.5 wt.% NaCl solution, the corrosion behaviour for all nanocomposite was studied by means of EIS investigations. The study included the evaluation of the inhibition zone of the nanoparticles and the antimicrobial properties of the nanocomposite. It was found that the nanoparticles of Al and Ag provide excellent antibacterial properties. The epoxy nanocomposite with Al NP showed the migration of ions in the range from 0.75 to 1 mg/L in a wastewater solution for 30 days, indicating a potential for antimicrobe activity. The 1% Al NP epoxy nanocomposite showed good anticorrosion and antibacterial properties and demonstrated great potential for applications in pipelines.

**Keywords:** corrosion protection; nanoparticles; epoxy coating; antibacterial activity



**Citation:** Samardžija, M.; Stojanović, I.; Vuković Domanovac, M.; Alar, V. Epoxy Coating Modification with Metal Nanoparticles to Improve the Anticorrosion, Migration, and Antibacterial Properties. *Coatings* **2023**, *13*, 1201. <https://doi.org/10.3390/coatings13071201>

Academic Editor: Jinyang Xu

Received: 9 June 2023

Revised: 1 July 2023

Accepted: 3 July 2023

Published: 4 July 2023



**Copyright:** © 2023 by the authors. Licensee MDPI, Basel, Switzerland. This article is an open access article distributed under the terms and conditions of the Creative Commons Attribution (CC BY) license (<https://creativecommons.org/licenses/by/4.0/>).

## 1. Introduction

The 21st century is marked by the study of nanotechnology and the production of nanostructured materials. Nanoparticles (NPs) are a wide class of materials that includes particulate substances with sizes between 1 and 100 nm [1]. The use of nanoparticles in different fields such as molecular biology, physics, organic and inorganic chemistry, medicine, and material science is of growing interest in future applications [2]. In recent years, scientists and researchers have been motivated to develop coatings with new features, such as the possibility of the migration of substances due to the improvement of anticorrosive and antibacterial properties. As a result, nanoparticles began to be incorporated into the polymer material. The material obtained was defined as a nanocomposite, which implies a composition of at least two immiscible phases, and one of them in the nanometer scale [3]. The ability of nanocomposite material to release nanoparticles is considered very harmful if applied in the food packaging industry [4], but its application on the surface of drainage pipes is a new idea for protection against microorganisms. Cast iron pipes have been widely used in water distribution systems for more than 150 years due to their high mechanical strength and cost effectiveness [5]. With the development of urbanization and industrialization, the amount of wastewater produced and discharged increased significantly year by year. Consequently, problems such as corrosion, damage, a reduction in the water transport capacity, and an increase in the habitat of pathogenic and opportunistic bacteria

are becoming serious [6,7]. To achieve corrosion protection, organic coatings and corrosion inhibitors are widely used, but the limitations of these materials, such as high cost, heavy contamination, and operational difficulties, has not been completely overcome [8]. Polymer nanocomposite coatings are a new generation of coatings which have recently been used for the protection of drainage pipes from corrosion due to their superior mechanical strength, stiffness, improved barrier properties against oxygen and moisture, increased heat, wear, and use in the simple repair of damaged structures [9,10]. Similarly, a new class of “nanometallo-antibiotics” consisting of numerous metal NPs has appeared, which involves investigating their antimicrobial properties [11]. It is clear that some metal nanoparticles are effective antimicrobial agents against several pathogenic microorganisms, and their action depends on size, shape, and surface charge [12,13]. Mejía and co-authors [14] developed a new thin antibacterial coating with long-term effectiveness based on silver release that has an antibacterial effect. According to the research of Tahir and co-authors, the incorporation of silver nanoparticles (Ag NP) into the epoxy resin reduces the occurrence of bubbling and delamination of the coating and improves the durability of the coating [15]. Epoxy antimicrobial coatings are of great interest for the protection of surfaces, since the survival of microorganisms on the surface environment can be detrimental to materials [16]. Microbially induced corrosion (MIC) can be defined as the process by which biological agents (live organisms) cause changes in the material properties, leading to the structural lowering in quality or value [17]. Considering the proven antibacterial efficacy of metal and metal oxide nanoparticles in an organic coating with clear known mechanisms of action against bacteria for silver, silver oxide, titanium dioxide, iron oxide, and zinc oxide, potential materials with the same effect as nickel and aluminum remain poorly researched [16,18,19].

Nickel is a metal relatively resistant to atmospheric corrosion, but it also has huge potential for the development of antibacterial properties [20,21]. The bactericidal action of nickel nanoparticles (Ni NP) has shown a strong effect with particle sizes in the range of 10–100 nm [21]. Aluminum nanoparticles (Al NP) also have high corrosion resistance, but due to the ability to create a passive oxidation layer their antibacterial potential increases [4]. It can be concluded that certain metal powder nanoparticles have a cytotoxic and genotoxic effect on bacteria, and their intercalation in the epoxy coating creates the potential for antibacterial protection. In this study, the effect of the Al NP, Ni NP, and Ag NP in an epoxy coating on the anticorrosion, migration, and the antibacterial property was investigated. In our current work, the composition and distribution of particles for these coatings were characterized using SEM and EDS investigations. The EIS technique was used to characterize the anticorrosion properties of the modified epoxy coating and epoxy nanocomposite. The migration of nanoparticles from the epoxy coating into the wastewater was observed for 30 d, and the possibility of antibacterial action of nanocomposite was tested according to ISO 22196.

## 2. Materials and Methods

### 2.1. Materials

The metallic substrate used during this study was gray cast iron with chemical composition 2.5 C, 1.5 Si, 1.05 Mn, 0.5 P, 0.07 S, and Fe in balance (wt.%). The epoxy coatings that we used in this work were based on diglycidyl ether of bisphenol A, and the polyamine hardener was obtained from Hempel (Umag, Croatia). Aluminum, nickel, and silver nanoparticles with an average particle size of about 100 nm were provided by Guangzhou Hongwu Material Technology Co., Ltd., Guangzhou, China. The morphology of the powder nanoparticles was observed from the SEM micrographs, EDS, and XRF (Figure 1).

According to Figure 1a–c, the Al and Ni NPs showed spherical particles and the Ag NPs within irregular shapes. All nanoparticles showed different sizes. The small nanoparticles had a very large surface area to volume ratio, which gave them huge energy and high reactivity. The agglomerates with average particle sizes from 223.4 to 620.7 nm were observed in Figure 1a,b. The XRF analysis of the elemental composition of the nanoparticle powder showed a high proportion of Al, Ag, and Ni nanoparticles (Table 1).



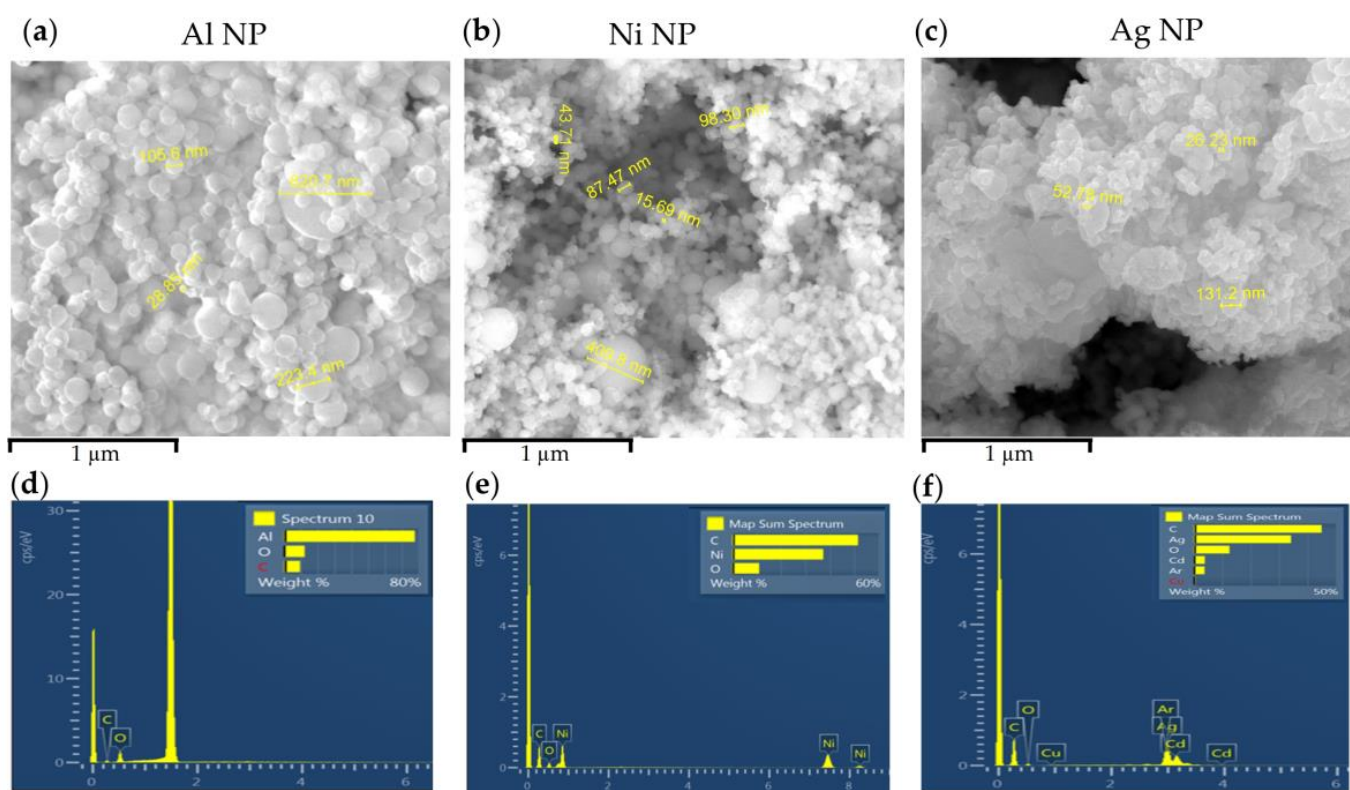


Figure 1. SEM image and EDS analysis of the (a,d) Al, (b,e) Ni, and (c,f) Ag nanoparticles.

Table 1. The XRF analysis of the elemental composition of the nanoparticle powder.

Al NP			Ni NP			Ag NP		
Elements	wt.%	+/-	Elements	wt.%	+/-	Elements	wt.%	+/-
Al	98.85	0.24	Ni	99.21	0.25	Ag	98.94	0.32
Cr	0.08	0.01	Cu	0.28	0.05	Cr	0.41	0.10
Fe	0.03	0.43	Si	0.26	0.05	Co	0.33	0.04
Residue	1.04	0.01	Co	0.11	0.02	Si	0.33	0.02
Total	100	-	Residue	0.14	0.01	Total	100	-
			Total	100				

## 2.2. Preparation of the Epoxy Coating/Nanocomposite

The epoxy coating was formulated by taking epoxy paint and polyamine hardener in the mass ratio of 4:1. Four formulations of prepared coatings are shown in Table 2.

At ambient temperature, various nanoparticles were incorporated into the epoxy coating under sonicate agitation for 20 min with a delay in the process due to the cooling of the nanocomposite. Polyamine hardener was added to the nanocomposite and mechanically stirred using a glass stirrer.

Before applying the coating, the panels of 9.5 cm × 0.9 cm × 15 cm gray cast iron were abrasively blasted and cleaned with ethanol (70 wt.%). The nanocomposite mixture was applied using a film applicator with a wet film thickness of 150 μm. The samples were kept at room temperature for 24 h, and then another layer of nanocomposites was applied in the opposite direction. The samples were left at room temperature (25 °C) for 7 days.

**Table 2.** The chemical composition of the tested samples.

Sample	Epoxy Coating (g)	Hardener (g)	m (Al NP) (g)	m (Ni NP) (g)	m (Ag NP) (g)	Thickness ( $\mu\text{m}$ )
Epoxy Coating	30	7.5	-	-	-	249.1
1% Al NP Nanocomposite	30	7.5	0.4545	-	-	256.1
1% Ni NP Nanocomposite	30	7.5	-	0.4545	-	266.5
1% Ag NP Nanocomposite	30	7.5	-	-	0.4545	264.9

### 2.3. Characterization of the Epoxy Coating/Nanocomposite

To evaluate the size of the nanoparticles, the quality of dispersion, and the appearance of the agglomerate of nanoparticles in the nanocomposite, scanning electron microscopy (SEM) (TESCAN Brno, Brno, Czech Republic) and energy-dispersive X-ray spectroscopy (EDS) analyses were used.

To investigate the anticorrosion behavior of Al, Ni, and Ag nanocomposites, electrochemical impedance spectroscopy (EIS) (VersaSTAT 3, AMETEK Scientific 131 Instruments, Princeton applied research, Berwyn, PA, USA) was used. These measurements were performed in a three-electrode electrochemical cell in a 3.5 wt.% NaCl solution. The coated gray cast iron was used as the working electrode, with a test area of 19.75 cm<sup>2</sup>, a saturated calomel electrode was used as a reference electrode, and the graphite electrode was used as an auxiliary electrode. The frequency scan range of 0.1 to 10<sup>5</sup> Hz with an amplitude of 10 mV was used. The impedance data were fitted using the ZSimpWin software (AMETEK, Berwyn, PA, USA) (Version 3.2).

The samples of epoxy coating, 1% Al NP epoxy nanocomposite, 1% Ni NP epoxy nanocomposite, and 1% Ag NP epoxy nanocomposite were placed in contact with simulation wastewater according to the DIN EN 877 [22]. For the assessment of Al<sup>3+</sup>, Ni<sup>2+</sup>, and Ag<sup>+</sup> ions' migration from the epoxy coating, 10 g of each sample was immersed in 100 mL simulated wastewater for 30 days. In this study, samples were kept in the dark at a temperature of 40 °C. The temperature for this study was chosen according to the real conditions in drainage pipes. The mass concentration, electrical conductivity, and pH value of the wastewater were determined after 10, 20, and 30 days. The mass concentration of Al<sup>3+</sup>, Ni<sup>+</sup>, and Ag<sup>+</sup> ions in wastewater was determined with the flame atomic absorption spectrometry (F-AAS) technique (Perkin Elmer Analyst 700, Waltham, MA, USA). The conductivity and pH values were measured with a pH/EC meter (HI5521-02, HANNA instruments, Woonsocket, RI, USA).

The antibacterial properties of the Al, Ni, and Ag were investigated with a well-diffusion method [23]. For this purpose, *P. aeruginosa* was used as a Gram-negative bacterial strain, and *B. subtilis* as a Gram-positive bacterial strain. The 24 h aged active bacterial cultures were poured into the Muller Hinton culture medium. The nanoparticle samples dissolved in distilled water (100 g/mL) were added from the stock into each well. The zone of inhibition was measured using a ruler. After 24 h, the appearance of the inhibition zone was observed.

The antibacterial activities of nanocomposites were tested according to ISO 22196:2011 against *P. aeruginosa* and *B. subtilis* [24]. The surface of the epoxy coating, 1% Al epoxy nanocomposite, 1% Ni epoxy nanocomposite, and 1% Ag epoxy nanocomposite were cut to size 50 mm × 50 mm and inoculated with 0.4 mL of 10<sup>5</sup> CFU bacterial suspensions. All samples were covered with polyethylene foil dimensions of 40 mm × 40 mm ( $\pm$  1 mm) and a thickness of 0.06 mm. All samples were placed in a Petri dish and incubated at 35 °C ( $\pm$ 1 °C) and 90% relative humidity (RH) ( $\pm$ 5%) for 24 h ( $\pm$ 1 h). The number of viable bacterial cells was determined by plating different dilutions on plate count agar, incubating the plates for 24 h at 37 °C, and then visually counting the colonies [25]. All experiments are representative of repeated trials. Sample error bars on plots represent  $\pm$  SD. The

measurement of the inhibition zone was carried out in four sections (rotation by 45°) using a ruler with a length of 15 cm. The measurements were repeated three times.

### 3. Results and Discussion

#### 3.1. SEM and EDS Analysis of Epoxy Coating/Nanocomposite

The morphology of epoxy coating and 1 wt.% of Al, Ni, and Ag nanocomposites were investigated using SEM analysis. Figure 2a shows the SEM images of epoxy coating without nanoparticles, which indicates a rough surface morphology with a large addition of other coating components such as fillers, additives, pigments and similar. The EDS analysis confirms the presence of aluminum particles in the initial sample (Figure 2b,c). It was assumed that these microparticles of aluminum were used as a pigment in the epoxy coating. The presence of these particles in the initial epoxy coating showed small irregularities and the appearance of agglomerates (Figure 2b). The EDS analysis of the initial epoxy coating (Figure 2c) determined the percentage of the aluminum microparticles, and this was 0.85%.

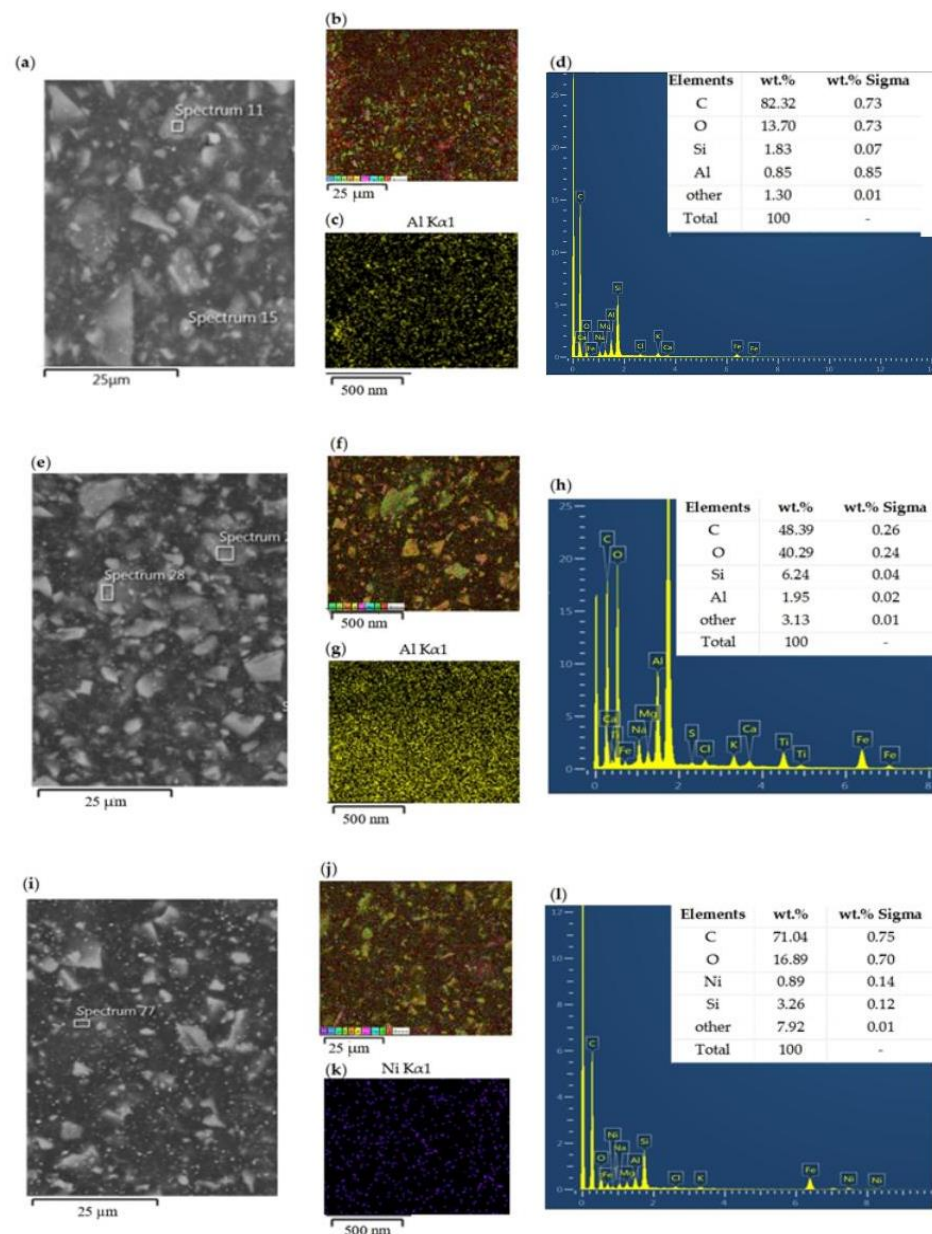
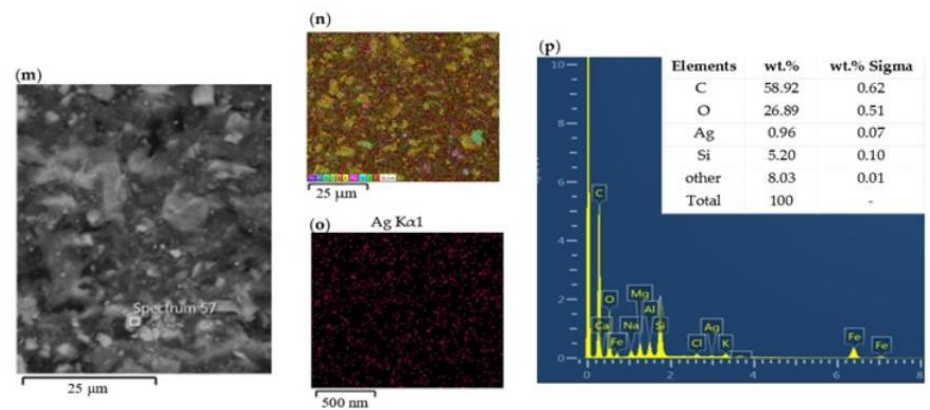


Figure 2. Cont.



**Figure 2.** The SEM and EDS analyses of (a,b) epoxy coating, (e,f) 1% Al NP epoxy nanocomposite, (i,j) 1% Ni NP epoxy nanocomposite, and (m,n) 1% Ag NP epoxy nanocomposite. The EDS mapping and element weight percentages of distribution of microparticles of (c,d) Al in epoxy coating, and nanoparticles of (g,h) Al, (k,l) Ni, and (o,p) Ag in the nanocomposite.

With the addition of nanoparticles, the rough surface morphology of nanocomposites remained the same (Figure 2e,i,m). The action of the sonication process improved the distribution of the added aluminum particles (Figure 2g). The EDS analysis confirmed the uniform distribution of Ni and Ag nanoparticles within the epoxy coating, shown in Figure 2k,o. Furthermore, EDS analysis determined that all nanocomposite samples contained a certain percentage of nanoparticles that deviated very slightly from the added 1% nanoparticles (Figure 2d,h,l,p).

### 3.2. EIS Analysis of Epoxy Coating/Nanocomposite

The EIS measurements were performed to investigate the effects of the addition of Al, Ni, and Ag nanoparticles on the corrosion protection properties of the epoxy coating in a 3.5 wt.% NaCl solution with different immersion times. According to the electrochemical behavior of the various prepared nanocomposites, the model of the equivalent circuit with three resistance elements was chosen (Figure 3). This model demonstrated electrolyte resistance,  $R_e$ , coating capacitance,  $CPE_{coat}$ , coating resistance,  $R_{coat}$ , charge transfer resistance,  $R_{ct}$ , and double layer capacitance,  $CPE_{dl}$  [26]. The behavior of the CPE was shown by the parameter phase shift,  $n$  ( $-1 \leq n \leq 1$ ); when  $n = 0$ , the CPE represented a pure resistor, if  $n = -1$ , the CPE stood for an inductor, and if  $n = +1$ , the CPE represented a pure capacitor [27].

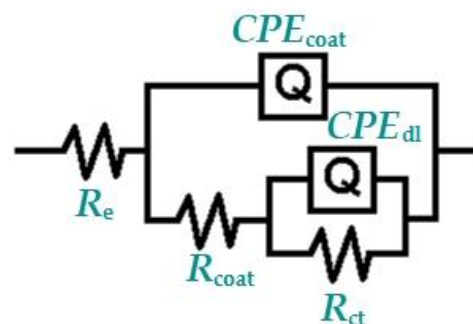


**Figure 3.** The equivalent circuits used for fitting the Nyquist and Bode plots for coating.

The Nyquist and Bode plots for the epoxy coating, 1% Al epoxy nanocomposite, 1% Ni epoxy nanocomposite, and 1% Ag epoxy nanocomposite after 24 h and 10 days of immersion in 3.5 wt.% NaCl solution are illustrated in Figure 4a–d. The calculated values

of the EIS parameters were reported in Table 3. The coating protection efficiency (%CPE) also listed in the table was calculated using the equation [28]:

$$\%CPE = \frac{R_{\text{coat with NP}} - R_{\text{coat without NP}}}{R_{\text{coat with NP}}} \quad (1)$$

where  $R_{\text{coat with NP}}$  is the resistance of Al, Ni, or Ag nanocomposites, and  $R_{\text{coat without NP}}$  is the resistance of the epoxy coating.

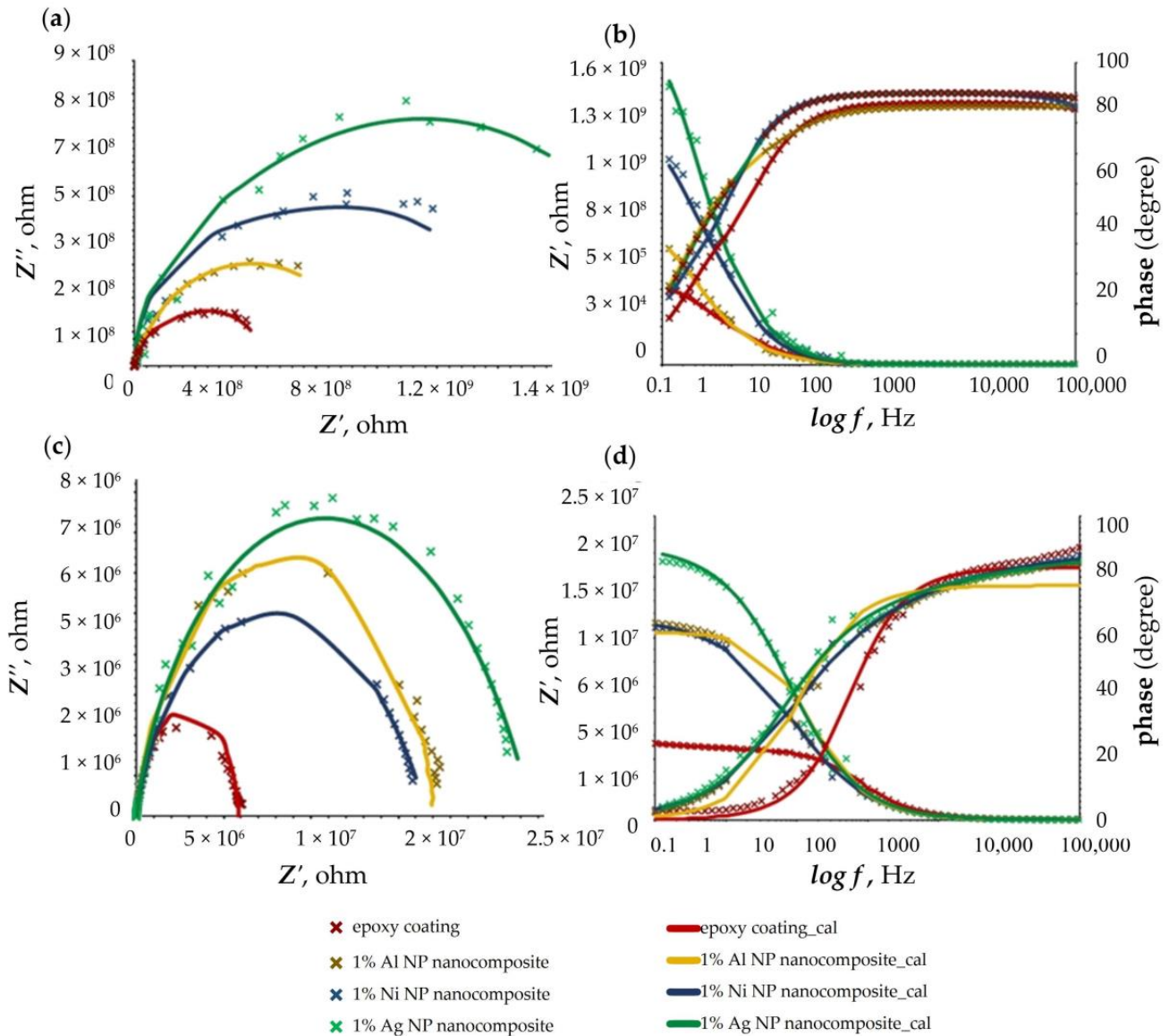


**Figure 4.** The (a,c) Nyquist and (b,d) Bode plots for epoxy coating, 1% Al epoxy nanocomposite, 1% Ni epoxy nanocomposite, and 1% Ag epoxy nanocomposite after (a,b) 24 h and (c,d) 10 days of exposure to 3.5 wt.% NaCl solution.

After immersion, as shown in Figure 4, the electrochemical response of the prepared nanocomposites showed one-time constants. The Nyquist diagrams for epoxy coating had the lowest value of  $R_{\text{coat}}$ , implying that the presence of nanoparticles prolonged the use of the gray cast iron. The nanocomposite with 1% of Ag NP showed the best corrosion resistance, followed by the 1% Ni NP nanocomposite and 1% Al NP nanocomposite (Figure 4a). All samples achieved a constant phase angle value extending from the medium frequency range (100 Hz) to the high frequency range ( $10^5$  Hz) after 24 h exposure in

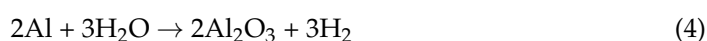
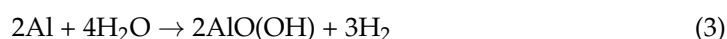
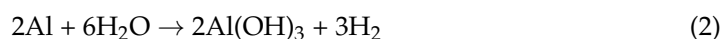
3.5 wt.% NaCl solution (Figure 4b). With increasing immersion time (after 10 days), the resistance decreased due to the penetration of the electrolyte through the nanocomposite layer, and the corrosion resistance for 1% Ni and 1% Al nanocomposites became equal (Figure 4a,c). Figure 4c shows the deviation of the Nyquist diagrams from a perfect semicircle. This phenomenon is referred to as frequency dispersion, and has been attributed to the roughness and non-uniformity of a working electrode, fracture structures, and the formation of porous layers [29]. This behavior can be observed in the Bode diagram, where the constant area of the phase angle value decreased, indicating that all samples had started to degrade (Figure 4d).

**Table 3.** Electrochemical parameters of the EIS experiments for all sample after 24 h, and 10 days of exposure to 3.5 wt.% NaCl solution at room temperature.

Samples	$R_e, \Omega$	$R_{coat}, \Omega$	$CPE_{coat}, Ssec^m$	$n$	$R_{ct}, \Omega$	$CPE_{dl}, Ssec^n$	$n$	$CPE, \%$
<b>After 24 h</b>								
Epoxy Coating	195.9	$2.55 \times 10^8$	$4.8 \times 10^{-10}$	0.9641	$1.76 \times 10^8$	$2.32 \times 10^{-9}$	0.9305	-
1% Al NP Nanocomposite	116.8	$5.68 \times 10^8$	$6.97 \times 10^{-11}$	0.9379	$2.034 \times 10^8$	$5.67 \times 10^{-10}$	0.9505	54.87
1% Ni NP Nanocomposite	204.1	$7.90 \times 10^8$	$2.72 \times 10^{-12}$	1	$4.42 \times 10^8$	$1.69 \times 10^{-9}$	1	67.72
1% AgNP Nanocomposite	217.1	$8.89 \times 10^8$	$5.95 \times 10^{-12}$	1	$8.81 \times 10^8$	$2.12 \times 10^{-10}$	1	71.32
<b>After 10 days</b>								
Epoxy Coating	153.9	$5.87 \times 10^6$	$7.35 \times 10^{-10}$	0.924	$4.87 \times 10^4$	$4.19 \times 10^{-9}$	0.9951	-
1% Al NP Nanocomposite	100.0	$1.67 \times 10^7$	$5.63 \times 10^{-10}$	0.9102	$2.35 \times 10^6$	$3.85 \times 10^{-10}$	0.9862	64.85
1% Ni NP Nanocomposite	165.3	$2.34 \times 10^7$	$1.32 \times 10^{-11}$	0.9589	$3.34 \times 10^6$	$7.53 \times 10^{-10}$	0.9357	74.91
1% AgNP Nanocomposite	135.5	$2.57 \times 10^7$	$3.64 \times 10^{-11}$	0.9525	$4.73 \times 10^6$	$9.23 \times 10^{-10}$	0.9768	77.16

Based on Table 3, the double layer capacitance between the coating surface/electrolyte solutions ( $CPE_{coat}$  value) increased with time. This showed that the absorption level of the electrolyte solution in the nanocomposite had increased, but its resistance was still better than that of the epoxy coating. Further inspection of the table revealed that the  $n$  values were close to unity, implying that the interface behaved nearly capacitively. The addition of nanoparticles increased the value of %CPE. In all nanocomposites, the efficiency improved with time. The reason for such behavior could be nanoscale inorganic particles that cause better barrier properties. When metals interact with their surroundings, they can be converted into a more chemically stable form such as oxide, hydroxide, or sulfide, and thus provide better corrosion resistance [30,31].

Figure 5 illustrates the reaction between Al, Ni, and Ag NP and electrolyte, and the protection mechanism of the Al, Ni, and Ag nanocomposites in contact with corrosive electrolyte. When metallic aluminum comes into contact with oxygen, it becomes very reactive. A thin layer of alumina (4 nm thickness) forms in about 100 picoseconds on any exposed aluminum surface, which acts as a protective covering for further oxidation [32]. The Al NPs form an aluminum oxide layer on its surface in contact with the electrolyte, according to the following equations [33]:



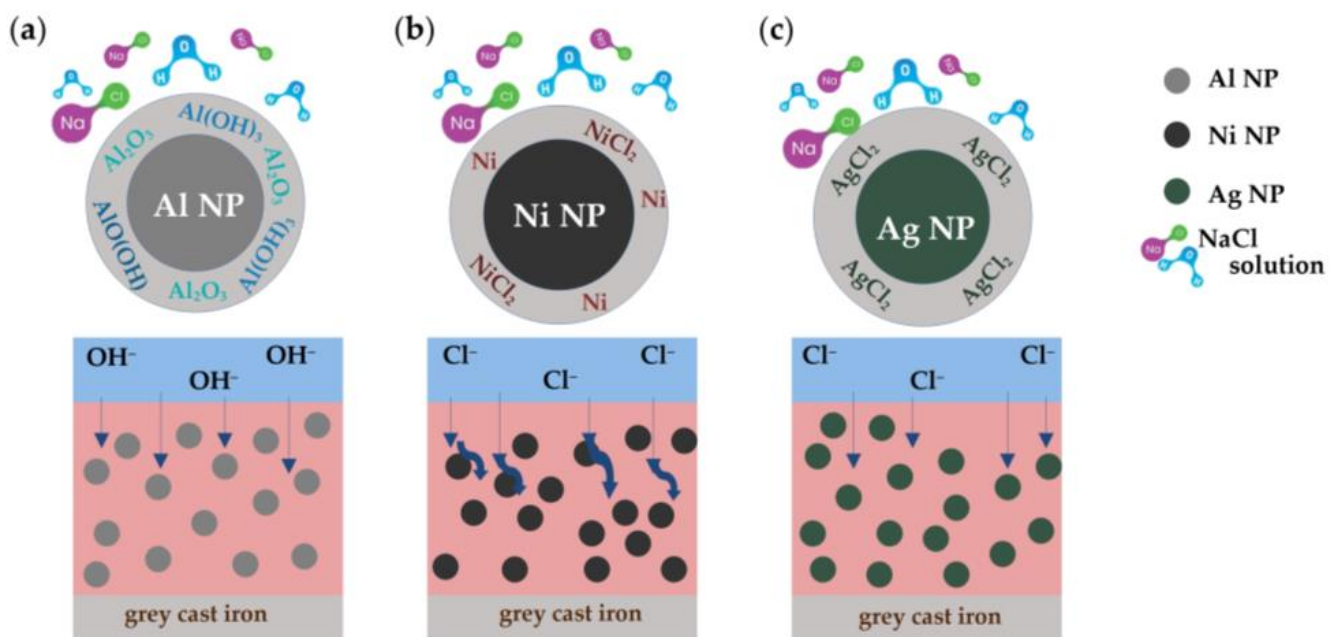


**Figure 5.** Protection mechanisms of (a) Al, (b) Ni, and (c) Ag nanoparticles in the epoxy coating in contact with NaCl solution.

The volume of formed aluminum oxides is greater than the volume of nanoparticles, which can prevent the further penetration of the corrosive medium, prolong the path of penetration of the corrosive medium into the coating, and ultimately delay the onset of corrosion (Figure 5a) [34,35].

The Ni NPs did not show passive behavior in the epoxy coating because the 3.5 wt.% NaCl solution had a pH value of 7. Nickel did not react with water, and small amounts of chloride ions can be exposed on its surface. According to Pourbex's diagram, passive oxide films should appear at a pH value of 10 [20,36]. From these results, we can conclude that only Ni NPs and a small part of the formed NiCl<sub>2</sub> acted to increase the corrosion resistance of nickel nanocomposites. The nickel nanocomposite system did not have the ability to close the micropores formed in the epoxy coating during exposure to a corrosive medium. The effectiveness of this coating dropped, as can be seen in Figure 4c,d.

The Ag NPs have the property of releasing Ag<sup>+</sup> ions, which gives them the ability to react with other chemical species in the environment. Since silver is a noble metal ( $E^{\circ}/V = 0.79$  vs. SHE), its affinity for oxygen will be low, so a layer of AgCl will form on its surface when exposed to 3.5 wt.% NaCl solution [36,37]. The generation of insoluble AgCl leads to the formation of a chemical barrier inside the epoxy coating. Ag NPs act as a chemical barrier against the further penetration of corrosive species from the electrolyte to the grey cast iron substrate [38].

### 3.3. Antibacterial Activity of the Al, Ni, and Ag Nanoparticles

The antibacterial activity of Al, Ni, and Ag nanoparticles was tested against various bacterial strains: *P. aeruginosa*, and *B. subtilis*. Figure 6 represents the antibacterial activity of nanoparticles for various bacteria in a well-diffusion technique. Arithmetic means of measurement results are given with measurement uncertainty  $U = 1.5$  mm,  $k = 2$ , and  $P = 95\%$ , where  $U$  is expanded measurement uncertainty,  $k$  the presented coverage factor, and  $P$  is confidence level.

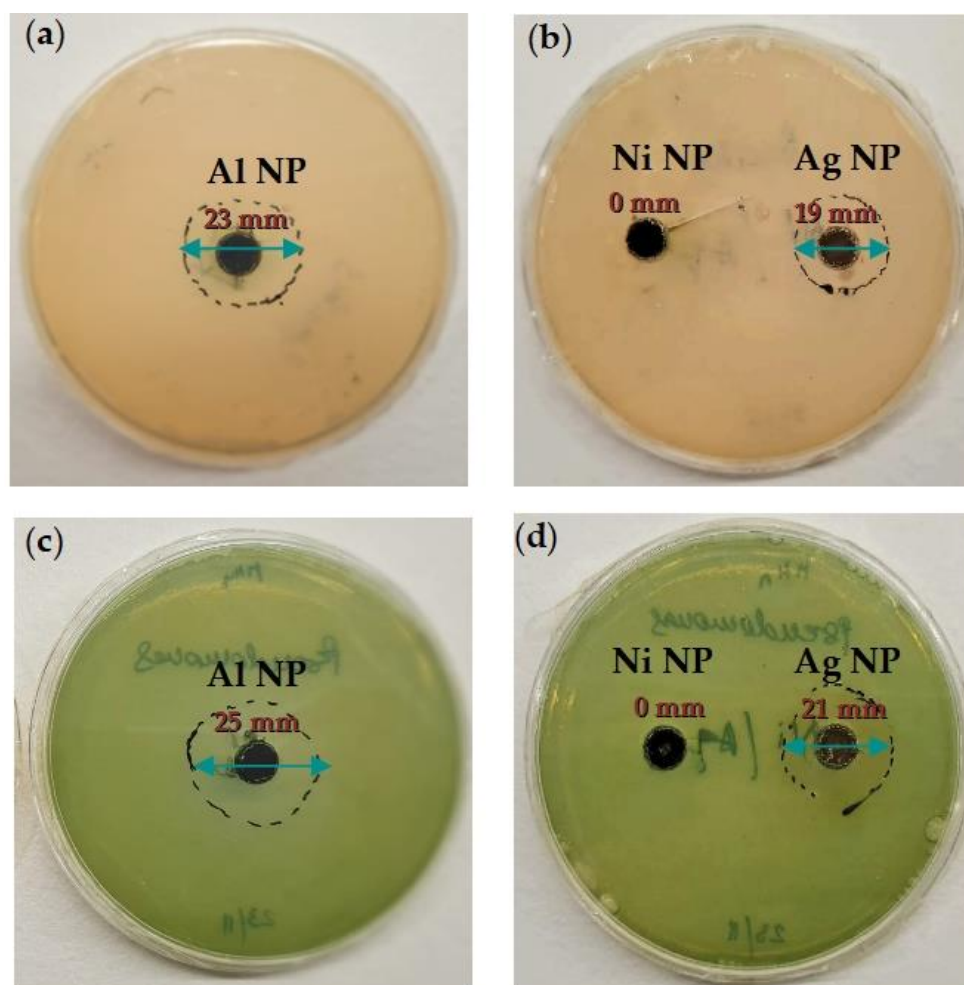


**Figure 6.** Zone of inhibition of (a) Al, and (b) Ni, and Ag nanoparticles against *B. subtilis*, and (c) Al, and (d) Ni, and Ag against *P. aeruginosa*.

The results indicated that Al and Ag nanoparticles showed effective antibacterial activity compared to Ni nanoparticles. The diameter of the inhibitory zone shows that Al NP had a larger zone of inhibition than Ag NP. In this respect, it was found that the Al and Ag NP were poisonous to both Gram-positive and Gram-negative bacteria. Nickel nanoparticles showed a very small inhibition zone, due to the large range of nanoparticle sizes. Typically, smaller NPs have better interaction with the bacteria due to their ability to penetrate a cell and inhibit bacteria growth [11,13]. Asghari and co-authors revealed that *P. aeruginosa* showed a high survival rate against Ni NPs and therefore can survive at quite high concentrations of Ni NPs [39]. It was assumed that due to their large size range and the possibility of agglomeration in aqueous media, Ni NPs could not enter the membrane of bacterial cells (*P. aeruginosa* and *B. subtilis*) to attach to functional groups of proteins to cause their denaturation [40].

### 3.4. Migration Ability and Antibacterial Activity of the Nanocomposites

A migration of nanoparticles from epoxy coating is a very important test because it provides a new property for drainage pipe protection. Figure 7 demonstrated the migration of Al and Ni nanoparticles from the epoxy coating into simulated wastewater. Released  $\text{Ag}^+$  ions from the epoxy coating reacted with  $\text{Cl}^-$  ions from the wastewater to form a white precipitate of silver(I) chloride. This is the reason why the actual concentration of  $\text{Ag}^+$  ions released could not be determined with F-AAS techniques. In Figure 7, the concentration of  $\text{Ag}^+$  ions in the wastewater was below the detection limit of the instrument.



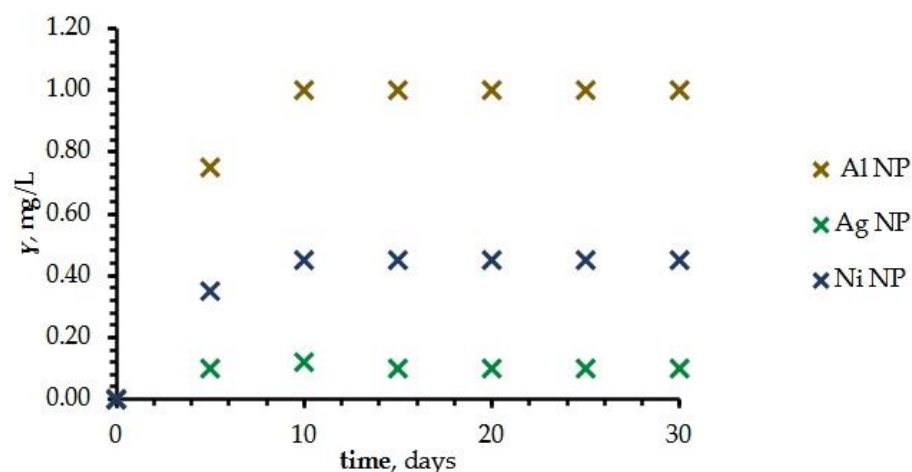


**Figure 7.** The mass concentration of the migration of Al, Ag, and Ni nanoparticles from epoxy coating to simulated wastewater.

The nanoparticles with 1% of Al NP showed significant migration, while nanocomposites with Ag and Ni nanoparticles showed the lowest value of migration from epoxy coating to the wastewater (Figure 7). The amount of migrated Al NP gradually increased in the beginning, but after 10 days of exposure the wastewater assumed a constant value of aluminum concentration (1 mg/L). For all samples, the pH-value increased very slightly, from 7.723 to 8.791, while the electrical conductivity showed a significant increase for the Al NP nanocomposite, from 1.085 to 2.083 mS/cm.

The migration of nanoparticles from the epoxy coating was stimulated by the action of the wastewater. Aluminum nanoparticles were the only ones capable of forming an oxide film on their surface. The resulting oxide film, with its passivity, closed the micropores of the epoxy and did not allow the oxidation and migration of other nanoparticles located further from the surface of the epoxy coating. The incorporation of certain metals and metal-oxides in the epoxy polymers also led to the development of 'active' materials that prevented the growth of microorganisms, and hence preserved the quality of water pipes during the transportation of wastewater. According to ISO 22196, the antibacterial properties of the epoxy coating (control sample) and nanocomposites were determined by measuring the reduction in antibacterial activity. Consistent with the ISO guidelines, the reduction in antibacterial activity was estimated using the following equation [41]:

$$\text{reduction of antibacterial activity} = \frac{(CFU_{0h} - CFU_{24h})}{CFU_{0h}} \times 100 \quad (5)$$

where  $CFU_{0h}$  is the bacterial colony forming units obtained for the control samples before incubation, and  $CFU_{24h}$  is the bacterial colony forming units observed for the test conditions for the nanocomposites after incubation.

The antibacterial activity of the epoxy coating and nanocomposites against *P. aeruginosa* and *B. subtilis* after a 24 h exposition period is presented in Figure 8 and the reduction in antibacterial activity in Table 4.

**Table 4.** Average values of bacterial reductions of epoxy coating and 1% Al NP, 1% Ag NP, and 1% Ni NP in nanocomposite against *P. aeruginosa* and *B. subtilis* after 24 h.

	Nanocomposite			
	Epoxy Coating	1% Al NP	1% Ag NP	1% Ni NP
<i>P. aeruginosa</i>	4.17 ± 0.09	61.46 ± 2.64	45.83 ± 4.05	11.46 ± 0.92
<i>B. subtilis</i>	3.44 ± 0.11	55.31 ± 0.16	42.19 ± 1.41	11.25 ± 0.15

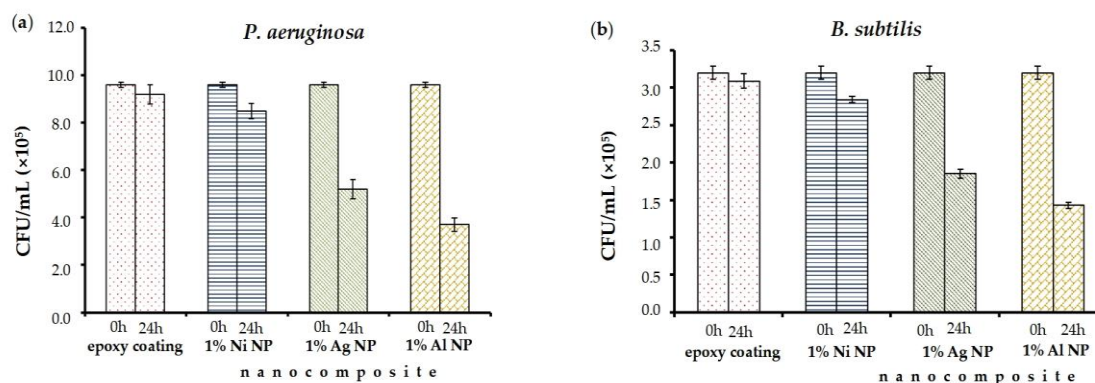
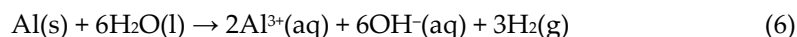


**Figure 8.** Antibacterial activity of epoxy coating, and 1% Al, 1% Ag, and 1% Ni epoxy nanocomposite on (a) *P. aeruginosa* and (b) *B. subtilis* during 24 h according to the ISO 22196 standard.

Based on the evaluation of bacteria (Figure 8), we concluded that after 24 h incubation the highest live count of *P. aeruginosa* and *B. subtilis* was observed on the epoxy coating samples and samples containing 1% of Ni NP in the nanocomposite (Table 4). The nanocomposite with 1% of Al NP exhibited the highest antibacterial effect, with a reduction of  $61.46 \pm 0.09\%$  for *P. aeruginosa* and  $55.31 \pm 0.16\%$  for *B. subtilis* (Figure 8, Table 4). The 1% of Ag NP in the epoxy coating showed the second-greatest antimicrobial potential, and achieved a  $45.83 \pm 4.05\%$  cell reduction for *P. aeruginosa* and  $42.19 \pm 1.41\%$  for *B. subtilis*, respectively, after 24 h incubation. However, the average leaching potential of Al NP was better than Ag NP in the epoxy coating (Figure 7). In contact with aqueous media, the Al NP formed an aluminum oxide and smaller amounts of aluminum hydroxide and oxyhydroxide [34]. The attraction between nanoparticles and bacteria depends on the surface charge of the nanoparticles and the bacteria [42]. Gram-positive bacteria (*B. subtilis*) consist of a thick layer of peptidoglycan, which is embedded in teichoic acid, while Gram-negative bacteria (*P. aeruginosa*) have a layer of lipopolysaccharide at the external surface. The teichoic acid and lipopolysaccharides impart a negative charge to the surface of bacterial cells [43]. The negatively charged bacterial surfaces of *P. aeruginosa* and *B. subtilis* strongly attract the resulting highly positively charged oxides, for example  $\text{Al}_2\text{O}_3$  [44]. Better electrostatic attraction between bacteria and particles will result in better antibacterial action, which is visible in Figure 6c and Figure 8a. Table 4 shows that less antibacterial activity was evident in samples exposed to the bacterium *B. subtilis* due to the thick outer cell wall, which can hinder NP penetration into the thick peptidoglycan layer.

In contact with corrosive media, Al NPs react with water molecules and the following redox reactions occur[45]:



In the oxidation reaction, the  $\text{Al}^{3+}$  ion is formed, which is toxic to bacteria. Also, the resulting oxidation products can release the  $\text{Al}^{3+}$  ion, which will affect the life of the bacteria [41]. The mechanism of action of  $\text{Al}^{3+}$  ions has not been fully clarified yet. Cell penetration and the adsorption or diffusion of NPs at the cell surface is often the initial step in the stages involved in some microbial cell inhibition [46]. According to literature [47], an increased  $\text{Al}^{3+}$  concentration can stimulate reactive oxygen species (ROS), which can act as the main factor in DNA damage in bacterial cells.

#### 4. Conclusions

The influence of nanoparticles in the epoxy coating leads to the modification of the internal defects in the coating due to the filling of voids and blocking of easy access to channels. Nanoparticles that could react with a corrosive medium prolong the path of

penetration of corrosive species from the electrolyte to the metal substrate. Likewise, the resulting corrosion product on the nanoparticle is dangerous for lower organisms and can be used for the formation of a new property of the coating. These studies showed that Al and Ag nanoparticles embedded in nanocomposites can significantly improve the anticorrosive properties and inhibit bacteria, while Ni NPs have lower efficiency. Due to remarkable properties like high reactivity, the ability to form a homogeneous structure, bacterial resistance, cost-effectiveness, and unexplored literature, Al NPs attracted our enormous interest and will continue to serve for detailed analysis so that they can be applied as a protective additive in epoxy coating for the protection of pipelines.

**Author Contributions:** Conceptualization, M.S., V.A. and M.V.D.; methodology, M.S. and M.V.D.; software, M.S.; validation, M.S. and M.V.D.; formal analysis, M.S.; investigation, M.S. and M.V.D.; resources, V.A. and I.S.; data curation, M.S.; writing—original draft preparation, M.S.; writing—review and editing, M.S.; visualization, M.S.; supervision, V.A., I.S. and M.V.D.; project administration, V.A. and I.S.; funding acquisition, V.A. All authors have read and agreed to the published version of the manuscript.

**Funding:** This research was funded by “Development of anticorrosion protection system for multipurpose pipe use”, Grant Number KK.01.1.1.07.0045. This work was supported by the European Regional Development Fund under the Operational Program Competitiveness and Cohesion 2014–2020.

**Institutional Review Board Statement:** Not applicable.

**Informed Consent Statement:** Not applicable.

**Data Availability Statement:** Not applicable.

**Acknowledgments:** We thank Michaela Hruškova Hasan (University of Zagreb, Faculty of Mining, Geology, and Petroleum Engineering) for the use of flame atomic absorption spectrometry technique and helpful advice.

**Conflicts of Interest:** The authors declare no conflict of interest.

## References

1. Khan, I.; Saeed, K.; Khan, I. Nanoparticles: Properties, applications, and toxicities. *Arab. J. Chem.* **2019**, *12*, 908–931. [[CrossRef](#)]
2. Jamkhande, P.G.; Ghule, N.W.; Bamer, A.H.; Kalaskar, M.G. Metal nanoparticles synthesis: An overview on methods of preparation, advantages and disadvantages, and applications. *J. Drug Deliv. Sci. Technol.* **2019**, *53*, 101174. [[CrossRef](#)]
3. Nguyen-tri, P.; Nguyen, T.A.; Carriere, P.; Xuan, C.N. Nanocomposite Coatings: Preparation, Characterization, Properties, and Applications. *Int. J. Corros.* **2018**, *2018*, 19. [[CrossRef](#)]
4. Tanveer, M.; Farooq, A.; Ata, S.; Bibi, I.; Sultan, M.; Iqbal, M.; Jabeen, S.; Gull, N.; Islam, A.; Khan, R.U.; et al. Aluminum nanoparticles, chitosan, acrylic acid and vinyltrimethoxysilane based hybrid hydrogel as a remarkable water super-absorbent and antimicrobial activity. *Surf. Interfaces* **2021**, *25*, 101285. [[CrossRef](#)]
5. Zhang, G.; Li, B.; Liu, J.; Luan, M.; Yue, L.; Jiang, X.T.; Yu, K.; Guan, Y. The bacterial community significantly promotes cast iron corrosion in reclaimed wastewater distribution systems. *Microbiome* **2018**, *6*, 222. [[CrossRef](#)]
6. Wang, J.; Liu, G.; Wang, J.; Xu, X.; Shao, Y.; Zhang, Q.; Liu, Y.; Qi, L.; Wang, H. Current status, existent problems, and coping strategy of urban drainage pipeline network in China. *Environ. Sci. Pollut. Res.* **2021**, *28*, 43035–43049. [[CrossRef](#)]
7. Sun, H.; Shi, B.; Lytle, D.A.; Bai, Y.; Wang, D. Formation, and release behavior of iron corrosion products under the influence of bacterial communities in a simulated water distribution system. *Environ. Sci. Process. Impacts* **2014**, *16*, 576–585. [[CrossRef](#)]
8. Lou, Y.; Chan, W.; Cui, T.; Qian, H.; Huang, L.; Ma, L.; Hao, X.; Zhang, D. Microbiologically influenced corrosion inhibition of carbon steel via biomineralization induced by *Shewanella putrefaciens*. *Mater. Degrad.* **2021**, *5*, 59. [[CrossRef](#)]
9. Brindha, T.; Rathinam, R.; Dheenadhayalan, S.; Sivakumar, R. Nanocomposite Coatings in Corrosion Protection Applications: An Overview. *Orient. J. Chem.* **2021**, *37*, 1062–1067.
10. Kausar, A. A review of high performance polymer nanocomposites for packaging applications in electronics and food industries. *J. Plast. Film Sheeting* **2020**, *36*, 94–112. [[CrossRef](#)]
11. Zheng, K.; Setyawati, M.I.; Leong, D.T.; Xie, J. Antimicrobial silver nanomaterials. *Coord. Chem. Rev.* **2018**, *357*, 1–17. [[CrossRef](#)]
12. Rai, M.; Shegokar, R. Metal Nanoparticles in Pharma. In *Metal Nanoparticles in Pharma*; Springer International Publishing: Cham, Switzerland, 2017; pp. 1–493.
13. Franco, D.; Calabrese, G.; Guglielmino, S.P.P.; Conoci, S. Metal-Based Nanoparticles: Antibacterial Mechanisms and Biomedical Application. *Microorganisms* **2022**, *10*, 1778. [[CrossRef](#)]
14. Giraldo Mejia, H.F.; Yohai, L.; Pedetta, A.; Herrera Seitz, K.; Procaccini, R.A.; Pellice, S.A. Epoxy-silica/clay nanocomposite for silver-based antibacterial thin coatings: Synthesis and structural characterization. *J. Colloid Interface Sci.* **2017**, *508*, 332–341. [[CrossRef](#)]

15. Hussain, Z.; Tahir, S.A.; Mahmood, K.; Ali, A.; Arshad, M.I.; Ikram, S.; Nabi, M.A.U.; Ashfaq, A.; Rehman, U.U.; Muddassir, Y. Synthesis and characterization of silver nanoparticles with epoxy resin. *Dig. J. Nanomater. Biostructures* **2020**, *15*, 873–883. [[CrossRef](#)]
16. Manjumeena, R.; Venkatesan, R.; Duraibabu, D.; Sudha, J.; Rajendran, N.; Kalaichelvan, P.T. Green Nanosilver as Reinforcing Eco-Friendly Additive to Epoxy Coating for Augmented Anticorrosive and Antimicrobial Behavior. *Silicon* **2015**, *8*, 277–298. [[CrossRef](#)]
17. Chaudhari, B.; Panda, B.; Šavija, B.; Paul, S.C. Microbiologically Induced Concrete Corrosion: A Concise Review of Assessment Methods, Effects, and Corrosion-Resistant Coating Materials. *Materials* **2022**, *15*, 4279. [[CrossRef](#)]
18. Shen, W.; Zhang, T.; Ge, Y.; Feng, L.; Feng, H.; Li, P. Multifunctional AgO/epoxy nanocomposites with enhanced mechanical, anticorrosion and bactericidal properties. *Prog. Org. Coat.* **2021**, *152*, 106130. [[CrossRef](#)]
19. Shetty, P.; Bhushan, S.; Vidya, A.; Kodialbail, S. Biocorrosion Behavior of Epoxy—Based Multilayer Nanocomposite Coatings. *J. Bio-Tribo-Corrosion* **2023**, *9*, 45. [[CrossRef](#)]
20. Leygraf, C.; Wallinder, I.O.; Tidblad, J.; Graedel, T. Appendix I: The Atmospheric Corrosion Chemistry of Silver. In *Atmospheric Corrosion*, 2nd ed.; John Wiley & Sons, Inc.: Hoboken, NJ, USA, 2016; pp. 337–347.
21. Majeed, H.M.; Wadee, S.A. Antibacterial Activity and Mechanism of Nickel Nanoparticles against Multidrug Resistant *Pseudomonas aeruginosa*. *Ann. Trop. Med. Public Health* **2019**, *22*, 157–168. [[CrossRef](#)]
22. EN 877; Cast Iron Pipes and Fittings, Their Joints and Accessories for the Evacuation of Water from Buildings—Requirements, Test Methods and Quality Assurance. European Committee for Standardization: Brussels, Belgium, 2006.
23. ISO/TS 16782; Clinical Laboratory Testing—Criteria for Acceptable Lots of Dehydrated Mueller-Hinton Agar and Broth for Antimicrobial Susceptibility Testing. International Organization for Standardization: Geneva, Switzerland, 2016.
24. ISO 22196; Plastics—Measurement of Antibacterial Activity on Plastics Surfaces. International Organization for Standardization: Geneva, Switzerland, 2007.
25. ISO 4833-1; Microbiology of the Food Chain—Horizontal Method for the Enumeration of Microorganisms—Part 1: Colony Count at 30 °C by the Pour Plate Technique. International Organization for Standardization: Geneva, Switzerland, 2018.
26. Ghanbari, A.; Attar, M.M. A study on the anticorrosion performance of epoxy nanocomposite coatings containing epoxy-silane treated nano-silica on mild steel substrate. *J. Ind. Eng. Chem.* **2015**, *23*, 145–153. [[CrossRef](#)]
27. Obot, I.B.; Madhankumar, A. Synergistic effect of iodide ion addition on the inhibition of mild steel corrosion in 1 M HCl by 3-amino-2-methylbenzylalcohol. *Mater. Chem. Phys.* **2016**, *177*, 266–275. [[CrossRef](#)]
28. Samardžija, M.; Alar, V.; Špada, V.; Stojanović, I. Corrosion Behaviour of an Epoxy Resin Reinforced with Aluminium Nanoparticles. *Coatings* **2022**, *12*, 1500. [[CrossRef](#)]
29. Solomon, M.M.; Gerengi, H.; Kaya, T.; Umoren, S.A. Performance Evaluation of a Chitosan/Silver Nanoparticles Composite on St37 Steel Corrosion in a 15% HCl Solution. *ACS Sustain. Chem. Eng.* **2017**, *5*, 809–820. [[CrossRef](#)]
30. Anjum, M.J.; Ali, H.; Khan, W.Q.; Zhao, J.; Yasin, G. Chapter 11—Metal/Metal Oxide Nanoparticles as Corrosion Inhibitors, 1st ed.; Elsevier: Amsterdam, The Netherlands, 2020; pp. 181–201.
31. Jain, P.; Patidar, B.; Bhawsar, J. Potential of Nanoparticles as a Corrosion Inhibitor: A Review. *J. Bio-Tribo-Corros.* **2020**, *6*, 43. [[CrossRef](#)]
32. Geoprincy, G.; Nagendhra Gandhi, N.; Renganathan, S. Novel antibacterial effects of alumina nanoparticles on *Bacillus cereus* and *Bacillus subtilis* in comparison with antibiotics. *Int. J. Pharm. Pharm. Sci.* **2012**, *4*, 544–548.
33. Niroumandrad, S.; Rostami, M.; Ramezanzadeh, B. Effects of combined surface treatments of aluminium nanoparticle on its corrosion resistance before and after inclusion into an epoxy coating. *Prog. Org. Coat.* **2016**, *101*, 486–501. [[CrossRef](#)]
34. Samardžija, M.; Kurtela, M.; Vuković Domanovac, M.; Alar, V. Anticorrosion and Antibacterial Properties of Al NP—Epoxy Nanocomposite Coating on Grey Cast Iron. *Coatings* **2023**, *13*, 898. [[CrossRef](#)]
35. Feichtenschlager, B.; Pabisch, S.; Svehla, J.; Peterlik, H.; Sajjad, M.; Koch, T.; Kickelbick, G. Epoxy Resin Nanocomposites: The Influence of Interface Modification on the Dispersion Structure—A Small-Angle-X-ray-Scattering Study. *Surfaces* **2020**, *3*, 664–682. [[CrossRef](#)]
36. Pavapootanont, G.; Wongpanya, P.; Viyanit, E.; Lothongkum, G. Corrosion behavior of Ni steels in aerated 3.5-wt.% NaCl solution at 25 °C by potentiodynamic method. *Eng. J.* **2018**, *22*, 1–12. [[CrossRef](#)]
37. Keast, V.J. Atmospheric Corrosion of Silver and Silver Nanoparticles. *Corros. Mater. Degrad.* **2022**, *3*, 221–234. [[CrossRef](#)]
38. Bordbar, S.; Rezaeizadeh, M.; Kavian, A. Improving thermal conductivity and corrosion resistance of polyurea coating on internal tubes of gas heater by nano silver. *Prog. Org. Coat.* **2020**, *146*, 105722. [[CrossRef](#)]
39. Asghari, E.; Kaltschmidt, B.P.; van Merwyk, L.; Huser, T.; Kaltschmidt, C.; Hutten, A. *Pseudomonasaeruginosa* Clusters Toxic Nickel Nanoparticles to Enhance Survival. *Microorganisms* **2022**, *10*, 2220. [[CrossRef](#)] [[PubMed](#)]
40. Hussain, A.; Ahmad, M.N.; Jalal, F.; Yameen, M.; Falak, S.; Noreen, S.; Naz, S.; Nazir, A.; Iftikhar, S.; Soomro, G.A.; et al. Investigating the antibacterial activity of POMA nanocomposites. *Polish J. Environ. Stud.* **2019**, *28*, 4191–4198. [[CrossRef](#)]
41. Fonseca, S.; Cayer, M.; Ahmmed, K.M.T.; Khadem-moharam, N.; Charette, S.J.; Brouard, D. Characterization of the Antibacterial Activity of an SiO<sub>2</sub> Nanoparticulate Coating to Prevent Bacterial Contamination in Blood Products. *Antibiotics* **2022**, *11*, 107. [[CrossRef](#)]
42. Mukherjee, A.; Mohammed Sadiq, I.; Prathna, T.C.; Chandrasekaran, N. Antimicrobial activity of aluminium oxide nanoparticles for potential clinical applications. *Sci. Microb. Pathog. Commun. Curr. Res. Technol. Adv.* **2011**, *4*, 245–251.
43. Li, Z.; Ma, J.; Ruan, J.; Zhuang, X. Using Positively Charged Magnetic Nanoparticles to Capture Bacteria at Ultralow Concentration. *Nanoscale Res. Lett.* **2019**, *14*, 195. [[CrossRef](#)]

44. Jiang, W.; Mashayekhi, H.; Xing, B. Bacterial toxicity comparison between nano- and micro-scaled oxide particles. *Environ. Pollut.* **2009**, *157*, 1619–1625. [[CrossRef](#)] [[PubMed](#)]
45. Yasakau, K.A.; Zheludkevich, M.L.; Lamaka, S.V.; Ferreira, M.G.S. Mechanism of corrosion inhibition of AA2024 by rare-earth compounds. *J. Phys. Chem. B* **2006**, *110*, 5515–5528. [[CrossRef](#)] [[PubMed](#)]
46. Sharmin, S.; Rahaman, M.M.; Sarkar, C.; Atolani, O.; Islam, M.T.; Adeyemi, O.S. Nanoparticles as antimicrobial and antiviral agents: A literature-based perspective study. *Heliyon* **2021**, *7*, 5515–5528. [[CrossRef](#)]
47. Gudkov, S.V.; Burmistrov, D.E.; Smirnova, V.V.; Semenova, A.A.; Lisitsyn, A.B. A Mini Review of Antibacterial Properties of Al<sub>2</sub>O<sub>3</sub> Nanoparticles. *Nanomaterials* **2022**, *12*, 2635. [[CrossRef](#)] [[PubMed](#)]

**Disclaimer/Publisher's Note:** The statements, opinions and data contained in all publications are solely those of the individual author(s) and contributor(s) and not of MDPI and/or the editor(s). MDPI and/or the editor(s) disclaim responsibility for any injury to people or property resulting from any ideas, methods, instructions or products referred to in the content.

## Article 2

M. Samardžija, V. Alar, V. Špada, I. Stojanović, Corrosion Behaviour of an Epoxy Resin Reinforced with Aluminium Nanoparticles, *Coatings*, 12 (2022), 1500.


### Author Contributions:

Marina Samardžija	conceptualisation, methodology, software, validation, formal analysis, investigation, data curation, writing—original draft preparation, writing—review and editing, visualisation
Vesna Alar	conceptualization, methodology, validation, resources, supervision, project administration
Vedrana Špada	software, validation, formal analysis,
Ivan Stojanović	validation, resources, project administration, funding acquisition

This paper is published in an open access journal (<https://doi.org/10.3390/coatings12101500>).

## Article

# Corrosion Behaviour of an Epoxy Resin Reinforced with Aluminium Nanoparticles

Marina Samardžija <sup>1,\*</sup> , Vesna Alar <sup>2</sup>, Vedrana Špada <sup>3</sup> and Ivan Stojanović <sup>2</sup>

<sup>1</sup> Department of Chemistry, Faculty of Mining-Geology-Petroleum Engineering, University of Zagreb, 10110 Zagreb, Croatia

<sup>2</sup> Department of Welded Structures, Faculty of Mechanical Engineering and Naval Architecture, University of Zagreb, 10000 Zagreb, Croatia

<sup>3</sup> Istrian University of Applied Sciences, Riva 6, 52100 Pula, Croatia

\* Correspondence: marina.samardzija@rgn.hr; Tel.: +385-1-5535-912

**Abstract:** During exploitation, the properties of the epoxy coating deteriorate and therefore, it is necessary to modify it with metal particles. In this paper, spherical aluminium nanoparticles (Al NP) of 100 nm with 99.9% purity were used to modify the epoxy coating for the better corrosion protection of grey cast iron. Pure Al has a high corrosion resistance and can form a thin protective film that prevents its further oxidation, thus, becoming inert and environmentally friendly. To examine these facts, different concentrations (0.5, 0.75, 1.0, 3.0, and 6.0 wt.%) of Al nanoparticles were dispersed in the epoxy coating. The surface of the modified nanocomposite coating was analysed using scanning electron microscopy (SEM) and energy dispersive spectrometry (EDS). Furthermore, the physical properties such as colour, thickness, hardness, and adhesion to the cast iron surface were tested as well. The same properties were tested by exposing the sample plates to corrosive conditions in the climate chamber. Their anticorrosion properties were investigated using electrochemical impedance spectroscopy (EIS) by their immersion in 3.5 wt.% NaCl solution as a corrosive medium. The coating with 0.75% Al NP showed the best corrosion resistance after 10 days of exposure in salt water, while the sample with 1.0% Al NP showed the best corrosion resistance after exposure to the icing/deicing process.

**Keywords:** epoxy; aluminium nanoparticles; coating; anticorrosion



**Citation:** Samardžija, M.; Alar, V.; Špada, V.; Stojanović, I. Corrosion Behaviour of an Epoxy Resin Reinforced with Aluminium Nanoparticles. *Coatings* **2022**, *12*, 1500. <https://doi.org/10.3390/coatings12101500>

Academic Editor: Kyong Yop Rhee

Received: 6 September 2022

Accepted: 4 October 2022

Published: 8 October 2022

**Publisher's Note:** MDPI stays neutral with regard to jurisdictional claims in published maps and institutional affiliations.



**Copyright:** © 2022 by the authors. Licensee MDPI, Basel, Switzerland. This article is an open access article distributed under the terms and conditions of the Creative Commons Attribution (CC BY) license (<https://creativecommons.org/licenses/by/4.0/>).

## 1. Introduction

Cast iron is a material that is commonly used for drainage pipe systems as it is resistant to varying and moderately high internal pressures [1]. This material has also a high corrosion resistance [2], but when it is exposed to an aggressive medium, it is subject to electrochemical corrosion and a special form of corrosion known as graphitic corrosion or graphitisation of cast iron [3]. The most effective way of dealing with this issue is to apply a multi-layered coating system. For this purpose, epoxy coatings are used as they have good protective barrier properties, high adhesion to the metal substrate [4], are easy to apply, and are not expensive. During the exploitation process, the properties of the epoxy coating deteriorate and this leads to blistering and the creation of micropores and microcracks [5]. Consequently, these organic coatings need to be modified. Organic coatings consist of pigments that are dispersed in a binder; this is usually epoxy resin. Due to the complex composition of the epoxy coatings, it is not possible to predict what effects the ingredients will have on the coating properties as thinners and solvents for paints and varnish mixtures of organic liquids are used [6].

When looking for a new and efficient anticorrosion system, some promising initial results are given by nanocomposite systems. With the development of nanotechnology, researchers have started using nanoparticles to modify epoxy resins. The epoxy coating

containing nanoparticles (nanocomposite) showed great improvements, as the nanoparticles have a large specific surface area, are described by a quantum-mechanical method, and show a tunnelling effect [6,7]. Their small size enables the blocking of the micropores and increases the anticorrosion properties [8]. Compared to traditional micro-sized materials, the nanomaterials can more effectively improve the corrosion resistance of the waterborne coating at lower weight percentages [9]. There are different methods of incorporating nanoparticles into the epoxy matrix. Not only the morphology, arrangements, and volume fractions of the nanomaterials have an important effect on the properties of waterborne nanocomposite coatings, but also the dispersion quality of the nanomaterials in the polymer resins is crucial for the properties of the waterborne nanocomposite coatings [9]. According to the research of Shen and co-authors, light mechanical stirring enables the uniform dispersion of 1.0% of silver(II) oxide nanoparticles in pure epoxy resin [6]. Moreover, the author Xavier successfully dispersed the nickel(II) oxide nanoparticles in the polymer matrix at a stirring speed of 3000 rpm and by using acetone as a solvent [10].

By adding nano aluminium, which is a non-toxic material, environmentally friendly coatings can be developed. Several studies have considered the desirable anti-corrosion properties resulting from the addition of nano Al to water-based coatings [11]. The purpose of the study by Bello and co-authors is to achieve the improvement of the mechanical properties of the epoxy resin by using aluminium nanoparticles (Al NP). The authors showed the improvement of the mechanical properties of it, but did not investigate the impact of Al NPs on the corrosive medium [12]. Penna and co-authors dispersed 2.0% and 3.0% Al NPs in alcohol solutions and obtained an epoxy coating with super-hydrophobic properties [13]. Liang and co-authors claimed that the best corrosion protection is achieved with 5 wt.% Al NP using mixers and solvents [14]. The effectiveness of the anticorrosive nanocomposite depends on the properties of the nanoparticles, the barrier property of the polymer matrix, and the dispersion of the nanoparticles. The influence of mechanical mixing on the dispersion of Al NPs in the polymer matrix is presented in this paper. This research showed that this method of nanocomposite preparation can be used to incorporate Al NPs up to 1.0%.

This paper aims to establish the maximum concentration to which the nanocomposite coating can be developed by mechanical mixing of nano- and micro-particles of aluminium without adding solvents. This study is useful because the nanocomposite that is obtained in such a way shows excellent corrosion resistance and extends the life of a pipe. The high electrochemical reactivity and tendency of the aluminium nanoparticles to react with oxygen and moisture cause an oxide layer to form on their surface that prevents further corrosion [15]. Moreover, by using affordable devices for obtaining the nanocomposites, the epoxy coating is affordable for its use in the industry. To achieve a favourable outcome, in this paper, a combination of micro- and nanoparticles was used. A modified epoxy coating was characterised using a scanning electron microscope (SEM) and energy-dispersive X-ray spectroscopy (EDS), whereas the corrosion behaviour was investigated in a simulated marine solution (3.5% NaCl) and through the icing process at  $-5\text{ }^{\circ}\text{C}$  in the climate chamber. In this study, grey cast iron was investigated.

## 2. Materials and Methods

### 2.1. Material

The chemical composition of cast iron is as follows: 1.54 wt.% Si, 24.52 wt.% C, and 73.94 wt.% Fe. The microstructure of the cast iron that was used in this study is shown in Figure 1.

Figure 1 presents a typical microstructure of cast iron containing graphite. The graphite form in the cast iron is classified according to ISO 945-1:2017 [16]. The view of the cast iron microstructure in Figure 1 shows the flake graphite that, according to the standard, is marked as type IA.



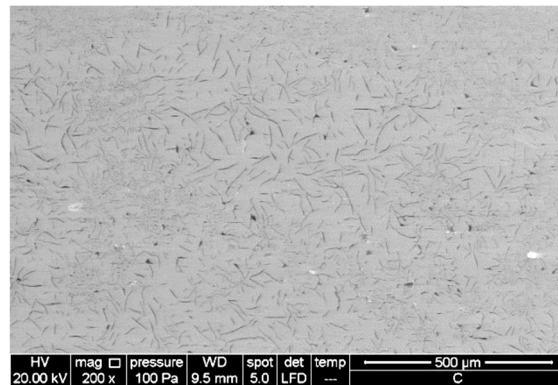


**Figure 1.** Microstructure of grey cast iron microstructure in the unetched state.

To remove corrosion products from the metal substrate, ethanol (70 wt.%) was used. Aluminium nanoparticles (100 nm in size) whose chemical composition is shown in Figure 2 were obtained from Guangzhou Hongwu Material Technology Co., Ltd. (Guangzhou, China).

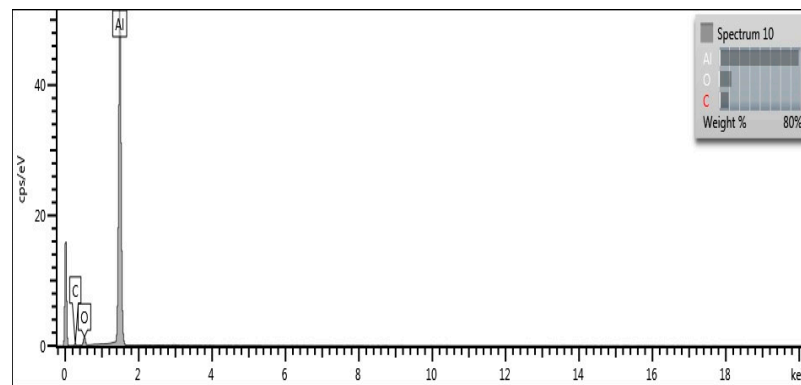


**Figure 2.** Chemical composition of Al NP.

The epoxy coating was prepared using epoxy resin (Bisphenol A, Hempel, Croatia) and hardeners (polyamine, Hempel, Zagreb, Croatia). For removing bubbles from epoxy resin, isopropanol was used.

## 2.2. Preparation of the Epoxy Coatings

Grey cast iron plates with dimensions of 9.5 cm × 0.9 cm × 15 cm were used as substrates. The surfaces of grey cast iron were cleaned with abrasive blasting ( $R_z$  of 136.7 μm) and ethanol to remove surface contaminants. To find the best concentration of Al NPs which may improve the anticorrosion protection of the epoxy coating, different weight percentages of Al NPs were dispersed in the epoxy coating. Table 1 shows the composition of the prepared nanocomposites.

**Table 1.** Incorporation of aluminium nanoparticles in epoxy resin and thickness of the obtained nanocomposites.

Sample	Epoxy Resin (g)	Hardener (g)	Al NP (%)	Thickness (μm)
blank_epoxy	30	7.5	0	207.2
0.50%_Al	30	7.5	0.50	228.1
0.75%_Al	30	7.5	0.75	235.4
1.0%_Al	30	7.5	1.0	229.7
3.0%_Al	30	7.5	3.0	212.3
6.0%_Al	30	7.5	6.0	226.7

Aluminium nanoparticles were added to the epoxy resin and mixed using a glass stick. Thereafter, the nanocomposites were put in a dispersing device (Ika T25, ultra turrax disperser, IKA<sup>®</sup>-Werke GmbH & Co. KG, Staufen, Germany) at a speed of 3000 rpm for 3 min. After that, the hardener was added, and everything was mixed using a glass stick until a homogeneous mixture was obtained as shown in Figure 3. The epoxy resin and hardener were added in a ratio of 1:4. No solvents were added during the dispersion process. The obtained nanocomposites were applied to a previously degreased grey cast iron substrate using an applicator (150  $\mu\text{m}$ ). To remove bubbles in the nanocomposite coating, immediately after the application, the coating was sprayed with isopropanol. Then, the samples were dried at 100  $^{\circ}\text{C}$  for 40 min. After cooling, another layer of nanocomposites was applied in the opposite direction (150  $\mu\text{m}$  applicator). The drying time was the same as for the previous layer. The samples were left at room temperature (25  $^{\circ}\text{C}$ ) for 7 days and then tested again (Figure 3).

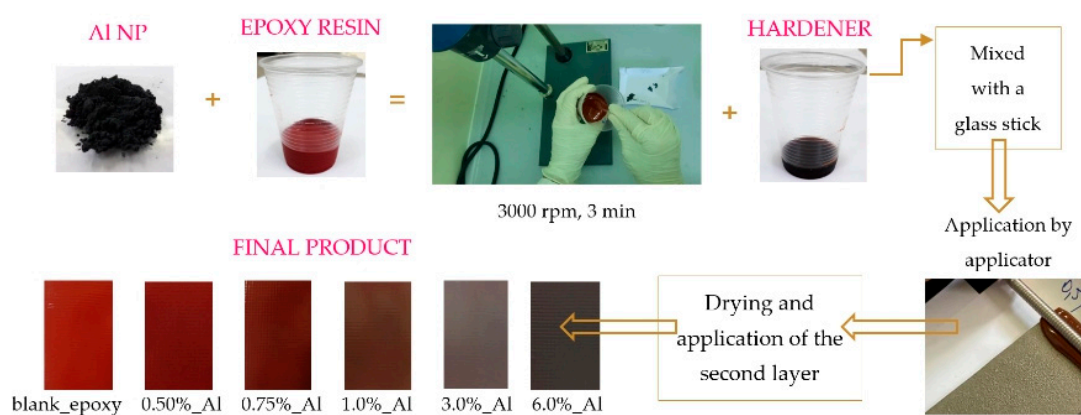


**Figure 3.** Description of modified nanocomposite coating preparation, application, and drying.

The homogeneity of the nanocomposite coating layer was investigated using a scanning electron microscope (SEM) (TESCAN Brno, Brno, Czech Republic) at a high vacuum, with 10 kV, a spot size of 3, and a work distance of 6 mm. The size distribution and dispersion of nanoparticles, the homogeneity of the layer, and the occurrence of agglomeration were observed. The microanalysis of the chemical composition of the sample was conducted using the energy-dispersive (EDS, INCA PentaFET, Oxford, United Kingdom) detector.

The change in colour of the nanocomposite coating was determined using RAL colour chart (RAL gGmbH, Siegburger, Germany). Elcometer<sup>®</sup>456 (Elcometer Limited, Edge Lane, Manchester, UK) was used to assess the thickness of the nanocoating sample. Measurements were performed on ten different locations per sample. The hardness of the coating was tested according to ISO 868:2003 [17]. The testing was performed using PosiTector SHD Shore Hardness Durometer (DeFlesko Corporation, Ogdensburg, NY, USA). The Elcometer 510 Automatic Pull-Off Adhesion Tester (Elcometer 510, model T, Manchester, UK) was used to measure the strength of the bond between the nanocomposite coating and the grey cast iron substrate. Aluminium dollies (20 mm diameter) were adhered to the topcoat surface using a two-part epoxy adhesive (Araldite resin and Araldite hardener). The coating adhesion was tested after 24 h.

To test the coating stability at low temperatures, the samples were placed in the climatic chamber (Climatic chamber Kambic KK-190 CHLT, CiK Solutions GmbH, Karlsruhe, Germany). The first test cycle lasted 24 h, the samples were placed at 5  $^{\circ}\text{C}$  with 0% humidity. In the second cycle that followed the first one, the temperature was lowered to  $-5$   $^{\circ}\text{C}$  for 2 h. This was followed by an intermediate step where the conditions in the chamber varied from 3  $^{\circ}\text{C}/\text{h}$  to 10  $^{\circ}\text{C}$ . The third test cycle at 10  $^{\circ}\text{C}$  and 70% humidity lasted 1440 min. After the icing/deicing process, the physical and chemical properties of samples were tested after they reached room temperature.

Open-circuit potential (OCP) was first obtained over a period of 20 min to study the changes in the corrosion potential of the coatings. Electrochemical Impedance Spectroscopy (EIS) was used to evaluate the resistance of the nanocomposite coating in 3.5% NaCl solution, pH = 7.554, while it was open to the atmosphere. For this purpose, VersaSTAT 3 Potentiostat/Galvanostat (AMETEK Scientific 131 Instruments, Princeton applied research, Berwyn, PA, USA) was used. Measurements were performed in the frequency range from 100 kHz to 0.1 Hz, a potential amplitude of 10 mV at a room temperature of  $25 \pm 2$  °C, while we recorded 10 points per decade. Measurements were conducted using an electrochemical cell with the coated sample as the working electrode of  $19.625 \text{ cm}^2$ . The saturated calomel electrode was used as a reference electrode and the graphite rod as the counter electrode. The ZSimWin software was used to interpret data.

Each measurement was implemented in three replications for checking the repeatability of data.

### 3. Results and Discussion

#### 3.1. Characterisation of Aluminium Nanoparticles (Al NP)

The visual analysis showed that the Al NP was dark grey. According to the data that were obtained by the manufacturer (Figure 2), the nanoparticles contained high-purity aluminium (99.92%). The SEM analysis was used to determine the form and the size of Al NPs that were dispersed in the epoxy matrix. The surface morphology of the Al NP is shown in Figure 4.

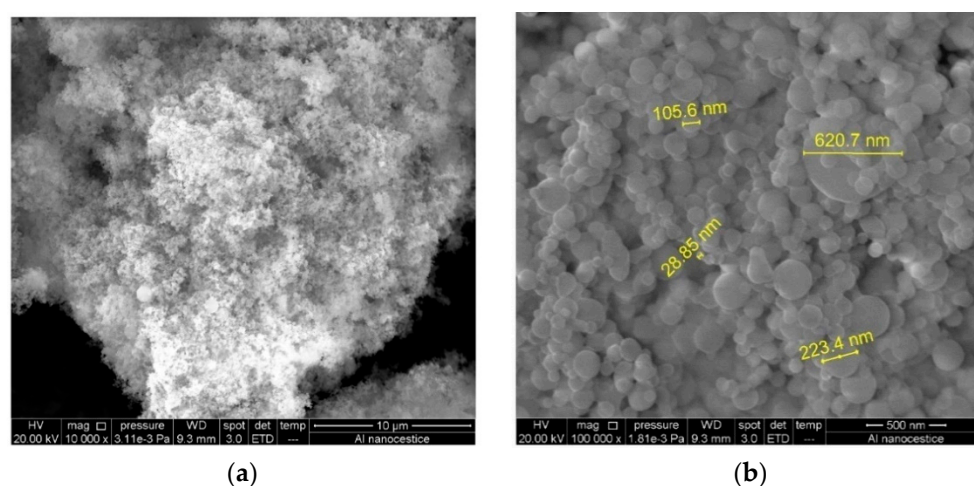


**Figure 4.** SEM analysis of (a) Al NP surface morphology and (b) size of aluminium nanoparticles in metal powder.

Figure 4a shows the nanoparticles in the form of a fluffy powder. At a higher magnification (Figure 4b), the spherical particles without pores that formed larger aggregates were visible. The estimated size was around 100 nm. Even though the size of the particles was not evenly distributed, these nanoparticles were characterised by an excellent dispersion and a high degree of hardness. According to the available literature, these nanoparticles belong to the group of zero-dimensional (0D) nanomaterials. Spherical 0D nanoparticles have a tendency for physical or chemical crosslinking with polymer resins, and the high crosslinking density of the water-borne resins is responsible for a high degree of curing. However, the surface activity of 0D nanoparticles is usually high, which leads to their aggregation. The agglomeration of the nanoparticles leads to the creation of new defects in the nanocomposite coating, which not only can damage the performance of the coating barrier, but also lowers its mechanical properties [9]. The tendency of the nanoparticles to form larger agglomerates was observed by adding greater quantities of Al NPs in the epoxy matrix.

### 3.2. Characterisation of Nanocomposite

The SEM and EDS analyses established that the initial epoxy coating without the nanoparticles contains Al<sub>2</sub>O<sub>3</sub> microparticles. Thus, by adding the Al NP, the concentration of the aluminium changed, as is shown in Table 2. Table 2 shows the Al NPs' added masses and results which were obtained by the EDS analysis.

**Table 2.** Obtained chemical composition of aluminium in epoxy coating.

Sample	<i>m</i> (Al NP), g	EDS(Al), %
blank epoxy	0.0000	0.96
0.50%_Al	0.1884	1.04
0.75%_Al	0.2915	1.19
1.0%_Al	0.3794	1.61
3.0%_Al	1.1598	2.21
6.0%_Al	2.3936	4.11

By adding the Al NPs to the epoxy matrix, the content by weight continually increased up to the mass concentration of 1% (Table 2). For samples in which 3.0 and 6.0% Al NP was added, the EDS analysis showed that there was a lower concentration of it. This was probably due to the formation of larger accumulations of nanoparticles and their uneven dispersion. Figure 5 shows the SEM micrographs that were obtained by analysing the cast iron surface that was coated with (a) the epoxy matrix without Al NP, and with (b) 0.50% Al NP, (c) 0.75% Al NP, (d) 1.0% Al NP, (e) 3.0 % Al NP, and (f) 6.0% Al NP before their immersion in an aggressive medium.

The SEM analysis showed that the epoxy matrix without adding the Al NPs had irregularities and alien particles, and the surface was not homogeneous. By adding the Al NP, the surface of the obtained nanocomposite presented many more irregularities and a higher concentration of brighter points. Figure 5b–f shows the slight differences in the surface morphology of the modified samples. The SEM analysis shows that, compared to the epoxy coating without the Al NP, the presence of the Al NP changed the morphology of the epoxy coating, and this effect was visible when we added 0.5% Al NP.

To determine the composition of the epoxy matrix and how the amount of the aluminium in the samples changed, the EDS analysis of each sample was carried out (Figure 6). The EDS analysis of the epoxy matrix without adding the Al NPs (Figure 6a) determined the percentage of the aluminium microparticles, and this was 0.96%. It was assumed that these microparticles of aluminium were used as a pigment in the epoxy paints. The presence of all of these elements in the blank epoxy matrix showed small irregularities as determined by the SEM analysis (Figure 5). By adding the Al NPs, the EDS analysis also detected Al that was already present in the epoxy matrix. This analysis showed a combination of micro- and nanoparticles of aluminium. The concentration of microparticles was constant, and the proportion of the Al NPs increased. A trend of increasing Al NP concentration was observed in the samples up to 1.0% (Figure 6b–d).

The EDS analysis could not detect a trend of increasing Al NP content due to the appearance of agglomerates in the 3% and 6% samples, and a drop in concentration appeared (Figure 6e,f). Inside the agglomerate, there were accumulated nanoparticles that were not well dispersed in the epoxy matrix, thus reducing the proportion over the entire surface.

To determine the homogeneity of the Al NP dispersion in the epoxy matrix, the EDS mapping for the epoxy matrix without adding Al NPs and for the nanocomposite with 1.0% Al NP and 6.0% Al NP was conducted (Figure 7).

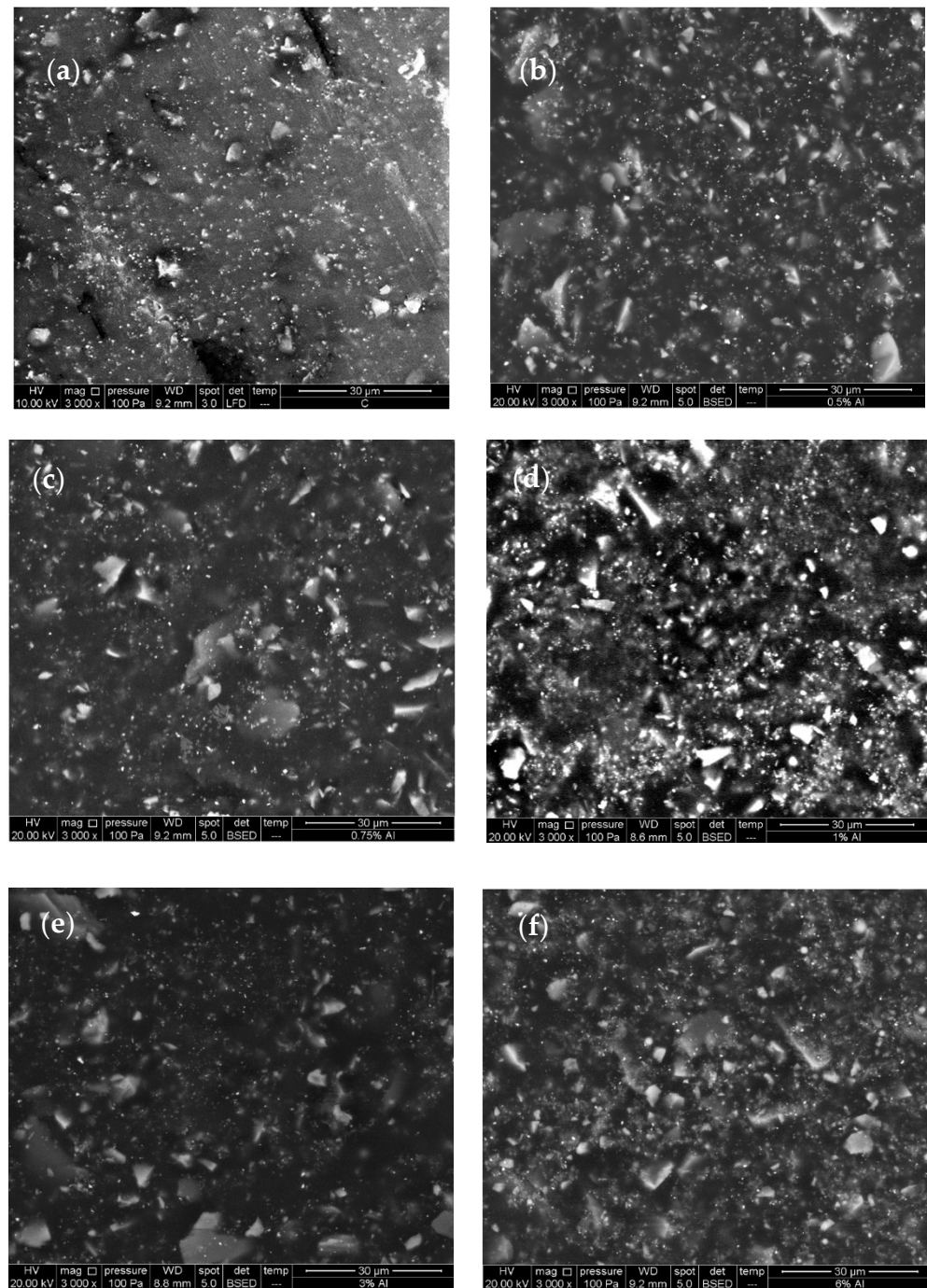


**Figure 5.** SEM micrographs obtained for the surface of (a) blank epoxy and epoxy coating with (b) 0.50% Al nanoparticles, (c) 0.75% Al nanoparticles, (d) 1.0% Al nanoparticles, (e) 3.0% Al nanoparticles, and (f) 6.0% Al nanoparticles.

The EDS mapping of the epoxy matrix without adding the Al NPs (Figure 7a) showed a rough non-homogeneous distribution of elements. By adding the Al NPs and using a mechanical mixer (Figure 7e,i), the nanocomposite obtained a smoother, homogeneous structure. The distribution of the elements of carbon and oxygen (Figure 7b,c,f,g,j,k) was even throughout the surface of all of the samples. The best aluminium distribution was observed in the sample with 1.0% Al NP (Figure 7h), whereas in the epoxy matrix (Figure 7d) and the sample with 6.0% Al NP (Figure 7l), agglomerates were observed. Microparticles and agglomerates of aluminium that serve as a pigment in the epoxy matrix were present in the epoxy matrix (Figure 7d). However, by adding the Al NPs and using a mechanical

mixer at 3000 rpm, these microparticles were broken and the micro and nano aluminium particles were evenly distributed. By adding a higher concentration of Al NPs (Figure 71), the saturation of the coating with the nanoparticles increased, and the nanoparticles began to interact and agglomerate. For the incorporation of a higher concentration of Al NPs in the epoxy matrix, a different method of sample preparation should be used.

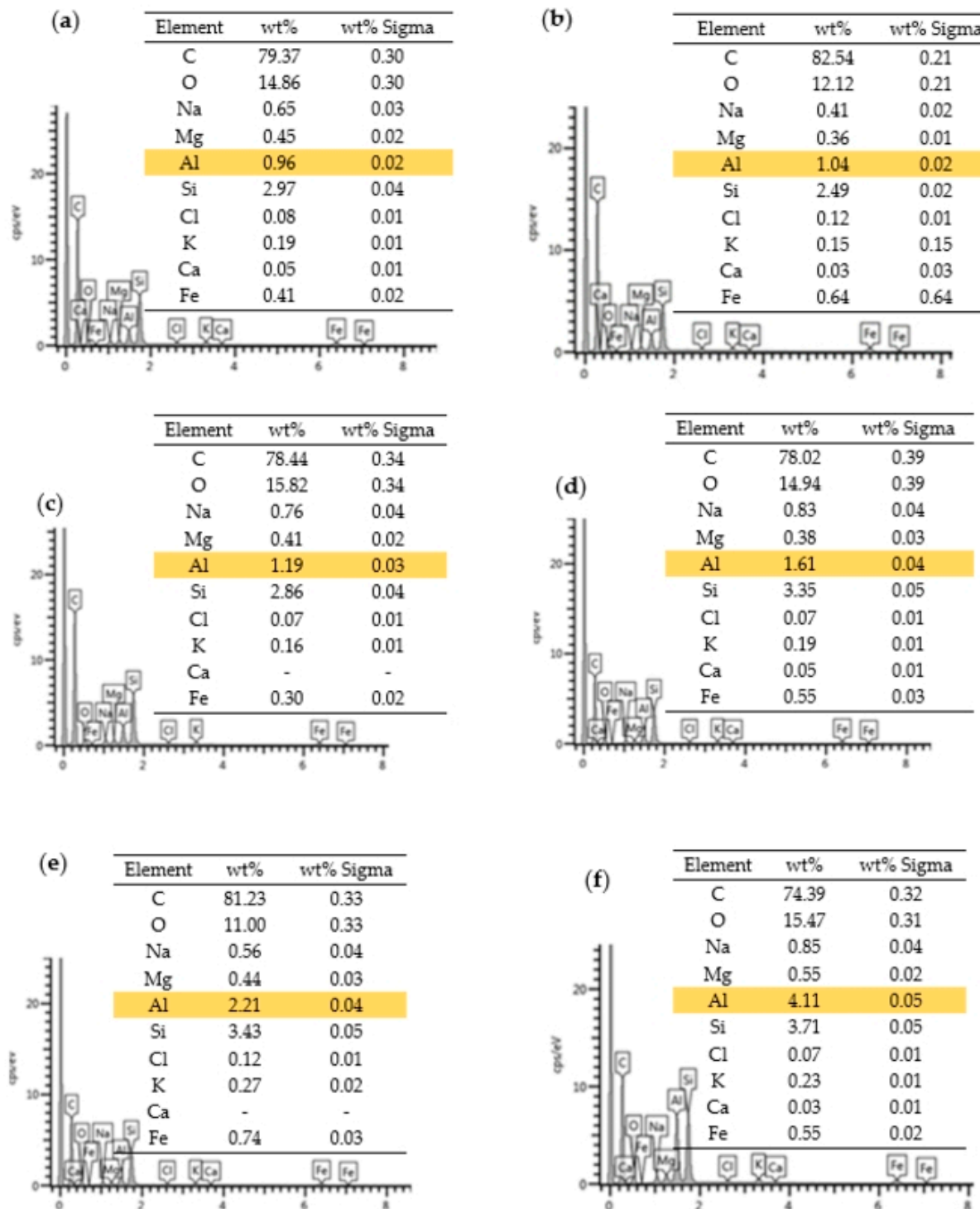


**Figure 6.** EDS spectra and overview of chemical composition of (a) epoxy matrix without Al NP and epoxy matrix with (b) 0.5%, (c) 0.75%, (d) 1.0%, (e) 3.0%, and (f) 6.0% Al NP.

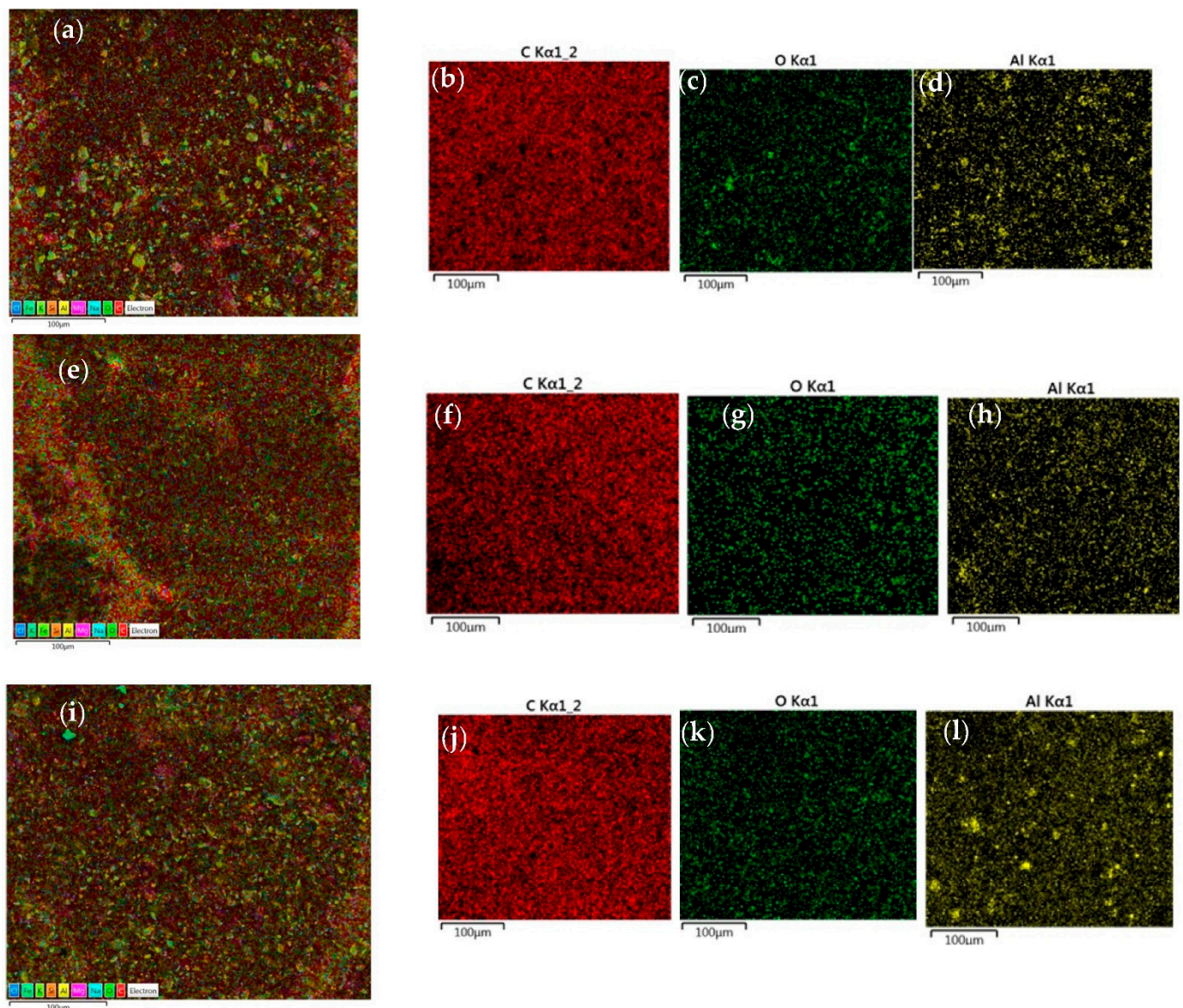


**Figure 7.** EDS mapping of the epoxy matrix (a) without adding Al NP, with (e) 1.0% Al NP and (i) 6.0% Al NP. Overview of the distribution of carbon (C), oxygen (O), and aluminium (Al) in epoxy coating (b–d) without adding Al NPs and with (f–h) 1.0% Al NP and (j–l) 6.0% Al NP.

### 3.3. Physical Properties of Coatings

The nanoparticles that were effectively dispersed in the epoxy matrix improved the mechanical properties of the composite [18] and affected the corrosion resistance of the coating [19]. The physical properties that were tested included discoloration, hardness, and coating adhesion to the metal substrate. Testing in climatic chambers was conducted under conditions that are typical for moderate winter continental climates that prevail in closed, non-heated premises. Table 3 shows the change in colour of the epoxy matrix with and without adding Al NPs and after the icing/deicing process.

By adding a higher concentration of the Al NPs in the epoxy matrix (Table 3), the colour of the nanocomposite became reddish grey to fully grey, as shown in Figure 3. After the samples had been exposed to the icing/deicing process, no discoloration was observed (Table 3). The results of coating hardness tests according to the Shore D scale before and after the icing/deicing process are shown in Table 4.

**Table 3.** Discoloration testing results for the epoxy matrix without and with adding Al NPs before and after the icing/deicing process.

Samples	Blank-Epoxy	0.50%_Al	0.75%_Al	1.0%_Al	3.0%_Al	6.0%_Al
non-exposed samples	RAL 3013	RAL 8015	RAL 8016	RAL 8017	8019	RAL 7015
icing/deicing process	RAL 3013	RAL 8015	RAL 8016	RAL 8017	8019	RAL 7015

**Table 4.** Results of coating hardness testing for epoxy matrix with and without adding Al NPs before and after the icing/deicing process.

Samples	Blank-Epoxy	0.50%_Al	0.75%_Al	1.0%_Al	3.0%_Al	6.0%_Al
non-exposed samples	83.4	83.0	83.6	83.4	84.4	83.5
icing/deicing process	82.0	83.6	80.6	80.8	82.8	83.2

The figures in Table 4 show that by adding different concentrations of Al NPs the coating hardness remained the same. It can be concluded that the Al NPs do not change the elastic properties of the coating and do not have an effect on the wear and tear resistance of the coating. After exposing the samples to the icing and deicing processes, there was no visible difference in the hardness of coatings compared to those of the non-tested samples. The results of the measurements show a high degree of the surface hardness which was characterised by a durable film with a predicted good wear. The dry adhesion strength of the epoxy matrix and nanocomposite on the surface of the cast iron was tested with the pull-off method. The pull-off adhesion test results for all of the samples are shown in Table 5.

**Table 5.** Adhesion test results for epoxy matrix with and without adding Al NPs as well as before and after the icing/deicing process.

Samples/MPa	Blank-Epoxy	0.50%_Al	0.75%_Al	1.0%_Al	3.0%_Al	6.0%_Al
non-exposed samples	8.34	13.00	15.56	-	13.97	12.14
icing/deicing process	8.31	13.24	14.49	-	13.45	10.93
	9.53	14.01	14.89	-	12.84	10.57
	8.98	13.58	14.47	-	13.25	13.01

The pull-off adhesion test results show an increased adhesion capability on the base material with the addition of the Al NP (Table 5). The adhesion of the sample containing 1.0% Al NP could not be established because the adhesion bond between the cast iron and the nanocomposite was high, and separation occurred between the glue and the dolly. All of the other samples showed adhesion loss in the nanocomposite layer, which confirms the good properties of the glue that was used [20]. The testing in the climatic chamber did not contribute to the reduction in the adhesion to the base material in either sample.

### 3.4. EIS Measurement

The EIS measurements were carried out to determine the influence of the increase in Al NP content in the epoxy matrix on the corrosion resistance in a 3.5% NaCl solution and in the climatic chamber. In the study of corrosion and corrosion mitigation of several metals in the sodium chloride solutions, the EIS measurements were used to report the kinetic parameters for the electron transfer reactions at the electrode/environment interface [21].

The equivalent electric circuit (EEC) model that is shown in Figure 8 was used to describe the impedance spectra. According to the available literature for organic coatings, a model with three resistors was selected. The model consists of the electrolyte resistance



( $R_s$ ), coating resistance ( $R_{coat}$ ), and coating capacity ( $CPE_{coat}$ ), charge transfer resistance ( $R_{ct}$ ), and constant phase element which represents a double-layer capacitance between the metal and the electrolyte solution ( $CPE_{dl}$ ) [22]. The Constant Phase Element (CPE) was used instead of the double-layer capacitance ( $C_{dl}$ ) when the capacitive loop deviated from a true semicircle. The CPE represents a real imperfect system that defines the non-heterogeneity of the surface ( $CPE_{coat}$ ) and the non-homogeneity of the charge distribution ( $CPE_{dl}$ ) [23].

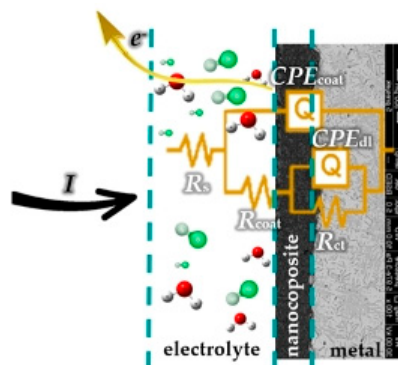


**Figure 8.** Equivalent circuit model employed to fit the impedance data.

The OCP measurement showed an insignificant change in the electrode potential. Compared to the blank epoxy, the OCP value of the nanocomposite was even lower. By increasing the Al NP concentration, the potential decreased to more negative values. After the immersion of the samples in 3.5 wt.% NaCl solution, the OCP values of the blank epoxy and of the samples with 0.5%, 0.75%, 1.0%, 3.0%, and 6.0% Al NP were approximately  $-36.80$  mV,  $-62.56$  mV,  $-79.74$  mV,  $-94.67$  mV,  $-102.44$  mV, and  $-129.74$  V, respectively.

The Nyquist and the Bode plots for the epoxy matrix without the Al NPs and the prepared nanocomposites with 0.5%, 0.75%, 1.0%, 3.0%, and 6.0% Al NPs are shown in Figure 9. The impedance spectrum was recorded immediately after the immersion in 3.5% NaCl solution (Figure 9a,b), and after 10 days or 240 h (Figure 9c,d). For the samples that were exposed to the icing and de-icing processes in the climatic chamber, the impedance spectrum was also recorded (Figure 9e,f).

The EIS spectra for the samples that were immediately immersed in the aggressive media (Figure 9a,b) showed that the sample with 1.0% Al NP had the best resistance. In the beginning, the samples did not achieve a full semicircle, meaning that the coating was very strong, the electrolyte had not damaged the coating's substrate, and the impressed current could not pass because the coating provided a sufficiently high resistance. By adding the Al NP, the coating resistance increased until it reached a concentration of 1.0% Al NP, whereas by adding 3.0 and 6.0% Al NP, the resistance decreased. This was due to the agglomeration of the nanoparticles that began to appear at concentrations higher than 1.0%. In these cases, the nanoparticles were not well coated with the epoxy matrix. For the incorporation of a higher concentration of the nanoparticles in the epoxy, the coating should be prepared differently, for instance: a longer mixing period with a cooling period or the use of a different type of mixer and/or mixing device. After 240 h (Figure 9c,d), all of the samples took on the shape of a regular semicircle, meaning that the coating became weaker and could not provide satisfactory resistance to the passage of the current. Despite the drop in resistance, the coating still provided satisfactory resistance. The greater the obtained semicircle diameter was, the greater the resistance of the coated surface to corrosion was [24]. The best resistance to the aggressive medium after 240 h was provided by the sample with 0.75% Al NP (Figure 9c,d). After exposing the samples to the conditions in the climatic chamber (Figure 9e,f), the recorded EIS spectra showed an improvement in the electrochemical properties of the coatings, which might be due to the influence of the humid environment and low temperature on the nanoparticles. In all of the samples, only one capacitive loop was visible, which may be attributed to very good coating adhesion to the base material [25] and good barrier properties [26]. The coating resistance ( $R_p$ ) and

the constant phase element ( $CPE_{coat}$ ) were calculated according to the shown EEC model (Figure 8) for all of the samples that were immersed immediately and after 240 h in 3.5% NaCl solution and thereafter, exposed in the climatic chamber (Figure 10a,b).

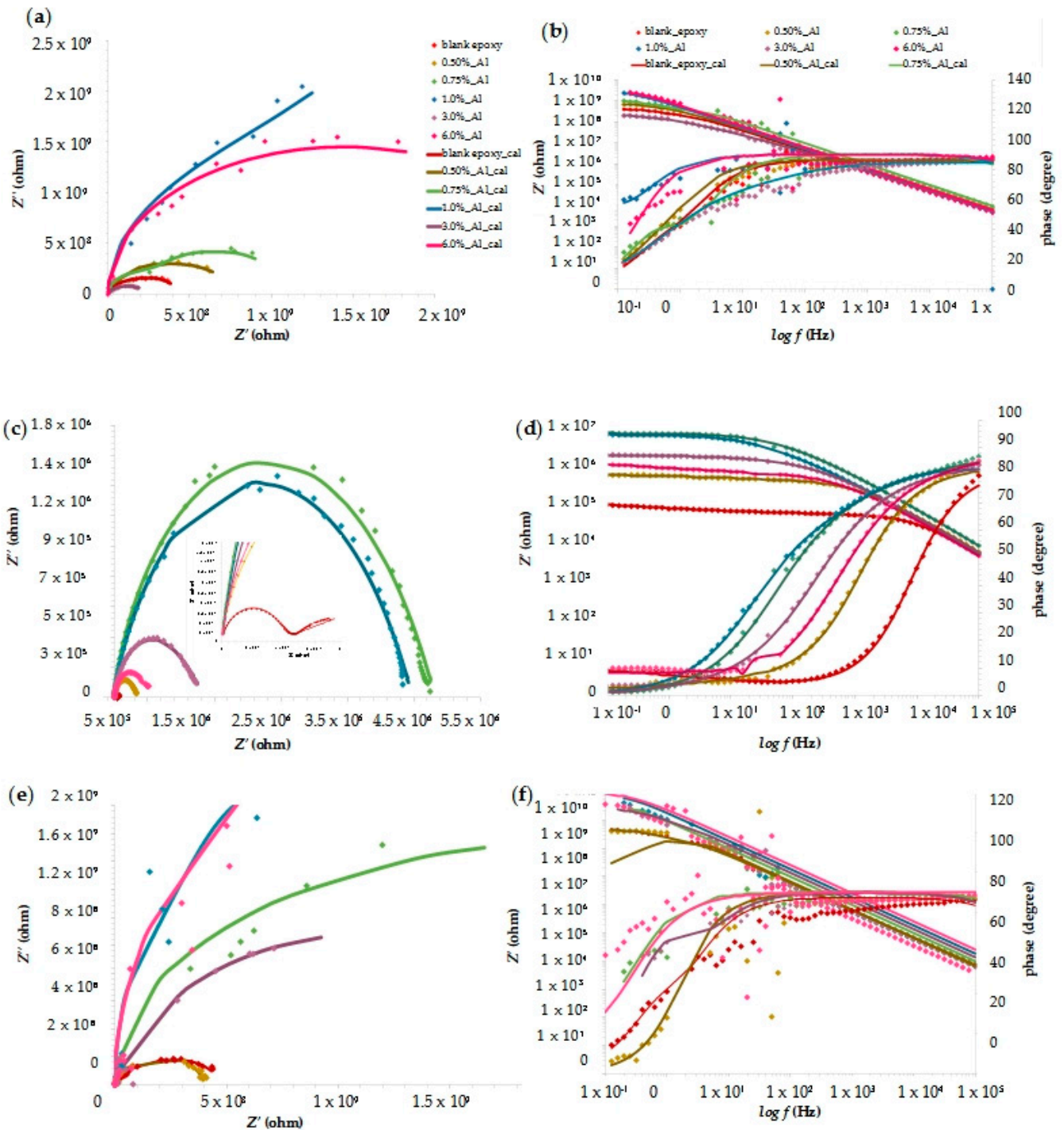
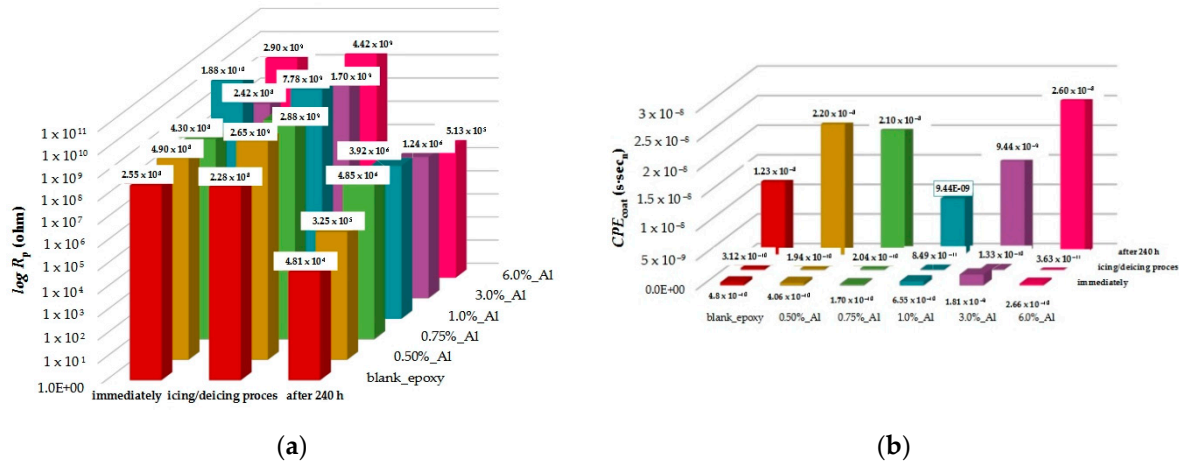


Figure 9. Nyquist and Bode plots for samples immersed immediately (a,b), after 10 days (c,d), and samples (e,f) exposed to corrosion conditions in climatic chamber.

By exposing the samples to the corrosive medium, the  $R_{coat}$  value decreased, which was accompanied by an increase in the  $CPE_{coat}$  value. After 240 h of immersing the samples in a corrosive medium, the increased values of  $CPE_{coat}$  showed that the coating absorbed water and it may be assumed that the corrosive medium reached the surface of the grey cast iron. Such behaviour was most noticeable in the sample with 6.0% Al NP. For the

samples that were placed in the climatic chamber, there was no change in the values for  $CPE_{coat}$ , which would mean that the increase in the resistance was due to the influence of the low temperature on the nanoparticles.



**Figure 10.** Overview of (a) coating resistance ( $R_p$ ) and (b) constant phase element ( $CPE_{coat}$ ) for epoxy matrix without Al NP, and prepared nanocomposites with 0.50%, 0.75%, 1.0%, 3.0%, and 6.0% Al NP, immediately and after 240 h exposure in aggressive medium (3.5% NaCl), and after testing in climatic chamber.

The obtained values which are shown in Figure 10 for coating resistance ( $R_{coat}$ ) were used to calculate the nanocomposite protection efficiency using the following equation [27]:

$$Coating\ protection\ efficiency = \frac{(R_{coat\ with\ Al\ NP} - R_{coat\ without\ Al\ NP})}{R_{coat\ with\ Al\ NP}} \cdot 100\% \quad (1)$$

The calculated nanocomposite efficiency is shown in Table 6 for each sample that contained Al NPs after 240 h of exposure in the electrolyte solution and after their exposure in the climatic chamber (icing and deicing process).

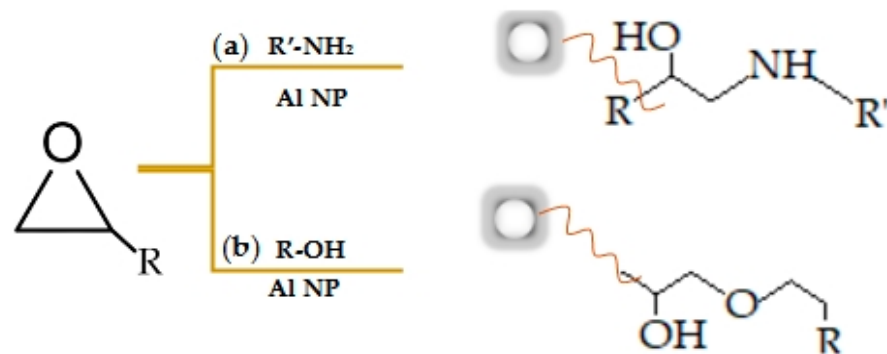
**Table 6.** Calculated coating protection efficiency (CPE, %) for non-modified and modified epoxy coating immersed immediately and after 240 h in 3.5% NaCl and after the icing/deicing process.

Samples	0.50%_Al	0.75%_Al	1.0%_Al	3.0%_Al	6.0%_Al
immediately	47.96	40.70	98.64	-	91.21
after 240 h	85.20	99.01	98.77	96.12	90.62
icing/deicing process	91.40	92.08	97.07	86.59	94.84

The sample that contained 1.0% Al NP showed the best efficiency which was continuously maintained after its exposure to the aggressive medium and the climatic chamber. In all of the other samples, the efficiency improved with time. The reason for such behaviour was a high electrochemical reactivity and the tendency of the nanoparticles to react with oxygen. Under the influence of moisture, an oxide layer formed on their surface which prevented their further corrosion [15]. Although the samples with 3.0% and 6.0% Al NP showed a lower resistance due to the effect of agglomeration, their efficiency was very high, and they could be classified into the category of acceptable coatings. The incorporation of higher concentrations of nanoparticles in the epoxy coating should be the subject of future study.

By increasing the concentration of the aluminium nanoparticles (up to 1.0%) in the epoxy matrix, the adhesion of the epoxy coating to the metal substrate increased. The occurrence of an adhesion enhancement implies that there was a good compatibility between

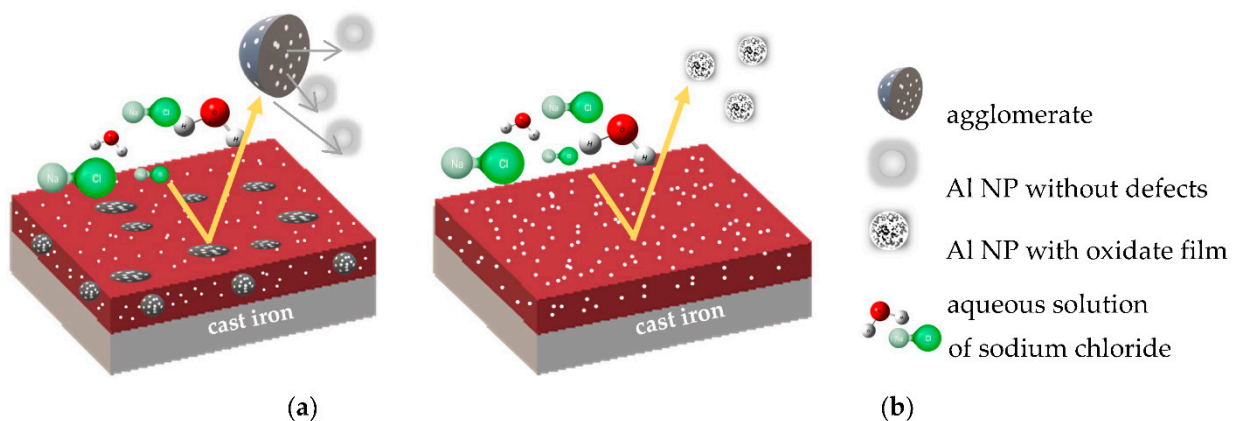
the Al NPs and the epoxy matrix. The possible reactions between the nanoparticles (which were well dispersed in the epoxy matrix) and the epoxy resin are shown in Figure 11.



**Figure 11.** Possible reactions of incorporation of Al NP (a) into the added hardener (amine) and (b) directly in the epoxy matrix.

By adding the hardener, the aliphatic amine initiated the curing by the nucleophilic attack of the amine group at the epoxy ring of the monomer (Figure 11a) [28]. Aluminium nanoparticles can enter into a chemical reaction with the hardener that is contained in the epoxy resin due to their small size. According to the chemical reaction in Figure 11b, the epoxy matrix, that is in a chain, contains hydroxyl groups that serve as sites for the creation of strong electromagnetic bonding attraction between the epoxy and metal molecules [29]. In this way, the aluminium nanoparticle is directly incorporated into the epoxy matrix.

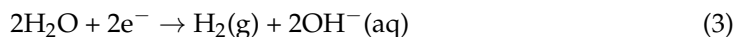
The increase in the concentration of the Al NPs in the epoxy matrix (more than 3%) leads to the formation of agglomerates. Agglomeration, which is caused by the poor dispersion of nanomaterials, can cause inhomogeneity in the nanocomposite (Figure 12a). Such a structure will show a significant decrease in the anticorrosive protection of the nanocomposite during its exposure to an aggressive medium (3.5 wt.% NaCl).



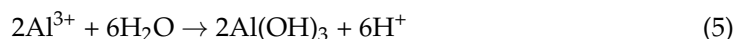
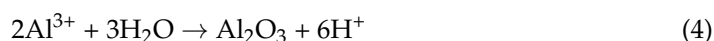
**Figure 12.** Graphic image of different influences of the electrolyte on the system (a) with agglomerates and (b) without agglomerates.

Figure 12b shows the behaviour of the nanocomposite where no agglomeration occurred, that is, the figure shows the successful incorporation of the nanoparticles in the organic film which is based on the reactions in Figure 11. Pure aluminium that is in contact with air or moisture is a thermodynamically reactive metal with an extremely negative value of the standard electrode potential ( $-1.66$  V). However, in neutral aqueous solutions, the aluminium showed a positive potential value of  $-0.6$  V, meaning that a thin protective layer was formed on its surface [30]. When it is in contact with the aqueous solution of NaCl and by the influence of the impressed current  $I$ , during the measurement of the EIS

spectrum, the aluminium nanoparticles will oxidise, which will lead to a reduction in the amount of water according to the following equations:



The aqueous solution is a weak electrolyte, which means that it consists more of water molecules than it does of ions, and thus the formed aluminium ions can react with water molecules ( $\text{H}_2\text{O}$ ) and form hydroxide ions ( $\text{OH}^{-}$ ). The corrosion reactions that occurred on the Al NP surface in the neutral medium are [15]:



The oxide layer on the nanoparticles provides a certain protection against the electrolyte by inhibiting the reaction of the electrolyte penetration into the structure of the epoxy matrix [31]. The electrolyte penetration is accelerated by the presence of chloride ions ( $\text{Cl}^{-}$ ), which are among the most corrosive halogen elements. Due to their relatively small size and high mobility,  $\text{Cl}^{-}$  ions can penetrate the aluminium oxide layer and thus, reduce the corrosion resistance of the nanocomposite [30].

#### 4. Conclusions

This paper investigates the influence of different concentrations of Al NPs in an organic coating to increase its anti-corrosive properties. All of the studies that have been conducted so far have aimed to achieve the desired coating properties. Among these, the most relevant are the increase in the coating resistance against an aggressive media, environmental friendliness, and low production costs that are acceptable for the industry. The research that has been carried out has brought some new findings which will help to improve the incorporation of larger quantities of nanoparticles in the epoxy matrix.

The aluminium nanopowder that was used in this paper consists of high-purity spherical nanoparticles. The SEM and EDS analysis established that by incorporating Al NPs in the epoxy matrix, no agglomeration occurred until the aluminium concentration in the coating reached 1.61%. The addition of Al NPs in the epoxy matrix was accompanied by a change in the colour of the nanocomposite from red to grey. By analysing the hardness of the nanocomposite, it has been established that by adding different concentrations of Al NP, the hardness of the coating remained the same, which also occurred after exposing the sample to the icing/deicing process. The results of testing the adhesion of the nanocomposite to the substrate of the cast iron showed an exceptional increase concerning the epoxy matrix. The recorded EIS spectra indicate that all of the nanocomposite samples showed exceptional resistance to the action of salt water and the icing/deicing process.

**Author Contributions:** Conceptualisation, M.S. and V.A.; methodology, M.S. and V.A.; software, M.S. and V.Š.; validation, M.S., V.A., V.Š. and I.S.; formal analysis, M.S. and V.Š.; investigation, M.S.; resources, V.A. and I.S.; data curation, M.S.; writing—original draft preparation, M.S.; writing—review and editing, M.S.; visualisation, M.S.; supervision, V.A.; project administration, V.A. and I.S.; funding acquisition, I.S. All authors have read and agreed to the published version of the manuscript.

**Funding:** This research was funded by “Development of anticorrosion protection system for multipurpose pipe use”, grant number KK.01.1.1.07.0045. This work was supported by the European Regional Development Fund under the Operational Program Competitiveness and Cohesion 2014–2020.

**Institutional Review Board Statement:** Not applicable.

**Informed Consent Statement:** Not applicable.

**Data Availability Statement:** Not applicable.

**Conflicts of Interest:** The authors declare no conflict of interest.

## References

1. Melchers, R.E. Post-perforation external corrosion of cast iron pressurised water mains. *Corros. Eng. Sci. Technol.* **2017**, *52*, 541–546. [[CrossRef](#)]
2. Kadhim, L. The Corrosion Behavior and Wear Resistance of Gray Cast Iron. *Kufa J. Eng.* **2018**, *9*, 118–132. [[CrossRef](#)]
3. Jur, T.; Middleton, J.; Yurko, A.; Windham, R.; Grey, J. Case Studies in Graphitic Corrosion of Cast Iron Pipe. *J. Fail. Anal. Prev.* **2021**, *21*, 376–386. [[CrossRef](#)]
4. Khodaei, P.; Shabani-Nooshabadi, M.; Behpour, M. Epoxy-Based nanocomposite coating reinforced by a zeolite complex: Its anticorrosion properties on mild steel in 3.5 wt % NaCl media. *Prog. Org. Coat.* **2019**, *136*, 105254. [[CrossRef](#)]
5. Wang, M.; Wang, J.; Hu, W. Preparation and corrosion behavior of Cu-8-HQ@HNTs/epoxy coating. *Prog. Org. Coat.* **2020**, *139*, 105434. [[CrossRef](#)]
6. Shen, W.; Zhang, T.; Ge, Y.; Feng, L.; Feng, H.; Li, P. Multifunctional AgO/epoxy nanocomposites with enhanced mechanical, anticorrosion and bactericidal properties. *Prog. Org. Coat.* **2021**, *152*, 106130. [[CrossRef](#)]
7. Guo, D.; Xie, G.; Luo, J. Mechanical properties of nanoparticles: Basics and applications. *J. Phys. D. Appl. Phys.* **2014**, *47*, 013001. [[CrossRef](#)]
8. Yuan, H.; Qi, F.; Zhao, N.; Wan, P.; Zhang, B.; Xiong, H.; Liao, B.; Quyang, X. Graphene oxide decorated with titanium nanoparticles to reinforce the anti-corrosion performance of epoxy coating. *Coatings* **2020**, *10*, 129. [[CrossRef](#)]
9. Yao, H.; Li, L.; Li, W.; Qi, D.; Fu, W.; Wang, N. Application of nanomaterials in waterborne coatings: A review. *Resour. Chem. Mater.* **2022**, *3*, 2772–4433. [[CrossRef](#)]
10. Xavier, J.R. Electrochemical, mechanical and adhesive properties of surface modified NiO-epoxy nanocomposite coatings on mild steel. *Mater. Sci. Eng. B Solid-State Mater. Adv. Technol.* **2019**, *260*, 114639. [[CrossRef](#)]
11. Xue, L.; Xu, L.; Li, Q. Effect of nano Al pigment on the anticorrosive performance of waterborne epoxy coatings. *J. Mater. Sci. Technol.* **2007**, *23*, 563–567.
12. Bello, S.A.; Agunsoye, J.O.; Adebisi, J.A.; Hassan, S.B. Effect of aluminium particles on mechanical and morphological properties of epoxy nanocomposites. *Acta Period. Technol.* **2017**, *48*, 25–38. [[CrossRef](#)]
13. Penna, M.O.; Silva, A.A.; Rosário, F.F.; De Souza, C.S.; Soares, B.G. Organophilic nano-alumina for superhydrophobic epoxy coatings. *Mater. Chem. Phys.* **2020**, *255*, 123543. [[CrossRef](#)]
14. Liang, Y.; Liu, F.C.; Nie, M.; Zhao, S.; Lin, J.; Han, E.H. Influence of Nano-Al Concentrates on the Corrosion Resistance of Epoxy Coatings. *J. Mater. Sci. Technol.* **2013**, *29*, 353–358. [[CrossRef](#)]
15. Niroumandrad, S.; Rostami, M.; Ramezanzadeh, B. Effects of combined surface treatments of aluminium nanoparticle on its corrosion resistance before and after inclusion into an epoxy coating. *Prog. Org. Coat.* **2016**, *101*, 486–501. [[CrossRef](#)]
16. *ISO 945-1*; Microstructure of cast irons—Part 1: Graphite classification by visual analysis. International Organization for Standardization: Geneva, Switzerland, 2017.
17. *ISO 868*; Plastic and ebonite—Determination of indentation hardness by means of a durometer (Shore hardness). International Organization for Standardization: Geneva, Switzerland, 2003.
18. Long, J.; Li, C.; Li, Y. Enhancement of Mechanical and Bond Properties of Epoxy Adhesives Modified by SiO<sub>2</sub> Nanoparticles with Active Groups. *Polymers* **2022**, *14*, 2052. [[CrossRef](#)]
19. Fu, X.; Shen, Z.; Chen, X.; Lin, J.; Cao, H. Influence of element penetration region on adhesion and corrosion performance of Ni-base coatings. *Coatings* **2020**, *10*, 895. [[CrossRef](#)]
20. Nascimento Silva, M.; Kassab, E.; Ginoble Pandoli, O.; Leite de Oliveira, J.; Pereira Quintela, J.; Bott, I.S. Corrosion behaviour of an epoxy paint reinforced with carbon nanoparticles. *Corros. Eng. Sci. Technol.* **2020**, *55*, 603–608. [[CrossRef](#)]
21. Alam, M.A.; Samad, U.A.; Sherif, E.-S.M.; Poulouse, A.M.; Mohammed, J.A.; Alharthi, N.; Saeed, M.; Al-Zahrani, S.M. Influence of SiO<sub>2</sub> content and exposure periods on the anticorrosion behavior of epoxy nanocomposite coatings. *Coatings* **2020**, *10*, 118. [[CrossRef](#)]
22. Njoku, D.I.; Cui, M.; Xiao, H.; Shang, B.; Li, Y. Understanding the anticorrosive protective mechanisms of modified epoxy coatings with improved barrier, active and self-healing functionalities: EIS and spectroscopic techniques. *Sci. Rep.* **2017**, *7*, 1–15. [[CrossRef](#)]
23. Margarit-Mattos, I.C.P. EIS and organic coatings performance: Revisiting some key points. *Electrochim. Acta.* **2020**, *354*, 136725. [[CrossRef](#)]
24. Sherif, E.S.M.; Alam, M.A.; Al-Zahrani, S.M. Fabrication of different protective coatings and studying their mechanical properties and corrosion behavior in sodium chloride solutions. *Int. J. Electrochem. Sci.* **2015**, *10*, 373–387.
25. Scully, J.R.; Silverman, D.C.; Kendig, M.W. *Electrochemical Impedance: Analysis and Interpretation*; ASTM Publication: Philadelphia, PA, USA, 1993.
26. Liu, X.; Xiong, J.; Lv, Y.; Zuo, Y. Study on corrosion electrochemical behavior of several different coating systems by EIS. *Prog. Org. Coat.* **2009**, *64*, 497–503. [[CrossRef](#)]
27. Chilkoor, G.; Sarder, R.; Islam, J.; Arun Kumar, K.E.; Ratnayake, I.; Star, S.; Bharat, K.J.; Sereda, G.; Koratkar, N.; Meyyappan, M.; et al. Maleic anhydride-functionalized graphene nanofillers render epoxy coatings highly resistant to corrosion and microbial attack. *Carbon N. Y.* **2020**, *159*, 586–597. [[CrossRef](#)]

28. Feichtenschlager, B.; Pabisch, S.; Svehla, J.; Peterlik, H.; Sajjad, M.; Koch, T.; Kickelbick, G. Epoxy Resin Nanocomposites: The Influence of Interface Modification on the Dispersion Structure—A Small-Angle-X-ray-Scattering Study. *Surfaces* **2020**, *3*, 664–682. [[CrossRef](#)]
29. Schmidt, R.G.; Bell, J.P. Epoxy Adhesion to Metals. *Adv. Polym.* **1986**, *75*, 33–71.
30. Vargel, C. *Corrosion of Aluminium*, 2nd ed.; Elsevier: Amsterdam, The Netherlands, 2019.
31. Karlsson, P.; Palmqvist, A.E.C.; Holmberg, K. Surface modification for aluminium pigment inhibition. *Adv. Colloid Interface Sci.* **2006**, *128–130*, 121–134. [[CrossRef](#)]

## Article 3

M. Samardžija, M. Kurtela, M. Vuković Domanovac, V. Alar, Anticorrosion and Antibacterial Properties of Al NP–Epoxy Nanocomposite Coating on Grey Cast Iron, *Coatings*, 13 (2023), 898.

### Author Contributions:

Marina Samardžija	conceptualization, methodology, software, validation, formal analysis, investigation, data curation, writing—original draft preparation, writing—review and editing, visualization
Marin Kurtela	software, validation, formal analysis, visualization, project administration
Marija Vuković Domanovac	methodology, visualization
Vesna Alar	conceptualization, resources, visualization, supervision, project administration, funding acquisition

This paper is published in an open access journal (<https://doi.org/10.3390/coatings13050898>).



## Article

# Anticorrosion and Antibacterial Properties of Al NP–Epoxy Nanocomposite Coating on Grey Cast Iron

Marina Samardžija <sup>1,\*</sup>, Marin Kurtela <sup>2</sup>, Marija Vuković Domanovac <sup>3</sup> and Vesna Alar <sup>2</sup>

<sup>1</sup> Department of Chemistry, Faculty of Mining-Geology-Petroleum Engineering, University of Zagreb, 10110 Zagreb, Croatia

<sup>2</sup> Department of Welded Structures, Faculty of Mechanical Engineering and Naval Architecture, University of Zagreb, 10000 Zagreb, Croatia; marin.kurtela@fsb.unizg.hr (M.K.); vesna.alar@fsb.unizg.hr (V.A.)

<sup>3</sup> Department of Industrial Ecology, Faculty of Chemical Engineering and Technology, University of Zagreb, 10000 Zagreb, Croatia; mvukovic@fkit.unizg.hr

\* Correspondence: marina.samardzija@rgn.unizg.hr; Tel.: +385-1-5535-912

**Abstract:** In this study, different concentrations of aluminium nanoparticles (Al NP) were incorporated into epoxy resin and epoxy paint. Here, we present a detailed systematic study of different methods of incorporating inorganic nanoparticles into epoxy coating. This work aims to obtain an epoxy coating with anticorrosion and antibacterial properties. The physical properties of coatings such as thickness, hardness, colour, and adhesion did not change with the addition of nanoparticles. According to the SEM and EDS analyses, the distribution effect of Al NPs in epoxy coating was better with ultrasonic homogenisation than with mechanical stirring. The EIS and SECM measurements were used to investigate corrosion resistance. The coating with 1.0 wt.% Al NP showed the best physical and chemical properties. SECM examination indicated that nanoparticles in epoxy resin increase the protection efficiency by 25.75% and in the epoxy paint by 40.89%. The results also showed the antibacterial activity of aluminium nanoparticles by inhibiting the growth of biofilm-forming bacteria such as *P. aeruginosa* and *B. subtilis*.

**Keywords:** electrochemical corrosion; microbiologically corrosion; Al nanoparticles; mechanisms



**Citation:** Samardžija, M.; Kurtela, M.; Vuković Domanovac, M.; Alar, V. Anticorrosion and Antibacterial Properties of Al NP–Epoxy Nanocomposite Coating on Grey Cast Iron. *Coatings* **2023**, *13*, 898. <https://doi.org/10.3390/coatings13050898>

Academic Editor: Heping Li

Received: 18 April 2023

Revised: 4 May 2023

Accepted: 8 May 2023

Published: 10 May 2023



**Copyright:** © 2023 by the authors. Licensee MDPI, Basel, Switzerland. This article is an open access article distributed under the terms and conditions of the Creative Commons Attribution (CC BY) license (<https://creativecommons.org/licenses/by/4.0/>).

## 1. Introduction

Grey cast iron has been widely used in pipes serving as water mains [1] due to its good thermal conductivity, relatively low melting temperature, high damping capacity, and excellent castability [2]. Unfortunately, these properties deteriorate when metals interact with certain elements that recur within their environments, a process technically called corrosion [3]. Corrosion is the irreversible damage or destruction of a material and as such is a very expensive and dangerous phenomenon that causes serious problems in the world [4,5]. The National Association of Corrosion Engineers (NACE International) estimates global losses caused by corrosion at USD 2.5 trillion per year and the average annual cost of corrosion in the pipeline industry is estimated at USD 7 billion to monitor, replace, and maintain these assets [6,7]. The most conventional method for protecting metal structures against corrosion is to isolate the metal from corrosive agents [8]. Researchers are continuously seeking new innovative coatings with good corrosion resistance and high antibacterial activity [9]. Typically, municipal wastewater that flows through pipes is composed of multiple pathogens and non-pathogenic bacteria, organic/inorganic chemicals, suspended and dissolved compounds, and similar [10,11].

Microbiologically influenced corrosion (MIC) is a serious type of corrosion, as it accounts for approximately 20% of total economic losses [12]. The microbiological community that exists in wastewater is usually a combination of various types of bacteria, among which are pathogenic forms such as opportunistic pathogens (*Enterobacter cloacae*, *Enterococcus faecalis*, *Escherichia coli*, *Klebsiella pneumoniae*, *Proteus vulgaris* or *Pseudomonas aeruginosa*),

obligate pathogens from *Salmonella* and *Shigella* genera and enteropathogenic strains of *Escherichia coli*. It can also contain viruses, protozoa, fungi, flatworms, roundworms, and similar [13,14]. The rod-shaped Gram-negative aerobic bacteria *P. aeruginosa* prefer moist environments such as urban runoffs and sewage effluents [15]. Furthermore, these bacteria have a high potential for developing great resistance to a wide range of currently available antimicrobial agents [16]. Likewise, the Gram-positive aerobic bacteria *B. subtilis* are widely present in the environment and show a capability to deal with heavy metals and dyes in polluted waters [17]. The presence of an energy source, carbon source, redox mediators, and water are important factors for bacterial colonization of any surface. Then, the metabolic activities of these colonized bacteria influence the electrochemical reactions initiating MIC. Secretion of extracellular polymeric substances (EPS) and biofilm formation on the material surfaces are crucial steps that enhance the probability of metal corrosion and MIC [18].

Recently, with the development of nanotechnology [19], the term “nanocomposite” has appeared with at least one dimension on the nanometre scale [20]. Nanoparticles have been widely used as resin fillers to block micropores and improve the corrosion resistance and the mechanical properties of the resins due to their great surface-to-volume proportion with respect to conventional macroscopic materials [4]. The purpose of the study by Manjumeena and co-authors [21] was to obtain a nanocomposite with dual properties. According to their study, silver nanoparticles show great antibacterial properties due to their ability to release  $\text{Ag}^+$  from nanoparticles which can damage the cell wall and cause oxidative stress. Talabi and co-authors [22] developed polymer nanocomposites with antibacterial properties. They showed that  $\text{Cu}^{2+}$  ions, which are released from copper nanoparticles, cause the denaturation of proteins in the bacterial membrane, by binding to DNA, which results in the cell not being able to replicate further. The surface-to-volume ratio of a nanoparticle is 35%–45% times higher as compared to large particles or atoms. This unique extrinsic property of the specific surface area of the nanoparticle is a contributory factor for its high value, and it also influences different intrinsic properties such as strong surface reactivity which is size dependent [23]. Due to all these properties of nanoparticles and the high viscosity of epoxy coating, it is hard to uniformly mix nano-size fillers into epoxy coating [15]. According to the available literature, there are different methods of incorporating nanoparticles into epoxy coating. In our last article, we employed strong mechanical stirring for the preparation of a nanocomposite of epoxy matrix and aluminium nanoparticles (Al NP) [24].

Pure aluminium is a metal that is soft, ductile, and corrosion-resistant [25]. Control over nano aluminium powder size has been crucial for changing properties. Slight changes in particle size can have a dramatic effect on surface area and therefore surface area-dependent properties such as rheology, powder mixing, dispersion, surface adsorption of condensed species, and bulk density [26]. Likewise, metal nanoparticles showed antibacterial behaviour against a wide series of bacteriological organisms [27]. Our interest is the development of a new anticorrosive and antibacterial nanocomposite coating to protect grey cast iron. The coating was fabricated with the addition of aluminium nanoparticles (Al NP) in a different ratio. In [24], the mechanical procedure for the preparation of the Al NP nanocomposite coating and its anticorrosive properties were demonstrated. In this paper, we investigated the influence of ultrasonic dispersion of Al NPs in an organic coating. Furthermore, in this study, we investigated the antibacterial properties of the metal powder of Al NPs. For all these purposes, we used electrochemical techniques (EIS and SECM), scanning electron microscopy (SEM), energy-dispersive X-ray spectroscopy (EDS) analyses, devices for establishing mechanical properties (Elcometer<sup>®</sup> 456, PosiTector<sup>®</sup> SHD, Elcometer 510) and bacteria (*P. aeruginosa* and *B. subtilis*) for the determination of antibacterial properties.

## 2. Materials and Methods

### 2.1. Materials

In this study, grey cast iron was investigated. The elemental composition of grey cast iron is shown in Table 1.

**Table 1.** The chemical composition of the grey cast iron.

Element	C	Si	Mn	P	S	Fe
Percent (%)	2.5	1.5	1.05	0.5	0.07	balance

Grey cast iron plates with dimensions of 9.5 cm × 0.9 cm × 15 cm were used as substrates. The surface of the grey cast iron was cleaned with abrasive blasting and ethanol (70 wt.%). Two epoxy coatings were used in the work. The first coating was prepared using pure epoxy resin (Bisphenol A, West System, UK) and hardener (polyamine, West System, UK) in a ratio of 3.5 to 1. The second coating was prepared using epoxy paint (Hempel, Croatia) and hardener (polyamine, Hempel, Croatia) in a ratio of 4 to 1. Aluminium nanoparticles (Al NP) with an average particle size of 100 nm were provided by Guangzhou Hongwu Material Technology Co., Ltd., Guangzhou, China.

### 2.2. Preparation of the Epoxy Coatings

The obtained Al NPs were used to prepare nanocomposites of Al NP–epoxy coating. In this method, different concentrations of Al NPs (0.50, 0.75, and 1.0 wt.%) were added to the epoxy solution. The procedure for the epoxy coating modified by Al NP is illustrated in Figure 1.

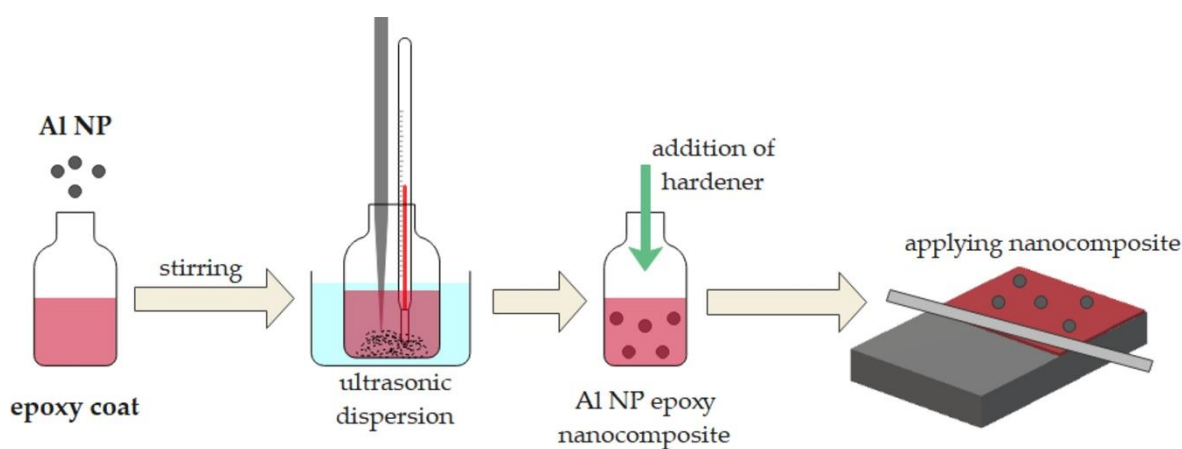


**Figure 1.** Preparation of the Al epoxy nanocomposite coating.

Al NPs were mixed with epoxy resin and epoxy paint (epoxy coating) using ultrasonic agitation for 20 min with a delay in the process due to the cooling of the nanocomposite. The hardener was added to the prepared samples and stirred until complete homogenisation. The obtained mixture was applied to the grey cast iron substrate using an applicator (150 μm). Then, the samples were dried under atmospheric conditions. After 24 h, another layer of nanocomposites was applied in the opposite direction (150 μm). The samples were left at room temperature (25 °C) for 7 days.

### 2.3. Coating Characterisation

The morphology of the Al NP samples was investigated by scanning electron microscope (SEM) (TESCAN Brno, Brno, Czech Republic). The size distribution and dispersion of nanoparticles, the homogeneity of the layer, and the occurrence of agglomeration were observed. The coated samples were also characterised using the energy-dispersive (EDS) detector.

Elcometer<sup>®</sup>456 (Elcometer Limited, Edge Lane, Manchester, UK) was used to assess the thickness of the nanocoating sample. Measurements were performed on ten different locations per sample. The change in the colour of the nanocomposite coating was determined using the RAL colour chart (RAL gGmbH, Siegburger, Germany). The hardness of the nanocomposite was tested according to ISO 868:2003 [28]. The testing was evaluated using PosiTector SHD Shore Hardness Durometer (DeFlesko Corporation, Ogdensburg, NY, USA). An adhesion test was performed to examine the effect of the coating strength of metal using an automatic Pull-Off Adhesion Tester (Elcometer 510, model T, Manchester, UK). The aluminium dollies (20 mm diameter) were glued on the Al NP nanocomposite using a two-part epoxy adhesive (Araldite resin and Araldite hardener). Complete curing of the adhesive was achieved by keeping the sample at 25 °C for 24 h.

The coating samples were exposed to the humidity chamber (Humidity Cabinet Model AB6), and the climatic chamber (Climatic chamber Kambic KK-190 CHLT, CiK Solutions GmbH, Karlsruhe, Germany). The humidity test was conducted according to EN ISO 6270-2 for five days [29]. To test the coating stability at low temperatures, the samples were placed in the climatic chamber for five days. The test cycle was set up in ten steps in which the temperatures changed from −5 °C, with 0% humidity, to 10 °C, with 70% humidity. The samples were left at each temperature for 8 h. The accelerated testing was performed on two samples per coating. After the humidity test, and the icing/deicing process, the physical properties of the samples were tested after they reached room temperature.

The corrosion protection performance of the epoxy coating and Al NP–epoxy nanocomposite were studied in 3.5 wt.% NaCl solution by EIS (VersaSTAT 3, AMETEK Scientific 131 Instruments, Princeton applied research, Berwyn, PA, USA). Open-circuit potential (OCP) was first obtained over a period of 20 min to study the changes in the corrosion potential of the coatings. The electrochemical cell consisted of a graphite rod as the auxiliary electrode, a saturated calomel electrode as the reference, and the epoxy coating and/or Al NP–epoxy nanocomposite specimen as the working electrode. The frequency range of 0.1 to 10<sup>5</sup> Hz with an amplitude of 10 mV was used. The impedance data were fitted using the ZSimpWin software. The Intermittent Contact-Scanning Electrochemical Microscopy (ic-ac-SECM) (M470, BioLogic, France) test of epoxy resin, epoxy paint, and epoxy nanocomposite with 1% of Al NP was used to observe real impedance distribution over a certain area. The 3DIsoPlot program was used to obtain the topography of the samples in 3D view. A three-electrode system, immersed in tap water, was above the surface of the nanocomposite. This three-electrode system consisted of the Ag/AgCl/KCl (saturated) reference electrode, the platinum sheet as the counter electrode, and of the UltraMicroElectrode (UME) probe for measuring the local electrochemical activity. The UME probe with 10 µm diameter platinum wire was used.

*Pseudomonas aeruginosa* and *Bacillus subtilis* were taken as the test bacteria. The antibacterial activity of the Al NP was performed using the well-diffusion method [30]. The final densities of the bacterial suspensions' cells were about 10<sup>8</sup> and 10<sup>7</sup> CFU/mL, respectively. The bacterial culture was inoculated from fresh colonies on agar plates into 20 mL Muller Hinton culture medium. The nanoparticle samples dissolved in distilled water (100 µg/mL) were added from the stock into each well. The zone of inhibition was measured using a ruler. After 24 h, the appearance of the inhibition zone was observed.

### 3. Results and Discussion

#### 3.1. Characterisation of Al NP

The SEM microstructure of Al NPs is shown in Figure 2a. The surface of nanoparticles is a fluffy powder with spherical properties. To determine the composition of Al NP, the EDS analysis was carried out.

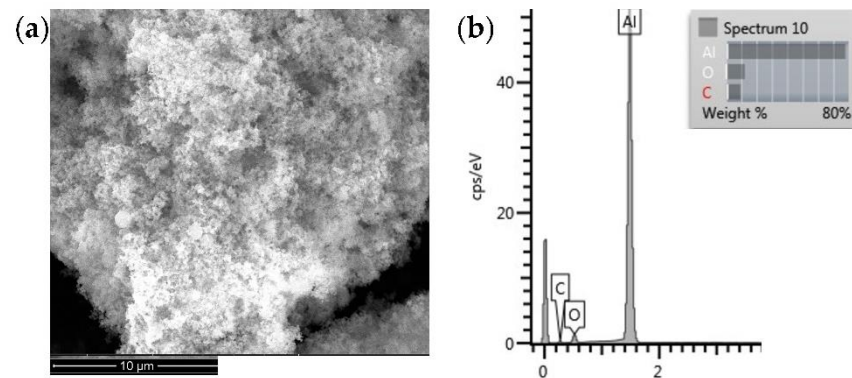


**Figure 2.** SEM image (a) and EDS profile (b) of pure Al NP.

The EDS analysis of Al NPs (Figure 2b) determined the mass fraction of the aluminium nanoparticles of about 80%. Spectrum minor elements such as O and C were due to contamination.

### 3.2. Evaluation of Mechanical Properties

Epoxy paint and epoxy paint nanocomposites with 0.50%, 0.75%, and 1.0% of Al NP were exposed to the humidity (ISO 6270-2) and climatic chambers. According to ISO 12944-6, nanocomposites were classified as corrosivity category C4 and durability up to 15 years [31]. After exposure of the samples to the corrosive media, mechanical properties were observed (Table 2).

**Table 2.** Results of changing thickness, hardness, adhesion force, and colours of epoxy paint and nanocomposite paint samples in different corrosion conditions.

	Samples	Epoxy Paint	0.5%_Al	0.75%_Al	1.0%_Al
thickness, µm	unexposed	249.9	278	256.4	275.5
	humidity chamber	275.9	263	263.2	285.6
	climatic chamber	248.8	259.9	271	292.3
Hardness, Shore D	unexposed	83.4	83.8	82.8	82.0
	humidity chamber	83.2	80.3	80.0	80.2
	climatic chamber	81.0	83.0	81.4	81.8
adhesion, MPa	unexposed	8.34 8.31	9.59 9.42	12.10 10.30	13.47 14.18
	humidity chamber	9.85 10.20	10.87 11.52	11.89 12.56	13.24 12.12
	climatic chamber	10.11 10.52	16.57 13.56	13.15 13.16	12.43 11.41
RAL colours	unexposed	3013	8015	8016	8017
	humidity chamber	3013	8015	8016	8017
	climatic chamber	3013	8015	8016	8017

According to Table 2, it is evident that there was no change in the thickness and hardness of the coating on the samples despite the addition of Al NPs and the exposure of the coating to corrosive conditions. The adhesion of the coating to the metal substrate showed a small increase with the addition of Al NPs. The results showed that the direct addition of Al NPs to the epoxy paint reduced the stress in the coating. The particle effect, the uniform dispersion of the filler in the epoxy paint, and the strength of the bond with the paint contribute to a better stress transfer. The strengthening mechanism was due to

the tight bond between the nanoparticles and the epoxy paint, which can limit the mobility of the polymer chains [32]. Samples that were exposed to the humid and air-conditioned chambers showed a smaller increase in adhesion. An increase in the adhesion force could be caused by increasing or decreasing temperature and moisture in the humidity and climatic chambers. As shown in the paper, the addition of Al NPs to the epoxy matrix significantly changed the colour of the coating [24].

### 3.3. Evaluation of Anticorrosion Properties

The impedance data were analysed using the equivalent electrical circuits (EEC) shown in Figure 3. The model's outer and inner circles corresponded to the high and low-frequency loops, respectively. Indeed, the outer circle was used to characterise the coating properties. The inner circle of EEC with two-time constants, was the feature of the double layer formed at the coating/metal interface [33]. Figure 3 shows that the first resistance encountered by the alternating current was the electrolyte resistance,  $R_s$ , which had a negligibly small value. The coating resistance,  $R_{coat}$ , provided another resistance to the passage of current. At the phase boundary between solid and liquid, an electrical double layer appeared, representing the capacity of the coating,  $CPE_{coat}$ . After a long time of exposure of the coating to an aggressive medium, damage occurred to the epoxy paint and thus the electrolyte could more easily reach the surface of the grey cast iron the alternating current encountered a charge transfer resistance,  $R_{ct}$ , which also had its capacity,  $CPE_{dl}$  [34].

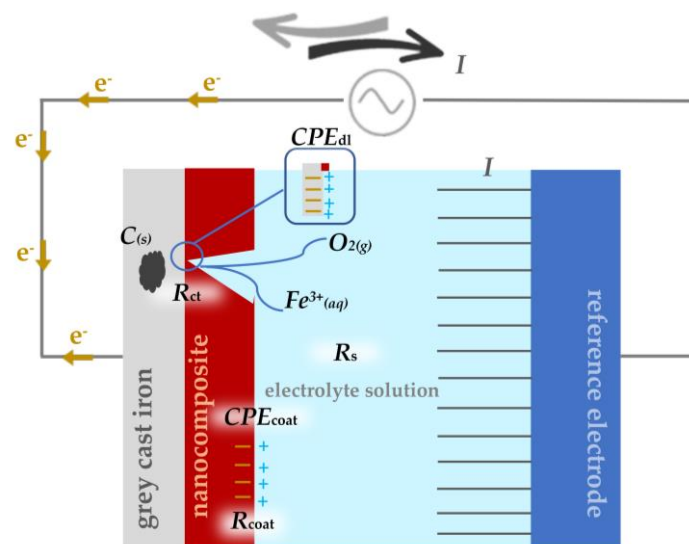


**Figure 3.** The equivalent electrical circuits used for describing the impedance response of epoxy coating and nanocomposite with 0.5, 0.75, and 1.0% Al NP.

Figure 3 shows the electrochemical mechanism of corrosion destruction on the surface of grey cast iron, which is called graphitization. When the aggressive medium reaches the surface of grey cast iron, it will initiate the anodic dissolution of iron by leaving free graphite [35]. To slow down this process, the epoxy resin and the epoxy paint were modified with Al NPs, and tests were performed in a 3.5 wt.% NaCl solution using alternating current.

The EIS results for the epoxy paint and nanocomposite samples with different concentrations of Al NPs (0.50, 0.75, 1.0%) were presented in Nyquist and Bode diagrams (Figure 4a,b). The measurement was made immediately after immersion in 3.5 wt.% NaCl solution. The results showed coating resistance,  $R_{coat}$ , which reflected the anti-penetrating ability of the coating to electrolyte solution [36]. All samples showed a single capacitive loop, meaning that there was no electrolyte penetration. Pure epoxy showed a lower coating resistance value, while the samples with 0.50 and 0.75% Al NPs had slightly higher resistances. The increase in resistance was significantly more pronounced in the sample containing 1.0% Al NPs. Nanoparticles embedded in the coating resisted the passage

of current and provided high resistance. The large resistance values in the Nyquist plot were confirmed by the Bode phase angle in Figure 4b. The Bode phase angle plots were further analysed to explain the effectiveness of the coating. All tested samples achieved a constant phase angle value extending from the medium frequency range (100 Hz) to the high frequency range ( $10^5$  Hz) during the entire exposure time, which indicated that the coating had not started to degrade. In the case of short-term immersion in the electrolyte, the properties of the protective coating remained intact.

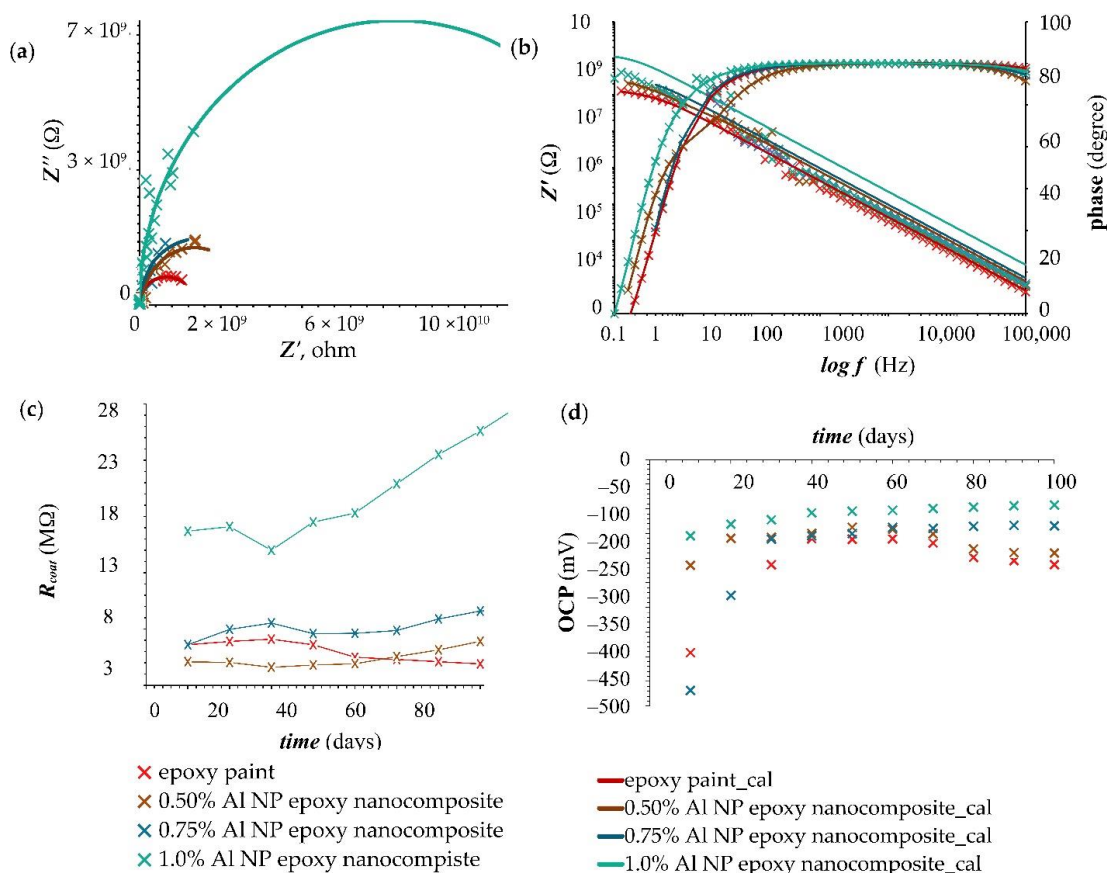


**Figure 4.** Nyquist and Bode plots of (a,b) epoxy paint and epoxy paint with different concentrations of Al NP immediately immersed in 3.5 wt.% NaCl solution. Corrosion resistance values (c) for samples in 3.5 wt.% NaCl solution during a 100-day immersion. Variations of OCP values (d) for samples during a 100-day immersion.

The value of  $R_{coat}$  for the blank epoxy coating (paint) without nanoparticles and for the coatings with different concentrations (0.50, 0.75, and 1.0%) of Al NP in the epoxy paint at different interval times over a 100-day immersion in 3.5 wt.% NaCl solution is shown in Figure 4c,d.

After 10 days, the epoxy paint showed the same resistance as the nanocomposite sample with 0.75% Al NPs. With a longer exposure time (after 50 days), the resistance of the blank epoxy gradually began to decrease (Figure 4c). Constant resistance values in all nanocomposite samples were maintained for 50 days, after which there was a slight increase in resistance in samples with 0.50% and 0.75% Al NPs, while the sample with 1.0% Al NPs showed a larger increase (Figure 4c). The obtained results indicated that it took 50 days to form an oxide film in the epoxy paint. The higher the concentration of nanoparticles, the greater the formation of the oxide film and the better the coating protection. Figure 4c shows that the highest resistance was achieved with the nanocomposite sample containing 1.0% Al NPs. This sample showed the highest resistance immediately at the beginning of the measurement. The increase in corrosion resistance could be attributed to a higher

concentration of nanoparticles that created better adhesion and compatibility with the epoxy matrix, reduced the transport paths for the passage of corrosive electrolyte through the system coating, led to a decrease in the capacitance of the coating, and reduced corrosion reactions [16,30].

Open-circuit potential (OCP) is the potential of a working electrode when no current is applied to the cell [37]. In Figure 4d, all samples showed a constant OCP value after 50 days. After 100 days of exposure to an aggressive medium, the epoxy paint showed the highest negative potential value, which indicated weaker protective properties. Nanocomposites showed a more positive potential value that balanced out after 50 days indicating the beginning of the formation of a protective oxidative film. The values of the parameters shown on the equivalent circuit are listed in Table 3.

**Table 3.** EIS parameters values after fitting with equivalent circuit for epoxy paint and epoxy paint with different concentrations of Al NPs immediately immersed in 3.5 wt.% NaCl solution.

Parameters	Epoxy Paint	0.50% Al NP-Epoxy Nanocomposite	0.75% Al NP-Epoxy Nanocomposite	1.0% Al NP-Epoxy Nanocomposite
$R_s, \Omega$	479.0	495.0	481.0	313.4
$R_{coat}, \Omega$	$1.78 \cdot 10^8$	$1.80 \cdot 10^9$	$1.93 \cdot 10^9$	$1.87 \cdot 10^{10}$
$CPE_{coat}, S \cdot sec^n$	$4.22 \cdot 10^{-9}$	$1.47 \cdot 10^{-10}$	$2.60 \cdot 10^{-10}$	$2.76 \cdot 10^{-11}$
$n$	1	1	1	1
$R_{ct}, \Omega$	$1.17 \cdot 10^9$	$8.38 \cdot 10^8$	$1.30 \cdot 10^9$	$2.87 \cdot 10^9$
$CPE_{dl}, S \cdot sec^n$	$3.65 \cdot 10^{-10}$	$2.05 \cdot 10^{-10}$	$3.01 \cdot 10^{-9}$	$7.22 \cdot 10^{-11}$
$n$	1	1	0.84	0.8

Considering the results reported in Table 3, CPE is a constant phase element of the double layer showing its capacitive properties, which depend on the empirical constant  $n$ . The  $CPE_{coat}$  value of the nanocomposite decreased by adding nanoparticles to the epoxy paint. The lower value of  $CPE_{coat}$  indicates superior corrosion resistance due to low electron storage.

To detect the presence of the aluminium oxide film, EDS microanalysis was performed at a point on the surface of the powder sample obtained by the reaction between Al NPs and distilled water (Figure 5).

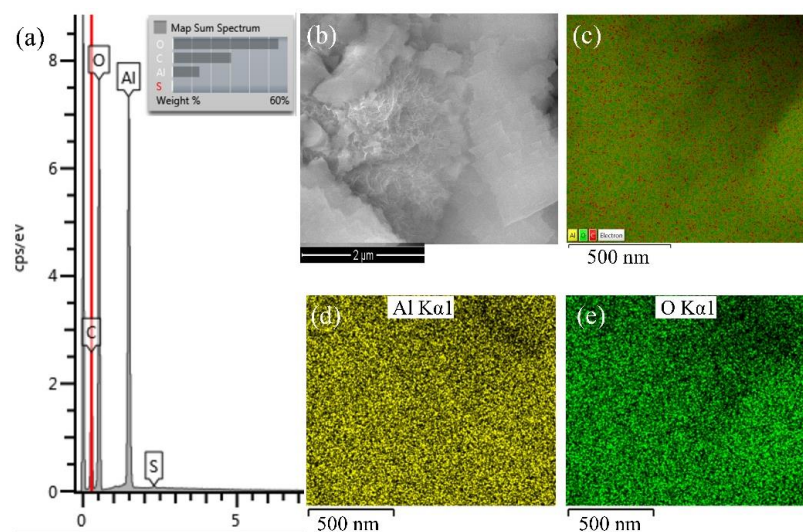


**Figure 5.** Results of (a) Surface spectrum, (b) SEM image, (c) collective colouring of surface maps of prepared aluminium oxide particles and partially coloured maps of the distribution of individual chemical elements in aluminium oxide particles: (d) Al K series, and (e) O K series.



Observing the size of the formed particles, an increase in the volume of the particles was visible in Figure 5a. The display of partial colours for aluminium and oxygen elements indicated that aluminium oxidation had occurred (Figure 5b,c). The EDS analysis cannot detect the presence of hydrogen in the compound, so according to the literature, the reactions that occur at the interface between Al NPs and a neutral aqueous medium are shown in Figure 6 [38].

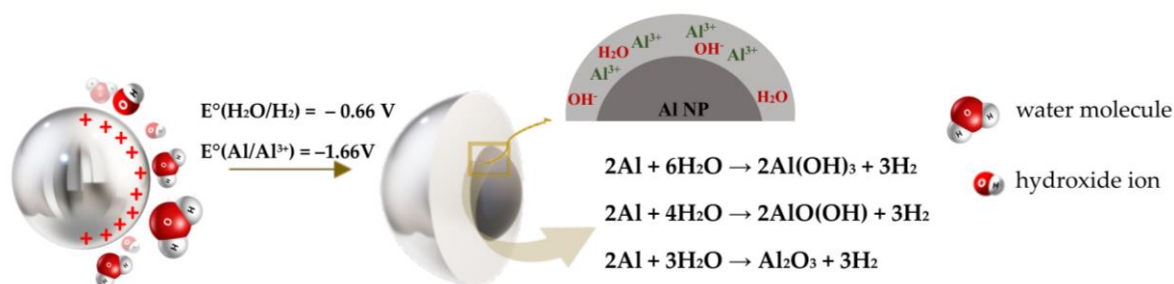


**Figure 6.** Mechanism of aluminium nanoparticle oxidation.

The oxidation process of a metal nanoparticle included two mechanisms, as shown in Figure 6. A nanoparticle in contact with an aqueous medium became electrically positively charged and, using van der Waals interactions, began to attract  $\text{OH}^-$  ions and the negative polar part of the  $\text{H}_2\text{O}$  molecule. After physical adsorption, due to the existence of a driving force (potential difference), Al NP oxidation and  $\text{H}_2\text{O}$  reduction occurred. The resulting oxidized products together with the metal surface created a chemisorbed monolayer [39,40]. The aqueous solution was a weak electrolyte, which means that it consisted more of water molecules than ions, and thus the formed aluminium ions could react with water molecules ( $\text{H}_2\text{O}$ ) and form hydroxide ions ( $\text{OH}^-$ ) [38]. According to the literature, the first possible reaction product is  $\text{Al}(\text{OH})_3$  (bayerite). The second possible reaction product is  $\text{AlO}(\text{OH})$  (boehmite). The third possible reaction product is  $\text{Al}_2\text{O}_3$  (alumina). These reactions are all thermodynamically favourable over a wide temperature range from room temperature to temperatures far above the melting point of aluminium ( $660^\circ\text{C}$ ). In addition, all these reactions are highly exothermic [41]. The outer layer consisted of a mixture of  $\text{Al}_2\text{O}_3$  and a hydrated layer, mostly in the form of amorphous  $\text{Al}(\text{OH})_3$ , while the inner part was mostly made of  $\text{Al}_2\text{O}_3$  and a small amount of aluminium oxyhydroxide in the form of  $\text{AlO}(\text{OH})$ . Such a coating ( $\text{Al}_2\text{O}_3$ - $\text{AlO}(\text{OH})$ ) was characterised by continuity and resistance to certain electrolytes ( $3.91 < \text{pH} < 8.64$ ) [39]. The layers may have different thicknesses and chemical compositions depending on the methods used for the production and passivation of the powders [42]. The oxide layer thickness remained stable for at least 30 days, showing that the native oxide acted as a passivation layer preventing further oxidation [43]. Consolidation of inorganic fillers into the polymeric coating formulation can diminish porosity and draw out the lifetime of the composite coating [44].

The appearance of a protective oxidative film on the surface of nanoparticles led to an increase in corrosion resistance. The mechanism of formation, the connection of Al NPs with epoxy paint, and the degradation of Al NPs in epoxy paint are shown in Figure 7.

According to literature data [26,45,46], by adding a hardener, the aliphatic amine started hardening by nucleophilic attack of the amine group on the epoxy ring of the monomer (Figure 7). At the same time, the nanoparticle could react with both the hardener and the epoxy paint due to its small size. When the epoxy ring was opened, the hydroxyl groups that serve as bonding sites became strong electromagnetic bonds between the epoxy and the metal molecules. At the beginning of exposure to an aggressive medium, the nanoparticles were well embedded in the epoxy paint, which protected them from rapid oxidation. To prevent the oxidation of Al NPs, layers of organic and inorganic coatings could be applied to their surface [42]. The protective barrier properties of the epoxy paint decreased over time. Organic polymeric coatings mostly protect against corrosion by forming a barrier to disengage the metal from the surrounding environment. Nonetheless,

all polymeric coatings are porous to destructive species, for example, oxygen, water, and chloride particles [44]. The used aluminium nanoparticles in contact with the aqueous medium formed an aluminium oxide and smaller amounts of aluminium hydroxide and oxyhydroxide. Due to good dispersion, and interfacial compatibility of composites, a “maze effect” can be formed to prevent the penetration of corrosive media, prolong the penetration path of corrosive media in the coating, and ultimately delay the occurrence of corrosion [47]. This whole mechanism of protection of grey cast iron relied on a cathodic passivation process in which the aluminium in the coating acted as the sacrificial anode and protected the iron. According to the obtained EIS data (Figure 4c), an aluminium oxide film was formed after the sample had been immersed in an aggressive medium for 50 days. As a result, we can conclude that as the aggressive medium started to diffuse through the epoxy coating, more and more nanoparticles were completely and/or partially oxidized and the corrosion resistance increased (Figure 6).

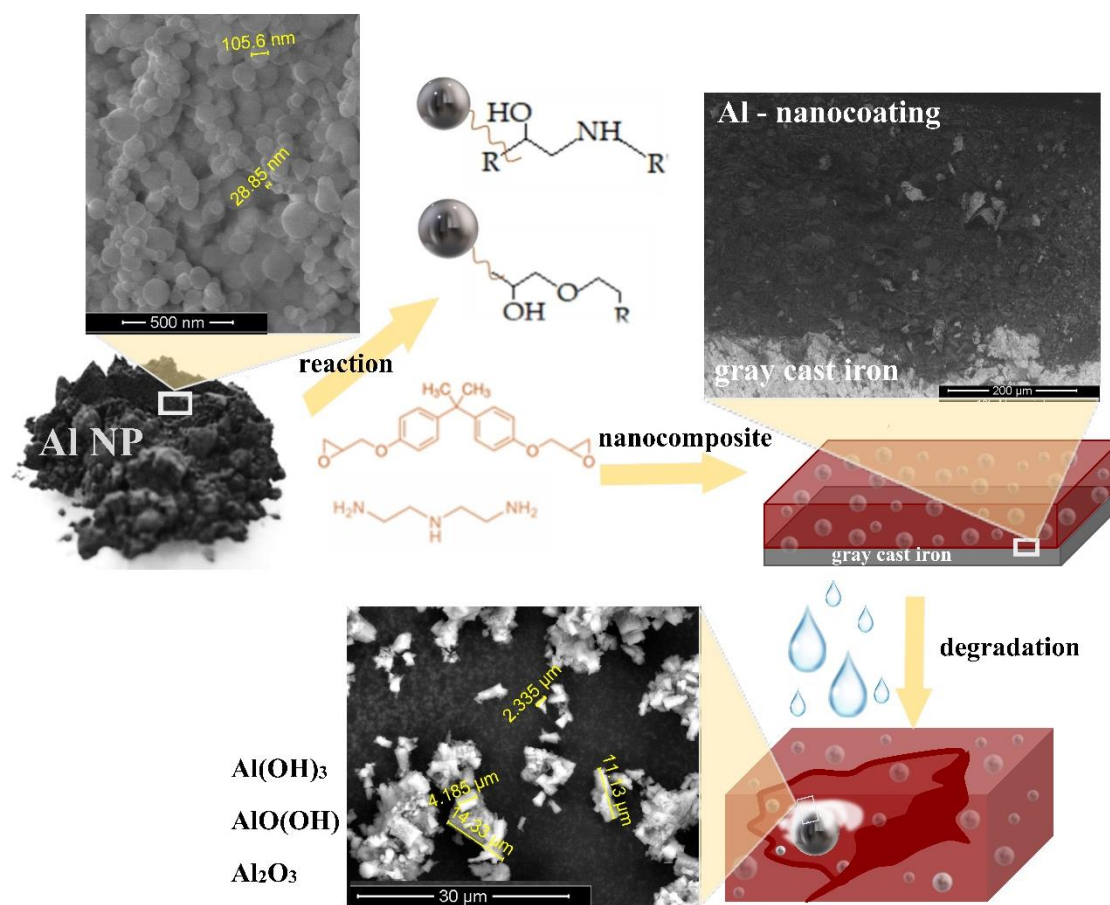


**Figure 7.** The mechanism of nanoparticle interaction with the epoxy paint and hardener, the degradation of the nanocomposite, and the formation of an oxidation film on the Al NP.

### 3.4. Surface Characterisation of 1.0% Al NP–Epoxy Nanocomposite

#### 3.4.1. SEM/EDS Analysis

As 1.0% Al NP–epoxy nanocomposite was found to be the formulation with the best anticorrosion properties, the surface of the same sample was tested. The cross-sectional SEM image of the nanocomposite with 1.0% Al NPs prepared in epoxy paint is shown in Figure 8a,b.

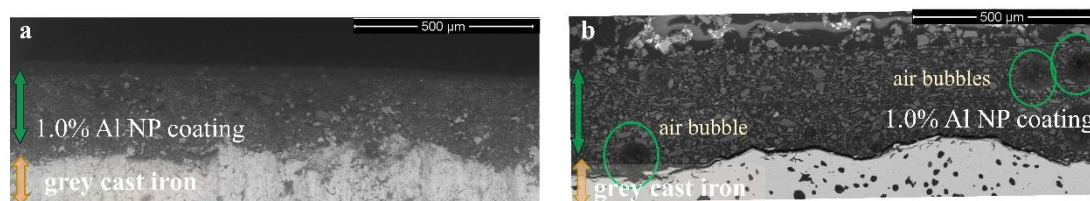


**Figure 8.** SEM cross-sectional morphology of nanocomposite with 1% Al NP prepared using (a) ultrasonic homogeniser and (b) mechanical mixing.

Figure 8 shows the result of two methods of preparing a nanocomposite containing 1.0% Al NPs. The preparation of the nanocomposite using ultrasonic mixing is shown in Figure 8a, while Figure 8b shows the nanocomposite prepared using a mechanical mixer. The results of mechanical mixing were published in the paper [24] and showed that the anticorrosive properties of the coating had improved in a short period of time. The reason for the short application of this nanocomposite was the appearance of air bubbles, as shown in Figure 8b. By applying ultrasonic mixing, better anticorrosive properties were achieved over a longer period. Figure 8a shows a cross-section of the nanocomposite, without air bubbles. Table 4 shows the advantages and disadvantages of both methods for the preparation of the nanocomposite material.

**Table 4.** Advantages and disadvantages of using mechanical and ultrasonic mixing in the preparation of nanocomposite coating.

	+	–
<b>Mechanical stirring</b>	Faster preparation of the sample It is not necessary to cool the Sample quiet mode of operation	Complicated handling of the device Complicated cleaning of the mechanical mixer The appearance of trapped air bubbles The appearance of nanoparticle agglomerates at higher concentrations
<b>Ultrasonic stirring</b>	Easy handling of the device Simple probe cleaning Easy air removal Better dispersion of nanoparticles	Heating the sample Longer sample preparation As the viscosity decreases, the device makes more noise

Better corrosion resistance and stability of the sample were obtained by ultrasonic preparation of nanocomposites due to better dispersion of nanoparticles and the absence of air bubbles. During sample preparation, air bubbles were released due to the heating of the coating. As the viscosity of the liquid decreased with the increase in temperature, air bubbles were released more easily. A risk of degradation of the base polymer, however, existed during processing [48]. To avoid this unwanted process, the epoxy paint must be heated to the temperature recommended by the manufacturer. Loss of solvent from the nanocomposite during preparation did not affect the reduction of anticorrosive properties.

Figure 9a shows the EDS spectra and chemical composition of the cross-section of the nanocomposite with 1% Al NP, which was prepared using an ultrasonic homogeniser in epoxy paint. SEM analysis of the sample is shown in Figure 9b. Figure 9d,e show the EDS distribution map of aluminium and oxygen in the cross-section of the nanocomposite with 1% Al NPs. The incorporation of Al NPs showed a uniform and homogeneous distribution in the entire measurement area of the nanocomposite cross-section. Additionally, according to the partial staining, we see that there was no formation of aluminium agglomerates. In the pure epoxy resin, as shown by the EDS analysis in Figure 10, the Al NPs were evenly distributed and remained at the nanoscale, which confirms that the nanoparticles did not start to form agglomerates.

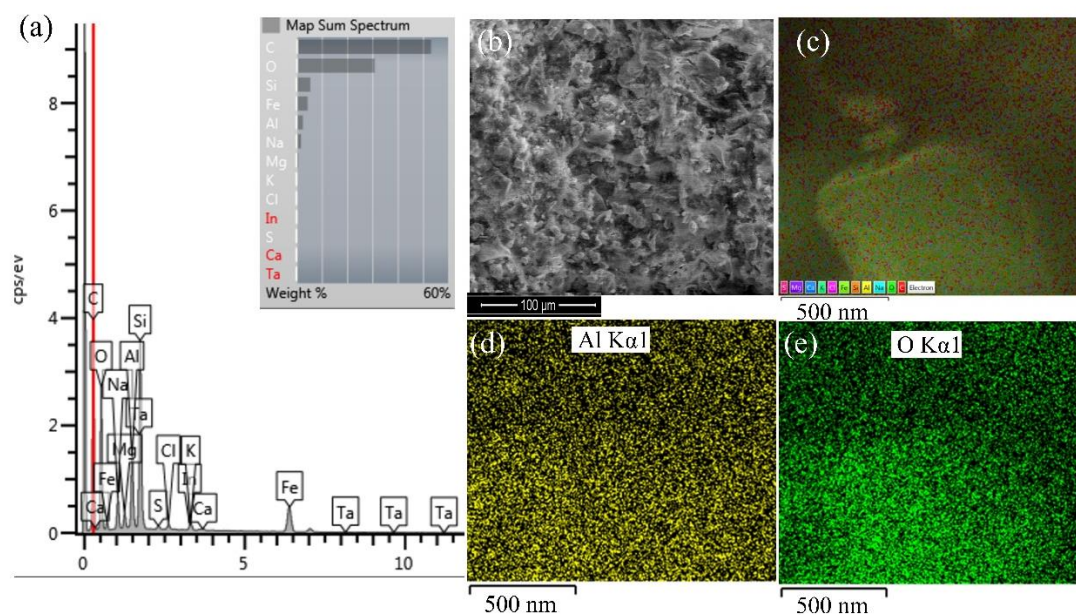


**Figure 9.** Results of (a) cross-sectional spectrum of the sample surface (b) SEM image of the sample surface (c) EDS cross-section map, and distribution of (d) aluminium and (e) oxygen in 1% Al NP-epoxy paint nanocomposite coating.

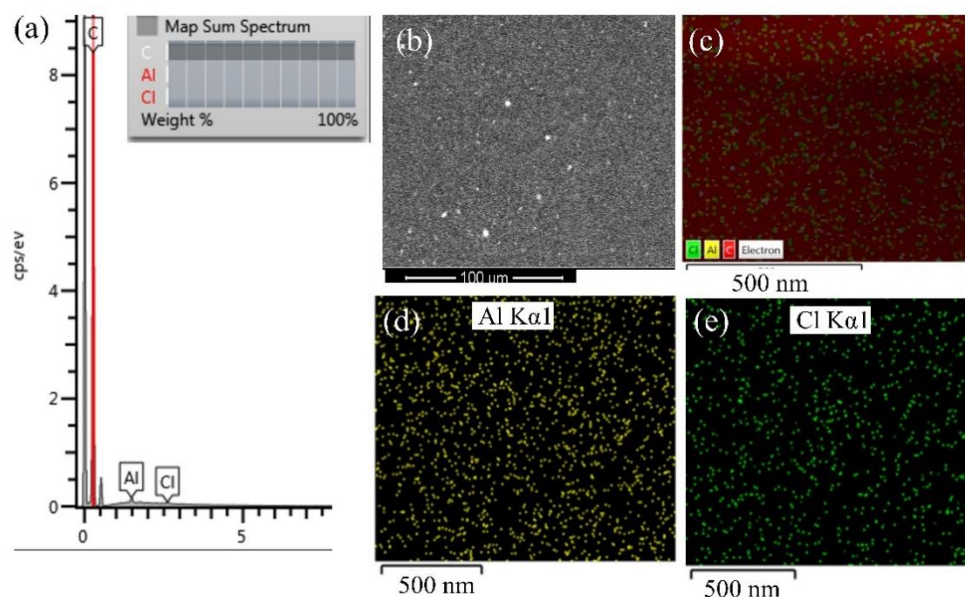


**Figure 10.** Results of (a) cross-sectional spectrum of the sample surface (b) SEM image of the sample surface (c) EDS cross-section map, and distribution of (d) aluminium and (e) chlorine in 1% Al NP-epoxy resin coating.

### 3.4.2. ic-ac-SECM Analysis

SECM provides electrochemical activity and topographic information about the surface reactions at the micrometre scale in aqueous environments [49]. We used this technique for the characterisation of the influence of the nanoparticles in the epoxy resin and epoxy paint. In the first experiment, it was necessary to find the appropriate vibration frequency so that the ultramicroelectrode (UME) could react with the surface (Figure 11). The piezo sensor was used to determine the distance of the UME from the surface of the sample. During the AC characterisation, the frequency applied to the piezo was automatically swept up to 600 Hz and the signal gain was recorded. The amplitude was 0.1.

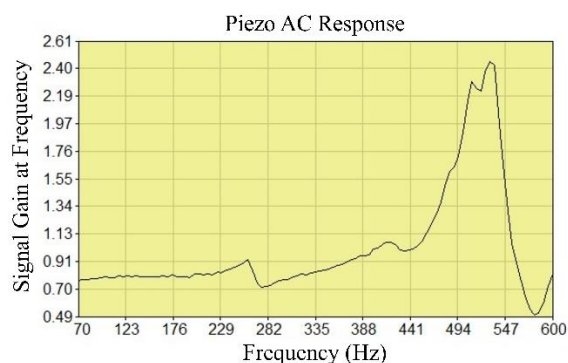


**Figure 11.** Determination of the vibration frequency of the UME.

The real impedance measured was the result of the surface activity and constant distance between the UME and the sample surface. The measurements were performed in tap water (Figure 11). The topography of the surface was determined on samples that did not contain nanoparticles and on samples obtained by ultrasonic mixing of epoxy resin and epoxy paint with 1.0% Al NPs.

The distribution of real impedance resistance values on the surface of pure epoxy resin, epoxy paint, 1.0% Al NP–epoxy resin, and 1.0% Al NP–epoxy paint nanocomposite coating is shown in Figure 12. The UME that recorded the topography moved along the  $x$ -axis from 0 to 0.5 mm, the  $y$ -axis from  $-0.25 \mu\text{m}$  to  $0.25 \mu\text{m}$ , and the  $z$ -axis was set to the constant distance determined by the piezo sensor.

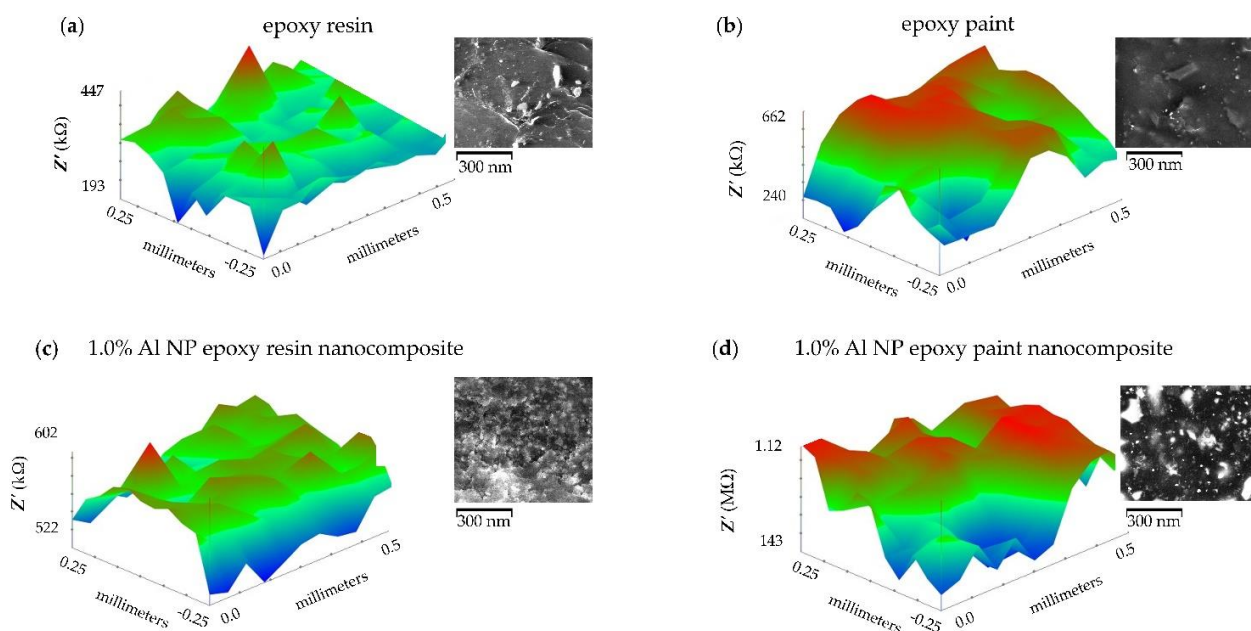


**Figure 12.** ic-ac-SECM distribution of real impedance per surface for samples: (a) epoxy resin, (b) epoxy paint, (c) 1.0% Al NP–epoxy resin nanocomposite, (d) 1.0% Al NP–epoxy paint nanocomposite coating immersed in tap water.

There is a small variation in the measured values of the impedance (from 522 to 602 kOhms) of the epoxy resin indicating a homogeneous structure (Figure 12a). A larger difference in real impedance distribution was observed in the epoxy paint sample (Figure 12b). The occurrence of localised peaks was surrounded by boundaries of higher impedance. The reason for the increase could be interpreted as the result of the effect of added coating components, such as additives in the epoxy paint. In the case of the sample containing 1.0% Al NPs in the epoxy resin, the impedance distribution was uniform, which resulted in

a homogeneous structure (Figure 12c). The sample containing 1.0% Al NPs in the epoxy paint showed the greatest resistance but also a large distribution of resistance (Figure 12d). A deviation in the impedance resistance values appeared due to the densely distributed aluminium nanoparticles located right next to the surface and inside the coating itself. The aluminium particles, located right next to the surface, reacted with the UME and allowed the current to flow, thus increasing the value of the current. Particles that were further from the surface were not able to have a complete impact on the UME, but the epoxy resin came to the fore, and the current flow decreased.

The obtained values which are shown in Figure 12 for coating resistance were used to calculate the nanocomposite protection efficiency (CPE) using the following equation [24]:

$$CPE = \frac{Z'_{coatwithAlNP} - Z'_{coatwithoutAlNP}}{Z'_{coatwithAlNP}} \quad (1)$$

The calculated nanocomposite efficiency obtained by ic-ac-SECM measurement of epoxy, epoxy paint, 1.0% Al NP–epoxy resin nanocomposite, and 1.0% Al NP–epoxy paint nanocomposite coating immersed in tap water, is shown in Table 5.

**Table 5.** Calculated coating protection efficiency (CPE, %) for non-modified and modified epoxy coating immersed in tap water.

Samples	Epoxy Resin	1.0% Al NP–Epoxy Resin Nanocomposite	Epoxy Paint	1.0% Al NP–Epoxy Paint Nanocomposite
$Z'_{max}$ (k $\Omega$ )	447	602	662	1120
CPE (%)	-	25.75	-	40.89

Nanoparticles in pure epoxy resin increase the protection efficiency by 25.75% and in the epoxy paint by 40.89%.

### 3.5. Evaluation of Antibacterial Properties

To develop a nanocoating with antibacterial properties, we investigated the antibacterial activity of Al NPs. Inorganic nanoparticles with antimicrobial activity are emerging as a new class of additives to coating materials to fulfil the increasing general demands for achieving dual properties of nanocomposites [21]. In the literature, there is almost no data on the toxicity of pure Al NPs, most of the literature studies aluminium oxide nanoparticles (alumina).

The antibacterial activity of Al NP nanoparticles against *P. aeruginosa* (Gram-negative) and *B. subtilis* (Gram-positive) was measured using the well-diffusion method (Figure 13a,b).

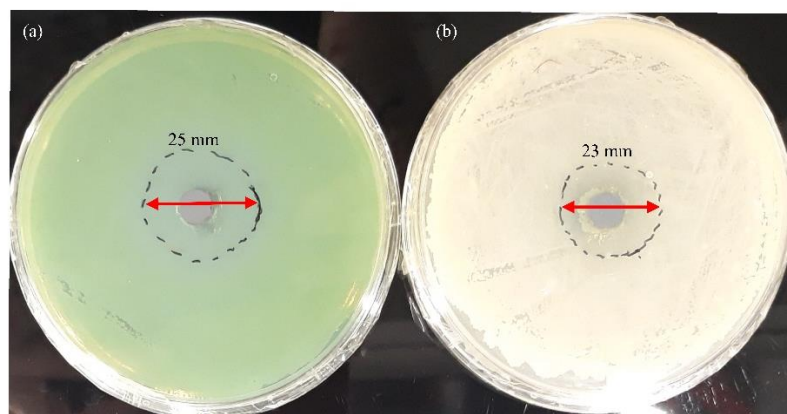


**Figure 13.** Antibacterial activity of pure Al NPs. Zone of inhibition of Al NP against (a) *P. aeruginosa* and (b) *B. subtilis* after 24 h.

The inhibition zone diameter indicated that Al NPs had a great antimicrobial effect (Figure 13a,b). Pure Al NPs produced zones of inhibition of 25 mm against *P. aeruginosa* and 23 mm against *B. subtilis*. In general, differences in the cell wall structure between Gram-positive and Gram-negative bacteria could affect the interaction between NPs and bacteria. Gram-positive bacteria had a thick outer cell wall formed by a thick peptidoglycan layer with hard polysaccharide chains linked by peptides. The thick outer cell wall could hinder NP penetration into the thick peptidoglycan layer [50]. It is known that, in an aerobic environment, pure aluminium reacts with oxygen and forms a thin oxide layer on its surface [51]. Factors that may be responsible for the antibacterial effect of aluminium oxide are (i) zeta potential and size of nanoparticles and (ii) formation of reactive oxidizing species (ROS) [52,53].

#### 4. Conclusions

- (1) The Al NP nanocomposite was successfully dispersed in the epoxy resin and epoxy paint, without agglomerates and the appearance of air bubbles, which was confirmed by SEM, EDS, and SECM analyses.
- (2) Electrochemical tests confirm that the addition of Al NPs to the epoxy paints significantly increases the impedance values. The enhanced corrosion protection performance in the presence of spherical Al NPs was attributed to the cathodic passivation process. After a longer exposure time, oxides form on the Al NP surface, close the pores, and provide greater resistance to the aggressive medium. When the added content of Al NPs was 1.0 wt.%, the nanocomposite displayed the best mechanical and corrosion protection properties.
- (3) The tests of antimicrobial properties against two typical bacteria of *P. aeruginosa* and *B. subtilis* indicate that the surface antibacterial layer of Al NPs possesses excellent antimicrobial properties.
- (4) According to the obtained results, we believe that this Al NP–epoxy nanocomposite represents a multifunctional coating with excellent anticorrosive and antibacterial properties.

**Author Contributions:** Conceptualization, V.A. and M.S.; methodology, M.S. and M.V.D.; software, M.S. and M.K.; validation, M.S. and M.K.; formal analysis, M.S. and M.K.; investigation, M.S.; resources, V.A.; data curation, M.S.; writing—original draft preparation, M.S.; writing—review and editing, M.S.; visualization, M.S., M.K., M.V.D. and V.A.; supervision, V.A.; project administration, V.A. and M.K.; funding acquisition, V.A. All authors have read and agreed to the published version of the manuscript.

**Funding:** This research was funded by “Development of anticorrosion protection system for multipurpose pipe use”, grant number KK.01.1.1.07.0045. This work was supported by the European Regional Development Fund under the Operational Program Competitiveness and Cohesion 2014–2020.

**Institutional Review Board Statement:** Not applicable.

**Informed Consent Statement:** Not applicable.

**Data Availability Statement:** Not applicable.

**Conflicts of Interest:** The authors declare no conflict of interest.

#### References

1. Melchers, R.E. Post-perforation external corrosion of cast iron pressurised water mains. *Corros. Eng. Sci. Technol.* **2017**, *52*, 541–546. [[CrossRef](#)]
2. Heikh, A.H.; Sarkar, A.; Singh, J.K.; Sohail, M.A.K.; Alharthi, N.; Ghosh, M. Corrosion Characteristics of Copper-Added Austempered Gray Cast Iron (AGCI). *Materials* **2019**, *12*, 503.
3. Umoren, S.A.; Solomon, M.M. Recent Developments on the Use of Polymers as Corrosion Inhibitors—A Review. *Open Mater. Sci. J.* **2014**, *8*, 39–54. [[CrossRef](#)]
4. Jain, P.; Patidar, B.; Bhawsar, J. Potential of Nanoparticles as a Corrosion Inhibitor: A Review. *J. Bio-Tribo-Corros.* **2020**, *6*, 1–12. [[CrossRef](#)]

5. Koch, G.; Varney, J.; Thompson, N.; Moghissi, O.; Gould, M.; Payer, J. International Measures of Prevention, Application, and Economics of Corrosion Technologies Study. *NACE Int.* **2016**, *2016*, 2–3.
6. Koch, G.H.; Brongers, M.P.H.; Thompson, N.G.; Virmani, Y.P.; Payer, J.H. Cost of Corrosion Study Unveiled. *NACE Int.* **2015**, 95–126.
7. Kania, H. Corrosion and Anticorrosion of Alloys/Metals: The Important Global Issue. *Coatings* **2023**, *13*, 216. [[CrossRef](#)]
8. Ferreira, E.S.; Giacomelli, C.; Giacomelli, F.C.; Spinelli, A. Evaluation of the inhibitor effect of L-ascorbic acid on the corrosion of mild steel. *Mater. Chem. Phys.* **2004**, *83*, 129–134. [[CrossRef](#)]
9. Ammar, A.U.; Shahid, M.; Ahmed, M.K.; Khan, M.; Khalid, A.; Khan, Z.A. Electrochemical study of polymer and ceramic-based nanocomposite coatings for corrosion protection of cast iron pipeline. *Materials* **2018**, *11*, 332. [[CrossRef](#)]
10. Foorginezhad, S.; Dargah, M.M.; Firoozirad, K.; Aryai, V.; Razmjou, A.; Abbassi, R.; Garaniya, V.; Beheshti, A.; Asadnia, M. Recent Advances in Sensing and Assessment of Corrosion in Sewage Pipelines. *Process. Saf. Environ. Prot.* **2020**, *147*, 192–213. [[CrossRef](#)]
11. Lv, M.; Du, M. A review: Microbiologically influenced corrosion and the effect of cathodic polarization on typical bacteria. *Rev. Environ. Sci. Biotechnol.* **2018**, *17*, 431–446. [[CrossRef](#)]
12. Slekovec, C.; Plantin, J.; Cholley, P.; Thouverez, M.; Talon, D.; Bartrand, X.; Hocquet, D. Tracking Down Antibiotic-Resistant *Pseudomonas aeruginosa* Isolates in a Wastewater Network. *PLoS ONE* **2012**, *7*, e49300. [[CrossRef](#)] [[PubMed](#)]
13. Perelomov, L.; Sizova, O.; Rahman, M.M.; Perelomova, I.; Minkina, T.; Sokolov, S.; Atroshchenko, Y. Metal-Tolerant Bacteria of Wastewater Treatment Plant in a Large City. *Sustainability* **2022**, *14*, 11335. [[CrossRef](#)]
14. Cyprowski, M.; Stobnicka-Kupiec, A.; Lawniczek-Walczyk, A.; Bakal-Kijek, A.; Gołofit-Szymczak, M.; Górný, R.L. Anaerobic bacteria in wastewater treatment plant. *Int. Arch. Occup. Environ. Health* **2018**, *91*, 571–579. [[CrossRef](#)]
15. Roulová, N.; Mot'ková, P.; Brožková, I.; Pejchalová, M. Antibiotic resistance of *Pseudomonas aeruginosa* isolated from hospital wastewater in the Czech Republic. *J. Water Health* **2022**, *20*, 692–701. [[CrossRef](#)] [[PubMed](#)]
16. Zhao, X.; Yan, L.; Xu, X.; Zhao, H.; Lu, Y.; Wang, Y.; Jiang, C.; Shao, D.; Zhu, J.; Shi, J. Synthesis of silver nanoparticles and its contribution to the capability of *Bacillus subtilis* to deal with polluted waters. *Appl. Microbiol. Biotechnol.* **2019**, *103*, 6319–6332. [[CrossRef](#)]
17. Balakrishnan, A.; Jena, G.; Pongachira George, R.; Philip, J. Polydimethylsiloxane–graphene oxide nanocomposite coatings with improved anti-corrosion and anti-biofouling properties. *Environ. Sci. Pollut. Res.* **2021**, *28*, 7404–7422. [[CrossRef](#)] [[PubMed](#)]
18. Saravanan, P.; Jayamoorthy, K.; Ananda Kumar, S. Design and characterization of non-toxic nano-hybrid coatings for corrosion and fouling resistance. *J. Sci. Adv. Mater. Devices* **2016**, *1*, 367–378. [[CrossRef](#)]
19. Bertani, R.; Bartolozzi, A.; Pontefisso, A.; Quaresimin, M.; Zappalorto, M. Improving the antimicrobial and mechanical properties of epoxy resins via nanomodification: An overview. *Molecules* **2021**, *26*, 5426. [[CrossRef](#)]
20. Yuan, H.; Qi, F.; Zhao, N.; Wan, P.; Zhang, B.; Xiong, H.; Liao, B.; Ouyang, X. Graphene oxide decorated with titanium nanoparticles to reinforce the anti-corrosion performance of epoxy coating. *Coatings* **2020**, *10*, 129. [[CrossRef](#)]
21. Manjumeena, R.; Venkatesan, R.; Duraibabu, D.; Sudha, J.; Rajendran, N.; Kalaichelvan, P.T. Green Nanosilver as Reinforcing Eco-Friendly Additive to Epoxy Coating for Augmented Anticorrosive and Antimicrobial Behavior. *Silicon* **2016**, *8*, 277–298. [[CrossRef](#)]
22. Talabi, H.K.; Adewuyi, B.O.; Olaniran, O.; Ayekusibe, P.O. Reinforcement Efficiency of Copper Nanoparticles on Epoxy Matrix Bactericide Composite. *J. Chem. Technol. Metall.* **2021**, *56*, 321–326.
23. Jamkhande, P.G.; Ghule, N.W.; Bamer, A.H.; Kalaskar, M.G. Metal nanoparticles synthesis: An overview on methods of preparation, advantages and disadvantages, and applications. *J. Drug Deliv. Sci. Technol.* **2019**, *53*, 101174. [[CrossRef](#)]
24. Samardžija, M.; Alar, V.; Špada, V.; Stojanović, I. Corrosion Behaviour of an Epoxy Resin Reinforced with Aluminium Nanoparticles. *Coatings* **2022**, *12*, 1500. [[CrossRef](#)]
25. *Aalco Aluminium Alloy Specifications Datasheet*; Aalco Metals Ltd.: Wednesbury, UK, 2016; pp. 1–6.
26. Pesiri, D.; Aumann, C.; Bilger, L.; Booth, D.; Carpenter, R.D.; Dxe, R.; O'Neill, E.; Shelton, D.; Walter, K.C. Industrial scale nano-aluminum powder manufacturing. *J. Pyro.* **2007**, *714*, 1–16.
27. Kumar, A.M.; Khan, A.; Suleiman, R.; Qamar, M.; Saravanan, S.; Dafalla, H. Bifunctional CuO/TiO<sub>2</sub> nanocomposite as nanofiller for improved corrosion resistance and antibacterial protection. *Prog. Org. Coatings* **2017**, *114*, 9–18. [[CrossRef](#)]
28. *ISO 868*; Plastic and Ebonite—Determination of Indentation Hardness by Means of a Durometer (Shore Hardness). International Organization for Standardization: Geneva, Switzerland, 2003.
29. *ISO 6270-2*; Paints and Varnishes—Determination of Resistance to Humidity—Part 2: Condensation (In-Cabinet Exposure with Heated Water Reservoir). International Organization for Standardization: Geneva, Switzerland, 2017.
30. Chaudhary, R.G.; Tanna, J.A.; Gandhare, N.V.; Rai, A.R.; Juneja, H.D. Synthesis of nickel nanoparticles: Microscopic investigation, an efficient catalyst and effective antibacterial activity. *Adv. Mater. Lett.* **2015**, *6*, 990–998. [[CrossRef](#)]
31. *ISO 12944-6*; Paints and Varnishes—Corrosion Protection of Steel Structures by Protective Paint Systems—Part 6: Laboratory Performance Test Methods. International Organization for Standardization: Geneva, Switzerland, 2018.
32. Wei, H.; Xia, J.; Zhou, W.; Zhou, L.; Hussian, G.; Li, Q.; Ostrikov, K.K. Adhesion and cohesion of epoxy-based industrial composite coatings. *Compos. B Eng.* **2020**, *193*, 108035. [[CrossRef](#)]
33. Sherif, E.S.M.; Alam, M.A.; Al-Zahrani, S.M. Fabrication of Different Protective Coatings and Studying their Mechanical Properties and Corrosion Behavior in Sodium Chloride Solutions. *Int. J. Electrochem. Sci.* **2015**, *10*, 373–387.



34. Margarit-Mattos, I.C.P. EIS and organic coatings performance: Revisiting some key points. *Electrochim. Acta* **2020**, *354*, 136725. [[CrossRef](#)]
35. Chilkoor, G.; Sarder, R.; Islam, J.; Kumar, K.E.A.; Ratnayake, I.; Star, S.; Jasthi, B.K.; Sereda, G.; Koratkar, N.; Meyyappan, M.; et al. Maleic anhydride-functionalized graphene nanofillers render epoxy coatings highly resistant to corrosion and microbial attack. *Carbon N. Y.* **2020**, *159*, 586–597. [[CrossRef](#)]
36. Shankar, A.R.; Anandkumar, B.; Thinaharan, C.; George, R.P.; Rooby, J.; Philip, J.; Kamachi Mudali, U. Corrosion Evaluation of Buried Cast Iron Pipes Exposed to Fire Water System for 30 years. *Trans. Indian Inst. Met.* **2020**, *73*, 9–21. [[CrossRef](#)]
37. Liu, X.; Xiong, J.; Lv, Y.; Zuo, Y. Study on corrosion electrochemical behavior of several different coating systems by EIS. *Prog. Org. Coatings* **2009**, *64*, 497–503. [[CrossRef](#)]
38. Dave, P.N.; Chopda, L.V.; Sahu, L. Applications of Nanomaterials in Corrosion Protection Inhibitors and Coatings. *ACS Symp. Ser.* **2022**, *1418*, 189–212.
39. Trentin, A.; Pakseresht, A.; Duran, A.; Castro, Y.; Galusek, D. Electrochemical Characterization of Polymeric Coatings for Corrosion Protection: A Review of Advances and Perspectives. *Polymers* **2022**, *14*, 2306. [[CrossRef](#)]
40. Niroumandrad, S.; Rostami, M.; Ramezanzadeh, B. Effects of combined surface treatments of aluminium nanoparticle on its corrosion resistance before and after inclusion into an epoxy coating. *Prog. Org. Coatings* **2016**, *101*, 486–501. [[CrossRef](#)]
41. Kurtela, M.; Šimunović, V.; Stojanović, I.; Alar, V. Effect of the cerium (III) chloride heptahydrate on the corrosion inhibition of aluminum alloy. *Mater. Corros.* **2019**, *71*, 125–147. [[CrossRef](#)]
42. Chernavskii, P.A.; Peskov, N.V.; Mugtasimov, A.V.; Lunin, V.V. Oxidation of metal nanoparticles: Experiment and model. *Russ. J. Phys. Chem.* **2007**, *1*, 394–411. [[CrossRef](#)]
43. Petrovic, J.; Thomas, G. Reaction of Aluminum with Water to Produce Hydrogen, a Study of Issues Related to the Use of Aluminum for On-Board Vehicular Hydrogen Storage. *U.S. Dep. Energy* **2008**, *1*, 1–26.
44. Gromov, A.A.; Strokova, Y.I.; Teipel, U. Stabilization of metal nanoparticles—A chemical approach. *Chem. Eng. Technol.* **2009**, *32*, 1049–1060. [[CrossRef](#)]
45. Gerard, D.; Gray, S.K. Aluminium plasmonics. *J. Phys. D. Appl. Phys.* **2015**, *48*, 184001. [[CrossRef](#)]
46. Schmidt, R.G.; Bell, J.P. Epoxy Adhesion to Metals. *Adv. Polym.* **1986**, *75*, 33–71.
47. Feichtenschlager, B.; Pabisch, S.; Svehla, J.; Peterlik, H.; Sajjad, M.; Koch, T.; Kickelbick, G. Epoxy Resin Nanocomposites: The Influence of Interface Modification on the Dispersion Structure—A Small-Angle-X-ray-Scattering Study. *Surfaces* **2020**, *3*, 664–682. [[CrossRef](#)]
48. Taylor, P.; Halder, S.; Ghosh, P.K.; Goyat, M.S.; Ray, S. Ultrasonic dual mode mixing and its effect on tensile properties of SiO<sub>2</sub>-epoxy nanocomposite. *J. Adhes. Sci. Technol.* **2013**, *27*, 37–41.
49. Xavier, J.R.; Nallaiyan, R. Application of EIS and SECM Studies for Investigation of Anticorrosion Properties of Epoxy Coatings containing ZrO<sub>2</sub> Nanoparticles on Mild Steel in 3.5% NaCl Solution. *J. Fail. Anal. Prev.* **2016**, *16*, 1082–1091. [[CrossRef](#)]
50. Slavin, Y.N.; Asnis, J.; Häfeli, U.O.; Bach, H. Metal nanoparticles: Understanding the mechanisms behind antibacterial activity. *J. Nanobiotechnol.* **2017**, *15*, 1–20. [[CrossRef](#)]
51. Karlsson, P.; Palmqvist, A.E.C.; Holmberg, K. Surface modification for aluminium pigment inhibition. *Adv. Colloid Interface Sci.* **2006**, *128–130*, 121–134. [[CrossRef](#)]
52. Prashanth, P.A.; Raveendra, R.S.; Krishan, R.H.; Ananda, S.; Bhagya, N.P.; Nagabhushana, B.M. Synthesis, characterizations, antibacterial and photoluminescence studies of solution combustion-derived  $\alpha$ -Al<sub>2</sub>O<sub>3</sub> nanoparticles. *J. Asian Ceram. Soc.* **2015**, *3*, 345–351. [[CrossRef](#)]
53. Gudkov, S.V.; Burmistrov, D.E.; Smirnova, V.V.; Semenova, A.A.; Lisitsyn, A.B. A Mini Review of Antibacterial Properties of Al<sub>2</sub>O<sub>3</sub> Nanoparticles. *Nanomaterials* **2022**, *12*, 2635. [[CrossRef](#)]

**Disclaimer/Publisher’s Note:** The statements, opinions and data contained in all publications are solely those of the individual author(s) and contributor(s) and not of MDPI and/or the editor(s). MDPI and/or the editor(s) disclaim responsibility for any injury to people or property resulting from any ideas, methods, instructions or products referred to in the content.

## Article 4

M. Samardžija, I. Stojanović, M. Kurtela, V. Alar, Influence of aluminum nanoparticles in epoxy resin and epoxy coating for anticorrosion and antibacterial protection in pipeline industry, *J. Appl. Polym.* (2023), e55002.

### Author Contributions:

Marina Samardžija	conceptualization, data curation, formal analysis, software, writing – original draft, writing – review and editing
Ivan Stojanović	project administration, supervision, validation
Marin Kurtela	methodology, project administration, software, supervision
Vesna Alar	funding acquisition, methodology, project administration, supervision

This paper is published in an open access journal (<https://doi.org/10.1002/app.55002>).

Marina Samardžija

**Pošiljatelj:** APP Editorial Office <appmc@wiley.com>  
**Poslano:** 27. studenog 2023. 16:59  
**Prima:** Marina Samardžija  
**Predmet:** RE: app.20232160R1 Marked for Production - CEMID:17ef87e55d9891a]  
0  
**Zastavica uputa za daljnji rad:** Upute za daljnji rad  
**Stanje zastavice:** Obilježen zastavicom

Dear Dr. Samardžija,

Thank you for your message. Articles are published according to our format and author guidelines,

If you wish to use the published article in your dissertation, that's subject to approval from your university and we allow that to be done.

If you have further questions, please let us know.

Best Regards,  
Journal of Applied Polymer Science

-----Original Message-----

From: Marina Samardžija <marina.samardzija@rgn.unizg.hr>  
Sent: Friday, November 24, 2023 2:54 AM

To: APP Editorial Office <appmc@wiley.com>  
Subject: RE: app.20232160R1 Marked for Production - [EMID:17ef87e55d9891aO]

Dear,

thank you for accepting the article "Influence of aluminium nanoparticles in epoxy resin and epoxy coating for anticorrosion and antibacterial protection in pipeline industry".

I have a question and I hope I can ask it simply.

I am a PhD student, and I am doing my doctoral thesis according to the Scandinavian model, where I will submit four papers. Among those works is this paper, which I plan to publish at your Journal.

If I do not choose open access, can you provide me with a document in which the publisher allows automatic publication of the article within the framework of the doctoral dissertation?

Thank you.  
Kind regards,  
Marina Samardžija

## RESEARCH ARTICLE

# Influence of aluminum nanoparticles in epoxy resin and epoxy coating for anticorrosion and antibacterial protection in pipeline industry

Marina Samardžija<sup>1</sup>  | Ivan Stojanović<sup>2</sup> | Marin Kurtela<sup>2</sup> | Vesna Alar<sup>2</sup>

<sup>1</sup>Department of Chemistry, Faculty of Mining Geology and Petroleum Engineering University of Zagreb, Zagreb, Croatia

<sup>2</sup>Department of Welded Structures, Faculty of Mechanical Engineering and Naval Architecture, University of Zagreb, Zagreb, Croatia

**Correspondence**

Marina Samardžija, Department of Chemistry, Faculty of Mining Geology and Petroleum Engineering University of Zagreb, Pierottijeva 6, 10000 Zagreb, Croatia.

Email: [marina.samardzija@rgn.unizg.hr](mailto:marina.samardzija@rgn.unizg.hr)

**Funding information**

European Regional Development Fund, Grant/Award Number: KK.01.1.1.07.0045

**Abstract**

In the present work, the effect of aluminum nanoparticles inside epoxy resin and epoxy paint for the purpose of extending the service life of drainage pipes. The nanocomposite samples were analyzed with scanning electronic microscopy (SEM) and energy dispersive x-ray analysis (EDX) to evaluate the dispersion of nanoparticles. Performed quantitative tests including electrochemical techniques, such as the method of electrochemical impedance spectroscopy (EIS) and scanning electrochemical microscopy (SECM) to determine impedance resistance on macro and micro levels. The antibacterial resistance of the nanocomposite samples was tested in the presence of *Pseudomonas aeruginosa* and *Bacillus subtilis*. All nanocomposite samples show an improvement in the measurement of impedance resistances and an increase in antibacterial effect by about 60% compared to the sample without nanoparticles.

**KEYWORDS**

corrosion, electrochemical impedance spectroscopy, nanoparticles, organic coating, scanning electrochemical microscopy

## 1 | INTRODUCTION

Cast iron was widely used as a common material for water mains more than 50 years ago and it is subjected to different levels of deterioration due to corrosion and loading.<sup>1,2</sup> Nowadays, one of the leading global problems is the generation of increasing amounts of wastewater. Empirical records compiled from a variety of sources suggest that globally more than 330 km<sup>3</sup> year<sup>-1</sup> of municipal wastewater is produced.<sup>3</sup> Over half of the population living in clusters in the European Union produces on a daily basis wastewater that amounts to 41.5 million m<sup>3</sup>.<sup>4</sup> An excessive amount of wastewater, affects the strength of the material, mechanical properties, physical appearance, as well as its operation and lead to degradation of infrastructure.<sup>5</sup> Gray cast irons undergo a unique form of deterioration, known as graphitic corrosion.<sup>6</sup> In the

process, the ferrous iron component of the cast iron pipe wall exposed to the water media will leached out (anodic action), leaving behind a graphite matrix.<sup>7,8</sup> The corrosion can cause degradation of the external and internal pipeline surfaces. The external corrosion is governed by reactions between the outer surface of the pipeline and the surrounding atmosphere, including moisture, soils, and similar.<sup>9</sup> Except for electrochemical corrosion, damage to pipelines can occur by microbiologically influenced corrosion.<sup>10</sup> The microorganism influences internal corrosion immensely which is primarily governed by the nature/source/composition of wastewater in residential and industrial pipelines, types of pollutants, including nutrients, pathogens, and so on.<sup>9</sup> The bacteria that we can find in wastewater are *Escherichia coli*, *Salmonella* spp., *Pseudomonas aeruginosa*, *Citrobacter*, *Enterobacter*, *Hafnia*, *Klebsiella*, *Serratia*, *Bacillus subtilis*,

and *Yersinia*.<sup>11–13</sup> The mechanism of action of bacteria and metal substrates was described in detail in their works by Blackwood<sup>14</sup> and Lv and co-authors,<sup>15</sup> where they describe the cathodic depolarization theory and extracellular electron transfer and microbiologically induced corrosion caused by microbial products. To illustrate, different studies showed that the acquisition of iron is important for the survival of Gram-negative bacteria *P. aeruginosa* which means that they will replenish their need for iron from the metal surface.<sup>16,17</sup> One of the mechanisms of interaction between metal/bacteria is extracellular electron transfer. These mechanisms include direct electron transfer and electron transfer which require redox mediators.<sup>14</sup> Besides metal/bacteria interaction, the metal corrosion process also can be accelerated by biofilm.<sup>18</sup> Research showed that extracellular polymer substances (EPS) produced by Gram-positive bacteria *B. subtilis* were the main component of the biofilm formed on the metal surface and provided the biologically active compound that affected the corrosion process.<sup>19,20</sup>

Due to all these reasons, researchers wanted to develop a new generation of protective coating that will have anticorrosive and antibacterial properties.<sup>21</sup> Nanoparticles have proven to be a good tool for achieving this goal. Besides their ability to stop the reaction of the surface and control the corrosion rate by blocking active sites of the metal surfaces, they also provide hardness, straightness, durability, optical qualities, and thermal stability.<sup>22</sup> By adding aluminum nanoparticles (Al NP) into epoxy coating anticorrosion and antibacterial coatings can be developed.<sup>23</sup> The ability of Al NPs to release the Al<sup>3+</sup> ion and create a passive oxidation layer gives the possibility of creating a nanocomposite system for the protection of drainage pipes against chemical and microbiological environmental factors.<sup>24,25</sup>

In the present research, we want to investigate whether there is a difference in the anticorrosive and antibacterial effectiveness of Al NPs in pure epoxy resin and epoxy paint. The formation of an aluminum oxidation film on a nanocomposite coating applied to the surface of gray cast iron was also investigated. A comparison between the resin and commercially available anticorrosive paints was made.

## 2 | EXPERIMENTAL SECTION

### 2.1 | Materials

Elemental compositions of the gray cast iron specimens are 2.5 wt% C, 0.4 wt% Mn, 1.0 wt% Si, 0.4 wt% P, and the remainder is Fe. Coating formulations were prepared by

reacting West System 105 epoxy resin, and epoxy paint purchased from Hempel with polyamine-containing hardener. Aluminum nanoparticles (Al NP) with an average particle size of 100 nm were provided by Guangzhou Hongwu Material Technology Co.

### 2.2 | Apparatus

#### 2.2.1 | Surface characterization

Scanning electron microscope (SEM) analysis was carried out using a TESCAN Brno microscope at a high vacuum, with 10 kV, a spot size of 3, and a work distance of 6 mm. The size distribution and dispersion of nanoparticles and microanalysis of the chemical composition of the sample were conducted using the energy-dispersive detector (EDS) from INCA PentaFET.

#### 2.2.2 | Mechanical properties of nanocomposite

Elcometer<sup>®</sup>456 (Elcometer Limited, Edge Lane, Manchester, UK) was used to observe the thickness of all samples. The hardness of the coating and nanocomposite was determined by the PosiTector SHD Shore Hardness Durometer (DeFlesko Corporation, Ogdensburg, NY, USA). The hardness of the nanocomposite was tested according to ISO 868:2003.<sup>26</sup> The automatic Pull-Off test was used to measure the adhesion force between coating and metal (Elcometer 510, model T, Manchester, UK). The coating samples and nanocomposite were exposed to the salt chamber (Ascott Analytical Equipment Limited, model S450, Staffordshire, UK). According to HRN EN ISO 9227, the samples had been in the salt chamber for 10 days (240 h).<sup>27</sup>

#### 2.2.3 | Thermal properties

Differential scanning calorimetry (DSC) thermograms were recorded on a Mettler Toledo DSC 822e calorimeter using N<sub>2</sub> flow. The samples weighing about 10 mg were heated from 25°C to 150°C at a rate of 10°C/min and kept at that temperature for 5 min to forget the thermal history of the sample preparation (first heating cycle). The samples were cooled to –100°C at a speed of 10°C/min and heated to 150°C at a speed of 10°C/min (second heating cycle). From the second heating cycle, the values of the glass transition temperature,  $T_g$ , were read. Cooling was carried out with liquid nitrogen. Thermogravimetric analysis (TGA) was recorded on a TGA analyzer

Q500. The samples weighing around 10 mg were analyzed in a stream of nitrogen (60 mL/min) in the temperature range of 25–600°C with a heating rate of 10°C/min.

### 2.2.4 | Electrochemical measurements

Electrochemical impedance spectroscopy (EIS) was recorded on the VersaSTAT 3 Potentiostat/Galvanostat instrument. EIS was used to evaluate the resistance of the epoxy resin, 1% Al NP epoxy resin nanocomposite, epoxy paint, and 1% Al NP epoxy paint nanocomposite in 3.5% NaCl solution, pH = 7.554, while it was open to the atmosphere. Measurements were performed in the frequency range from 100 kHz to 0.1 Hz, with a potential amplitude of 10 mV at a room temperature of  $25 \pm 2^\circ\text{C}$ . Measurements were conducted using an electrochemical cell with the coated sample as the working electrode of  $19.625\text{ cm}^2$ . The saturated calomel electrode was used as a reference electrode and the graphite rod as the counter electrode. The ZSimWin software was used to interpret data.

A model intermittent contact – alternating current – Scanning ElectroChemical Microscopy (ic-ac-SECM) from BioLogic was used to make measurements on the epoxy resin, 1% Al NP epoxy resin nanocomposite, epoxy paint, and 1% Al NP epoxy paint nanocomposite in tap water. For a more detailed view, a smaller area ( $50\text{ mm} \times 50\text{ mm}$ ) of a sample was studied using a smaller step size. A 10- $\mu\text{m}$  diameter Pt ultramicroelectrode (UME) was used as the probe, with the platinum electrode used as the counter electrode, and an Ag/AgCl electrode as a reference. The 3D Iso Plot software was used to interpret data. All experiments were carried out at room temperature.

### 2.2.5 | Migration and antibacterial activity of nanocomposite

The samples of epoxy resin, 1% Al NP epoxy resin nanocomposite, epoxy paint, and 1% Al NP epoxy paint nanocomposite were placed in contact with simulation wastewater according to the DIN EN 877.<sup>28</sup> All samples (10 g) were exposed in the 100 mL simulated wastewater for 30 days in 40°C. The mass concentration, electrical conductivity, and pH value of the wastewater were determined after 10, 20, and 30 days. The mass concentration of  $\text{Al}^{3+}$  ions in wastewater was determined with the Aluminium Test (MColorTest™, 0.1–6 mg/L Al). The conductivity and pH values were measured with a pH/EC meter (HI5521–02, HANNA instruments, Woonsocket, RI, USA).

The antibacterial performance of coatings and nanocomposites was assessed using *P. aeruginosa* and *B. subtilis* in accordance with ISO 22196:2011.<sup>29</sup> The antibacterial surfaces for the tests were epoxy resin, 1% Al NP epoxy resin nanocomposite, epoxy paint, and 1% Al NP epoxy paint nanocomposite measuring  $50\text{ mm} \times 50\text{ mm}$  and inoculated with 0.4 mL of  $10^5$  CFU bacterial suspensions. All samples were covered with polyethylene foil dimensions of  $40\text{ mm} \times 40\text{ mm}$  ( $\pm 1\text{ mm}$ ) and a thickness of 0.06 mm and were placed in a Petri dish and incubated at 35°C ( $\pm 1^\circ\text{C}$ ) and 90% relative humidity (RH) ( $\pm 5\%$ ) for 24 h. The plating of different dilutions on plate count agar was used to determine a few viable bacterial cells. The measurements were repeated three times.

### 2.3 | Preparation of nanocomposite

The substrate used for depositing the coating was gray cast iron plates of  $15 \times 9.5 \times 0.9\text{ cm}$ . Surfaces of gray cast iron were cleaned with abrasive blasting ( $R_z$  of 136.7  $\mu\text{m}$ ) and ethanol to remove surface contaminants. Two groups of samples with different epoxy coatings were prepared. The first group of samples was made of pure epoxy resin mixed with 1.0% Al NP. The second group of samples contained epoxy paint mixed with 1.0% Al NPs. Mixing of 1.0% Al NPs into epoxy resin and paint was performed with an ultrasonic homogenizer at an amplitude of 30 for 20 min. The ultrasonic probe heated the sample and therefore the process was stopped for cooling. After that, the hardener was added, and everything was mixed with a glass stick until a homogeneous mixture was obtained. The epoxy resin and hardener were added in a ratio of 3.5:1, and epoxy paint and hardener were added in a ratio of 4:1. No solvents were added during the dispersion process. Pure epoxy resin, 1% Al NP in epoxy resin, epoxy paint, and 1.0% Al NP in epoxy paint were applied to the surface of gray cast iron. The obtained nanocomposite was twice applied to a previously degreased gray cast iron substrate using an applicator (150  $\mu\text{m}$ ). The samples were left at room temperature (25°C) for 7 days and then tested.

## 3 | RESULTS AND DISCUSSION

### 3.1 | The SEM and EDS analysis

Figure 1 shows the SEM and EDS images of pure epoxy resin and 1% Al NP epoxy resin nanocomposite. As shown in Figure 1a, the pure epoxy resin exhibited a smooth surface area with many shrinkage holes and

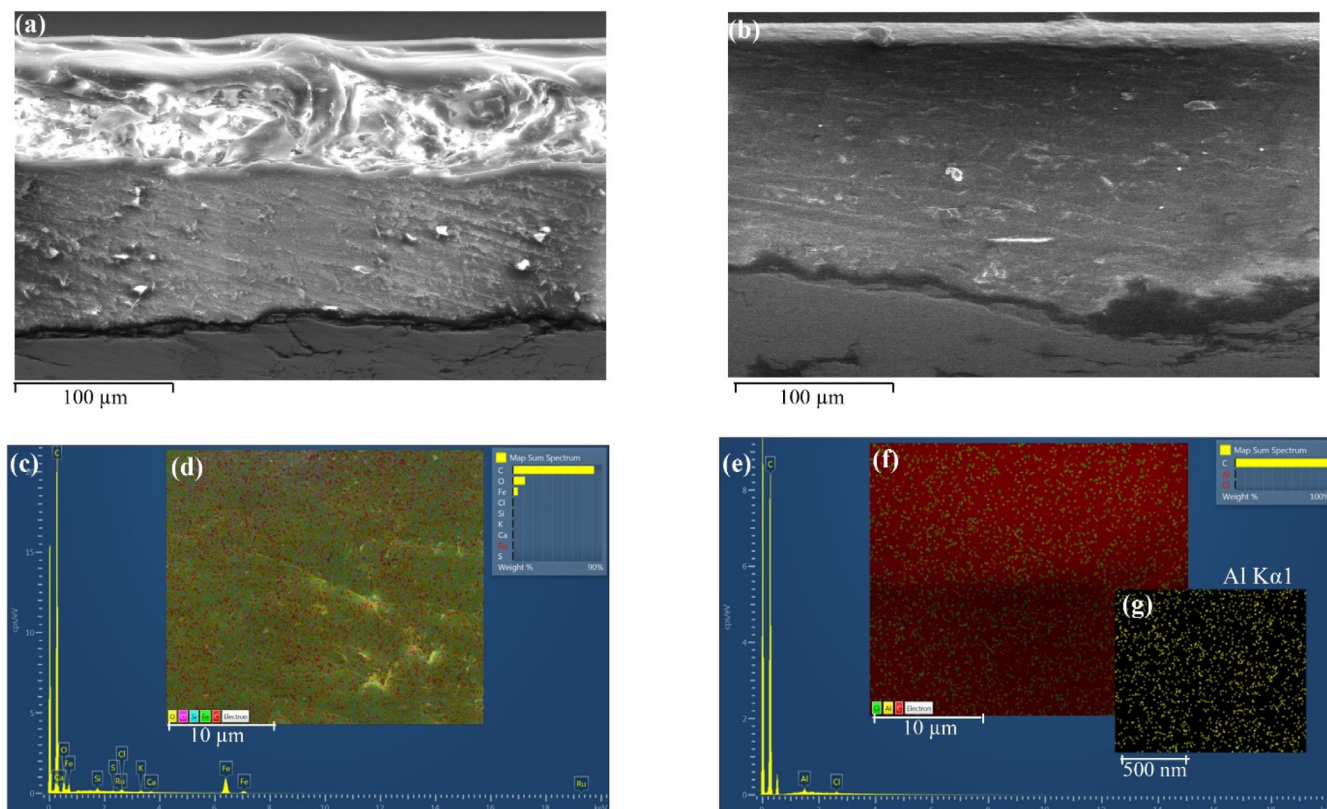


**FIGURE 1** The SEM-EDS chemical composition and mapping analysis of the (a, c, d) epoxy resin, (b, e, f) 1% Al NP epoxy resin nanocomposite, and (g) Al NP distribution in epoxy resin. [Color figure can be viewed at [wileyonlinelibrary.com](http://wileyonlinelibrary.com)]

pinholes on the surface of the coating. The EDS analyses confirmed that the epoxy resin did not contain Al NP (Figure 1c). In addition, C, O, and Fe elements have been monitored on the surface (Figure 1d). The SEM analysis of 1% Al NP epoxy nanocomposite in Figure 1b shows a smooth surface area without cracks and defects. As shown in Figure 1e,f, the 1% of Al NP in epoxy resin shows excellent dispersion. Figure 1e shows the homogeneous and uniform distribution of Al NP in the epoxy resin. Al NPs did not agglomerate due to the action of the ultrasonic probe.

The SEM and EDS mapping of the epoxy paint showed a rough non-homogeneous structure (Figure 2a,d). Pure epoxy paint, before modification, contained a small number of aluminum microparticles (Figure 2c, d). Figure 2e shows clusters of agglomerates larger than 500 nm in size. By adding the Al NPs and using an ultrasonic homogenizer (Figure 2b) the nanocomposite obtained a smoother, homogeneous structure. The EDS analysis (Figure 2f,g) revealed that the concentration of aluminum particles increased. The distribution of the elements of aluminum (Figure 2h) was uniform and homogeneous, without the formation of agglomerates. The ultrasonic homogenizer, in addition to the good distribution of nanoparticles, was also effective in breaking up the aluminum agglomerates that were added as pigments.

### 3.2 | Mechanical resistance of Al NP epoxy nanocomposite

The results of the effect of Al NP on the mechanical properties of epoxy resin and epoxy paint are shown in Table 4. Mechanical properties, such as thickness, hardness, adhesion, and color change, were tested after 10 days of exposure of the samples to the salt chamber. According to HRN EN ISO 6270-2, the samples had been in the chamber for 10 days (240 h).

According to Table 1, it is evident that the addition of 1% Al NP did not change the thickness and hardness of the coating. Adhesion of the coating to the metal substrate showed a small increase with the addition of Al NPs to the epoxy paint. A significant change is visible in the color change of the coating. Exposure of the samples in the salt chamber did not significantly affect the change in the mechanical properties of all samples.

### 3.3 | Differential scanning calorimetry

All samples were analyzed using Differential scanning calorimetry (DSC) to obtain the  $T_g$  values. The DSC curves of all samples show a transition that is related to the glass transition temperature ( $T_g$ ). The obtained  $T_g$

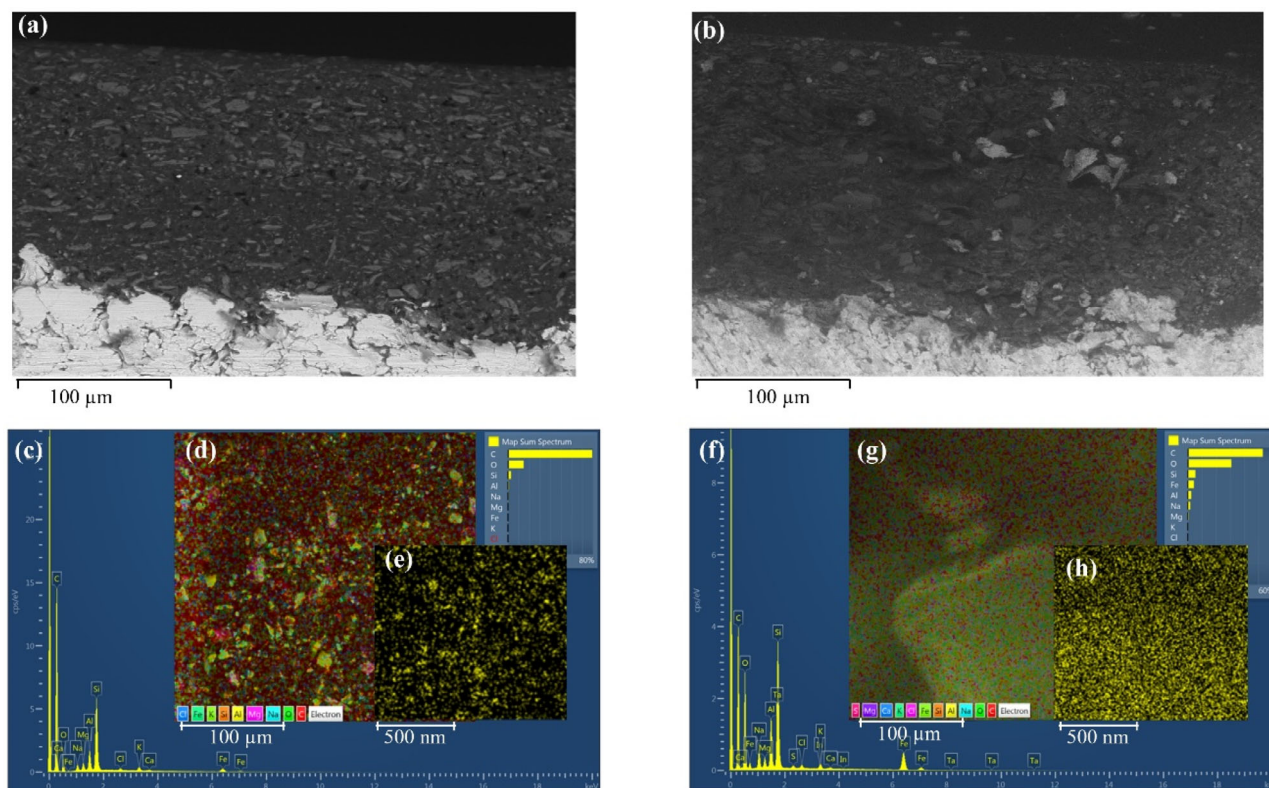


FIGURE 2 The SEM-EDS chemical composition and mapping analysis of the (a, c, d) epoxy paint, (b, f, g) 1% Al NP epoxy paint nanocomposite, and (e, h) Al NP distribution in epoxy paint. [Color figure can be viewed at [wileyonlinelibrary.com](http://wileyonlinelibrary.com)]

range goes from  $-100^{\circ}\text{C}$  to  $140^{\circ}\text{C}$ . Table 2 shows the values of  $T_g$  for all samples.

According to Table 2, the results were evaluated to study the effects of Al NP modification on the  $T_g$  values of the coating. With the addition of Al NPs, it is evident that with an increase in the proportion of Al NPs, there is a shift of  $T_g$  to lower temperatures which means that the nanoparticles are not completely absorbed by the epoxy resin/paint and still have intact free nanoparticle surfaces.

### 3.4 | Thermogravimetric analysis

All samples were analyzed using Thermogravimetric analysis (TGA). Figure 3 illustrates the thermal stability behavior of pure epoxy resin, 1% Al NP epoxy resin nanocomposite, epoxy paint, and 1% Al NP epoxy paint nanocomposite whereas the TGA parameters are listed in Table 3.

The TGA curves for epoxy resin and 1% Al NP epoxy resin nanocomposites show that they decompose in two stages (Figure 3a,b). In both cases, the first stage of decomposition starts around  $100^{\circ}\text{C}$ , where the weight loss for epoxy resin is 13.29%, and for 1% Al NP epoxy

resin nanocomposites 11.05%. The second stage of weight loss, for both samples, started above  $300^{\circ}\text{C}$  during which the weight loss for both samples was approximately 80%.

From the obtained results according to Figure 3c,d, it can be concluded that epoxy paint and 1.0% Al NP epoxy nanocomposite are degraded in three stages. The first stage of weight loss started above  $100^{\circ}\text{C}$  and continued up to approximately  $400^{\circ}\text{C}$ . This may correspond to the removal of traces of solvents or other volatiles trapped during curing because of epoxies complex cross-linked structure and residues of reactants, as well as the decomposition of low molecular weight fractions of polymer.<sup>30</sup> The second and third stage weight loss started above  $400^{\circ}\text{C}$  and continued up to  $510^{\circ}\text{C}$  during which weight loss for blank epoxy coat and 1.0% Al NP epoxy nanocomposite were approximately 27.08, 32.51% and 13.43, 10.87%. The use of an ultrasonic homogenizer did not affect the loss of solvent during the preparation of the nanocomposite. Table 2 shows all results of TGA analysis for epoxy resin samples, 1% Al NP epoxy resin nanocomposite, epoxy paint, and 1% Al NP epoxy paint nanocomposite.

The results in Table 3 show that the nanocomposite samples show the same decomposition temperature interval as their starting samples (epoxy resin and epoxy



**TABLE 1** Results of mechanical resistance tests for epoxy resin, 1% Al NP epoxy resin nanocomposite, epoxy paint, and 1% Al NP epoxy paint before and after the exposure to the salt chamber.

	Samples	Epoxy resin	1% Al NP epoxy resin	Epoxy paint	1% Al NP epoxy paint
Thickness ( $\mu\text{m}$ )	Unexposed	251.20	254.90	249.90	255.50
	Salt chamber	252.00	261.60	254.40	259.50
Hardness (Shore D)	Unexposed	80.00	81.00	83.40	82.00
	Salt chamber	81.75	81.00	77.20	81.60
Adhesion (MPa)	Unexposed	8.32	9.11	8.34	13.47
		9.14	8.87	8.31	14.18
	Salt chamber	7.72	10.46	12.99	9.58
RAL colors	Unexposed	7.67	8.62	11.85	10.44
		025	7016	3013	8017
	Salt chamber	025	7016	3013	8017

**TABLE 2** DSC analysis of epoxy resin, 1% Al NP epoxy resin, epoxy paint, and 1% Al NP epoxy paint.

Samples	Epoxy resin	1% Al NP epoxy resin	Epoxy paint	1% Al NP epoxy paint
$T_g$ ( $^{\circ}\text{C}$ )	52.3	41.1	34.7	20.1

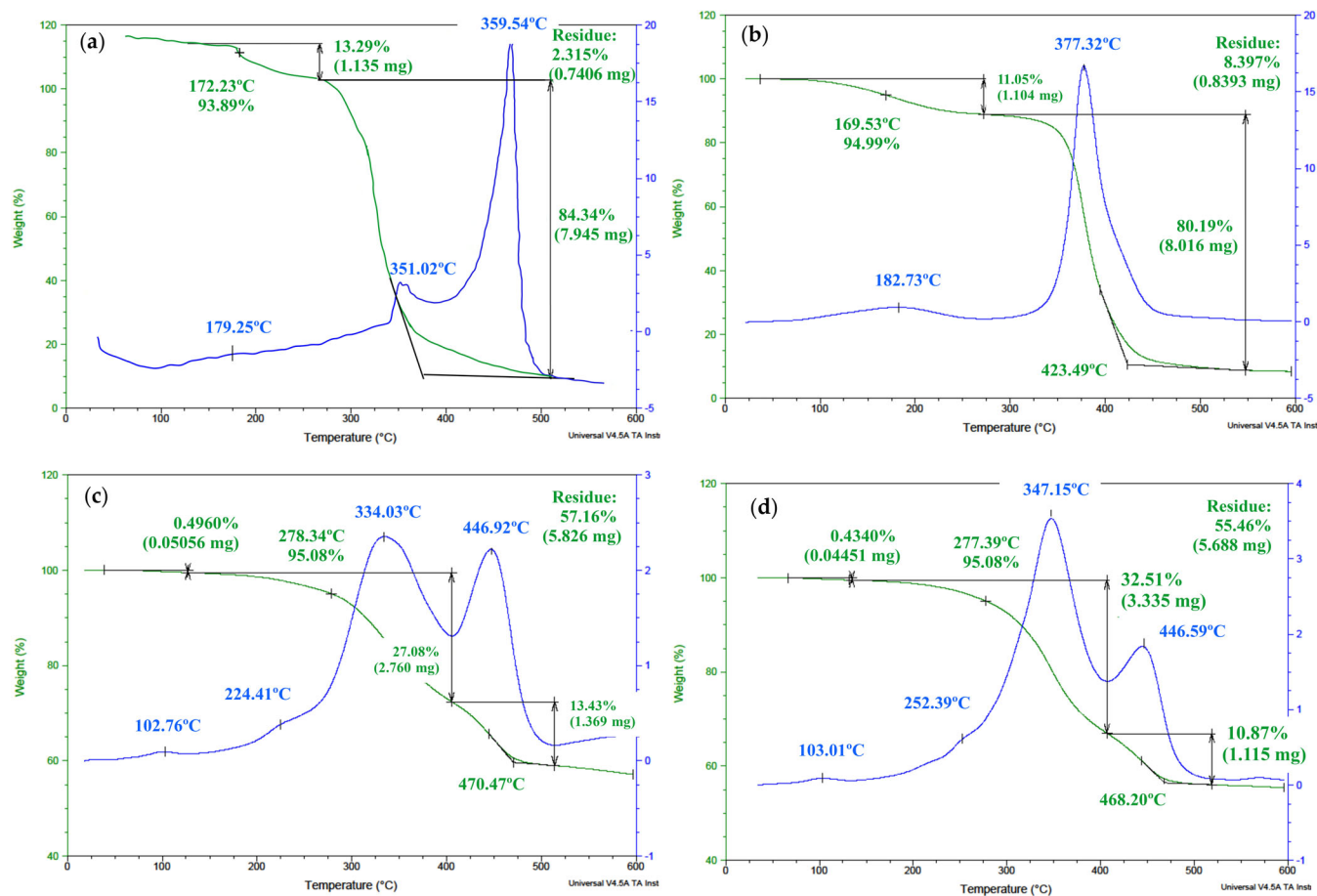


**FIGURE 3** TGA and DTG curves of: (a) epoxy resin, (b) 1% Al NP epoxy resin nanocoating, (c) epoxy paint, (d) 1% Al NP epoxy paint nanocoating. [Color figure can be viewed at [wileyonlinelibrary.com](http://wileyonlinelibrary.com)]

**TABLE 3** Results of thermal decomposition of epoxy resin, 1% Al NP epoxy resin nanocoating, epoxy paint, and 1% Al NP epoxy paint nanocoating.

Samples	Epoxy resin	1% Al NP epoxy resin nanocomposite	Epoxy paint	1% Al NP epoxy paint nanocomposite
$T_5$ (°C)	172.2	169.5	278.3	277.4
$T_{kon}$ (°C)	351.0	423.5	470.5	468.2
$T_{max}^1$ (°C)	179.3	182.7	102.8	103.0
$\Delta m_1$ (%)	13.3	11.1	0.49	0.43
$T_{max}^2$ (°C)	359.5	377.3	334.0	347.2
$\Delta m_2$ (%)	84.34	80.2	27.1	32.5
$T_{max}^3$ (°C)	–	–	446.9	446.6
$\Delta m_3$ (%)	–	–	13.4	10.9
Residue (600°C)	7.4	8.4	57.1	55.5

Note: <sup>1</sup>first step of decomposition, <sup>2</sup>second step of decomposition, and <sup>3</sup>third step of decomposition.

paint). In the first stage of decomposition ( $\Delta m_1$ ), solvent evaporation occurs, which occurs in all samples in an equal proportion for resin from 13.3% to 11.1%, and for paint from 0.43% to 0.49%. The mass loss in the second stage of decomposition ( $\Delta m_2$ ) for samples made with epoxy resin is equal. In the case of the epoxy paint sample with the addition of 1% Al NP, the mass loss increases in the second stage, while it decreases in the third stage of decomposition ( $\Delta m_3$ ). At 600°C, a large proportion of solid residue appears, which may be related to additives added to the coating.

### 3.5 | Electrochemical impedance spectroscopy

The study of electrochemical properties of coating and nanocomposite coating in corrosion media is of great importance for the assessment of the durability and protection of the applied coating system. This information can be obtained using Electrochemical impedance spectroscopy (EIS). Figure 4 shows the equivalent circuit model for the sample with a nanocomposite coat. In the EIS technique, an alternating electric signal over a wide range of frequencies is applied to the reference, working, and counter electrodes at ambient temperature. In this model,  $R_s$ ,  $R_{coat}$ , and  $R_{ct}$  represent the solution resistance, coat resistance, and charge-transfer resistance, respectively.  $CPE_{coat}$  and  $CPE_{dl}$  are the double-layer capacitance and coating capacitance, respectively.<sup>31</sup> In this work, the substrate on which the epoxy coat is applied is gray cast iron with a high carbon content. After a long exposure time in a corrosive electrolyte, the epoxy coat will loosen and begin to form pores and microcracks. When the

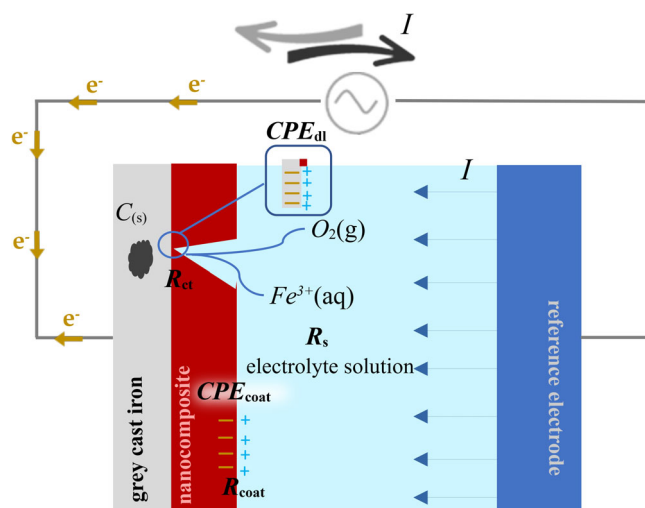


**FIGURE 4** An equivalent circuit model is employed to fit the impedance data.<sup>23</sup> [Color figure can be viewed at [wileyonlinelibrary.com](http://wileyonlinelibrary.com)]

corrosive medium reaches gray cast iron, the iron will dissolve and leave behind graphite (C) (Figure 4). To extend the life of gray cast iron, the epoxy coat is modified with Al NP.

Figure 5 gives the impedance spectra of the epoxy resin, 1% Al NP epoxy resin nanocomposite, epoxy paint, and 1% Al NP epoxy paint nanocomposite in 3.5 wt% NaCl solution after 24 hours. The semi-circular arc diameter in the Nyquist plot and the impedance value at the lowest frequency in the Bode plot provide information regarding the corrosion resistance of the coatings. A higher arc diameter and a high impedance value correspond to a high corrosion resistance.<sup>32</sup> The anticorrosive properties of Al NPs, without the influence of additives

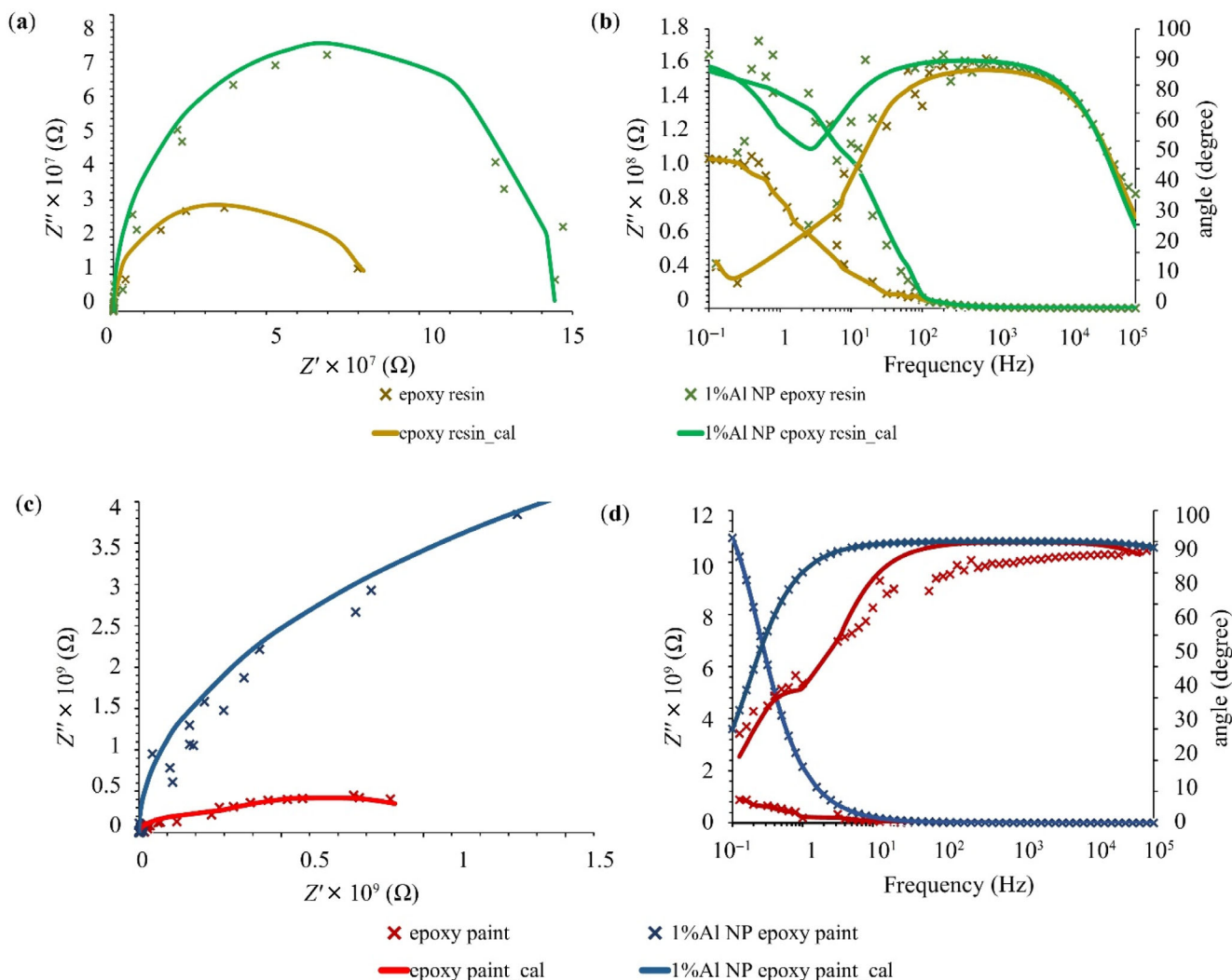


FIGURE 5 Nyquist and Bode plots of (a, b) epoxy resin and 1% Al NP epoxy resin nanocomposite, (c, d) epoxy paint, and 1% Al NP epoxy paint nanocomposite in 3.5 wt% NaCl solution after 24 h. [Color figure can be viewed at [wileyonlinelibrary.com](http://wileyonlinelibrary.com)]

in the coating, are shown in Figure 5a where Al NPs are embedded in pure epoxy resin. Figure 5b shows that the 1% Al NP epoxy resin nanocomposite should have two-time constants after 24 h of immersion in 3.5 wt% NaCl solution. Epoxy paint (Figure 5c) shows better corrosion resistance than pure epoxy resin (Figure 5a) and thus the incorporation of Al NPs into epoxy paint will show better properties. The 1% Al NP epoxy paint resin sample (Figure 5d) achieved a constant phase angle value extending from the medium frequency region (10 Hz) to the high-frequency region ( $10^5$  Hz) throughout the exposure time, indicating that the coating had not started to deteriorate. In the case of short-term immersion in the electrolyte, the properties of the protective coating remained intact. The epoxy paint sample shows a narrower constant area of the phase angle (Figure 5d), which can also be seen in the lower resistance value shown in the Nyquist diagram (Figure 5c).

After finding corrosion resistance for epoxy resin, 1% Al NP epoxy resin nanocomposite, epoxy paint, and 1% Al NP epoxy paint nanocomposite the coating protection efficiency (CPE) can be determined depending on the formula<sup>33</sup>:

$$CPE = \frac{Z'_{\text{coat with AlNP}} - Z'_{\text{coat without AlNP}}}{Z'_{\text{coat with AlNP}}} \times 100\% \quad (1)$$

The CPE was calculated using the following Equation (1), where  $Z'_{\text{coat with Al NP}}$  is the real impedance ( $\Omega$ ) of nanocomposite coating, and  $Z'_{\text{coat without Al NP}}$  is the real impedance of coating ( $\Omega$ ) which was obtained using an equivalent circuit model. In Table 4 calculated values are shown for CPE (%):

According to Table 4, the influence of Al NPs increases corrosion protection by 43.33%. In epoxy paint, the same amount of Al NP increased corrosion protection by 51.41%

compared to epoxy resin. The reason for this deviation could be attributed to the added additives and aluminum particles that were in the epoxy paint, which were additionally affected by the ultrasonic homogenizer. According to the EDS analysis (Figure 3h), after the addition of 1% Al NP and the action of the ultrasonic probe, the distribution of aluminum particles became uniform and more homogeneous than in the base epoxy paint (Figure 7d).

### 3.6 | Scanning electrochemical microscopy

Although electrochemical techniques provide powerful tools for the study of interfacial reactions, conventional

**TABLE 4** The CPE (%) values for all samples were obtained from the Nyquist plot.

Samples	<i>t</i> (h)	$R_p$ ( $\Omega$ )	CPE (%)
Epoxy resin	24	$8.5 \times 10^7$	43.33
1% Al NP + epoxy resin		$1.5 \times 10^8$	
Epoxy paint	24	$1.0 \times 10^9$	94.74
1% Al NP + epoxy paint		$1.9 \times 10^{10}$	

methods fall short in providing information about the electrochemical reactions occurring at the sample surface.<sup>34</sup> Therefore, in addition to the EIS measurement, a scanning electrochemical microscopy (SECM) analysis of the samples was made, which gives the surface a representation of the coating in different shades that correspond to the electrochemical activity of the surface during 30 days of exposure in a 3.5 wt% NaCl solution. In this study, ic-ac-SECM was used primarily to evaluate the effect of Al NP on the corrosion protection performance of epoxy resin and epoxy paint over gray cast iron in a 3.5% NaCl solution. The surface distribution of real impedance resistances on epoxy resin and 1% Al NP epoxy resin nanocomposite after 1, 15, and 30 days of exposure in 3.5 wt% NaCl solution is shown in Figures 6 and 7.

According to Figure 6, all samples show a uniform distribution of real impedance resistances, which indicates the homogeneity of the prepared samples. The epoxy resin sample containing 1% Al NP showed better corrosion resistance than the pure epoxy resin immediately after 1 day of exposure to a corrosive medium (Figure 6a). With a longer exposure time (after 30 days), the resistance of all samples is still reflected as constant (Figure 6a–f). In Figure 6f, the 1% Al NP epoxy resin

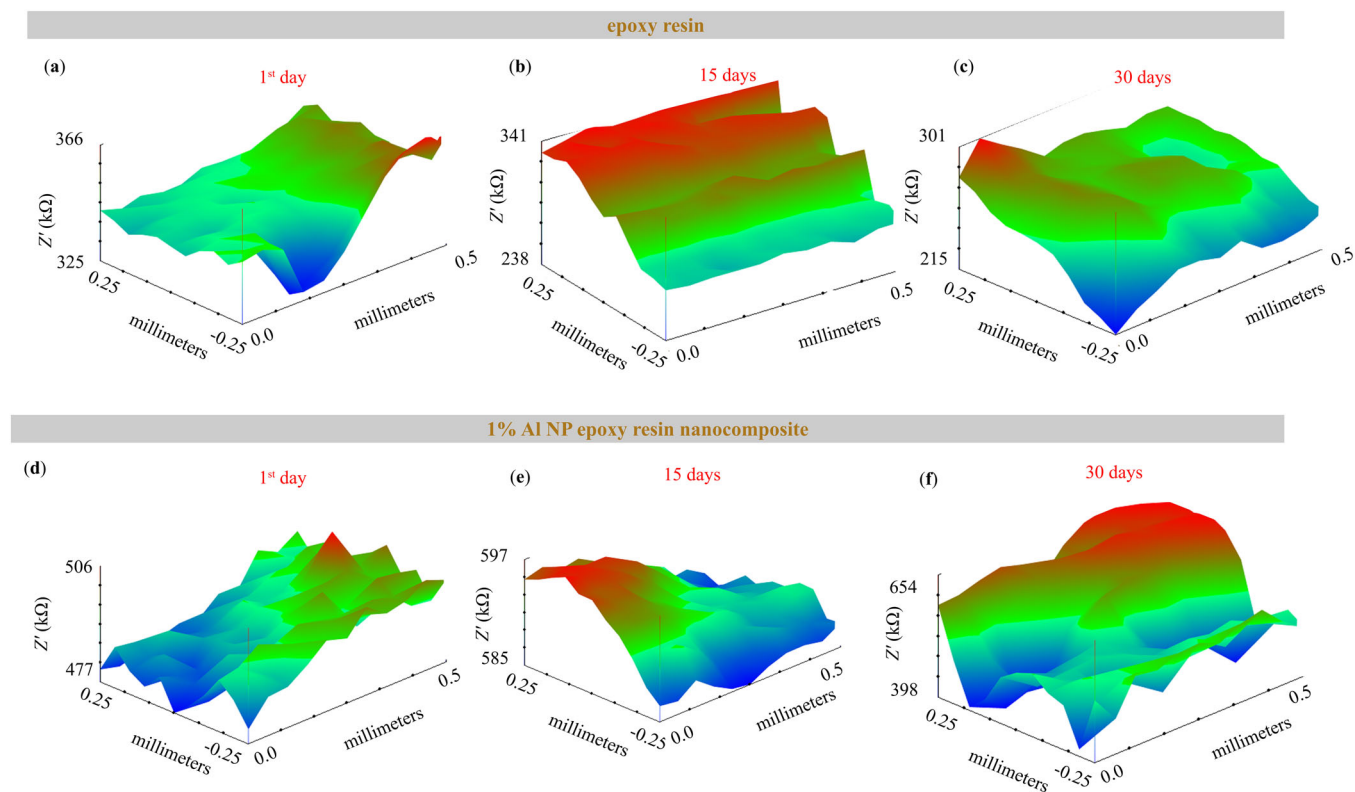


**FIGURE 6** IC-AC SECM distribution of real impedance ( $Z'$ ) for epoxy resin after (a) 1 day, 15 days, (c) 30 days, and 1% Al NP epoxy resin nanocomposite after (d) 1 day, (e) 15 days, and (f) 30 days in 3.5% NaCl solution. [Color figure can be viewed at [wileyonlinelibrary.com](http://wileyonlinelibrary.com)]

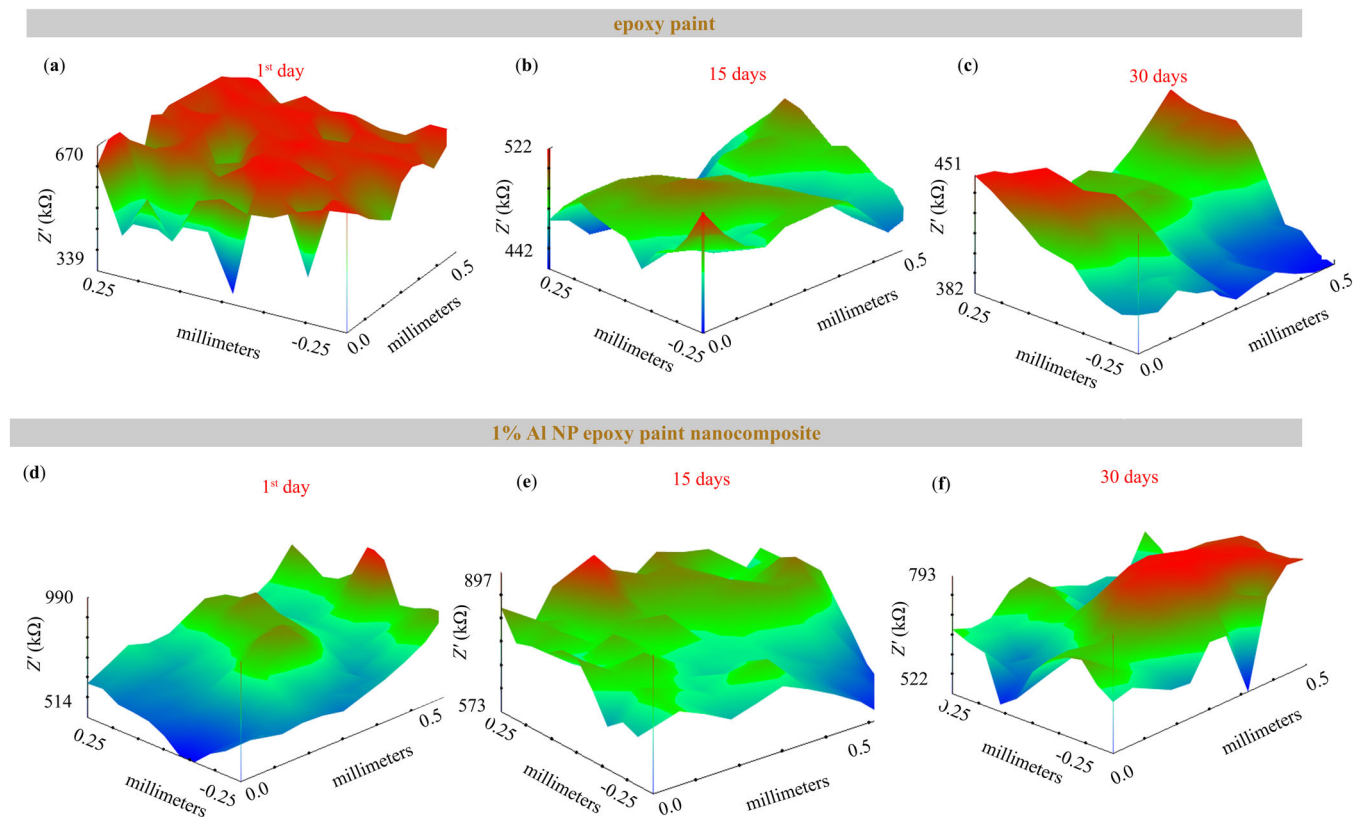


**FIGURE 7** IC-AC SECM distribution of real impedance ( $Z'$ ) for (a) epoxy paint after 24 h, (b) epoxy paint after 120 h, (c) 1% Al NP epoxy paint nanocomposite after 24 h, and (d) 1% Al NP epoxy paint nanocomposite after 120 h in 3.5% NaCl solution. [Color figure can be viewed at [wileyonlinelibrary.com](http://wileyonlinelibrary.com)]

nanocomposite sample shows an increasingly extended distribution of higher impedance resistances over the surface. The reason for this could be the reactivity of aluminum, in contact with the electrolyte Al NP reacts with water molecules,  $H^+$  and  $OH^-$  ions, and starts to form an oxide film on its surface.<sup>35</sup> The oxide film is very compact and the oxide volume is high compared to the metal involved by oxidation and closely adhered to the metal surface.<sup>36</sup> In addition, the Al NPs are superimposed parallel to each other in the coating film and play a “labyrinth” effect, thereby prolonging the permeation path and time of water and corrosion media to the substrate.<sup>37</sup>

According to Equation (1), calculate the CPE values for the epoxy resin and the 1% Al NP epoxy resin nanocomposite after 1, 15, and 30 days of exposure in a 3.5 wt % NaCl solution. Table 5 shows that for the sample 1% Al NP epoxy resin nanocomposite increased the CPE value by 15.21% after 15 days, which could indicate the formation of a protective oxide film on the Al NP surface.

The distribution of real impedances on the surface of epoxy paint and nanocomposite 1% Al NP epoxy paint is shown in Figure 7. The samples were exposed in 3.5 wt% NaCl solution for up to 30 days. All samples show small deviations of the real impedances on the surface, the

**TABLE 5** The CPE (%) values for epoxy resin and 1% Al NP epoxy resin nanocomposite obtained from ic-ac SECM topography after exposure in 3.5 wt. % NaCl solution for 1, 15, and 30 days.

Samples	$t$ (days)	$R_p$ (k $\Omega$ )	CPE (%)
Epoxy resin	1	366	27.67
1% Al NP + epoxy resin		506	
Epoxy resin	15	341	42.88
1% Al NP + epoxy resin		597	
Epoxy resin	30	301	53.98
1% Al NP + epoxy resin		654	

**TABLE 6** The CPE (%) values for epoxy paint and 1% Al NP epoxy paint nanocomposite were obtained from ic-ac SECM topography after exposure in 3.5 wt% NaCl solution for 30 days.

Samples	$t$ (days)	$R_p$ (k $\Omega$ )	CPE (%)
Epoxy paint	1	670	32.32
1% Al NP + epoxy paint		990	
Epoxy paint	15	522	39.09
1% Al NP + epoxy paint		857	
Epoxy resin	30	451	43.12
1% Al NP + epoxy paint		793	

cause of which may be a small inhomogeneity of the coating component. During 30 days of exposure to the epoxy paint in the corrosive electrolyte, there was no change in the resistance of the coating (Figure 7a–c). The addition of Al NPs to the epoxy paint increases the value of the relay impedance on the surface and thereby improves the anti-corrosion properties of the coating (Figure 7d). By exposing 1% Al NP epoxy paint in 3.5 wt% NaCl solution, the corrosion resistance is kept constant in the interval between 514 and 990 k $\Omega$  for 30 days (Figure 7d–f). Figure 7f shows that the surface of the coating is covered with all higher values of impedance

resistance, which could result in the formation of aluminum oxides.

According to Equation (1) calculate CPE values for epoxy paint and nanocomposite 1% Al NP epoxy paint after 1, 15, and 30 days of exposure in 3.5 wt% NaCl solution. The addition of Al NPs to the epoxy shows a coating color performance that increases and slightly increases with exposure time in the corrosive medium (Table 6).

The coating made of pure epoxy paint has a higher corrosion stability than the coating of epoxy resin (Figures 6 and 7) and because of this, the electrolyte penetration is more difficult and the Al NP in the epoxy paint

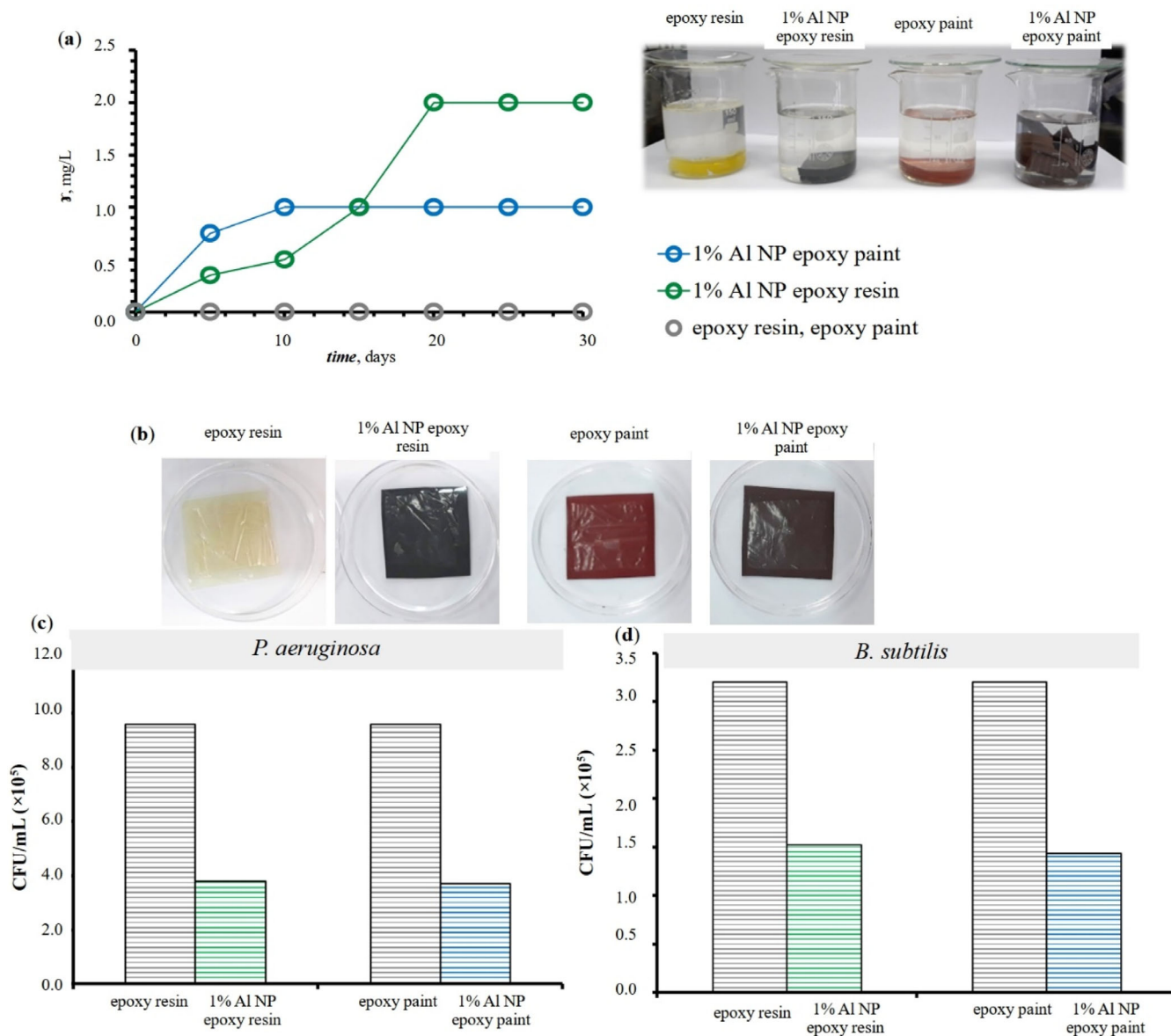


FIGURE 8 The mass concentration of the migration of (a)  $Al^{3+}$  ions from epoxy resin, epoxy paint, 1% Al epoxy resin nanocomposite, and 1% epoxy paint nanocomposite to simulated wastewater for 30 days. Antibacterial activity of epoxy resin, epoxy paint, 1% Al epoxy resin nanocomposite, and 1% epoxy paint nanocomposite on (c) *P. aeruginosa* and (d) *B. subtilis* after 24 h according to the ISO 22196 standard. [Color figure can be viewed at [wileyonlinelibrary.com](http://wileyonlinelibrary.com)]

**TABLE 7** Average values of bacterial activity of epoxy resin, 1% Al NP epoxy resin nanocomposite, epoxy paint, 1% Al NP epoxy paint nanocomposite against *P. aeruginosa* and *B. subtilis* according to JIS Z 2801 after 24 h.

Test bacteria	Contact time	Test substance	CFU (control) (mL)	CFU (test) (mL)	Reduction (%)	Log <sub>10</sub> (reduction)
<i>P. aeruginosa</i>	24 h	Epoxy resin	960,000	930,000	3.13	0.3887
		1% Al NP resin nanocomposite	960,000	380,000	60.42	
		Epoxy paint	960,000	920,000	4.17	0.39559
		1% Al NP paint nanocomposite	960,000	370,000	61.46	
<i>B. subtilis</i>	24 h	Epoxy resin	320,000	312,000	2.50	0.3123
		1% Al NP resin nanocomposite	320,000	152,000	52.50	
		Epoxy paint	320,000	309,000	3.44	0.3346
		1% Al NP paint nanocomposite	320,000	143,000	55.31	

will oxidize more slowly, and the CPE value will be a little lower.

### 3.7 | Migration and antibacterial activity of Al nanoparticles embedded in epoxy polymers

For polymer nanocomposites, degradation of the composite product itself, the fate of the nanoparticles in the polymer matrix, and the released nanoparticles play a key role in the antibacterial properties of epoxy coating. Release of Al NPs from epoxy resin, epoxy paint, and nanocomposite in simulated wastewater was measured at intervals of up to 30 days. According to Figure 8a, it was shown that the release rate of Al NP is faster in epoxy resin than in epoxy paint. Both samples after a certain time (10 days of exposure) show a constant mass concentration of aluminum in the wastewater. Pure aluminum has a greater affinity with oxygen and can be automatically oxidized in contact with water media to form an Al<sub>2</sub>O<sub>3</sub> passivation film.<sup>38</sup> The constant value of the mass concentration of aluminum in the wastewater could be the reason for the oxidation of Al NPs on the surface of the epoxy coating, and the release of new Al NPs due to the formation of aluminum oxide is possible. However, little data is available on the degradation of polymer nanocomposites, and the state of the imbedded nanoparticles during environmental exposures. The lack of this type of information hinders our ability to understand the release mechanisms and to predict the long-term release.<sup>39</sup>

The antibacterial activity of the epoxy resin, epoxy paint, 1% Al epoxy resin nanocomposite, and 1% epoxy paint nanocomposite was evaluated against the wastewater bacterial species *Pseudomonas aeruginosa* and *Bacillus subtilis* (Figure 8c,d).

According to Figure 8c,d, the highest nonlive count of bacteria was observed on the nanocomposites. The nanocomposite with 1% of Al NP in epoxy resin and epoxy paint exhibited the highest antibacterial effect, with a reduction of about 60.5% for *P. aeruginosa* and 54% for *B. subtilis* (Table 7).

According to Table 7, the nanocomposites showed a significant reduction in the number of all tested bacteria of about 0.33 log compared to the control epoxy coating during the exposure period of 24 h. These reduction values are satisfactory to demonstrate the antibacterial efficacy according to the criterion ( $\geq 2$  log) defined in the Japanese standard JIS Z 2801.<sup>40</sup>

According to the literature, the toxicity of Al NPs can be explained in two ways: (1) the released aluminum ion is toxic to living organisms,<sup>41</sup> (2) the formed aluminum oxides may inhibit bacterial growth.<sup>25</sup> It has been previously shown that the most toxic Al species are considered to be the monomeric Al<sup>3+</sup>.<sup>42,43</sup> The metal NPs slowly release metal ions able to puncture holes in the bacterial cell membrane and disrupt cellular processes from inside the cell.<sup>25,44</sup> The contract killing is the first possible mechanism for the ability of nanostructures to reduce the number of bacteria.<sup>45</sup> The aluminum ions are capable of interaction with many cellular components which has a negative impact on the homeostasis of microorganisms.<sup>42,43</sup> Aluminum binds to membrane components of cell walls and interferes with calcium metabolism. Moreover, for its positively charged species may interact with nucleic acids, thus distressing cellular functions. The second antibacterial mechanism of nanoparticles is the formation of extracellular and intracellular reactive oxygen species (ROS).<sup>45,46</sup> There is also evidence that Al<sup>3+</sup> toxicity can cause excessive generation of ROS and an increase in peroxidation and/ or breakdown of membrane lipids.<sup>47</sup> Aggregation of AlOxNPs on the surface of the bacterial cell also has a harmful effect.<sup>44</sup> Once the aluminum oxide

nanostructures are in contact with the bacteria, they can potentially cause the bacteria to rupture via irreparable mechanical damage to the bacterial membrane, increase oxidative stress within the bacterial cell and increased levels of free radicals can result in irreparable damage to nucleic acids, proteins, membranes, and organelles, which eventually leads to the activation of cell death.<sup>45</sup> It is important to note that the mechanisms of action are the complex result of multiple and often interconnected mechanisms that happen simultaneously and it is difficult to delineate their contributions in a complex biological system.<sup>46</sup>

## 4 | CONCLUSION

The aluminum nanocomposite was prepared, homogenized, and successfully used in epoxy resin and paint formulations to develop anticorrosion and antibacterial protection coating in the pipeline industry. It can be concluded that the addition of Al NPs in the epoxy coating improves the resistance to the electrolyte, but at the same time enables the migration of Al<sup>3+</sup> ions up to a certain concentration. It was also found that after 30 days of exposure to 3.5 wt% NaCl solution, the nanocomposite can form aluminum oxides. The influence of Al NPs in epoxy paint showed slightly better anticorrosion and antibacterial characteristics than the effect of Al NPs in pure epoxy resin. Such behavior is possible due to various additions and additives contained in the epoxy paint.

### AUTHOR CONTRIBUTIONS

**Marina Samardžija:** Conceptualization (lead); data curation (lead); formal analysis (lead); software (lead); writing – original draft (lead); writing – review and editing (lead). **Ivan Stojanović:** Project administration (lead); supervision (lead); validation (lead). **Marin Kurtela:** Methodology (supporting); project administration (lead); software (lead); supervision (supporting). **Vesna Alar:** Funding acquisition (lead); methodology (lead); project administration (lead); supervision (lead).

### ACKNOWLEDGMENTS

This work was supported by the European Regional Development Fund under the Operational Program Competitiveness and Cohesion 2014–2020. This research was funded by “Development of anticorrosion protection system for multipurpose pipe use,” grant number KK.01.1.1.07.0045.

### DATA AVAILABILITY STATEMENT

Research data are not shared.

### ORCID

Marina Samardžija  <https://orcid.org/0000-0001-9053-0627>

### REFERENCES

- [1] S. Rathnayaka, B. Shannon, D. Robert, J. Kodikara, *Struct. Infrastruct. Eng.* **2017**, *13*, 1553.
- [2] J. Ji, J. Hong Lai, G. Fu, C. Zhang, J. Kodikara, *Eng. Fail. Anal.* **2019**, *108*, 104239.
- [3] P. Drechsel, M. Qadir, D. Wichelns, *Wastewater: Economic asset in an urbanizing world*, World Springer, Switzerland **2015**.
- [4] L. Perelomov, O. Sizova, M. M. Rahman, I. Perelomova, T. Minkina, S. Sokolov, Y. Atroshchenko, *Sustainability* **2022**, *14*, 1.
- [5] S. Foorginezhad, V. Aryai, M. M. Dargah, R. Abbassi, *Process. Saf. Environ. Prot.* **2021**, *147*, 192.
- [6] R. Logan, M. Mulheron, D. Jesson, P. A. Smith, T. S. Evans, N. Clay-Michael, J. T. Whiter, *WIT Trans Built Environ.* **2014**, *139*, 411.
- [7] R. E. Melchers, *Corros. Eng. Sci. Technol.* **2017**, *52*, 541.
- [8] R. E. Melchers, C. Herron, R. Emslie, *Corros. Eng. Sci. Technol.* **2016**, *51*, 248.
- [9] A. Jana, T. K. Sarkar, A. Chouhan, D. Dasgupta, O. P. Khatri, D. Ghosh, *J. Mol. Liq.* **2022**, *364*, 119960.
- [10] S. Li, Y. Kim, K. S. Jeon, Y. Kho, *Met. Mater. Int.* **2000**, *6*, 281.
- [11] E. Ukpong, J. Udechukwu, *Glob. J. Eng. Res.* **2015**, *13*, 21.
- [12] C. Curutiu, F. Iordache, P. Gurban, V. Lazar, M. C. Chifiriuc, Elsevier Inc, Woodhead Publishing, Sawston, Cambridge **2019**.
- [13] S. Rahimi, O. Modin, F. Roshanzamir, A. Neissi, S. S. Alam, B. Seelbinder, S. Pandit, L. Shi, I. Mijakovic, *Chem. Eng. J.* **2020**, *397*, 125437.
- [14] D. Blackwood, *Corros. Mater. Degrad.* **2018**, *1*, 59.
- [15] M. Lv, M. Du, *Rev. Environ. Sci. Biotechnol.* **2018**, *17*, 431.
- [16] M. F. Moradali, S. Ghods, B. H. A. Rehm, *Front. Cell. Infect. Microbiol.* **2017**, *7*, 1.
- [17] S. P. Diggle, M. Whiteley, *Microbiology* **2020**, *166*, 30.
- [18] F. Teng, Y. T. Guan, W. P. Zhu, *Corros. Sci.* **2008**, *50*, 2816.
- [19] J. Errington, L. T. van der Aa, *Microbiology* **2020**, *166*, 425.
- [20] Y. S. Wang, L. Liu, Q. Fu, J. Sun, Z. Y. An, R. Ding, Y. Li, X. D. Zhao, *Sci. Rep.* **2020**, *10*, 1.
- [21] A. Mirmohseni, M. Azizi, M. S. S. Dorraji, *Prog. Org. Coat.* **2020**, *139*, 105419.
- [22] P. Jain, B. Patidar, J. Bhawsar, *J. Bio. Tribo-Corrosion* **2020**, *6*, 1.
- [23] M. Samardžija, M. Kurtela, M. Vuković Domanovac, V. Alar, *Coatings* **2023**, *13*, 898.
- [24] M. Tanveer, A. Farooq, S. Ata, I. Bibi, M. Sultan, M. Iqbal, S. Jabeen, N. Gull, A. Islam, R. U. Khan, S. H. Al-Mijalli, *Surf. Interfaces.* **2021**, *25*, 101285.
- [25] N. Doskocz, K. Affek, M. Załęska-Radziwiłł, *E3S Web Conf.* **2017**, *17*, 1.
- [26] ISO 868, *ISO copyright office*, Geneva, Switzerland, 2003.
- [27] ISO 12944-6, *ISO copyright office*, Geneva, Switzerland, 2018.
- [28] DIN EN 877, *German Institute for Standardisation*, Berlin, Germany, 2019.
- [29] ISO 22196, *ISO copyright office*, Geneva, Switzerland, 2007.
- [30] U. A. Samad, M. A. Alam, A. Chafidz, S. M. Al-Zahrani, N. H. Alharthi, *Prog. Org. Coat.* **2018**, *119*, 109.



- [31] H. Y. Xu, B. Li, X. Han, Y. Wang, X. R. Zhang, S. Komarneni, *J. Appl. Polym. Sci.* **2019**, *136*, 1.
- [32] A. Joseph, K. P. John Mathew, S. Vandana, *ACS Appl. Nano Mater.* **2021**, *4*, 834.
- [33] M. Samardžija, V. Alar, V. Špada, I. Stojanović, *Coatings* **2022**, *12*, 1500.
- [34] J. J. Santana, J. Izquierdo, R. M. Souto, *Coatings* **2022**, *12*, 637.
- [35] M. Kurtela, *PhD Thesis*, University of Zagreb (Zagreb, Croatia) 2021.
- [36] M. C. Reboul, B. Baroux, *Mater. Corros.* **2011**, *62*, 215.
- [37] Y. Bai, X. Jin, J. Xie, X. Lv, T. Gou, L. Zhang, J. Zhu, Y. Shao, H. Zhang, H. Zhang, B. Yuan, A. Yin, J. Nie, F. Cao, Z. Xu, *Coatings* **2022**, *12*, 1406.
- [38] L. Huang, K. Xiong, X. Wang, X. He, L. Yu, C. Fu, X. Zhu, W. Feng, *Metals (Basel)*. **2022**, *12*, 1049.
- [39] T. Nguyen, B. Pellegrin, C. Bernard, X. Gu, J. M. Gorham, P. Stutzman, D. Stanley, A. Shapiro, E. Byrd, R. Hettenhouser, J. Chin, *J. Phys. Conf. Ser.* **2011**, *304*, 012060.
- [40] JIS Z 2801, *JSA*, Japan. **2019**.
- [41] R. G. Pina, C. Cervantes, *Biol. Met.* **1996**, *9*, 311.
- [42] D. K. Chauhan, V. Yadav, M. Vaculik, W. Gassmann, S. Pike, N. Arif, V. P. Singh, R. Deshmukh, S. Sahi, D. K. Tripathi, *Crit. Rev. Biotechnol.* **2021**, *41*, 715.
- [43] P. Borotova, M. Drobny, A. Navratilova, M. Pozgajova, *Acta Fytotech. Zootech.* **2019**, *22*, 130.
- [44] S. V. Gudkov, D. E. Burmistrov, V. V. Smirnova, A. A. Semenova, A. B. Lisitsyn, *Nanomaterials* **2022**, *12*, 1.
- [45] P. Apelgren, K. Burnett, N. Ali, J. Bush, T. Karabacak, *Mater. Today Proc.* **2019**, *27*, 1.
- [46] D. Franco, G. Calabrese, S. P. P. Guglielmino, S. Conoci, *Microorganisms* **2022**, *10*, 1778.
- [47] L. Ponsone, A. Fabra, S. Castro, *Symbiosis* **2004**, *36*, 193.

**How to cite this article:** M. Samardžija, I. Stojanović, M. Kurtela, V. Alar, *J. Appl. Polym. Sci.* **2023**, e55002. <https://doi.org/10.1002/app.55002>

## 6. BIOGRAPHY OF THE AUTHOR

Marina Samardžija, [REDACTED] After finished high school, she enrolled at Faculty of Chemical Engineering and Technology in University of Zagreb. In 2013 completed her undergraduate study and with defending her bachelor thesis entitled “*Isomerization process of light paraffins*” earned univ. bacc. chem title. During her studies, she worked as a demonstrator in laboratory exercises in General Chemistry and was the winner of the Dean's award for work “*Rheological and thermal characterization of nanofluids*”. In 2015, she graduated at Faculty of Chemistry and Technology with defending her diploma thesis entitled “*Application of nanofluid in a plate heat exchanger*”. Her first employment was in 2016 at Faculty of Chemical Engineering and Technology in Department of General and Inorganic Chemistry where she worked as professional associate of the I. type in the system of science and higher education. In 2017, she supplemented her education with Pedagogical, Psychological, Didactic and Teaching Methodology Training at the Faculty of teacher Education in University of Zagreb. Next year, she started working as an assistant in Department of Chemistry in Faculty of Mining, Geology and Petroleum Engineering, as substitute for maternity. After she completed her maternity leave replacement, she was offered a position at the same institution that requires the enrolment of a doctorate. In 2020, she enrolled in the postgraduate doctoral course Chemical Engineering and Applied Chemistry at Faculty of Chemical Engineering and Technology in University of Zagreb. Under the supervision of her mentors, Assoc. Prof. Ivan Stojanović, PhD and Prof. Helena Otmačić Čurković, PhD, she started working on development of a nanocomposite system for corrosion and antibacterial protection consisting of an epoxy coating matrix and metal nanoparticles. The doctoral research resulted in the publication of four articles in scientific journals which are cited in Current Contents Connect. During her doctoral studies, she won three awards, namely:

1. 2022/2023-year, The prize for excellence in scientific – research work, technical field of research in 2022.
2. 2021/2022-year, The prize for the best e-college. Award for the implementation and active application of e-learning in the course Chemistry and water treatment.
3. 2020/2021- year, Prize for multimedia content in e-college. Award for the implementation and active application of e-learning in classes that took place in the Laboratory for the Analysis of Geological Materials

### **List of published papers:**

1. M. Samardžija, I. Stojanović, M. Kurtela, V. Alar, Influence of aluminum nanoparticles in epoxy resin and epoxy coating for anticorrosion and antibacterial protection in pipeline industry, *Journal of Applied Polymer Science*, (2023) e55002.
2. M. Samardžija, I. Stojanović, M. Vuković Domanovac, V. Alar, Epoxy Coating Modification with Metal Nanoparticles to Improve the Anticorrosion, Migration, and Antibacterial Properties, *Coatings*, 13 (2023) 7; 1201.
3. D. Božić, M. Samardžija, M. Kurtela, Z. Keran, B. Runje, Risk Evaluation for Coating Thickness Conformity Assessment, *Materials*, 16 (2023) 758, 15.
4. M. Samardžija, M. Kurtela, M. Vuković Domanovac, V. Alar, Anticorrosion and Antibacterial Properties of Al NP– Epoxy Nanocomposite Coating on Grey Cast Iron, *Coatings*, 13 (2023) 5, 898, 17.
5. M. Samardžija, V. Alar, V. Špada, I. Stojanović, Corrosion Behaviour of an Epoxy Resin Reinforced with Aluminium Nanoparticles, *Coatings*, 12 (2022) 10, 1500.
6. V. Alar, I. Stojanović, V. Šimunović, M. Kurtela, M. Samardžija, D. Ivaniš, Influence of acidic media and chlorides on protective properties of epoxy coatings, *Materials testing*, 64 (2022) 12, 1753-1764.
7. M. Samardžija, V. Alar, V. Špada, F. Kapor, Phosphating Modification with Metal Ions of Carbon Steel Surface to Improve the Influence of Anticorrosion Properties, *Technologies*, 10 (2022) 1, 3.
8. M. Samardžija, V. Alar, F. Aljinović, F. Kapor, Influence of phosphate layer on adhesion properties between a steel surface and an organic coating, *Rudarsko-geološko-naftni zbornik*, 37 (2022) 1, 11-17.

### **Lectures at international conferences:**

1. M. Samardžija, F. kapor, V. Alar, M. Kustela, Metode analize ispitivanja epoksidnih prvlaka, 26th International conference of materials protection and industrial finish, KORMAT 2024, 2024. (izvorni znanstveni rad, predavanje)
2. M. Samardžija, V. Alar, F. Kapor, B. Runje, I. Stojanović, The Influence of Different Preparations of Nanocomposite Coating on Protective Properties, International Conference MATRIB 2023 – Materials, Tribology & Recycling, 2023 (izvorni znanstveni rad, predavanje)

3. M. Samardžija, V. Alar, I. Stojanović, V. Špada, M. Kurtela. Aluminium nanocomposites epoxy coating for anticorrosion and antibacterial protection, MTECH 2023, 2023 (izvorni znanstveni rad, predavanje)
4. M. Samardžija, V. Alar, F. Kapor, Mikrobiološki Poticana Korozija Odvodnih Cijevi, 25th International conference of materials protection and industrial finish, KORMAT 2022, 2022 (izvorni znanstveni rad, predavanje)
5. M. Samardžija, Marina, G. Bilić, V. Alar, F. Kapor, Phosphate Coatings Modified with a Green Olive Leaf Extract for Corrosion Resistance on Carbon Steel, 3rd International Conference on Materials: corrosion, heat treatment, materials testing and tribology, MTECH 2021, 2021 (izvorni znanstveni rad, predavanje)

#### **Posters at the international conference:**

1. M. Samardžija, V. Alar, I. Stojanović, M. Kurtela, Application of EIS and SECM studies for investigation of anticorrosion properties of epoxy coatings. 28th Croatian Meeting of Chemists and Chemical Engineers, March 28-31, 2023. Rovinj, Croatia. 2023. str. 1-1. (sažetak izlaganja sa skupa)
2. M. Samardžija, M. Kurtela, V. Alar, I. Stojanović, B. Runje, Multifunctional Nanocomposites Epoxy Coating with Enhanced Mechanical, Anticorrosion and Bactericidal Properties Bruxelles: European Federation of Corrosion Publications, 2023. str. 1-1. (sažetak izlaganja sa skupa)
3. M. Samardžija, V. Alar, V. Špada, S. Jakovljević, B. Runje, Effect of Al and Ag nanoparticles on the anticorrosion and antibacterial properties of epoxy coating, MTECH 2023 – 4. međunarodna konferencija o materijalima: toplinska obrada i inženjerstvo površina, materijali i tribologija, korozija i ispitivanje materijala Zagreb: Hrvatsko društvo za toplinsku obradu i inženjerstvo površina, 2023. -, 1. (sažetak izlaganja sa skupa)
4. M. Samardžija, V. Alar, M. Kurtela, F. Kapor, Epoksidna prevlaka u zaštiti odvodnih cijevi, MATRIB 2022, 22th International Conference on Materials, Tribology & Recycling / Bušić, Matija ; Leder Horina, Jasna ; Tropša, Vlado (ur.). Varaždin: Hrvatsko društvo za materijale i tribologiju (HDMT), 2022. str. 56-56. (sažetak izlaganja sa skupa)
5. M. Kurtela, V. Alar, V. Šimunović, M. Samardžija, Modified Epoxy Coatings on Cast Iron, EUROCORR 2022 2022. str. 1-2. (sažetak izlaganja sa skupa)